Thermodynamic Properties of Spinor Bosons in Optical Lattices

Diploma Thesis by
Matthias Ohliger

Main Referee: Prof. Dr. Dr. h.c. Hagen Kleinert

submitted to the
Department of Physics
Freie Universität Berlin
May 2008

Contents

1 Introduction **1**

1.1 Bose-Einstein Condensation 1

1.2 Optical Lattices 2

1.3 Outline of Thesis 4

2 Spinor Bose Gases in Optical Lattices **7**

2.1 Experimental Realization 7

2.2 Details of Model 8

2.3 Bose-Hubbard Model for Spin-1 Bosons 10

3 Mott Insulator-Superfluid Transition **13**

3.1 Thermodynamics 13

3.2 System Properties Without Hopping 15

3.2.1 Unmagnetized Systen at Zero Temperature 15

3.2.2 Unmagnetized System at Finite Temperature 16

3.2.3 Magnetized Bose Gas 17

3.3 Mean-Field Hamiltonian 19

3.3.1 Decoupling of Hopping Term 19

3.3.2 Perturbation Theory 20

3.4 Phase Diagram at Zero Temperature 21

3.4.1 Landau Expansion 21

3.4.2 Limit of Vanishing Magnetization 24

3.5 Phase Diagram at Finite Temperature 27

3.5.1 Partition Function 27

3.5.2 Phase Boundary 30

4 Time-of-Flight **35**

4.1 Zero Temperature 35

4.1.1 Limit of Vanishing Interaction 35

4.1.2 Correlation Functions . . . 37
4.1.3 Time-of-Flight Pictures . . . 39
4.1.4 Visibility . . . 42
4.2 Finite Temperature . . . 43
4.2.1 Correlation Functions . . . 43
4.2.2 Particle Number . . . 44
4.2.3 Visibility . . . 45

5 Diagrammatic Green's Functions Approach 49
5.1 Preliminaries . . . 49
5.1.1 Scalar Bose-Hubbard Model . . . 49
5.1.2 Importance of Green's Functions . . . 50
5.1.3 Interaction Picture . . . 50
5.1.4 Partition Function . . . 51
5.2 Cumulant Decomposition . . . 52
5.3 Basic Diagrammatic Calculations . . . 54
5.3.1 Diagrammatic Rules . . . 54
5.3.2 Weights and Multiplicities . . . 54
5.3.3 Diagrammatic Series for Partition Function . . . 55
5.3.4 Calculation of Cumulants . . . 55
5.3.5 Free Energy . . . 56
5.3.6 Particle Number . . . 58
5.3.7 Specific Heat . . . 59
5.3.8 Green's Functions . . . 61
5.4 Diagrammatic Rules in Matsubara Space . . . 63

6 Further Development of Green's Functions Technique 65
6.1 Applications . . . 65
6.1.1 Time-of-Flight . . . 65
6.1.2 Phase Boundary . . . 67
6.1.3 Real-Time Green's Functions . . . 68
6.1.4 Dispersion Relations of Excitations . . . 70
6.1.5 Effective Masses . . . 73
6.1.6 Time-of-Flight from Resummed Green's Function . . . 75
6.1.7 Visibility from Resummed Green's Function . . . 80
6.1.8 Correlation Functions . . . 82

6.1.9 Extension to Spin-1 Systems . . . 83
6.2 Second Order . . . 84
6.2.1 Self-Energy . . . 85
6.2.2 Calculation of One-Loop Diagram . . . 85
6.2.3 One-Loop Corrected Phase Boundary at Zero Temperature . . . 89
6.2.4 Critical Properties of Mott Insulator-Superfluid Transition . . . 90
6.2.5 One-Loop Corrected Phase Boundary at Finite Temperature . . . 93
6.2.6 One-Loop Corrected Excitation Spectrum . . . 94

7 Summary and Outlook **97**

A Properties of Spin-1 Eigenstates **99**
A.1 Matrix Elements of Creation and Annihilation Operators . . . 99
A.1.1 Further Properties of Spin Operators . . . 100
A.1.2 Creation of Basis States from Vacuum State . . . 100
A.1.3 Recursion Relations . . . 102
A.2 Calculation of Normalization Constant of Eigenstates . . . 106
A.3 Relations Between Matrix Elements . . . 109
A.4 Calculation of Matrix Elements for Unmagnetized System . . . 109

B Correlation Function for Finite Temperature **111**

Bibliography **115**

List of Figures **121**

Danksagung **123**

Chapter 1

Introduction

1.1 Bose-Einstein Condensation

Concerning quantum statistics, there is a fundamental difference between particles with integer and with half-integer spin [1]. The former, called Bosons, have a symmetric total wave function and obey the Bose-Einstein statistics while the latter, called Fermions, have an anti-symmetric wave function and obey the Fermi-Dirac statistics. The anti-symmetry of the wave function of the Fermions leads to the Pauli exclusion principle which prevents more than one particle to occupy the same state. This constraint does not apply to Bosons where arbitrary occupation numbers are possible. The maybe most prominent example for a Boson is the photon but also atoms with integer total hyperfine spin F, like ^{23}Na and ^{87}Rb, are Bosonic particles. Only Bosonic atoms shall be discussed in the present thesis.
Already in the year 1924, Satyendranath Bose and Albert Einstein predicted that, for low enough temperatures, Bosons can macroscopically occupy their ground state state and form a collective, coherent quantum state which was later on called a Bose-Einstein condensate or shorter just a BEC. This transition happens when the thermal de-Broglie wave-length, i.e. the wave-length corresponding to a particle with the mean thermal momentum $p \approx \sqrt{2Mk_BT}$, where M is the Boson mass, becomes of the order of the mean separation between the particles. The critical wave-length reads

$$\lambda_c = \sqrt{\frac{2\pi\hbar^2}{Mk_BT_c}} \approx n^{-1/3} \quad , \tag{1.1}$$

where n is the particle density and T_c the critical temperature. Condition (1.1) means that the wave functions of the atoms overlap. Then, because of the Heisenberg uncertainty principle, they can no longer be thought of as distinct particles but must be described as a collective quantum object. Performing a more quantitative calculation yields the critical temperature where the condensation in a homogeneous system occurs at [2]

$$T_c = \frac{2\pi\hbar^2}{k_BM}\left[\frac{n}{\zeta(3/2)}\right]^{2/3} \tag{1.2}$$

with $\zeta(3/2) \approx 2.61$. The phase transition to the Bose condensed phase is very interesting because it takes place even in an ideal gas without interaction which means that Bose-Einstein condensation is a pure quantum-statistical effect, as discussed in detail in Ref. [3]. In contrast to that, the well-known classical phase transitions [4,5], as for example in ferromagnets, and also the quantum phase transitions [6] which are extensively discussed in this thesis in Chapters 3 and 6, are governed by the interplay between the interaction energy and the thermal or quantum fluctuations. As it would facilitate the experimental realization to have a high critical temperature, Eq. (1.2) tells us to increase the particle

density as much as possible. Unfortunately, this is not favorable: Even for moderate densities, "normal" condensation to a solid or a liquid would occur long before the BEC transition temperature is reached. Thus, one is forced to work with very dilute gases with a density of $n \approx 10^{14}\,\mathrm{cm}^{-3}$. Because of this, the critical temperature (1.2) is of the order of some hundred nano-Kelvin and therefore it took more than 70 years and the development of very sophisticated cooling and trapping methods [7] before Bose-Einstein condensation was reached experimentally. However, an effect closely related [8] was already observed in 1937: When Helium-4 is cooled below 2.17 K, it becomes superfluid which means that its viscosity drops to zero. This effect can be understood by the existence of a collective wave-function for a fraction of the liquid. But because of the large density, the interaction between the atoms is strong and the analogy to the effect predicted by Bose and Einstein is not perfect. Even at zero temperature less then 10% of the atoms are in the ground state, in contrast to 100% in an ideal gas of Bosons.
Bose-Einstein condensation in almost ideal gases was first realized in 1995 at JILA in Rubidium atoms [9] and at MIT in Sodium atoms [10]. In the latter experiment, about $6 \cdot 10^5$ atoms were used and the critical temperature was about 250 nK. In order to reach such ultra-low temperatures, various cooling-methods have been employed of which two should be sketched here (see Fig. 1.1). The first method is "laser cooling" [11]. When an atom absorbs a photon from a directed laser beam, it experiences a recoil while the following re-emission is isotropic and, therefore, transfers zero net-momentum. When the laser frequency is now chosen red-detuned with respect to the considered atomic transition frequency, absorption is only possible when the atom is flying towards the laser so that the Doppler shift compensates the detuning. Therefore, the atom gets slowed down. Using three pairs of lasers, i.e. one pair in every spatial dimension, allows to cool the atoms in the trap down to a few micro-Kelvin. Note that this method, which is sometimes also called "optical molasses", is only the simplest way of laser cooling while more sophisticated schemes are also used, e.g. Sisyphus cooling [7,12]. For the atoms to be not only cooled but also trapped, the most commonly used device is the magneto-optical trap [7]. The key idea behind it is to use a position-dependent magnetic field to induce a position-dependent Zeeman-splitting. As a result, the force exercised by the lasers becomes also position-dependent, yielding a net-force towards the center of the trap. Note that this trapping potential, which can be well approximated as being harmonic, destroys the homogeneity of the system so that (1.2) must be modified accordingly [2, 3]. However, when the trap is sufficiently flat, the concept of a homogeneous system is a suitable starting point.
In order to reach even lower temperatures, the method of "forced evaporative cooling" is used [13]. The idea behind this cooling method is the same as blowing onto a cup of coffee which is too hot to drink. The fastest atoms are removed and the remaining ones re-thermalize to a lower temperature. In a trap the fastest atoms with highest kinetic energy are most likely to be found farer away from the center. The magnetic trapping field induces a Zeeman splitting of the energies according to their total spin z-component m_F. When now a radio frequency wave with the frequency corresponding to the energy splitting of the outmost atoms is irradiated, spin flips are induced. For the resulting state the trapping field is not attractive but repulsive and, thus, the atoms are expelled from the trap. In order to reach the critical temperature for Bose-Einstein condensation, it is necessary to loose up to 90% of the initial number of atoms. Because we have just seen that all atoms in a magnetic trap are in the same spin state with $m_F = F$, we do not expect any spin dynamics. The spin degrees of freedom are said to be frozen. That is the reason why the description of the Bosons as spinless ones is accurate and the corresponding scalar theory is applicable. We will see in the next chapter how these spin degrees of freedom are released and how they can lead to interesting physical effects.

1.2 Optical Lattices

As discussed in the previous section, Bose-Einstein condensation is a phenomenon observable in ideal gases. Although all real gases do, of course, interact, those interactions can be weak when the density

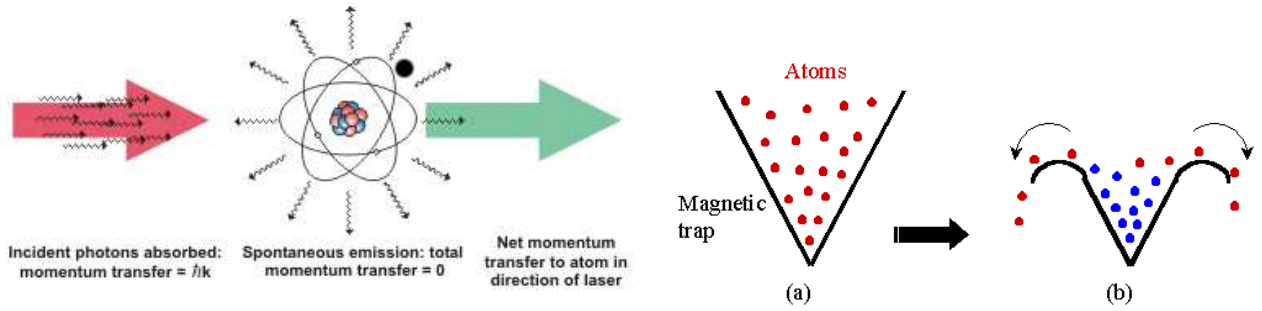

Figure 1.1: Schematic depiction of cooling methods. Left: Laser cooling [14]. Right: Evaporative cooling [15].

is sufficiently low. Therefore, they can usually be treated as a perturbation [3, 16]. The importance of interactions is notably enhanced when confining the Bosons in an optical lattice [17, 18]. Such a device is produced by reflected laser beams which form a standing wave. In such a standing wave the amplitude of the electric-field oscillates but its intensity, i.e. $I = |E|^2$, is stationary. In the simplest setting of lasers forming right angles, which is assumed troughout all this thesis, the intensity distribution reads

$$I(\mathbf{x}) = I_0 \sum_{i=1}^{D} \sin^2(2\pi x_i/\lambda) \quad , \tag{1.3}$$

where λ is the wave-length of the lasers and D the dimension of the system. We emphasize that it is experimentally possible to realize such settings for $D = 1, 2, 3$ and we will therefore address the question of dimensionality at the points where it occurs. The lasers are far detuned from atomic resonances and act on the atoms through the Stark effect, which means that the electric field of the laser-light induces dipole moments on the polarizable atoms which are then experiencing a force resulting from the gradient of the inhomogeneous electric light-field. This AC-Stark effect can be most easily understood in a classical model which considers the atom as a harmonic oscillator with a frequency corresponding to the atomic transition frequency next to the laser frequency. This model can be found in any textbook on classical mechanics, see for example Ref. [19]. The same result can also be obtained with the help of a simple semi-classical consideration, where the atom is considered as a two-level quantum system but the laser-light as a classical electromagnetic field, as it is, for example, discussed in Ref. [20]. If the laser-light is red-detuned, i.e. its frequency is lower than the one of the nearest atomic transition, the atoms are pushed towards higher laser intensities. Because this effect is proportional to the intensity of the laser light-field, the atoms experience the periodic potential

$$V(\mathbf{x}) = V_0 \sum_{i=1}^{D} \sin^2(2\pi x_i/\lambda) \quad , \tag{1.4}$$

where V_0 is called the lattice depth which is proportional to the intensity of the laser. The potential (1.4) describes a D-dimensional hypercubic lattice as it is depicted in Fig. 1.2. This situation resembles pretty much the situation in a crystal and can therefore serve as a model system for condensed-matter physics where we call the minima of the potential (1.4) "lattice sites". The interest in optical lattices as a model system stems from the fact that, unlike in condensed matter, the relevant parameters are experimentally controllable. Furthermore, there exist no defects, which make the treatment of ordinary crystals more complicated. After having understood the pure system, i.e. without defects, it is now possible to introduce disorder in a controlled way to study its effects [21, 22]. One detail, which should be mentioned at this point, is the fact that in all experiments, in addition to the optical lattice, a harmonic confining trap is used to prevent the atoms from escaping. Effects arising from

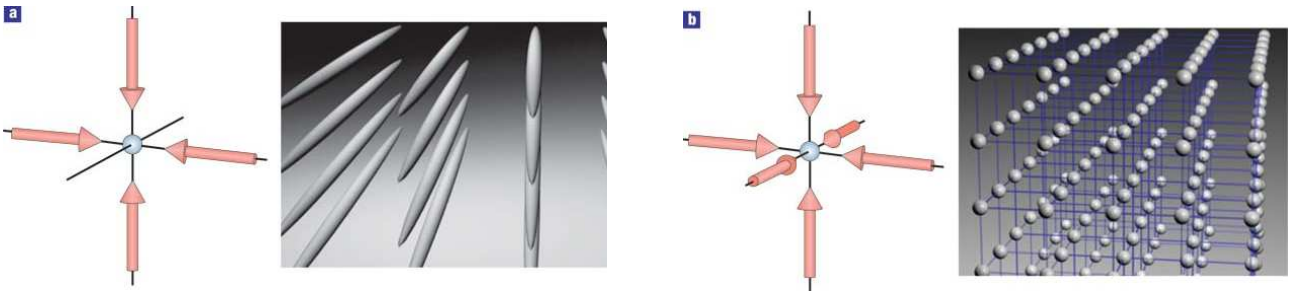

Figure 1.2: Schematic depiction of the lattice structure produced by counter-propagating lasers in two (a) and three (b) dimensions [30].

this additional potential are, for example, discussed in Ref. [23],
A groundbreaking accomplishment was the observation of the quantum phase transition from a superfluid to a Mott insulator in 2002 [17] according to a theoretical suggestion in Ref. [24]. More precisely, a Bose-Einstein condensate, which is characterized by a *delocalized* collective wave-function was transformed in an reversible way into a Mott insulator, which is a state with strongly localized atoms on the lattice sites, by changing the lattice depth V_0. The theoretical description of this transition is one main aim of this thesis.
In addition to serving as a model system, quantum gases also provide opportunities to study fundamental quantum effects like entanglement [25] and to investigate the basic concepts of quantum computation [26]. A further idea is to use ultra-cold atomic gases in optical lattices as a quantum emulator, i.e. to simulate Hamiltonians which are, for example, relevant for the problem of high-T_c superconductivity or which are discussed in quantum chromodynamics [27, 28].
Quantum effects in ultra-cold gases are not restricted to Bosons but also Fermions show interesting effects due to the formation of Bosonic Cooper pairs and their condensation [29].

1.3 Outline of Thesis

The work presented in this thesis is organized as follows: In **Chapter 2**, we consider Bosons in optical lattices which possess additional spinor degrees of freedom, where we focus on particles which can be described by an effective spin $F = 1$. We discuss the motivation to study this system, describe the experimental realization and derive an appropriate model, the "spin-1 Bose-Hubbard model", for a theoretical description.
In **Chapter 3**, we address the problem of the Mott insulator-superfluid transition in such a spinor system. We generalize the mean-field approximation commonly used to describe spinless Bosons and present the phase boundary for both zero and finite temperature. In the latter case an interesting effect arising from the interplay between thermal fluctuations and the spin-dependent interaction between the particles is observed.
Because it is possible [31], but experimentally difficult to perform in-situ measurements in a BEC, i.e. without destroying it, the most commonly used observation technique is time-of-flight measurement. It is performed by switching off the trapping potentials and letting the atoms expand freely. The aim of **Chapter 4** is to explain the observed pictures theoretically and to derive a quantitative measure, the visibility, out of it where we again include non-zero temperature and also resolve the different spin states.
To facilitate the following derivations and to make a connection to the large amount of existing literature and experiments on that system, we specify our discussion in **Chapter 5** to the scalar Bose-

Hubbard model, which describes effective spinless Bosons. We derive a diagrammatic approach to calculate both the free energy and the imaginary-time Green function perturbatively for deep lattices. In **Chapter 6**, this approach will be applied to calculate various properties of the system, especially the time-of-flight pictures, the phase boundary, and the spectrum of the excitations. For the latter, we introduce the Green function in real-time. We introduce a diagrammatic resummation technique, which allows us to obtain results that go beyond perturbation theory. With this technique, we calculate the phase diagram and compare it both to the well known mean-field result and to findings of other analytical and numerical methods. Furthermore, the critical properties of the quantum phase transitions are discussed.
In **Chapter 7** the presented work is summarized and a short outlook to related open questions is given.
The appendices are devoted to the presentation of details of calculations which are too technical to be included in the main part. In **Appendix A**, recursion relations for the coefficients, which arise in the perturbative treatment of the spin-1 problem in Chapter 3, are derived and some relations between them are stated. In **Appendix B**, we give some details of the calculation of the finite-temperature correlation functions of the spin-1 Bose-Hubbard model in Chapter 4.

Chapter 2

Spinor Bose Gases in Optical Lattices

As mentioned already in the introduction, the commonly used magneto-optical trap cannot store atoms in different hyperfine spin states and, therefore, no spin degrees of freedom exist in such traps. In order to observe spinor dynamics, one needs a trapping mechanism which traps atoms regardless of their spin state. This mechanism is explained below in Section 2.1. Most work, both theoretically and experimentally [16, 32, 33], was focused on atoms with effective spin $F = 1$ which we will exclusively consider in this thesis. Two examples for such species are ^{23}Na and ^{87}Rb. However, there are also efforts to understand the additional features resulting from effective spin $F = 2$, which can also be realized in ^{87}Rb, for example the existence of a cyclic phase in addition to the ferromagnetic and anti-ferromagnetic phases known for $F = 1$ [34, 35].

2.1 Experimental Realization

In order to see effects resulting from the spin properties, one needs a trap in which, for a given spin multiplet F, particles with all possible projections of the spin on the z-axis $m_F = -F, \ldots, +F$ can be stored. This is possible by reloading the gas into an all-optical trap which is sometimes also called an optical dipole trap [36]. Here, as the name suggests, no magnetic fields but only lasers are used. They act on the atoms with the same mechanism as an optical lattice, i.e. the Stark effect which was described above. Thus, it is possible to trap atoms with laser beams which have a Gaussian beam profile. In a red-detuned laser the atoms are concentrated in the center of the beam where the intensity of the light-field is maximal. If the laser is blue detuned, the situation is vice versa, i.e. the atoms are pushed towards smaller laser-intensities and therefore more complicated beam profiles must be used. These two situations are schematically shown in Fig. 2.1 together with a numerically calculated distribution of the laser light intensity. The mechanism of the interaction between the atom and the field of the laser light does not depend on the spin state of the atom, and, therefore, particles with arbitrary m_S can be trapped and the spin degrees of freedom are not frozen anymore. But despite of this feature of the optical dipole trap, which allows for new and interesting spin physics to be investigated, it has also two drawbacks: At first place, optical dipole traps are very shallow, they usually have no depths larger than one Millikelvin. The depth of a trap gives the maximal energy which atoms are allowed to have so that they still can be trapped. The depth of a magnetic trap is much higher and can reach more than hundred Millikelvin. The second disadvantage stems directly from the desired feature. Because all hyperfine components can be stored, no *forced* evaporative cooling is possible in an optical trap. Together with the small depth this means that it is often better to cool down the atoms to condensation temperature in a magnetic trap first and reload them then into an optical dipole trap. In that case it is feasible to use pulsed radio frequency in a way similar as in nuclear magnetic resonance (NMR) to flip a certain amount of the spins. Thus, it is possible

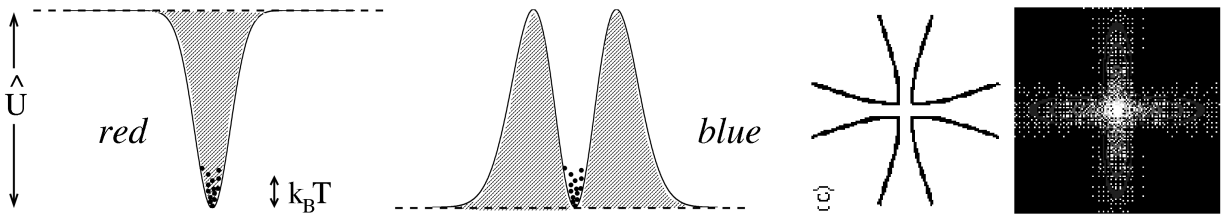

Figure 2.1: Left: Schematic illustration of red- and blue-detuned optical trap. Right: Calculated intensity profile of red-detuned trap with Gaussian beam profile [37].

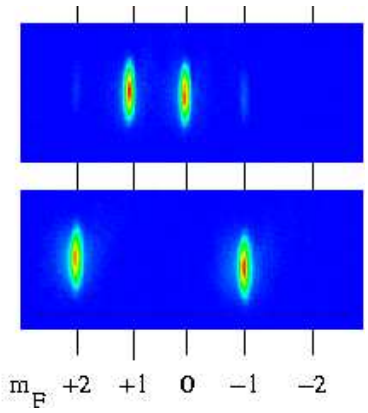

Figure 2.2: Different hyperfine components in a spinor BEC. Top and bottom are two experiments where different states where prepared [38].

to prepare the system in an arbitrary spin state. We will later see how these states can be separated experimentally. Two different initial states are shown in Fig. 2.2.

2.2 Details of Model

In this section, we describe more specifically the system under consideration. As it is used in most experiments, we consider a cubic lattice. We will mainly work in three dimensions but we will at some points also be interested in an arbitrary dimension. The optical lattice is created by three pairs of counter-propagating laser beams where the wave-length of the laser was given by 852 nm in the experiment described in Ref. [17] The depth of the lattice is described by V_0 which is measured in units of the recoil energy $E_R = \hbar^2 k_L^2/(2M)$ where $k_L = \pi/a$ is the lattice vector. Therefore, we get the following result for the single-particle potential:

$$V(\mathbf{x}) = V_0 \sum_{\nu=1}^{3} \sin^2(k_L x_\nu) \quad . \tag{2.1}$$

We note that the potential factorizes in three one-dimensional parts which is a special property of the (hyper)cubic lattice. In the following, we will neglect the additional harmonic confining potential and work with a translational invariant lattice with periodic boundary conditions.
It is known that the interaction potential between two atoms is quite complicated and can be best described by the empirical Lennard-Jones potential [39]. But when we neglect long-range forces like

	$c_2 < 0$ ferromagnetic example ^{87}Rb [44]	$c_2 > 0$ anti-ferromagnetic example ^{23}Na [45]
a_0	$50\,a_B$	$101.8\,a_B$
a_2	$55\,a_B$	$100.4\,a_B$

Figure 2.3: Experimentally determined s-wave scattering-lengths of the two most important Bosonic species used in optical lattice experiments. a_B is the Bohr radius.

Coulomb or dipolar interactions, the behavior can be very well described by a delta-like pseudo-potential [40]

$$V_{\rm int}(\mathbf{x_1}, \mathbf{x_2}) = \frac{4\pi\hbar^2 a_s}{M}\delta(\mathbf{x_1} - \mathbf{x_2}) \quad , \tag{2.2}$$

where the s-wave scattering length a_s is a parameter to be determined experimentally. Dipolar interactions are for example relevant when describing a Bose-Einstein condensate of chromium atoms because of their large magnetic dipole moment [41, 42].

Furthermore, we neglect three-body interactions which is acceptable because the particle density is very low. When two particles with hyperfine spins $F_1 = F_2 = 1$ scatter, there are two spin channels because the total spin $F_{\rm total}$ can either be 0 or 2. Note that $F_{\rm total} = 1$ is forbidden [43]. The most general two-particle time- and space-independent delta-interaction reads in second quantized form

$$\sum_{\alpha\beta\gamma\delta} \hat\Psi^\dagger_\alpha(\mathbf{x})\hat\Psi^\dagger_\beta(\mathbf{x})U_{\alpha\beta\gamma\delta}\hat\Psi_\gamma(\mathbf{x})\hat\Psi_\delta(\mathbf{x}) \tag{2.3}$$

with the fourth rank interaction tensor $U_{\alpha\beta\gamma\delta}$. Rotational invariance in spin space implies that (2.3) has only two irreducible terms and can be brought into the form [16, 43]

$$\frac{c_0}{2}\sum_{\alpha,\beta} \hat\Psi^\dagger_\alpha(\mathbf{x})\hat\Psi^\dagger_\beta(\mathbf{x})\hat\Psi_\beta(\mathbf{x})\hat\Psi_\alpha(\mathbf{x}) + \frac{c_2}{2}\sum_{\alpha,\beta,\gamma,\delta} \hat\Psi^\dagger_\alpha(\mathbf{x})\hat\Psi^\dagger_\gamma(\mathbf{x})\mathbf{F}_{\alpha\beta}\cdot\mathbf{F}_{\gamma\delta}\hat\Psi_\delta(\mathbf{x})\hat\Psi_\beta(\mathbf{x}) \quad , \tag{2.4}$$

where we have used the abbreviations

$$c_0 = 4\pi\hbar^2(a_0 + 2a_2)/3M \quad , \qquad c_2 = 4\pi\hbar^2(a_0 - a_2)/3M \tag{2.5}$$

with the two s-wave scattering lengths a_0, a_2 in the respective spin channels. The first term in (2.4) describes two Bosons coupling to total spin $F = 0$ while the second one corresponds to two particles which have total spin $F = 2$. Furthermore, $\mathbf{F}$ is the vector of the three spin-1 generators of the rotation group

$$F^x = \frac{1}{\sqrt{2}}\begin{pmatrix} 0 & 1 & 0 \\ 1 & 0 & 1 \\ 0 & 1 & 0 \end{pmatrix}, \quad F^y = \frac{1}{\sqrt{2}}\begin{pmatrix} 0 & -i & 0 \\ i & 0 & -i \\ 0 & i & 0 \end{pmatrix}, \quad F^z = \begin{pmatrix} 1 & 0 & 0 \\ 0 & 0 & 0 \\ 0 & 0 & -1 \end{pmatrix} \quad , \tag{2.6}$$

which fullfill the commutator relations $[F^\alpha, F^\beta] = i\sum_\gamma \epsilon_{\alpha\beta\gamma}F^\gamma$ and have the Casimir invariant $\mathbf{F}\cdot\mathbf{F} = F2$.

Most important for the system properties is the sign of c_2. If $c_2 < 0$, i.e. $a_2 > a_0$, the repulsion of particles with parallel spin is lower than the one between particles with antiparallel spin. Because of this, it is energetically favorable for the spins to align, which means that the ground state is ferromagnetic. For the opposite case $c_2 > 0$, i.e. $a_2 < a_0$, the situation is vice versa and the ground state is anti-ferromagnetic. The Bosons most used in experiments are ^{87}Rb and ^{23}Na for which the respective scattering lengths are given in Fig. 2.3.

2.3 Bose-Hubbard Model for Spin-1 Bosons

The Bose-Hubbard model provides the simplest way to describe the most important feature of a Bose gas in an optical lattice. This feature is the competition between the kinetic energy, which leads to the delocalization of the particles and to an uniform spatial distribution and the potential energy, which localizes the particles on the lattice sites due to a minimization of the repulsion. In order to derive the model, we start from the second quantized Hamiltonian for a spin-1 Bose gas in the grand-canonical ensemble [43, 46–48] which reads

$$\hat{H} = \sum_{\alpha} \int d^3x\, \hat{\Psi}^\dagger_\alpha(\mathbf{x}) \left[-\frac{\hbar^2}{2M}\nabla^2 + V_0 \sum_{\nu=1}^{3} \sin^2(k_L x_\nu) - \mu \right] \hat{\Psi}_\alpha(\mathbf{x}) - \eta \sum_{\alpha,\beta} \int d^3x\, \hat{\Psi}^\dagger_\alpha(\mathbf{x}) F^z_{\alpha\beta} \hat{\Psi}_\beta(\mathbf{x})$$
$$+ \frac{c_0}{2} \sum_{\alpha,\beta} \int d^3x\, \hat{\Psi}^\dagger_\alpha(\mathbf{x}) \hat{\Psi}^\dagger_\beta(\mathbf{x}) \hat{\Psi}_\beta(\mathbf{x}) \hat{\Psi}_\alpha(\mathbf{x}) + \frac{c_2}{2} \sum_{\alpha,\beta,\gamma,\delta} \int d^3x\, \hat{\Psi}^\dagger_\alpha(\mathbf{x}) \hat{\Psi}^\dagger_\gamma(\mathbf{x}) \mathbf{F}_{\alpha\beta} \cdot \mathbf{F}_{\gamma\delta} \hat{\Psi}_\delta(\mathbf{x}) \hat{\Psi}_\beta(\mathbf{x}) \quad . \tag{2.7}$$

Here η is an additional parameter which can be interpreted for the time being as an external magnetic field. Its exact meaning will be further explained in Subsection 3.1. Because of the Bosonic nature of the particles, the field operators fullfill the standard commutator relations

$$[\hat{\Psi}_\alpha(\mathbf{x}), \hat{\Psi}_\beta(\mathbf{x}')] = 0 \quad , \qquad [\hat{\Psi}^\dagger_\alpha(\mathbf{x}), \hat{\Psi}^\dagger_\beta(\mathbf{x}')] = 0 \quad , \qquad [\hat{\Psi}_\alpha(\mathbf{x}), \hat{\Psi}^\dagger_\beta(\mathbf{x}')] = \delta_{\alpha,\beta}\delta(\mathbf{x}-\mathbf{x}') \quad . \tag{2.8}$$

The first term in (2.7) results from the one-particle Hamiltonian, the second one is the Zeman energy in the magnetic field η, the third one describes the spin-independent interaction, and the last one the spin dependent interaction. As explained above, the lattice potential does not depend on the spin and we can therefore expand the field operators into spin-independent, orthonormal Wannier functions which are extensively discussed in Ref. [49]:

$$\hat{\Psi}_\alpha(\mathbf{x}) = \sum_i \hat{a}_{i,\alpha} w(\mathbf{x}-\mathbf{x}_i) \quad , \qquad \hat{\Psi}^\dagger_\alpha(\mathbf{x}) = \sum_i \hat{a}^\dagger_{i\alpha} w^*(\mathbf{x}-\mathbf{x}_i) \tag{2.9}$$

with

$$[\hat{a}_{i\alpha}, \hat{a}_{j\beta}] = 0 \quad , \qquad [\hat{a}^\dagger_{i\alpha}, \hat{a}^\dagger_{j\beta}] = 0 \quad , \qquad [\hat{a}_{i\alpha}, \hat{a}^\dagger_{j\beta}] = \delta_{\alpha,\beta}\delta_{i,j} \quad . \tag{2.10}$$

Here $w(\mathbf{x})$ is the Wannier function of the lowest Bloch band. Wannier functions are the Fourier transforms of the Bloch functions [23]. Because the Wannier functions are peaked on the lattices sites, they form a set of suitable basis states when considering particles in optical lattices. We do not consider excitations into higher bands which is reasonable because the band gap is much higher than any other energy scale in this problem. The Wannier functions are localized and, therefore, it is valid to say that $\hat{a}^\dagger_{i\alpha}$ creates a particle with $m_F = \alpha$ on site i. Now we insert the decomposition (2.9) into (2.7). In order to get a Hamiltonian we can work with, we must make an approximation: Because the Wannier functions are strongly localized on the lattice sites, we consider only on-site interactions, i.e. we assume

$$\int d^3\mathbf{x}\, |w(\mathbf{x}-\mathbf{x}_i)|^2 |w(\mathbf{x}-\mathbf{x}_j)|^2 \approx 0 \quad \text{if } i \neq j \quad . \tag{2.11}$$

Furthermore, we neglect all possible hopping processes which are not between the nearest neighboring sites, i.e. also assume

$$\int d^3\mathbf{x}\, w^*(\mathbf{x}-\mathbf{x}_i) \left[-\frac{\hbar^2}{2M}\nabla^2 + V_0 \sum_{\nu=1}^{3} \sin^2(k_L x_\nu) \right] w(\mathbf{x}-\mathbf{x}_j) \approx 0 \tag{2.12}$$

if i and j are not nearest neighbors. Note that for $i = j$ we only get an additional energy shift which is not of interest and is therefore also omitted. We now define the parameter

$$J_{ij} = -\int d^3\mathbf{x}\, w^*(\mathbf{x}-\mathbf{x}_i)\left[-\frac{\hbar^2}{2M}\nabla^2 + V_0\sum_{\nu=1}^{3}\sin^2(k_L x_\nu)\right] w(\mathbf{x}-\mathbf{x}_j) \quad . \tag{2.13}$$

Because of translational invariance and the fact that we only consider nearest-neighbor hopping, all J_{ij} are equal and we can drop the site indices. In the following, we will refer to J as the hopping matrix element. The interaction constants are defined by

$$U_{0,2} = c_{0,2}\int d^3\mathbf{x}\,|w(\mathbf{x}-\mathbf{x}_i)|^4 \quad . \tag{2.14}$$

We note that the interaction constants are directly proportional to the parameter $c_{0,2}$ defined in (2.5). That means that for $U_2 < 0$ we have a ferromagnetic and for $U_2 > 0$ an anti-ferromagnetic ground state. For ^{23}Na we find the ratio $U_2/U_0 = c_2/c_0 \approx +0.04$ [44]. In order to calculate J and $U_{0,2}$ from the experimental parameters V_0 and M, one needs to know the Wannier functions. They can either be calculated numerically or approximated by a Gaussian. The latter, also called the harmonic approximation, is widely used in literature but deviates quite strongly from the correct numerical result [23]. With (2.13) and (2.14) we obtain the Hamiltonian of the Bose-Hubbard Model for spin-1 Boson which reads

$$\hat{H} = \sum_i\Bigg[\frac{U_0}{2}\sum_{\alpha,\beta}\hat{a}^\dagger_{i\alpha}\hat{a}^\dagger_{i\beta}\hat{a}_{i\beta}\hat{a}_{i\alpha} + \frac{U_2}{2}\sum_{\alpha,\beta,\gamma,\delta}\hat{a}^\dagger_{i\alpha}\hat{a}^\dagger_{i\gamma}\mathbf{F}_{\alpha\beta}\cdot\mathbf{F}_{\gamma\delta}\hat{a}_{i\delta}\hat{a}_{i\beta} - \mu\sum_\alpha\hat{a}^\dagger_{i\alpha}\hat{a}_{i\alpha} - \eta\sum_{\alpha,\beta}\hat{a}^\dagger_{i\alpha}F^z_{\alpha\beta}\hat{a}_{i\beta}\Bigg] - J\sum_{<i,j>}\sum_\alpha\hat{a}^\dagger_{i\alpha}\hat{a}_{j\alpha} \quad , \tag{2.15}$$

where $\sum_{<i,j>}$ indicates the summation over all pairs of nearest neighbors. Defining the operators

$$\hat{n}_{i\alpha} = \hat{a}^\dagger_{i\alpha}\hat{a}_{i\alpha}\,, \quad \hat{n}_i = \sum_{i\alpha}\hat{n}_{i\alpha} \quad , \tag{2.16}$$

the spin-independent interaction term becomes $(U_0/2)\sum_i\hat{n}_i(\hat{n}_i-1)$. To simplify the spin-dependent interaction term, we rearrange

$$\sum_{\alpha,\beta,\gamma,\delta}\hat{a}^\dagger_{i\alpha}\hat{a}^\dagger_{i\gamma}\mathbf{F}_{\alpha\beta}\cdot\mathbf{F}_{\gamma\delta}\hat{a}_{i\delta}\hat{a}_{i\beta} = \sum_{\alpha,\beta,\gamma,\delta,\nu}(\hat{a}^\dagger_{i\alpha}F^\nu_{\alpha\beta}\hat{a}_{i\beta})(\hat{a}^\dagger_{i\gamma}F^\nu_{\alpha\delta}\hat{a}_{i\delta}) - \sum_{\alpha,\beta,\delta,\nu}F^\nu_{\alpha\beta}F^\nu_{\beta\delta}\hat{a}^\dagger_{i\alpha}\hat{a}_{i\delta} \quad . \tag{2.17}$$

Defining $\hat{\mathbf{S}}_i = \sum_{\alpha,\beta}\hat{a}^\dagger_{i\alpha}\mathbf{F}_{\alpha\beta}\hat{a}_{i\beta}$ and using $\mathbf{F}\cdot\mathbf{F} = 2$, Eq. (2.15) simplifies to [50]

$$\hat{H} = \sum_i\left[\frac{1}{2}U_0\hat{n}_i(\hat{n}_i-1) + \frac{1}{2}U_2(\hat{\mathbf{S}}_i^2 - 2\hat{n}_i) - \mu\hat{n}_i - \eta\hat{S}_i^z\right] - J\sum_\alpha\sum_{<i,j>}\hat{a}^\dagger_{i\alpha}\hat{a}_{j\alpha} \quad . \tag{2.18}$$

The reason why we have introduced the operator $\hat{\mathbf{S}}_i$ is the fact that it behaves like an angular momentum or spin operator. In order to see this, we first write down its components explicitly:

$$\begin{aligned}
\hat{S}_i^x &= \frac{1}{\sqrt{2}}(\hat{a}^\dagger_{i0}\hat{a}_{i1} + \hat{a}^\dagger_{i1}\hat{a}_{i0} + \hat{a}^\dagger_{i-1}\hat{a}_{i0} + \hat{a}^\dagger_{i0}\hat{a}_{i-1}) \quad , \\
\hat{S}_i^y &= \frac{1}{\sqrt{2}}(\hat{a}^\dagger_{i0}\hat{a}_{i1} - \hat{a}^\dagger_{i1}\hat{a}_{i0} + \hat{a}^\dagger_{i-1}\hat{a}_{i0} - \hat{a}^\dagger_{i0}\hat{a}_{i-1}) \quad , \\
\hat{S}_i^z &= \hat{a}^\dagger_{i1}\hat{a}_{i1} - \hat{a}^\dagger_{i-1}\hat{a}_{i-1} \quad .
\end{aligned} \tag{2.19}$$

The defining property of a spin operator is its commutator relation $[\hat{S}_j^\alpha, \hat{S}_k^\beta] = i\delta_{jk}\sum_\gamma \epsilon_{\alpha\beta\gamma}\hat{S}_j^\gamma$. It is easy to prove with the help of (2.10) and (2.19) that these relations are, indeed, fullfilled by our operator $\hat{\mathbf{S}}_i$. We also note that $\hat{\mathbf{S}}_i$, $\hat{S}_i^x$ and $\hat{n}_i$ commute with each other and therefore have common eigenstates which we will denote in complete analogy to the usual problems from atomic physics as $|S_i, m_i, n_i\rangle$ with $m_i = -S_i, -S_i+1, \ldots, S_i-1, S_i$. There is a restriction on the values of S_i which has interesting physical consequences worth to be discussed: If we add the two spins s_1 and s_2, the resulting total spin s can have all integer values from $|s_1 - s_2|$ to $s_1 + s_2$. Therefore we must have $S_i \leq n_i$. If $n_i = 1$, we must of course have $S_i = 1$. But because of the Bosonic nature of the system, S_i must be even if n_i is even and odd if n_i is odd. Therefore, sites with odd n_i can not be in a spin singlet state, a fact which will have interesting and important consequences later on. The eigenvalue equations, which define these states $|S_i, m_i, n_i\rangle$, are

$$\begin{aligned}
\hat{\mathbf{S}}_i^2|S_i, m_i, n_i\rangle &= S_i(S_i+1)|S_i, m_i, n_i\rangle \quad , \\
\hat{S}_i^z|S_i, m_i, n_i\rangle &= m_i|S_i, m_i, n_i\rangle \quad , \\
\hat{n}_i|S_i, m_i, n_i\rangle &= n_i|S_i, m_i, n_i\rangle \quad .
\end{aligned} \tag{2.20}$$

Furthermore, the states $|S_i, m_i, n_i\rangle$ are orthonormal, i.e.

$$\langle S_i, m_i, n_i|S_i', m_i', n_i'\rangle = \delta_{S_i,S_i'}\delta_{m_i,m_i'}\delta_{n_i,n_i'} \quad . \tag{2.21}$$

The eigenvalue equations (2.20) allow us solve the Hamiltonian (2.18) in the limit $J = 0$ exactly which is discussed in the next Chapter.

Chapter 3

Mott Insulator-Superfluid Transition

In this chapter, we discuss the behavior of a spin-1 system, which is described by the Bose-Hubbard model, at first place for $T = 0$ and later on for finite temperature. In the former case, we have three relevant energies describing the system, i.e. the spin-independent and spin-dependent on-site interaction energies U_0 and U_2 and, furthermore, the hopping energy J. As this is the situation of experimental relevance (see Fig. 2.3), we will focus in the following on the situation $U_0 \gg |U_2|$. If the spin-independent interaction energy U_0 dominates, the particles will be localized on the lattice sites in order to minimize the repulsive energy. This state is called a Mott insulator. If the kinetic term J, which corresponds to the hopping process, becomes important, the particles tend to delocalize and form a superfluid. An important difference between these two phases can be seen in their respective excitation spectrum. In the Mott-insulator phase, the spectrum is gapped, which can be easily understood for the following reason: If all Bosons are localized, it requires a finite energy to move a particle from one lattice site to another. In the limit $J \to 0$, this energy is just the interaction energy U_0. If a delocalized superfluid is present, the spectrum is gapless and long wavelength excitations with arbitrary low energy are possible. In the case of the system discussed here, the presence of an additional spin-dependent interaction will lead to interesting new effects in the case of an anti-ferromagnetic interaction. Although it is very weak, i.e. $U_2 \ll U_0$, the phase diagram will be affected in a qualitative way because of the formation of stabilized hyperfine spin singlet pairs. Another possible excitation in a spinor system is to flip one spin which is also gapped in the Mott phase with the energy scale of the gap given by U_2.
When temperature enters the situation, there exists a fourth relevant energy which is the mean thermal energy $k_B T$. Therefore, we examine in this chapter also how thermal fluctuations affect the quantum phase diagram. In the rest of this thesis we will, for reasons of convenience, always use units with $\hbar = k_B = 1$.

3.1 Thermodynamics

In this section, we briefly review thermodynamics as far as it is needed for our present discussion. Because it is much simpler, we will work throughout all this thesis in the grand-canonical ensemble. The thermodynamic potential used in this formalism is the grand-canonical free energy $\mathcal{F}$. It is connected to the inner energy U via

$$\mathcal{F} = U - TS - \mu N \quad , \tag{3.1}$$

where μ is the chemical potential [51]. Its physical meaning is the following: In the grand-canonical ensemble, there is a heat bath around the system, exactly like in the canonical ensemble. Additionally, the system is also coupled to a particle bath. The chemical potential μ is the energy needed to add

a particle from the particle bath to the system. For this reason, we have already included the term $-\mu N$ in the definition of our Hamiltonian (2.3). From (3.1) we can see that the total particle number N is given by

$$N = -\frac{\partial \mathcal{F}}{\partial \mu} \quad , \tag{3.2}$$

which provides a relation between the chemical potential μ and the mean particle number N. This allows us to fix the average particle number N by tuning μ. When we now take the limit $T \to 0$ of (3.2) and use the fact that the inner energy becomes the ground state energy, i.e. $U \overset{T\to 0}{\longrightarrow} E_{\mathrm{G}}$, we obtain from Eq. (3.1):

$$N = -\frac{\partial E_{\mathrm{G}}}{\partial \mu} \quad . \tag{3.3}$$

Motivated by the idea of a variable particle number and a chemical potential, we extend our grand-canonical approach even more by putting some kind of "magnetization bath" around our system. This is achieved by changing

$$\mathcal{F} \to \mathcal{F} - \eta M \quad , \tag{3.4}$$

which we have also already done when defining our Hamiltonian (2.3). In analogy to the meaning of μ, the parameter η is the energy needed to change the magnetization of the system by one. For this reason we shall call η the "magneto-chemical potential" [16]. From (3.4) we obtain

$$M = -\frac{\partial \mathcal{F}}{\partial \eta} \quad , \tag{3.5}$$

which reduces in the zero-temperature limit to

$$M = -\frac{\partial E_{\mathrm{G}}}{\partial \eta} \quad . \tag{3.6}$$

There is one notable difference between the chemical and the magneto-chemical potential. The former has no experimental realization, at least not in the homogeneous system which we consider here. This means that there is no knob we can turn to change μ. But for the latter we do have this knob. It is an external magnetic field, and in this situation η corresponds to the Zeeman splitting between two states differing by $\Delta m_F = 1$. This interpretation of η was used in Refs. [43, 52–54]. We will switch between those two different interpretations of η whenever it becomes necessary.
The thermal average of an arbitrary operator can be calculated as

$$\langle \hat{O} \rangle = \frac{1}{\mathcal{Z}} \mathrm{Tr}\{\hat{O} e^{-\beta \hat{H}}\} \quad , \tag{3.7}$$

where $\beta = 1/T$ is the inverse temperature. The grand-canonical partition function occurring in (3.7) reads

$$\mathcal{Z} = \mathrm{Tr}\{e^{-\beta \hat{H}}\} \quad . \tag{3.8}$$

There is an important connection between the grand-canonical free energy and the partition function which reads

$$\mathcal{F} = -\frac{1}{\beta} \log \mathcal{Z} \quad . \tag{3.9}$$

This allows to calculate N and M also from thermal averages. From (3.2), (3.8), and (3.9) we conclude

$$N = -\frac{\partial \mathcal{F}}{\partial \mu} = \frac{1}{\beta} \frac{\partial}{\partial \mu} \log \mathcal{Z} = \frac{1}{\beta \mathcal{Z}} \frac{\partial}{\partial \mu} \mathcal{Z} = \frac{N_S}{\mathcal{Z}} \mathrm{Tr}\{\hat{n} e^{-\beta \hat{H}}\} = N_S \langle \hat{n} \rangle \quad , \tag{3.10}$$

where $\hat{n}$ is the operator of the particle number *per site* and N_S the number of lattice sites. The calculation for M is exactly analogous and yields $M = N_S \langle \hat{S}^z \rangle$.

3.2 System Properties Without Hopping

Before considering the effects arising from hopping, we first have a look at the system in the absence of tunneling, i.e. for $J = 0$. This corresponds to a situation with infinite high potential walls between the lattice sites. For this situation, the Bose-Hubbard Hamiltonian (2.18) reduces to

$$\hat{\tilde{H}}_0 = \sum_i \left[\frac{1}{2} U_0 \hat{n}_i (\hat{n}_i - 1) + \frac{1}{2} U_2 (\hat{\mathbf{S}}_i^2 - 2\hat{n}_i) - \mu \hat{n}_i - \eta \hat{S}_i^z \right] \quad . \tag{3.11}$$

Because all sites are equivalent, we can drop the sum as well as the site index i and consider only the local Hamiltonian

$$\hat{H}_0 = \frac{1}{2} U_0 \hat{n}(\hat{n} - 1) + \frac{1}{2} U_2 (\hat{\mathbf{S}}^2 - 2\hat{n}) - \mu \hat{n} - \eta \hat{S}^z \quad . \tag{3.12}$$

We now determine the eigenstates and eigenvalues of this Hamiltonian. We know from Section 2.3 that $\hat{n}$, $\hat{\mathbf{S}}^2$, and $\hat{S}^z$ commutes and, therefore, we choose eigenstates of these three operators as a basis of the Hilbert space as already discussed above. The respective eigenvalues are given by Eq. (2.20). Thus, the eigenstates of the Hamiltonian (3.12) are

$$\hat{H}_0 |S, M, n\rangle = E_{S,m,n} |S, m, n\rangle \tag{3.13}$$

with the eigenvalues

$$E_{S,m,n} = \frac{1}{2} U_0 n(n-1) + \frac{1}{2} U_2 \left[S(S+1) - 2n \right] - \mu n - \eta m \quad . \tag{3.14}$$

3.2.1 Unmagnetized Systen at Zero Temperature

Because it is an interesting special case we will focus at first place on the case of a non-magnetized system, which corresponds to $\eta = 0$, and discuss later on modifications which occur when considering $\eta \neq 0$. In the former case, the eigenenergies (3.14) do not depend on the magnetic quantum number m, and therefore all eigenstates are $(2S + 1)$–fold degenerated. The nature of the ground state of the system crucially depends on the sign of U_2. An anti-ferromagnetic interaction is characterized by $U_2 > 0$, thus, in order to minimize the ground-state energy, S must be minimal according to (3.14). Therefore, the ground state is $|0, 0, n\rangle$ for even n and $|1, m, n\rangle$ with $m = 0, \pm 1$ for odd n.
Correspondingly, a ferromagnetic interaction is present for $U_2 < 0$, so S must be maximal in this case. This is realized by the state $|n, m, n\rangle$ with $m = -n, \ldots, n$ irrespectively of n being even or odd. In order to obtain a relation between the chemical potential μ and the particle number n, we consider the cases of even and odd n separately, but restrict ourselves to the anti-ferromagnetic case. If n is even we have $E_{1,n-1} < E_{0,n} < E_{1,n+1}$ and we conclude

$$(n-1)U_2 - 2U_2 \leq \mu \leq n\, U_0 \quad . \tag{3.15}$$

In the opposite case that n is odd, we have $E_{0,n-1} < E_{1,n} < E_{0,n+1}$, which leads to

$$(n-1)U_0 \leq \mu \leq nU_0 - 2U_2 \quad . \tag{3.16}$$

Note that (3.16) implies for anti-ferromagnetic interaction that there are no states with odd n when $U_2 > U_0/2$. Together, the two inequalities (3.15) and (3.16) allow us to plot the equation of state $n = n(\mu)$ as done in Fig. 3.1. The dependence of S on the chemical potential follows directly from the result for n because $S = 0$ for even and $S = 1$ for odd n.

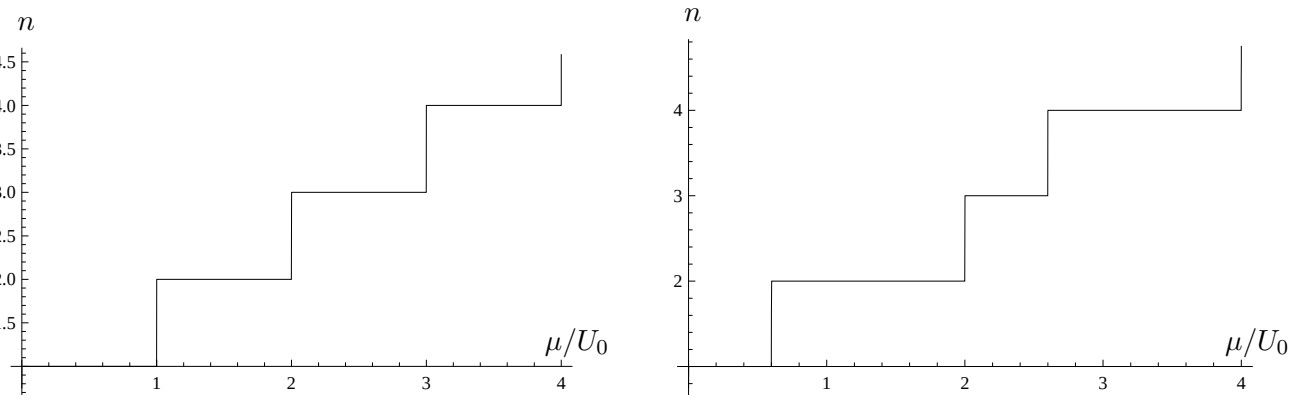

Figure 3.1: Dependence of the particle number per site on the chemical potential for the unmagnetized system at zero temperature. Left: $U_2 = 0$. Right: $U_2 = 0.2\,U_0$.

3.2.2 Unmagnetized System at Finite Temperature

In this subsection, we calculate at first place the mean particle number in dependence of the chemical potential for finite temperature. To perform this calculation, we use the known eigenstates of (3.12) as a base of the Hilbert space. Therefore, the partition function (3.8) reduces to

$$\mathcal{Z}^{(0)} = \sum_{n=0}^{\infty} \sum_{S} (2S+1) e^{-\beta E_{S,n}} \quad , \tag{3.17}$$

where the factor $2S+1$ accounts for the degeneracy with respect to the magnetic quantum number m and we have to keep in mind that S must be even (odd) when n is even (odd). We calculate the resulting thermal expectation value of the particle number per site according to (3.7)

$$\langle \hat{n} \rangle = \frac{\sum_{n,S} (2S+1) n\, e^{-\beta E_{S,n}}}{\sum_{n,S} (2S+1) e^{-\beta E_{S,n}}} \quad , \tag{3.18}$$

and also the total spin per site

$$\sqrt{\langle \hat{\mathbf{S}}^2 \rangle} = \sqrt{\frac{\sum_{n,S} (2S+1) S(S+1) e^{-\beta E_{S,n}}}{\sum_{n,S} (2S+1) e^{-\beta E_{S,n}}}} \quad . \tag{3.19}$$

When we plot the particle number per site against the chemical potential (see Fig. 3.2), we can clearly see that for an anti-ferromagnetic interaction, i.e. $U_2 > 0$, states with an even number of particles are favored. For ferromagnetic interaction, i.e. $U_2 < 0$, no even-odd dependence exists. This all agrees with the previously discussed case of $T = 0$. We note, furthermore, that the thermal fluctuation smooth out the respective curve, which was a step-function for $T = 0$ (see Fig. 3.2), and the equation of state $\langle \hat{n} \rangle = \langle \hat{n} \rangle(\mu)$ becomes a continuous, bijective function. In Fig. 3.3 (right), where the total spin per site is plotted, one can see that for low temperature this quantity is approximately zero in the regions which correspond to an even particle number per site and approximately one for odd particle number. This is expected as the respective zero-temperature ground state (2.20) is $|0, 0, n\rangle$ for the former and $|1, m, n\rangle$, $m = 0, \pm 1$ for the latter case. For larger temperature this even-odd dependence gets weaker. This effect is important also for the phase-boundary and will be explained in detail later on.

To get the zero temperature limit $\beta \to \infty$, we notice that, for large β, the main contribution to the sum in (3.18) results from the term with the smallest energy in the exponential function. In order to

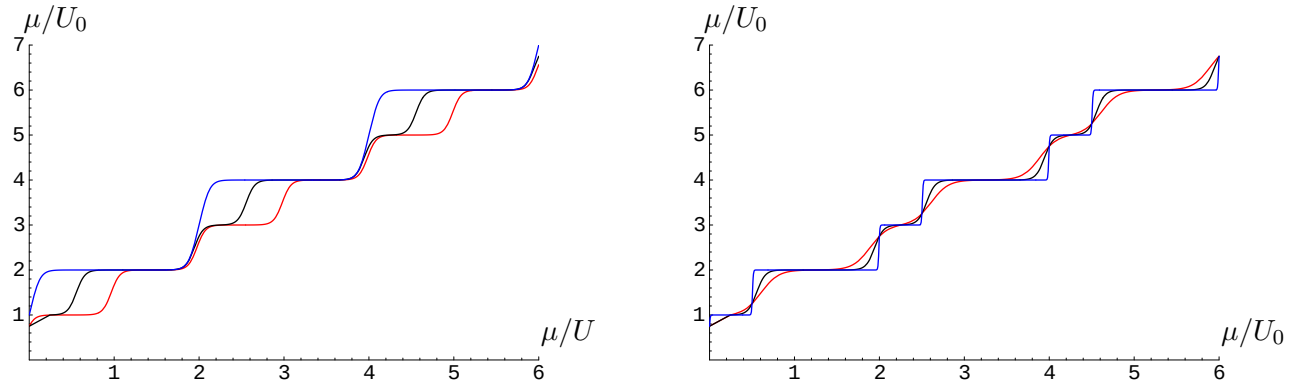

Figure 3.2: Dependence of the particle number per site on the chemical potential for the unmagnetized system, i.e. $\eta = 0$. Left: $k_BT/U_0 = 0.05$ and $U_2/U_0 = 0$ (red), $U_2/U_0 = 0.25$ (black), and $U_2/U_0 = 0.5$ (blue). Right: $U_2/U_0 = 0.25$ and $k_BT/U_0 = 0.1$ (red), $k_BT/U_0 = 0.05$ (black), and $k_BT/U_0 = 0.005$ (blue).

see this, we write (3.18) as

$$\langle \hat{n} \rangle = \frac{n_0(2S_0+1)e^{-\beta E_{S_0,n_0}}[1+\sum_{n,S}' n(2S+1)e^{-\beta(E_{S,n}-E_{S_0,n_0})}]}{(2S_0+1)e^{-\beta E_{S_0,n_0}}[1+\sum_{n,S}'(2S+1)e^{-\beta(E_{S,n}-E_{S_0,n_0})}]} \quad , \tag{3.20}$$

where n_0 and S_0 minimize the ground state energy E_{G} for a given chemical potential, and the prime on the sum denotes summation over all states but the ground state. Note that then $E_{S,n} - E_{S_0,n_0} > 0$ holds and, therefore, these terms vanish when β tends to infinity. This gives us the result

$$\langle \hat{n} \rangle \overset{T\to 0}{\longrightarrow} n_0 \tag{3.21}$$

for the particle number per site at $T = 0$. The same argument also holds for the total spin per site S.

3.2.3 Magnetized Bose Gas

Until now, we have considered a system with no magnetization where all states with the same total spin quantum number S are degenerated with respect to their magnetic quantum number m. When a finite magnetization exists, this degeneracy is lifted and the lowest energy state for given n and S is $|S, S, n\rangle$. We now consider the effect of the additional parameter η on the system properties. For a ferromagnetic interaction there is nothing interesting happening because the ground state is the state with maximal S for a given n as it is in the case without η which can be seen from Eq. (3.14). The only thing which changes is that, as discussed above, the degeneracy with respect to m is lifted, so the ground state becomes

$$E_{\mathrm{G}} = |n, n, n\rangle \quad . \tag{3.22}$$

For an anti-ferromagnetic interaction, things are more complicated. When η is large compared to U_2, it is energetically favorable to align all spins in the z-direction and, therefore, the ground state is a high spin state again. When η is small against U_2, the minimal energy is realized by pairing as many spins as possible, which leads to the ground state $|0, 0, n\rangle$ for even, and $|1, 1, n\rangle$ for odd n. We already note that, when we apply perturbation theory later on, the limit $\eta \to 0$ turns out to be non-trivial. The reason for that is that, for $\eta = 0$, the ground state for odd particle numbers per site is threefold degenerated and one has to use the degenerated perturbation theory which leads to different results. When η and U_2 are of the same order of magnitude, ground states with all allowed spin quantum

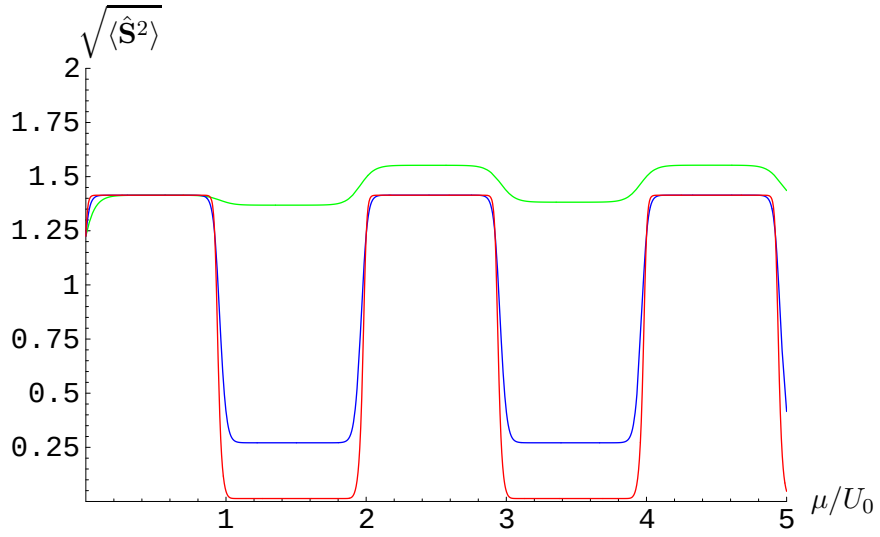

Figure 3.3: Dependence of the total spin per site on the chemical potential for the unmagnetized system, i.e. $\eta = 0$. $U_2/U_0 = 0.04$. $k_BT/U_0 = 0.01$ (red), $k_BT/U_0 = 0.02$ (blue), and $k_BT/U_0 = 0.05$ (green)

numbers between 0 and n are possible. To find the realized one, it is necessary to minimize $E_{S,S,n}$ for given parameters μ and η.
There is another special case where one has to be careful with degeneracies. This happens when the energies of two states with equal particle number but different total spins become equal. In order to find the corresponding values of η we set

$$E_{S,S,n} = E_{S+2,S+2,n} \quad . \tag{3.23}$$

Inserting (3.14) into (3.23) yields

$$\frac{\eta}{U_2} = S + \frac{3}{2} \quad . \tag{3.24}$$

At this critical η, which, of course, corresponds to a critical magnetization, we, therefore, expect some effect arising from the degeneracy of the states with the same particle number but different spin. This means, that spin flips are possible which do not cost any energy. Thus, we see that even in the limit of an infinitely deep lattice we have gapless excitations. We must, therefore, make the definition of a Mott insulator more precise and demand only that the particle and hole excitations, which move particles from one site to another, should have a gap.
For finite temperature, one can calculate the thermal averages of $\hat{S}^z$ and $\hat{n}$ according to (3.7) as

$$M = \langle \hat{S}^z \rangle = \frac{1}{\mathcal{Z}^{(0)}} \sum_{n=0}^{\infty} \sum_{S} \sum_{m=-S}^{S} m\, e^{-\beta E_{S,m,n}} \quad , \tag{3.25}$$

$$\langle \hat{n} \rangle = \frac{1}{\mathcal{Z}^{(0)}} \sum_{n=0}^{\infty} \sum_{S} \sum_{m=-S}^{S} n\, e^{-\beta E_{S,m,n}} \quad , \tag{3.26}$$

where the partition function (3.8) is given by

$$\mathcal{Z}^{(0)} = \sum_{n=0}^{\infty} \sum_{S} \sum_{m=-S}^{S} e^{-\beta E_{S,m,n}} \quad . \tag{3.27}$$

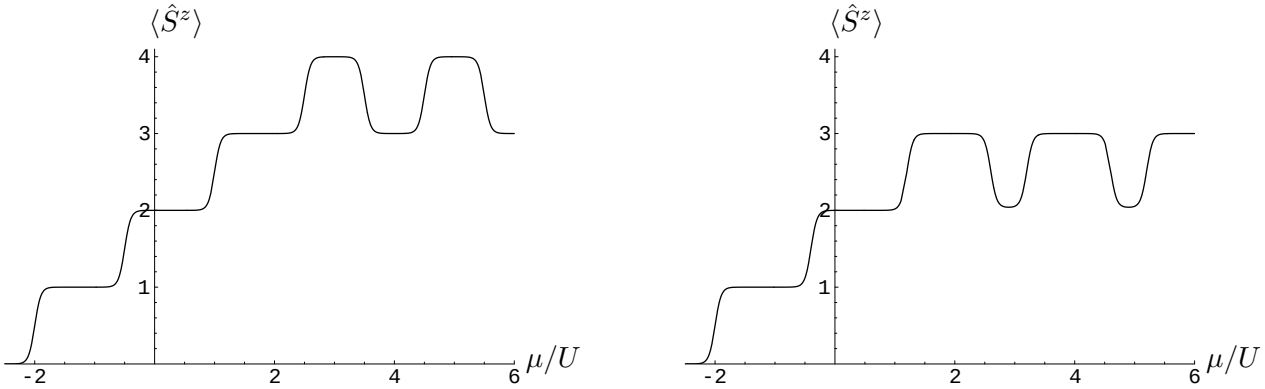

Figure 3.4: Dependence of the magnetization per site on the chemical potential for $k_BT/U_0 = 0.05$ and $\eta/U_0 = 2$. Left: $U_2/U_0 = 0.5$. Right: $U_2/U_0 = 0.6$.

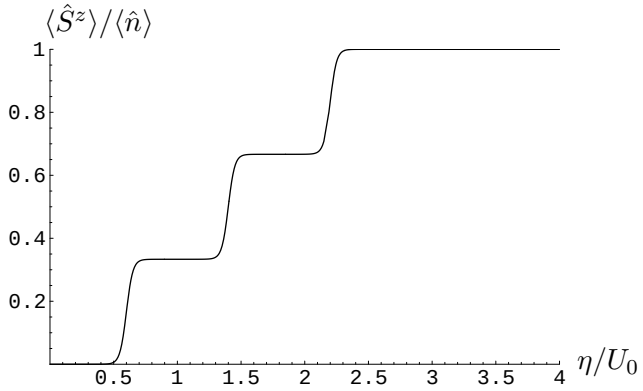

Figure 3.5: Dependence of the magnetization per particle on the magneto-chemical potential for $k_BT/U_0 = 0.05$, $\mu/U_0 = 5$, and $U_2/U_0 = 0.4$.

One can see in Fig. 3.4 that small changes in the spin-dependent interaction strength U_2 change the magnetic behavior in a qualitative way, while they change the mean particle number only quantitatively (see Fig. 3.2). We have also plotted the magnetization per particle against the magneto-chemical potential for a fixed μ in Fig. 3.5. Here one can see how η must be chosen to get the desired magnetization. The zero-temperature limit follows exactly as discussed in Subsection 3.2.2.

3.3 Mean-Field Hamiltonian

In this section, we introduce a crucial approximation to the hopping part of the Hamiltonian (2.18) which allows us to introduce a quantity which describes the collective behavior of the delocalized Bosons forming the superfluid.

3.3.1 Decoupling of Hopping Term

When we consider the Bose-Hubbard model in the strong-coupling limit, i.e. $J = 0$, we see that the unperturbed Hamiltonian (3.12) is local while the perturbation

$$\hat{H}_1 = -J \sum_{<i,j,>} \sum_{\alpha} \hat{a}^\dagger_{i\alpha} \hat{a}_{j\alpha} \tag{3.28}$$

is non-local which means that it couples different lattice sites. To simplify this term and to introduce an order parameter in view of the Landau theory [55,56], we decompose the creation and annihilation operators into their expectation values and fluctuations around them:

$$\hat{a}_{i\alpha} = \langle \hat{a}_{i\alpha} \rangle + \delta\hat{a}_{i\alpha} \quad , \qquad \hat{a}^\dagger_{i\alpha} = \langle \hat{a}^\dagger_{i\alpha} \rangle + \delta\hat{a}^\dagger_{i\alpha} \quad . \tag{3.29}$$

Rearranging (3.29) yields

$$\delta\hat{a}^\dagger_{i\alpha}\delta\hat{a}_{j\alpha} = \hat{a}^\dagger_{i\alpha}\hat{a}_{j\alpha} - \langle \hat{a}^\dagger_{i\alpha} \rangle \langle \hat{a}_{j\alpha} \rangle - \langle \hat{a}^\dagger_{i\alpha} \rangle \delta\hat{a}_{j\alpha} + \langle \hat{a}_{j\alpha} \rangle \delta\hat{a}^\dagger_{i\alpha} \quad . \tag{3.30}$$

We now assume the fluctuations to be small and, therefore, neglect the term which is quadratic in them, i.e. the one on the left-hand side in (3.30). This is known as the mean-field approximation. We also remember that our system is translationally invariant, so the expectation value of the operators must not depend on the site index i. Because of that, we can introduce the order parameters

$$\Psi_\alpha = \langle \hat{a}_{i\alpha} \rangle \quad , \qquad \Psi^*_\alpha = \langle \hat{a}^\dagger_{i\alpha} \rangle \tag{3.31}$$

and get from (3.30)

$$\hat{a}^\dagger_{i\alpha}\hat{a}_{j\alpha} \approx \Psi_\alpha \hat{a}^\dagger_{i\alpha} + \Psi^*_\alpha \hat{a}_{j\alpha} - \Psi^*_\alpha \Psi_\alpha \quad . \tag{3.32}$$

When we now insert this mean-field approximation into (2.18) and perform the summation over j, we get the Bose-Hubbard mean-field Hamiltonian

$$\hat{H}_{\mathrm{MF}} = N_S \hat{H}_0 - Jz \sum_i \sum_\alpha (\Psi_\alpha \hat{a}^\dagger_{i\alpha} + \Psi^*_\alpha \hat{a}_{i\alpha} - \Psi^*_\alpha \Psi_\alpha) \quad , \tag{3.33}$$

where $z = 2D$ is the number of nearest neighbors in the D-dimensional cubic lattice. As the mean-field Hamiltonian (3.33) is local, we can drop again drop the index i and the sum over it and consider an effective one-site problem.

3.3.2 Perturbation Theory

In order to be able to apply perturbation theory, we must know how the one-site mean-field perturbation Hamiltonian

$$\hat{H}_{\mathrm{1MF}} = -Jz \sum_\alpha (\Psi_\alpha \hat{a}^\dagger_\alpha + \Psi^*_\alpha \hat{a}_\alpha - \Psi^*_\alpha \Psi_\alpha) \tag{3.34}$$

acts on an eigenstate of the unperturbed Hamiltonian (3.12). Because the components of the order parameter Ψ_α, Ψ^*_α are c-numbers and not operators, this boils down to the calculation of $\hat{a}^\dagger_\alpha |S,m,n\rangle$ and $\hat{a}_\alpha |S,m,n\rangle$. For doing this, it is useful to recall what the creation and annihilation operators do in a physical sense. The creator $\hat{a}^\dagger_\alpha$ creates a spin-1 particle with its spin orientation specified by α. Because the z-component of the magnetic moment and, therefore, also of the spin is conserved, we have $\hat{a}^\dagger_\alpha |S,m,n\rangle \propto |S \pm 1, m+\alpha, n+1\rangle$. The quantum number of the total spin changes by ± 1 because one spin-1 particle is added. Correspondingly, $\hat{a}_\alpha$ annihilates a spin-1 particle. Therefore, we have $\hat{a}_\alpha |S,m,n\rangle \propto |S \pm 1, m-\alpha, n-1\rangle$. Thus, the results can be written in the following form:

$$\hat{a}^\dagger_\alpha |S,m,n\rangle = M_{\alpha,S,m,n} |S+1, m+\alpha, n+1\rangle + N_{\alpha,S,m,n} |S-1, m+\alpha, n+1\rangle \quad , \tag{3.35}$$

$$\hat{a}_\alpha |S,m,n\rangle = O_{\alpha,S,m,n} |S+1, m-\alpha, n-1\rangle + P_{\alpha,S,m,n} |S-1, m-1, n-1\rangle \quad , \tag{3.36}$$

where the respective coefficients M, N, O, and P are calculated recursively in detail in Appendix A.

3.4 Phase Diagram at Zero Temperature

The aim of this section is to calculate the phase boundary for the transition between a Mott insulator and a superfluid phase at zero temperature. We stress again that this is a pure quantum effect which is driven by *quantum* fluctuations in contrary to thermal phase transitions, like the melting of a crystal, which are driven by *thermal* fluctuations. This is the reason why it is called a quantum phase transition [6].

3.4.1 Landau Expansion

For the calculation of the phase diagram we use the Landau theory of phase transitions [4, 55]. In order to do this, we need an order parameter which is zero in one phase, i.e. the non-ordered phase, and finite in the other one, i.e. the ordered phase. In (3.31), we have introduced three complex order parameters Ψ_α, which can be combined to a complex vector

$$\mathbf{\Psi} = (\Psi_{-1}, \Psi_0, \Psi_1) \quad . \tag{3.37}$$

The quantity $\mathbf{\Psi}$ is a good choice for describing the Mott-insulator superfluid phase transition, because a non-zero $\mathbf{\Psi}$ means that there are particles which do not belong to one particular site but are delocalized over the whole system and form a superfluid. We keep in mind that our order parameter has three components because of the three different hyperfine states $m = 0, \pm 1$. We now write the energy of the system as a function of the order parameter and look for the minimum. Therefore, we expand the ground state energy E_G in powers of $\mathbf{\Psi}$ up to quadratic order and obtain

$$E_\mathrm{G}(\mathbf{\Psi}) = A^{(0)} + \mathbf{A}^{(1)} \cdot \mathbf{\Psi} + \sum_\alpha A^{(2)}_\alpha |\Psi_\alpha|^2 + \mathcal{O}(\mathbf{\Psi}^4) \quad . \tag{3.38}$$

We will see later on that there is no contribution to the energy which is linear in $\mathbf{\Psi}$, so the leading contribution is of the order $\mathbf{\Psi}^2$. To find the phase boundary, we set $A^{(2)}_\alpha = 0$ because a change of the sign of this coefficient means that the minimum of the energy shifts from zero to a finite value of the order parameter as it can bee seen in Fig. 3.6 (left). We work with a magnetized system as described in Subsection 3.2.3 and discuss the difficulties of the non-magnetized limit $\eta \to 0$ later on. We calculate the energy shifts to the eigenvalues (3.14) of the unperturbed Hamiltonian (3.12). Because many different ground states are possible as discussed in Subsection 3.2.3, we do this for the general state $\Phi_0 = |S, S, n\rangle$. We consider the mean-field hopping term (3.34) as a perturbation.
In order to get the first-order correction in $\hat{H}_\mathrm{1MF}$, we use the orthonormality of our basis states (2.21) and obtain

$$E^{(1)}_{S,S,n} = \langle S, S, n | \hat{H}_\mathrm{1MF} | S, S, n \rangle = Jz \sum_\alpha \Psi^*_\alpha \Psi_\alpha \quad . \tag{3.39}$$

The second-order corrections read with the abbreviation $\sum_{\phi'} = \sum_{(S',m',n') \neq (S,S,n)}$

$$E^{(2)}_{S,S,n} = \sum_{\phi'} \frac{|\langle S', m', n' | \hat{H}_\mathrm{1MF} | S, S, n \rangle|^2}{E_{S',m',n'} - E_{S,S,n}} = J^2 z^2 \sum_\alpha \sum_{\phi'} \frac{|\langle S', m', n' | \Psi_\alpha \hat{a}^\dagger_\alpha + \Psi^*_\alpha \hat{a}_\alpha | S, S, n \rangle|^2}{E_{S',m',n'} - E_{S,S,n}} + \dots \quad . \tag{3.40}$$

Using now (3.35) and (3.36), one can see that for every spin component all but four terms of the sum vanish. This leads to

$$E^{(2)}_{S,S,n} = J^2 z^2 \sum_\alpha \Psi^*_\alpha \Psi_\alpha \left(\frac{M^2_{\alpha,S,S,n}}{E_{S+1,S+\alpha,n+1} - E_{S,S,n}} + \frac{N^2_{\alpha,S,S,n}}{E_{S-1,S+\alpha,n+1} - E_{S,S,n}} + \frac{O^2_{\alpha,S,S,n}}{E_{S+1,S-\alpha,n-1} - E_{S,S,n}} + \frac{P^2_{\alpha,S,S,n}}{E_{S-1,S-\alpha,n-1} - E_{S,S,n}} \right) + \dots \quad . \tag{3.41}$$

Thus, we see that there are two contributions to the second order in $\mathbf{\Psi}$. Putting them together yields

$$E_{\mathrm{G}} = E_{S,S,n} + \sum_{\alpha} A^{(2)}_{\alpha,S,S,n} |\Psi_\alpha|^2 + \mathcal{O}(\mathbf{\Psi^4}) \quad , \tag{3.42}$$

where the coefficients are given by

$$A^{(2)}_{\alpha,S,S,n} = Jz - J^2 z^2 \Bigg(\frac{M^2_{\alpha,S,S,n}}{E_{S+1,S+\alpha,n+1} - E_{S,S,n}} + \frac{N^2_{\alpha,S,S,n}}{E_{S-1,S+\alpha,n+1} - E_{S,S,n}} + \frac{O^2_{\alpha,S,S,n}}{E_{S+1,S-\alpha,n-1} - E_{S,S,n}} + \frac{P^2_{\alpha,S,S,n}}{E_{S-1,S-\alpha,n-1} - E_{S,S,n}} \Bigg) \tag{3.43}$$

and we have used that the third order vanishes for symmetry reasons. When the first of the three coefficients (3.43) vanishes, the ground state of the system (3.42) changes from a state with $\mathbf{\Psi} = \mathbf{0}$ to one where one component Ψ_α is non-zero. From this, one can also see which of the three hyperfine spin components is populated first in the respective superfluid phase. In order to be able to plot a phase diagram we set

$$A^{(2)}_{\alpha,S,S,n} \stackrel{!}{=} 0 \quad . \tag{3.44}$$

The critical hopping parameter for the transition to a superfluid with a specified spin α reads

$$zJ_{c,\alpha}(\mu) = \Bigg(\frac{M^2_{\alpha,S,S,n}}{E_{S+1,S+\alpha,n+1} - E_{S,S,n}} + \frac{N^2_{\alpha,S,S,n}}{E_{S-1,S+\alpha,n+1} - E_{S,S,n}} + \frac{O^2_{\alpha,S,S,n}}{E_{S+1,S-\alpha,n-1} - E_{S,S,n}} + \frac{P^2_{\alpha,S,S,n}}{E_{S-1,S-\alpha,n-1} - E_{S,S,n}} \Bigg)^{-1} \quad . \tag{3.45}$$

To find the transition, which is realized for the given parameters, one has to look for the minimum of (3.45) with respect to the spin index α:

$$zJ_c(\mu) = \min_{\alpha} \, zJ_{c,\alpha}(\mu) \quad . \tag{3.46}$$

Note that our theory can only describe the transition from a Mott insulator to a superfluid. It is not capable to describe the transition between different phases within the superfluid which differ in the occupation of the three spin states. Therefore, it is not reasonable to interpret (3.46) for different α but one should consider only the minimum (3.46) as we have done.

For any finite η, the phase boundary always describes a transition to a superfluid with $\Psi_1 \neq 0$ or $\Psi_{-1} \neq 0$. We have calculated these phase boundaries for $U_2/U_0 = 0.04$ which is the value realized in ^{23}Na and plotted them in Fig. 3.7. In order to resolve the kinks in the phase boundary better, we consider a situation where the anti-ferromagnetic interaction is much stronger, i.e. $U_2/U_0 = 0.5$, and also the magneto-chemical potential is larger. The phase boundary corresponding to this situation is shown in Fig. 3.8. It is not realized in the commonly used alkali-metal gases but it is known that the scattering length and, therefore, also the interaction strength can be changed by using Feshbach resonances [57]. The origin of the kinks in the phase boundary is the fact that the transition changes qualitatively at this point between a superfluid phase with $\Psi_1 \neq 0$ and a corresponding one with $\Psi_{-1} \neq 0$. Thus, we have a tricritical point where three phases coincide. The reason for this behavior, which was also found in Ref. [50], is the following: Normally, we would expect, that the spin-component, which is aligned parallel to the magnetic field η, makes the transition to the superfluid phase first, i.e. for the lowest values of the hopping parameter J, because its energy is lowest. But when the chemical potential has a certain value, the energy gained is large when relaxing the condition that the spins per site S must

be odd for an odd particle number per site n. Then it is energetically favorable for the component aligned anti-parallel to the quantization axis to form a superfluid. Note also that the ground state of the second lobe in Fig. 3.8 is $|2,2,2\rangle$ and not the also allowed $|0,0,2\rangle$.
Now we describe the situation which is realized in experiments with a magnetic trap. As already discussed in the introduction, magnetic traps can capture only one hyperfine spin component. Therefore the situation to be considered is the limit of a fully polarized gas. As discussed in Subsection 3.2.3, the ground state for this situation is $|n,n,n\rangle$. We read off the needed coefficients from Appendix A.1:

$$M_{1,n,n,n} = \sqrt{n+1} \quad , \qquad M_{0,n,n,n} = 1 \quad , \tag{3.47}$$

$$M_{-1,n,n,n} = \sqrt{\frac{1}{2n+1}} \quad , \qquad N_{1,n,n,n} = 0 \quad , \tag{3.48}$$

$$N_{0,n,n,n} = 0 \quad , \qquad N_{-1,n,n,n} = -\sqrt{\frac{2n}{2n+1}} \quad , \tag{3.49}$$

$$O_{\alpha,n,n,n} = 0 \quad , \quad \text{for all } \alpha \quad , \qquad P_{1,n,n,n} = \sqrt{n} \quad , \tag{3.50}$$

$$P_{0,n,n,n} = 0 \quad , \qquad P_{-1,n,n,n} = 0 \quad . \tag{3.51}$$

When we now plug these coefficients into (3.45) and use (3.14), we find

$$zJ_{c,1} = \left[\frac{n+1}{n(U_0+U_2)-(\eta+\mu)} + \frac{n}{(1-n)(U_2+U_0)+(\eta+\mu)} \right]^{-1} \quad . \tag{3.52}$$

When one does the same for $zJ_{c,0}$ and $zJ_{c,-1}$ one can see that both are always larger than $zJ_{c,1}$. Therefore we have $zJ_c = zJ_{c,1}$.We simplify further by defining a new interaction strength by

$$U = U_0 + U_2 \quad . \tag{3.53}$$

Furthermore, we can remove the magneto-chemical potential, which is no more needed in the fully polarized gas, by redefining the chemical potential according to

$$\mu + \eta \to \mu \quad . \tag{3.54}$$

Inserting (3.53) and (3.54) into (3.52) yields finally

$$zJ_c = \left[\frac{n+1}{nU-\mu} + \frac{n}{(1-n)U+\mu} \right]^{-1} \quad , \tag{3.55}$$

which is exactly the mean-field result of the scalar Bose-Hubbard model in Ref. [58].
When we have performed the Landau expansion (3.42) and used (3.44) in order to find the phase boundary, we have implicitly assumed that the order parameter changes continuously from zero to a finite value. This is the characteristic of a second-order phase transition and it is surely true if the fourth-order coefficient in the Landau expansion (3.42), i.e. $A_\alpha^{(4)}$, is positive [55]. But this is not the only possibility: If $A^{(2)} > 0$, $A^{(4)} < 0$ and $A^{(6)} > 0$, the order parameter changes discontinuously from zero to a finite value Ψ_c when changing $A^{(4)}$ through the critical value, a behavior which is characteristic for a first-order phase transition [55]. There are some arguments that our system does, at least in some part of its phase diagram, show such a transition [50,59]. In Fig. 3.6, the two situations are shown schematically. The left picture corresponds to a second-order phase transition, while the right picture corresponds to a first-order one. Note that for simplicity reasons, we have only shown one scalar component of the order parameter. In order to clarify which situation is realized in the case discussed here, we have to calculate $A_\alpha^{(4)}$.

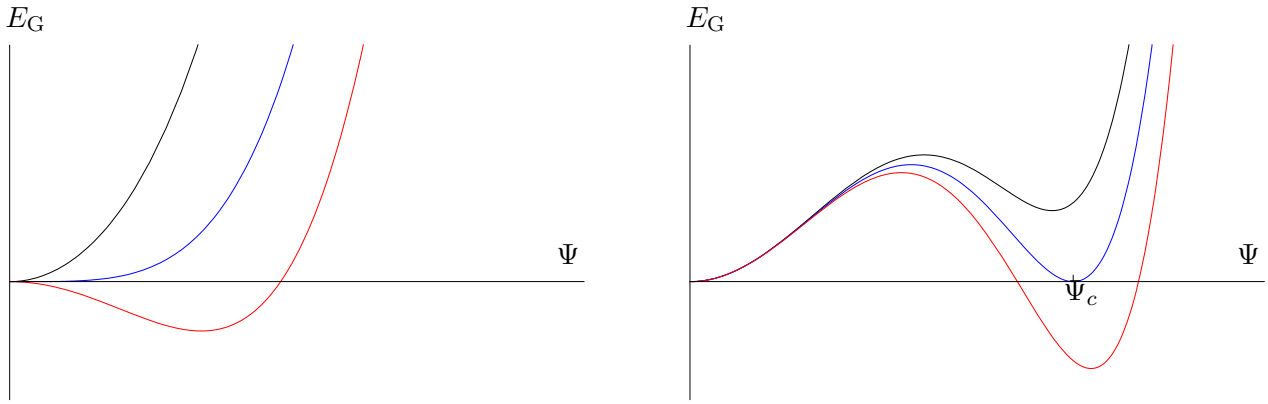

Figure 3.6: Dependence of the ground-state energy on the order parameter. Left: $A^{(4)} > 0$ and $A^{(2)} = 1$ (black), $A^{(2)} = 0$ (blue) and $A^{(2)} = -0.5$ (red). Right: $A^{(2)} > 0$ and $A^{(6)} > 0$. $A^{(4)} = -1.9$ (black), $A^{(4)} = -2$ (blue) and $A^{(4)} = -2.1$ (red).

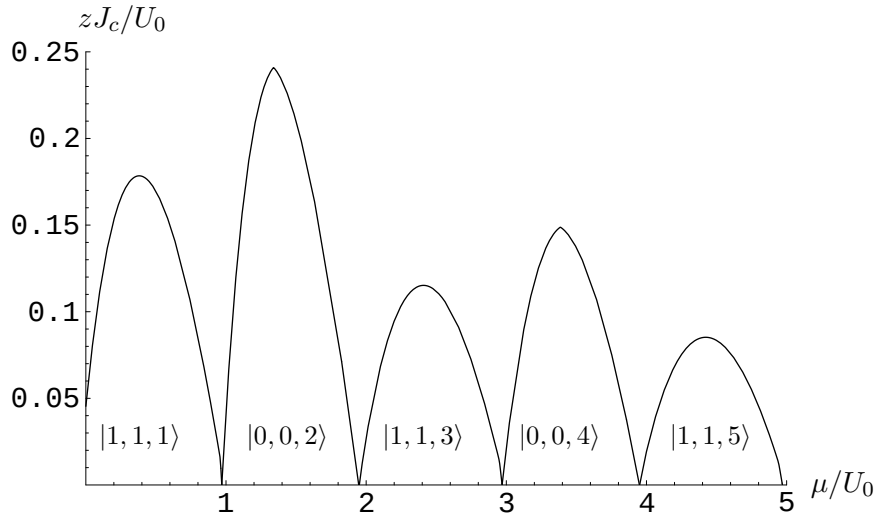

Figure 3.7: Zero-temperature phase boundary for the parameters $U_2/U_0 = 0.04$ and $\eta/U_0 = 0.05$.

3.4.2 Limit of Vanishing Magnetization

Calculating the limit of vanishing magnetization, which corresponds to the limit of $\eta \to 0$, is straightforward for *even* particle numbers per site. The energy eigenvalues (3.14) do no longer depend on m and we can drop this index. The ground state for $J = 0$ is $|0, 0, n\rangle$ as discussed in Section 3.2. Therefore, we get from (3.45)

$$zJ_{c,\alpha}(\mu) = \left[\frac{M^2_{\alpha,0,0,n}}{E_{1,n+1} - E_{0,n}} + \frac{O^2_{\alpha,0,0,n}}{E_{1,n-1} - E_{0,n}} \right]^{-1} , \tag{3.56}$$

which can be further evaluated with (3.14), and the matrix elements from Appendix A to

$$zJ_c = zJ_{c,\alpha} = 3/\left[\frac{n}{-\mu + U_0(n-1) - 2U_2} + \frac{n+3}{\mu - U_0 n} \right] . \tag{3.57}$$

Equation (3.57) is consistent with the result in Ref. [60], where only unmagnetized systems were discussed. One can easily see that the critical hopping approaches zero when one of the energy

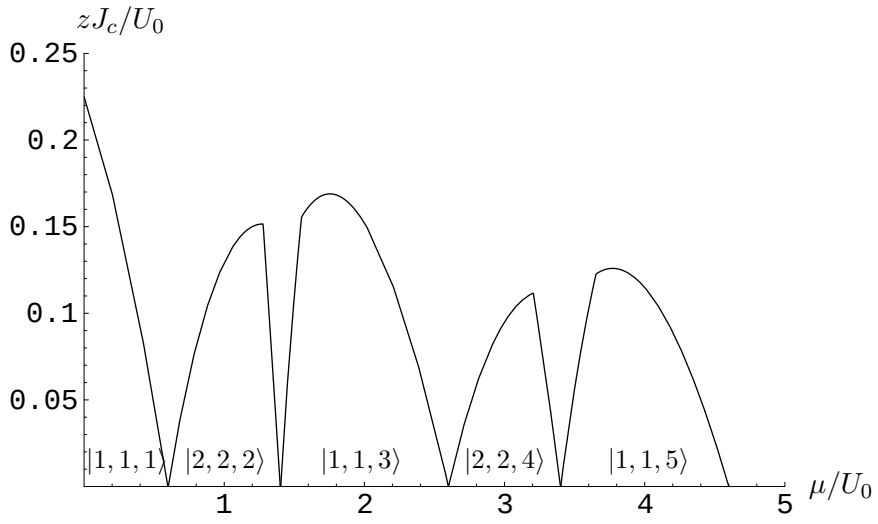

Figure 3.8: Zero-temperature phase boundary for the parameters $U_2/U_0 = 0.5$ and $\eta/U_0 = 0.9$.

differences in the denominators vanishes. This gives us the values of the chemical potential for which no Mott phase exists:

$$\mu_1 = U_0 n \quad , \tag{3.58}$$

$$\mu_2 = U_0(n-1) - 2U_2 \quad . \tag{3.59}$$

When we compare this with the dependence of the particle number on the chemical potential discussed in Subsection 3.2.1, we see that μ_1 in (3.58) is exactly the value of μ where the particle number increases by one. This means that it does not cost any energy to add another particle which, therefore, forms a superfluid even at infinitesimal hopping. Correspondingly, μ_2 in (3.59) indicates the boundary to the Mott lobe with $n-1$ Bosons per site, from which also the addition of one particle costs no energy.
The critical value (3.57) does not depend on α. That means that we can say nothing about the symmetry of the superfluid. We do not know which spin component is populated.
For odd particle numbers per site, the calculation of the phase diagram is not that simple because in the limit of $\eta \to 0$ the ground state for an odd number of particles per site is threefold degenerated, as the states $|1,0,n\rangle$ and $|1,\pm 1,n\rangle$ have the same energy. Therefore, one has to use degenerated perturbation theory which yields a different result for the phase boundary. This is a quite exhausting task because it involves diagonalizing a 3x3-matrix [60]. However, we can obtain the same result in a much easier way: Because of the degeneracy, the ground state is a superposition of the form

$$|\Phi_0\rangle = C_1|1,1,n\rangle + C_0|1,0,n\rangle + C_{-1}|1,-1,n\rangle \quad , \tag{3.60}$$

where the respective coefficients have to fullfill the normalization condition

$$|C_1|^2 + |C_0|^2 + |C_{-1}|^2 = 1 \quad . \tag{3.61}$$

We consider these three terms separately and calculate the phase boundaries corresponding to them. The aim of this consideration is to find the role played by the ground states $|1,0,n\rangle$ and $|1,-1,n\rangle$ which were not taken into account when performing the calculation for finite η. Thus, we use (3.45) not only for $m=1$ but also for $m=0$ and $m=-1$. Doing this yields

$$zJ_{c\alpha;m=0,\pm1}(\mu) = \left[\frac{M^2_{\alpha,S,m,n}}{E_{2,n+1} - E_{1,n}} + \frac{N^2_{\alpha,S,m,n}}{E_{0,n+1} - E_{1,n}} + \frac{O^2_{\alpha,1,m,n}}{E_{2,n-1} - E_{1,n}} + \frac{P^2_{\alpha,1,m,n}}{E_{0,n-1} - E_{1,n}} \right]^{-1} \quad . \tag{3.62}$$

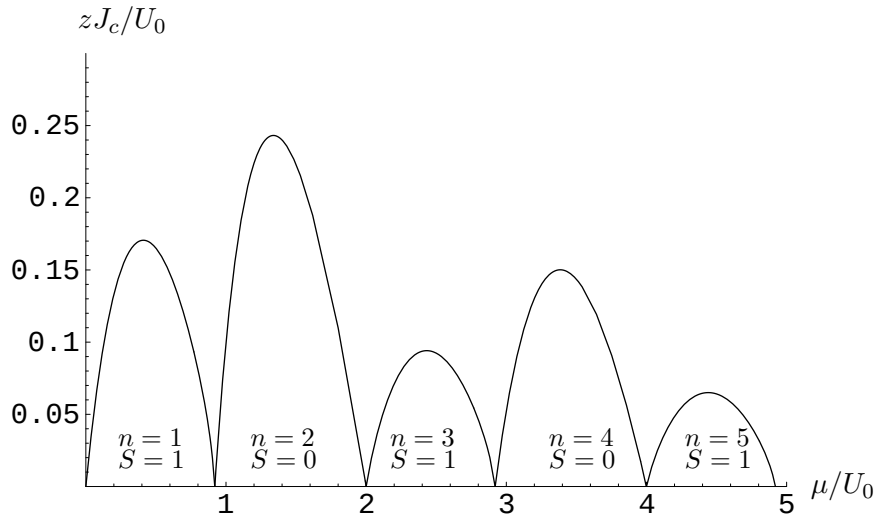

Figure 3.9: Zero-temperature phase boundary for vanishing magnetization and $U_2/U_0 = 0.04$.

The next step is to determine for which m the value of the critical hopping is minimal. When one also takes the minimum with respect to α, as done in (3.46), one can both determine which component of the ground state makes the transition and what kind the superfluid is. It turns out that the component with $m = 0$ forms the superfluid which has $\Psi_0 \neq 0$. This result is different from the one for finite η where we had $\Psi_1 \neq 0$ or $\Psi_{-1} \neq 0$. Thus, we get from (3.62) with the matrix elements from Appendix A the phase boundary

$$zJ_c = \left\{ \frac{4(n+4)}{15(-\mu + U_0 n + U_2)} + \frac{n+1}{3(-\mu + U_0 n - 2U_2)} + \frac{4(n-1)}{15[\mu - (n-1)U_0 + 3U_2]} + \frac{n+2}{3[\mu - (n-1)U_0]} \right\}^{-1} \quad , \quad (3.63)$$

which is plotted in Fig. 3.9. From (3.63) we expect a Mott lobe with a given particle number to have *four* points where the critical hopping is zero. But one has to keep in mind that (3.63) is only meaningful, when the particle number n minimizes the ground-state energy for a given chemical potential μ, as given by the inequalities (3.15) and (3.16).
In Fig. 3.10 we have plotted the first Mott lobe which has one particle per site and $S = 1$ both for zero and for very small magnetization. We clearly see, that a discontinuity occurs there. The reason for this feature is that for any finite η we assumed the ground state in the Mott-insulator phase to be $|1, 1, n\rangle$, which is of course true. But the states $|1, 0, n\rangle$ and $|1, -1, n\rangle$ have an only slightly higher energies. The energy difference to the former one is

$$\Delta E = E_{1,0,n} - E_{1,1,n} = \eta \quad . \quad (3.64)$$

Thus, when η is small, there will be some particles in this state because of quantum fluctuations. Therefore, we have found that our perturbative mean-field theory is not reliable in this regime. But other methods, e.g. the Gutzwiller variational ansatz do not have this problem [50, 53]. They predict a smooth behavior of the phase-boundary in the limit of vanishing magnetization. Unfortunately, they do not yield analytical, but only numerical result.

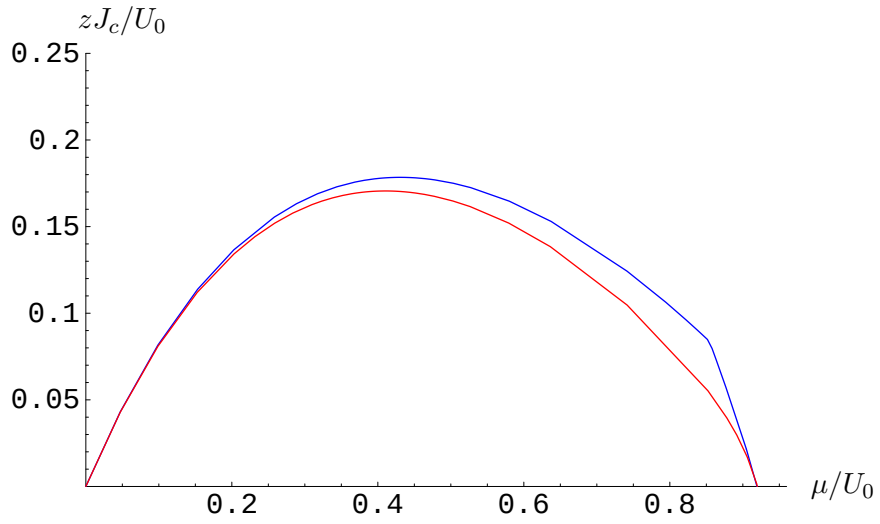

Figure 3.10: First Mott lobe ($S = 1$, $n = 1$) for $U_2/U_0 = 0.04$, $\eta/U_0 = 10^{-5}$ (blue) and $\eta = 0$ (red).

3.5 Phase Diagram at Finite Temperature

In the previous section, we have found the phase boundary between the Mott insulator and the superfluid phase at zero temperature. Because all experiments are, of course, performed at small but finite temperatures, it is desirable to extend our results in this respect. As all thermodynamic properties can be derived from the partition function (3.8), our first step is to calculate this important statistical quantity.

3.5.1 Partition Function

The definition of the partition function (3.8) involves the full Hamiltonian (2.18). Because we do not know its eigenstates, we use the Dirac picture in imaginary time to calculate $\mathcal{Z}$ at least perturbatively. In the Dirac picture, the time evolution of the operators is only determined by the unperturbed part of the Hamiltonian (3.12) and therefore easy to handle as

$$\hat{A}_{\mathrm{D}}(\tau) = e^{\hat{H}_0(\tau-\tau_0)}\hat{A}e^{\hat{H}_0(\tau_0-\tau)} \quad . \tag{3.65}$$

The time evolution of the states is given by

$$|\Psi_{\mathrm{D}}(\tau)\rangle = \hat{U}_{\mathrm{D}}(\tau,\tau')|\Psi_{\mathrm{D}}(\tau')\rangle \quad , \tag{3.66}$$

where the Dirac picture 4ution operator is given by [61]

$$\hat{U}_{\mathrm{D}}(\tau,\tau') = \hat{U}_0^{-1}(\tau,\tau_0)\hat{U}(\tau,\tau')\hat{U}_0(\tau',\tau_0) \quad . \tag{3.67}$$

This evolution operator satisfies the differential equation

$$\frac{d}{d\tau}\hat{U}_{\mathrm{D}}(\tau,\tau_0) = -\hat{H}_{1\mathrm{MF,D}}(\tau)\hat{U}_{\mathrm{D}}(\tau,\tau_0) \quad , \tag{3.68}$$

where $\hat{H}_{1\mathrm{MF,D}}$ is the Dirac picture representation of the mean-field hoping Hamiltonian (3.34). We transform Eq. (3.68) into an integral equation, while using the initial value condition

$$\hat{U}_{\mathrm{D}}(\tau_0,\tau_0) = 1 \quad , \tag{3.69}$$

and get

$$\hat{U}_{\mathrm{D}}(\tau,\tau_0) = 1 - \int_{\tau_0}^{\tau} d\tau_1 \hat{H}_{1\mathrm{MF,D}}(\tau_1)\hat{U}_{\mathrm{D}}(\tau_1,\tau_0) \quad . \tag{3.70}$$

This can be solved by iteration. Doing this up to second order yields

$$\hat{U}_{\mathrm{D}}(\tau,\tau_0) = 1 - \int_{\tau_0}^{\tau} d\tau_1 \hat{H}_{1\mathrm{MF,D}}(\tau_1) + (-1)^2 \int_{\tau_0}^{\tau} d\tau_1 \int_{\tau_0}^{\tau_1} d\tau_2 \hat{H}_{1\mathrm{MF,D}}(\tau_1)\hat{H}_{1\mathrm{D}}(\tau_2) + \mathcal{O}(\hat{H}_1)^3 \quad . \tag{3.71}$$

From this, one can easily write down the n-th order as

$$\hat{U}_{\mathrm{D}}^{(n)}(\tau,\tau_0) = (-1)^n \int_{\tau_0}^{\tau} d\tau_1 \int_{\tau_0}^{\tau_1} d\tau_2 \ldots \int_{\tau_0}^{\tau_{n-1}} d\tau_n \hat{H}_{1\mathrm{MF,D}}(\tau_1)\hat{H}_{1\mathrm{MF,D}}(\tau_2)\ldots\hat{H}_{1\mathrm{MF,D}}(\tau_n) \quad . \tag{3.72}$$

With the help of the imaginary-time ordering operator

$$\hat{T}\left[\hat{A}(\tau_1))\hat{A}(\tau_2)\right] = \Theta(\tau_1-\tau_2)\hat{A}(\tau_1)\hat{A}(\tau_2) + \Theta(\tau_2-\tau_1)\hat{A}(\tau_2)\hat{A}(\tau_1) \quad , \tag{3.73}$$

one can transform the respective integrals in a way that they all have the same boundaries of integration. Thus, Eq. (3.72) becomes

$$\hat{U}_{\mathrm{D}}^{(n)}(\tau,\tau_0) = \frac{1}{n!}(-1)^n \int_{\tau_0}^{\tau} d\tau_1 \int_{\tau_0}^{\tau} d\tau_2 \ldots \int_{\tau_0}^{\tau} d\tau_n \hat{T}\left[\hat{H}_{1\mathrm{MF,D}}(\tau_1)\hat{H}_{1\mathrm{MF,D}}(\tau_2)\ldots\hat{H}_{1\mathrm{MF,D}}(\tau_n)\right] \quad . \tag{3.74}$$

The factor $n!$ accounts for all the possible permutations of the n occurring operators. In the next step we transform the formula for the partition function (3.8). Multiplying it in a suitable way with an unity factor yields

$$\mathcal{Z} = \mathrm{Tr}\left\{e^{-\beta\hat{H}_0}e^{\beta\hat{H}_0}e^{-(\beta-0)\hat{H}}e^{-\hat{H}_0\cdot 0}\right\} \quad , \tag{3.75}$$

which can be written with the formula for the Dirac time-evolution operator (3.67) as

$$\mathcal{Z} = \mathrm{Tr}\left\{e^{-\beta\hat{H}_0}\hat{U}_{\mathrm{D}}(\beta,0)\right\} \quad . \tag{3.76}$$

Eq. (3.76) allows us to calculate the partition function perturbatively with the help of the Dyson series in (3.74). With the definition of the thermal average (3.7) and the notation, that the superscript $^{(0)}$ indicates averaging with respect to the unperturbed Hamiltonian (3.12), the partition function becomes

$$\mathcal{Z}^{(n)} = \frac{1}{n!}\mathcal{Z}^{(0)}(-1)^n \int_0^{\beta} d\tau_1 \int_0^{\beta} d\tau_2 \ldots \int_0^{\beta} d\tau_n \left\langle \hat{T}\left[\hat{H}_{1\mathrm{D}}(\tau_1)\hat{H}_{1\mathrm{D}}(\tau_2)\ldots\hat{H}_{1\mathrm{D}}(\tau_n)\right]\right\rangle^{(0)} \quad , \tag{3.77}$$

where the *unperturbed* partition function is given by (3.17). The standard technique in many-body theory to calculate correlation functions, like the ones occurring on the right-hand side of Eq. (3.77), is to use Wick's theorem [62, 63] which allows to decompose the arising n-point correlation functions into sums of products of 2-point correlation functions. Unfortunately, we cannot use this important theorem here because Wick's theorem is only valid if the unperturbed Hamiltonian is linear in the occupation number operator $\hat{n}$, i.e. the unperturbed system behaves like a harmonic oscillator

$$\hat{H}_{0\mathrm{har}} = \omega\hat{n} \quad . \tag{3.78}$$

This is not the case for the Bose-Hubbard Hamiltonian in the limit $J = 0$ (3.12), because it contains terms which are quadratic in $\hat{n}$. Therefore, we have to got back to (3.71), insert it into (3.76) and calculate the three arising terms separately. The first term just yields the unperturped partition function (3.17) again

$$\mathcal{Z}^{(0)} = \sum_{S,m,n} \langle S,m,n|e^{-\beta \hat{H}_0}|S,m,n\rangle = \sum_{S,m,n} e^{-\beta E_{S,m,n}} \quad , \tag{3.79}$$

while the second one gives the contribution

$$\mathcal{Z}^{(1)} = -\langle S,m,n|e^{-\beta \hat{H}_0} \int_0^\beta d\tau_1 Jz \sum_\alpha |\Psi_\alpha|^2 |S,m,n\rangle = -Jz\beta \sum_\alpha |\Psi_\alpha|^2 \sum_{S,m,n} e^{-\beta E_{S,m,n}} \quad . \tag{3.80}$$

The most interesting and complicated contribution stems from the third term. It reads

$$\mathcal{Z}^{(2)} = \sum_{S,m,n} \langle S,m,n|e^{-\beta \hat{H}_0} \int_0^\beta d\tau_1 \int_0^{\tau_1} d\tau_2 \hat{H}_{1\mathrm{D}}(\tau_1)\hat{H}_{1\mathrm{D}}(\tau_2)|S,m,n\rangle \quad . \tag{3.81}$$

Because we are only interested in terms up to quadratic order in the order parameter $\mathbf{\Psi}$, we skip the arising quartic term in (3.81). Therefore, we get

$$\begin{aligned}\mathcal{Z}^{(2)} = z^2 J^2 \sum_{S,m,n} e^{-\beta E_{S,m,n}} \int_0^\beta d\tau_1 \int_0^{\tau_1} d\tau_2 \langle S,m,n|e^{-\hat{H}_0\tau_1} \\ \times \sum_\alpha (\Psi_\alpha^* \hat{a}_\alpha + \Psi_\alpha \hat{a}_\alpha^\dagger) e^{\hat{H}_0\tau_1} e^{-\hat{H}_0\tau_2} \sum_\beta (\Psi_\beta^* \hat{a}_\beta + \Psi_\beta \hat{a}_\beta^\dagger) e^{\hat{H}_0\tau_2} |S,m,n\rangle + \ \ldots \quad .\end{aligned} \tag{3.82}$$

To simplify (3.82) further, we use the fact that the respective matrix elements have the properties

$$\begin{aligned}&\langle S,m,n|\hat{a}_\alpha \hat{a}_\beta^\dagger|S,m,n\rangle \propto \delta_{\alpha\beta} \quad , \\ &\langle S,m,n|\hat{a}_\alpha^\dagger \hat{a}_\beta|S,m,n\rangle \propto \delta_{\alpha\beta} \quad , \\ &\langle S,m,n|\hat{a}_\alpha \hat{a}_\beta|S,m,n\rangle = \langle S,m,n|\hat{a}_\alpha^\dagger \hat{a}_\beta^\dagger|S,m,n\rangle = 0 \quad ,\end{aligned} \tag{3.83}$$

which are simple consequences of (3.35), (3.36), and the orthonormality of the states (2.21). Using (3.83) in (3.82) yields

$$\begin{aligned}\mathcal{Z}^{(2)} = z^2 J^2 \sum_{S,m,n} e^{-\beta E_{S,m,n}} \int_0^\beta d\tau_1 \int_0^{\tau_1} d\tau_2 \sum_\alpha |\Psi_\alpha|^2 \Big[\langle S,m,n|e^{-\hat{H}_0\tau_1} \hat{a}_\alpha e^{\hat{H}_0(\tau_1-\tau_2)} \hat{a}_\alpha^\dagger e^{-\hat{H}_0\tau_2}|S,m,n\rangle \\ + \langle S,m,n|e^{-\hat{H}_0\tau_1} \hat{a}_\alpha^\dagger e^{\hat{H}_0(\tau_1-\tau_2)} \hat{a}_\alpha e^{-\hat{H}_0\tau_2}|S,m,n\rangle \Big] \quad .\end{aligned} \tag{3.84}$$

Now we remember from quantum mechanics, that one can act with operators on the left-hand site of a scalar product by taking the adjoint operator [61]. Doing this and using (3.35), (3.36) again, one obtains

$$\begin{aligned}\mathcal{Z}^{(2)} =& z^2 J^2 \sum_{S,m,n} e^{-\beta E_{S,m,n}} \int_0^\beta d\tau_1 \int_0^{\tau_1} d\tau_2 e^{E_{S,m,n}(\tau_2-\tau_1)} \sum_\alpha |\Psi_\alpha|^2 \Big[M^2_{\alpha,S,m,n} e^{E_{S+1,m+\alpha,n+1}(\tau_1-\tau_2)} \\ &+ N^2_{\alpha,S,m,n} e^{E_{S-1,m+\alpha,n+1}(\tau_1-\tau_2)} + O^2_{\alpha,S,m,n} e^{E_{S+1,m-\alpha,n-1}(\tau_1-\tau_2)} + P^2_{\alpha,S,m,n} e^{E_{S-1,m-\alpha,n-1}(\tau_1-\tau_2)} \Big] \quad .\end{aligned} \tag{3.85}$$

The next step is to calculate the following elementary imaginary-time integrals,

$$I_{S,m,n;S',m',n'} = \int_0^\beta d\tau_1 \int_0^{\tau_1} d\tau_2 \, e^{E_{S,m,n}(\tau_2-\tau_1)} e^{E_{S',m',n'}(\tau_1-\tau_2)} \quad , \tag{3.86}$$

yielding

$$I_{S,m,n;S',m',n'} = \frac{e^{-\beta(E_{S',m',n'}-E_{S,m,n})}-1}{(E_{S',m',n'}-E_{S,m,n})^2} + \frac{\beta}{E_{S',m',n'}-E_{S,m,n}} \quad . \tag{3.87}$$

Plugging (3.86) in (3.85), we get

$$\begin{aligned}\mathcal{Z}^{(2)} = z^2J^2 \sum_\alpha |\Psi_\alpha|^2 \sum_{S,m,n} e^{-\beta E_{S,m,n}} \big(& M^2_{\alpha,S,m,n} I_{S,m,n;S+1,m+\alpha,n+1} + N^2_{\alpha,S,m,n} I_{S,m,n;S-1,m+\alpha,n+1} \\ & + O^2_{\alpha,S,m,n} I_{S,m,n;S+1,m-\alpha,n-1} + P^2_{\alpha,S,m,n} I_{S,m,n;S-1,m-\alpha,n-1} \big) \quad . \end{aligned} \tag{3.88}$$

Inserting (3.87) there is one term which is proportional to β and a term which is independent of β. When performing the summation in (3.88), it turns out that the contribution arising from the latter vanishes. This can be shown by rearranging the terms and shifting summation indices suitably. Thus, the second-order result (3.88) becomes

$$\begin{aligned}\mathcal{Z}^{(0)} = z^2J^2 \sum_\alpha |\Psi_\alpha|^2 \sum_{S,m,n} e^{-\beta E_{S,m,n}} \Bigg(& \frac{M^2_{\alpha,S,m,n}}{E_{S+1,m+\alpha,n+1}-E_{S,m,n}} + \frac{N^2_{\alpha,S,m,n}}{E_{S-1,m+\alpha,n+1}-E_{S,m,n}} \\ & + \frac{O^2_{\alpha,S,m,n}}{E_{S+1,m-\alpha,n-1}-E_{S,m,n}} + \frac{P^2_{\alpha,S,m,n}}{E_{S-1,m-\alpha,n-1}-E_{S,m,n}} \Bigg) \quad . \end{aligned} \tag{3.89}$$

3.5.2 Phase Boundary

From the connection between the partition function and the grand-canonical free energy (3.9), the latter can be easily obtained to:

$$\mathcal{F} = \frac{1}{\beta}\log \mathcal{Z}^{(0)} - \frac{1}{\beta}\log\left[1 + \frac{\mathcal{Z}^{(1)}+\mathcal{Z}^{(2)}+\dots}{\mathcal{Z}^{(0)}}\right] \quad . \tag{3.90}$$

Using the Taylor series of the logarithm function up to quadratic order in its argument, one gets

$$\mathcal{F} = -\frac{1}{\beta}\log \mathcal{Z}^{(0)} - \frac{1}{\beta}\frac{\mathcal{Z}^{(1)}+\mathcal{Z}^{(2)}}{\mathcal{Z}^{(0)}} - \frac{1}{\beta}\frac{\mathcal{Z}^{(1)2}}{2\mathcal{Z}^{(0)2}} + \dots \quad . \tag{3.91}$$

With this formula, it is possible to write down the grand-canonical free energy as a series in the order parameter $\mathbf{\Psi}$, exactly as done with the ground-state energy in (3.42). The series reads

$$\mathcal{F}(\beta) = -\frac{1}{\beta}\log \mathcal{Z}_0 + \sum_\alpha A^{(2)}_\alpha(\beta)|\Psi_\alpha|^2 + \mathcal{O}(\mathbf{\Psi^4}) \tag{3.92}$$

with the coefficients

$$\begin{aligned}A^{(2)}_\alpha(\beta) = \frac{1}{\mathcal{Z}^{(0)}} \sum_{S,m,n} e^{-\beta E_{S,m,n}} \Bigg[-Jz + J^2z^2 \Bigg(& \frac{M^2_{\alpha,S,m,n}}{E_{S+1,m+\alpha,n+1}-E_{S,m,n}} + \frac{N^2_{\alpha,S,m,n}}{E_{S-1,m+\alpha,n+1}-E_{S,m,n}} \\ & + \frac{O^2_{\alpha,S,m,n}}{E_{S+1,m-\alpha,n-1}-E_{S,m,n}} + \frac{P^2_{\alpha,S,m,n}}{E_{S-1,m-\alpha,n-1}-E_{S,m,n}} \Bigg) \Bigg] \quad . \end{aligned} \tag{3.93}$$

Setting Eq. (3.93) equal to zero, the phase boundary follows in a completely analogous way to the zero-temperature case, yielding

$$zJ_{c,\alpha}(\mu,\beta) = \frac{\sum_{S,m,n} e^{-\beta E_{S,m,n}}}{\sum_{S,m,n} e^{-\beta E_{S,m,n}} \left[M^2_{\alpha,S,m,n}/(E_{S+1,m+\alpha,n+1} - E_{S,m,n}) + \dots \right]} \quad . \tag{3.94}$$

Before discussing this result, a few remarks on the phase diagram for the spinless or scalar Bose-Hubbard Model, which is shown in Fig. 3.11, should be made [64, 65]. It follows due to a similar reasoning as in Section 3.4 from (3.94) as the limit of a fully polarized system. The respective formula reads

$$zJ_c = \frac{\sum_{n=0}^{\infty} e^{-\beta E_n}}{\sum_{n=0}^{\infty} \left[\frac{n+1}{nU-\mu} + \frac{n}{(1-n)U+\mu} \right] e^{-\beta E_n}} \quad . \tag{3.95}$$

The phase boundaries in (3.11) are smeared out with higher temperature. This effect is especially visible in the space between the Mott lobes. In contrast to our zero-temperature result, there exists a Mott phase even for integer values of μ/U. This is easily understood. At finite temperature, the average value of the particle number per site in the Mott phase (see Fig. 3.2) is not integer anymore due to thermal fluctuations. Therefore, the addition of one particle does not change the situation as dramatically as in the zero-temperature case. In a rough estimate, the hopping must be of the order of the thermal energy $k_B T$ to form a superfluid. This can be easily seen by looking at the minima of the phase boundary in Fig. 3.11. On the tips of the lobes, the effect induced by temperature is much weaker because the avarge particle number per site is almost integer and thermal fluctuations are small.

After this excursion, we return to the system of spin-1 Bosons. We have plotted this result (3.94) in Fig. 3.12 for different temperatures but otherwise equal parameters as in Fig. 3.7. The shift of the phase boundary in the region *between* the lobes results from the same effect as in the scalar case and does not deserve further discussion. The interesting new feature is the fact that the phase boundaries for different temperature cross. The clear difference between odd and even particle numbers, which occurs for zero temperature, continuously vanishes for higher temperatures. To explain this, we recall the reason for this even-odd asymmetry. The stabilization of the Mott lobes with an even particle number per site is a result of the formation of spin-singlet pairs. The energy scale for their formation is given by the spin asymmetric interaction energy U_2. If now the thermal energy is larger than U_2, the singlet pairs are destroyed by thermal fluctuations, i.e. they melt. In Fig. 3.13, the phase diagram is shown for the same temperatures but much larger spin asymmetric interaction U_2. Here this effect is of course much weaker because the spin-dependent interaction is much larger and a substantial melting of the singlet pairs would only occur at much higher temperature.

We investigate now if our results reproduce correctly the zero-temperature limit of $T \to 0$. As already discussed in Subsection 3.2.2, the main contribution to the sums in (3.94) comes from the ground state. Let the ground state be $|S, S, n\rangle$. With the help of (3.20) we get from (3.94)

$$zJ_{c,\alpha}(\mu,\beta) \to \frac{e^{-\beta E_{S,m,n}}}{e^{-\beta E_{S,m,n}} \left(\frac{M^2_{\alpha,S,m,n}}{E_{S+1,m+\alpha,n+1} - E_{S,m,n}} + \dots \right)} \quad , \tag{3.96}$$

which yields

$$zJ_{c,\alpha}(\mu, T=0) = \left(\frac{M^2_{\alpha,S,m,n}}{E_{S+1,m+1,n+1} - E_{S,m,n}} + \dots \right)^{-1} \quad . \tag{3.97}$$

Thus, we have reproduced our zero-temperature result (3.45). As an interesting special case one can consider now the limit of vanishing magnetization $\eta \to 0$. In this case the unperturbed energies and

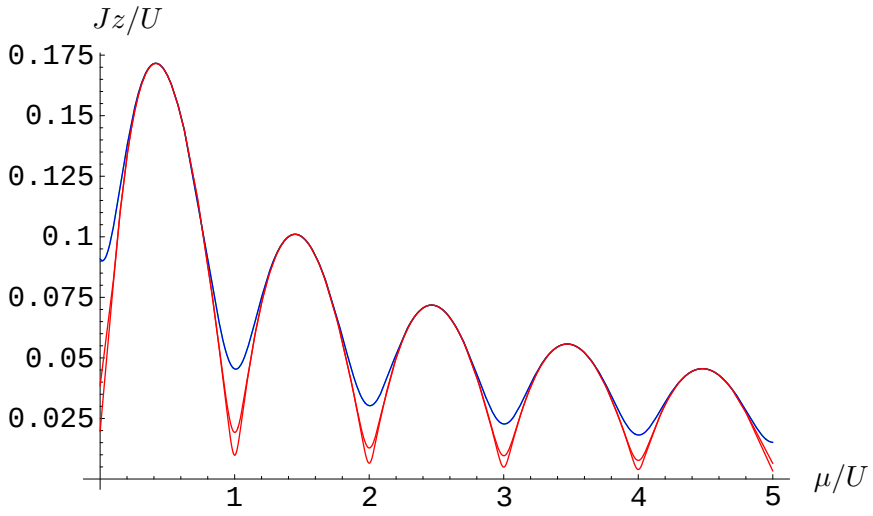

Figure 3.11: Phase diagram for effectively spinless Bosons for $k_BT/U_0 = 0.01$ (red), $k_BT/U_0 = 0.02$ (blue), and $k_BT/U_0 = 0.05$ (green).

also the integrals (3.87) only depend on the quantum numbers S and n. We introduce the definition

$$\tilde{M}_{\alpha,S,n} = \sum_m M^2_{\alpha,S,m,n} \tag{3.98}$$

and similar ones for the other matrix elements N, O, P. When we now rearrange the sums in (3.89), we can write the result in the more compact form

$$\mathcal{Z}_2 = J^2 z^2 \sum_\alpha |\Psi_\alpha|^2 \sum_{S,n} e^{-\beta E_{S,n}} \Big(\tilde{M}_{\alpha,S,n} I_{S,n;S+1,n+1} + \tilde{N}_{\alpha,S,n} I_{S,n;S-1,n+1} + \tilde{O}_{\alpha,S,n} I_{S,n;S+1,n-1} + \tilde{P}_{\alpha,S,n} I_{S,n;S-1,n-1} \Big) \quad . \tag{3.99}$$

Explicit formulas for $\tilde{M}$, $\tilde{N}$, $\tilde{O}$, and $\tilde{P}$ are given in Eq. (A.92). It turns out that they are equal for all spin components (e.g. $\tilde{M}_{\alpha,S,n} = \tilde{M}_{\beta,S,n}$). This means that also the Landau coefficients $A^{(2)}$ in Eq. (3.93) do not depend on α, a result which is expected from the zero-temperature calculation. Therefore, it seems that the superfluid does not have only a single component, as for finite η, where we had $\Psi_1 \neq 0$ or $\Psi_{-1} \neq 0$. To find out what the symmetry of the superfluid phase is in this special situation one has to calculate the next term in the Landau expansion (3.92), which is $A^{(4)}$.
Note, that we have exclusively discussed the transition to a superfluid phase. We have not considered different kinds of Mott phases which can be characterized by their magnetic properties and which were already discussed in Ref. [66].

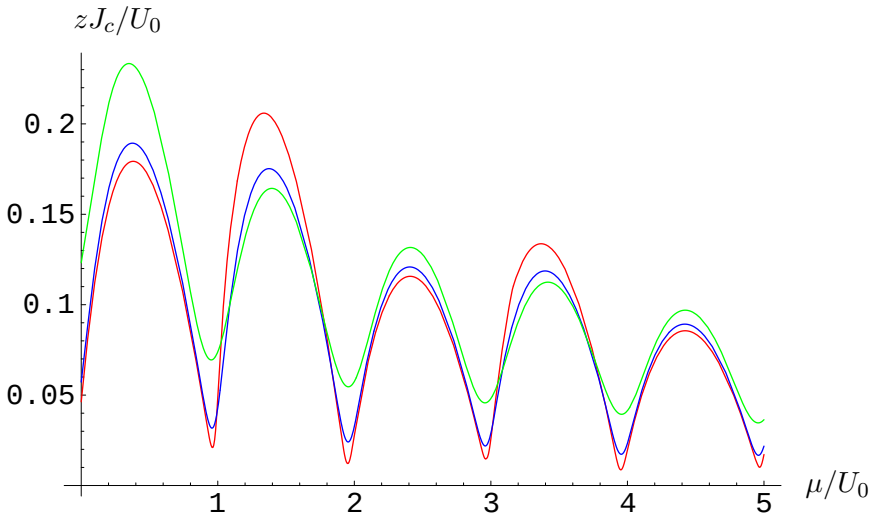

Figure 3.12: Phase boundary for the parameters $U_2/U_0 = 0.04$, $\eta/U_0 = 0.05$, as well as $k_BT/U_0 = 0.01$ (red), $k_BT/U_0 = 0.02$ (blue), and $k_BT/U_0 = 0.05$ (green).

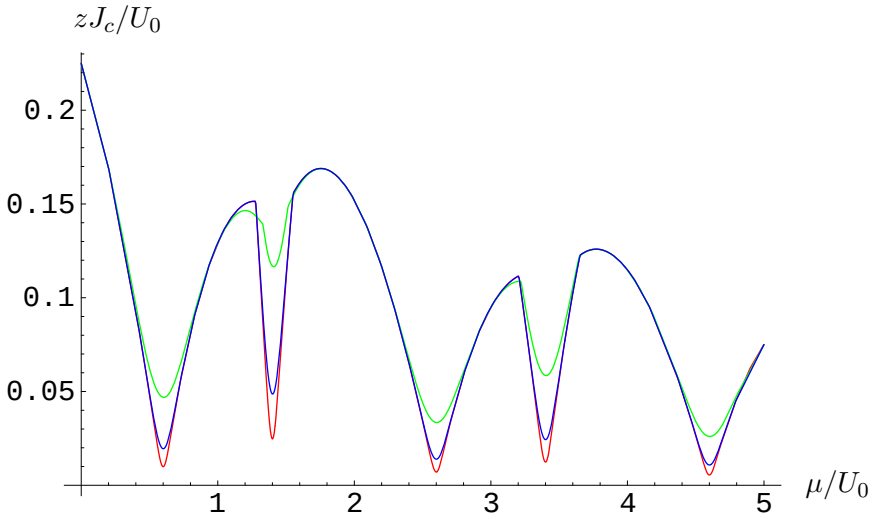

Figure 3.13: Phase boundary for the parameters $U_2/U_0 = 0.5$, $\eta/U_0 = 0.9$, and $k_BT/U_0 = 0.01$ (red), $k_BT/U_0 = 0.02$ (blue), and $k_BT/U_0 = 0.05$ (green).

Chapter 4

Time-of-Flight

In the previous chapter we have calculated the phase boundary between a Mott insulator and a superfluid phase. Unfortunately, the respective results are not comparable with experiments. As Bose-Einstein condensates are very small, they are hard to investigate directly. In spite of the fact that there are nevertheless possibilities to measure some properties by non-destructive in-situ measurements like phase-contrast imaging [31], the standard experimental technique to investigate them is a time-of-flight measurement. The key idea behind it is the following [67]: When the optical lattice and also the additional confining trap is turned off, the gas expands. After some holding time of approximately 100 ms, an absorption image of the cloud is taken. Because the size of the trapped gas is much smaller than the size of the expanded cloud, the initial system can be well approximated as being point-like. Furthermore, because of the low density, interactions after switching off the lattice can also be neglected. Under these assumptions, the time-of-flight picture stems from the initial momentum-space density $n(\mathbf{k})$. The faster a particle is, the farer it gets during a given expansion time. Of course the images are only two-dimensional and we, therefore, have to integrate $n(\mathbf{k})$ over one axis in order to get pictures which are comparable with the experimental data, see for example in Ref. [17].
The fact that we are dealing here with spinor Bosons, which have the three hyperfine spin components $m = 0, \pm 1$, provides an interesting way of getting additional information out of a time-of-flight picture. Because the different hyperfine spin components have different magnetic moments, as $\mu_z = m\mu_\mathrm{B}$ with the Bohr magneton μ_B, it is possible to separate the components during the expansion time by an additional inhomogeneous magnetic field [68, 69]. This is in complete analogy to the famous Stern-Gerlach experiment in which the quantum nature of magnetic moments and the existence of spin was discovered and which is extensively discussed in Ref. [70]. Our next goal should, therefore, be to calculate the spin resolved momentum space density $n_\alpha(\mathbf{k})$.

4.1 Zero Temperature

In this section, we consider a system at zero-temperature. Thus, we are dealing with pure quantum physics which is not obfuscated by thermal fluctuations.

4.1.1 Limit of Vanishing Interaction

Until now, we have considered the Bose-Hubbard model in the limit of strong interactions, which means that $J \ll U_0$. This allowed us to treat the hopping term in (2.18) as a perturbation. We will continue this consideration in the next subsection but in order to get some information about the system properties deep in the superfluid phase, we will in this section briefly discuss the opposite limit

$U_{0,2} \to 0$. For this situation the Hamiltonian (2.18) reads

$$\hat{H}_{U_0=U_2=0} = -\mu \sum_i \sum_\alpha \hat{a}^\dagger_{i\alpha}\hat{a}_{i\alpha} - J \sum_{<i,j>} \sum_\alpha \hat{a}^\dagger_{i\alpha}\hat{a}_{j\alpha} - \eta \sum_i \hat{S}^z_i \quad . \tag{4.1}$$

Using (2.19) and defining

$$\mu_\alpha = \begin{cases} \mu+\eta, & \alpha = 1 \\ \mu, & \alpha = 0 \\ \mu-\eta, & \alpha = -1 \end{cases} \quad , \tag{4.2}$$

we can write (4.1) as

$$\hat{H}_{U_0=U_2=0} = -\sum_\alpha \mu_\alpha \sum_i \hat{a}^\dagger_{i\alpha}\hat{a}_{i\alpha} - J \sum_{<i,j>} \sum_\alpha \hat{a}^\dagger_{i\alpha}\hat{a}_{j\alpha} \quad . \tag{4.3}$$

This Hamiltonian can be diagonalized by performing a Fourier transformation [71]. To this end, we write the creation and annihilation operators as

$$\hat{a}_{i\alpha} = \frac{1}{\sqrt{N_S}} \sum_{\mathbf{k}} \hat{a}_{\mathbf{k}\alpha} e^{-i\mathbf{k}\cdot\mathbf{r}_i} \quad , \qquad \hat{a}^\dagger_{i\alpha} = \frac{1}{\sqrt{N_S}} \sum_{\mathbf{k}} \hat{a}^\dagger_{\mathbf{k}\alpha} e^{i\mathbf{k}\cdot\mathbf{r}_i} \quad , \tag{4.4}$$

where N_S is the number of lattice sites. Note that we have to sum $\mathbf{k}$ over all vectors of the reciprocal lattice which are in the first Brillouin zone. Inserting (4.4) into (4.3) yields

$$\hat{H}_{U_0=U_2=0} = -\sum_\alpha \sum_{\mathbf{k}} \left[J(\mathbf{k}) + \mu_\alpha\right] \hat{a}^\dagger_{\mathbf{k}\alpha}\hat{a}_{\mathbf{k}\alpha} \tag{4.5}$$

with the lattice-dispersion relation

$$J(\mathbf{k}) = 2J \sum_{\nu=1}^{3} \cos(k_\nu a) \quad . \tag{4.6}$$

Introducing the density operators in momentum space, which read $\hat{n}_{\mathbf{k}\alpha} = \hat{a}^\dagger_{\mathbf{k}\alpha}\hat{a}_{\mathbf{k}\alpha}$, Eq. (4.5) becomes

$$\hat{H}_{U_0=U_2=0} = -\sum_\alpha \sum_{\mathbf{k}} \left[J(\mathbf{k}) + \mu_\alpha\right] \hat{n}_{\mathbf{k}\alpha} \quad . \tag{4.7}$$

The natural basis of eigenstates of this Hamiltonian is the momentum-space occupation number representation. The corresponding states will be denoted as

$$|(n_{\mathbf{k}_1,1}, n_{\mathbf{k}_2,1}, \ldots, n_{\mathbf{k}_m,1}), (n_{\mathbf{k}_1,0}, n_{\mathbf{k}_2,0}, \ldots, n_{\mathbf{k}_m,0}), (\ldots, \ldots, \ldots)\rangle \quad , \tag{4.8}$$

which we can shorten to $|\mathbf{n}_{\mathbf{k},1}, \mathbf{n}_{\mathbf{k},0}, \mathbf{n}_{\mathbf{k},-1}\rangle$. The respective eigenvalues are

$$E_{\mathbf{n}_{\mathbf{k},1},\mathbf{n}_{\mathbf{k},0},\mathbf{n}_{\mathbf{k},-1}} = -\sum_\alpha \sum_{\mathbf{k}} (\epsilon_{\mathbf{k}} + \mu_\alpha) n_{\mathbf{k}\alpha} \quad . \tag{4.9}$$

Because we are dealing here with Bosons, there is nothing like the Pauli principle, and at $T = 0$ all particles are in the ground state. From (4.9) we see that the energy has its minima at the maxima of $J(\mathbf{k})$ in Eq. (4.6). Thus, we get

$$\mathbf{k}_\alpha = \frac{2\pi}{a} \begin{pmatrix} h_\alpha \\ k_\alpha \\ l_\alpha \end{pmatrix} \quad ; \qquad h_\alpha,\, k_\alpha,\, l_\alpha = 0,\, 1, \ldots \quad . \tag{4.10}$$

Therefore, we can see that, for $T = 0$, all particles occupy the states given by (4.10). Thus, the time-of-flight picture is just an image of the reciprocal lattice. For the simple cubic lattice discussed here, the reciprocal lattice is also a simple cubic one [72] as it is shown in Fig. 4.3. We want to mention here the similarity to X-ray diffraction where also sharp peaks at the reciprocal lattice points exist which are called Bragg peaks. These peaks stem from the constructive interference of *electromagnetic* waves scattered at the atoms on the lattice sites while the peaks in our case stem from the interference of *matter* waves. The former are really non-interacting, while for the latter we have only used this assumption as a rough approximation deep in the superfluid phase. We will see in the next subsection that in the Mott phase, where interactions are important, the situation changes dramatically and the analogy with Bragg scattering gets destroyed.
Note that it is also, at least in principle, possible to take the limit of vanishing interaction as a starting point and consider the effects which are due to the interaction perturbatively. However, this approach does not yield a quantum phase transition, i.e. the system is superfluid for every value of the interaction strengths as discussed in Ref. [71]. Furthermore, there is some additional issue when considering the Bose-Hubbard model in the weak-coupling limit. When we have decomposed the wave function in (2.9), we have used the Wannier functions which are sharply peaked around the lattice sites. This enabled us to neglect all but the on-site interactions and all but the nearest neighbor hopping processes. These assumptions are surely no longer true when the optical lattice is switched off completely. This situation corresponds to a homogeneous Bose gas where all atoms are known to occupy the state with $\mathbf{k} = \mathbf{0}$ for $T = 0$ [73,74]. Thus, we expect the sharp interference peaks which are shown in Fig. 4.3 to be existent only for not too low lattice depths. For even lower lattices all peaks but the one in the middle, i.e. the one corresponding to $\mathbf{k} = \mathbf{0}$, should become weaker and completely disappear for vanishing lattice depth $V_0 \to 0$. This theoretical prediction is also confirmed by the experimental observations in Ref. [17].

4.1.2 Correlation Functions

After having roughly examined the limit of vanishing interaction, we now come back to the strong-coupling limit. In a first step, we calculate the correlation function of the creation and annihilation operators $\langle \hat{a}^\dagger_{k\alpha} \hat{a}_{l\alpha} \rangle$, which is first done for zero temperature and in the next subsection generalized to finite temperatures. For $T = 0$, the symbol $\langle \cdot \rangle$ denotes the quantum mechanical expectation value over the ground state of the system. The mean-field approach, which has been successfully employed to calculate phase boundaries, is not suitable here. The reason for this is the fact that the Hamiltonian (3.33) is local and, therefore, correlations between different lattice sites are zero in the whole Mott phase. A far better and conceptually even easier idea is to take the full Bose-Hubbard Hamiltonian (2.18) and employ the so-called strong-coupling expansion [75]. Here we use the hopping term (3.28) as a perturbation to calculate shifts to the eigenenergies and eigenstates with the help of Rayleigh-Schrödinger perturbation theory. Because we are dealing with a non-local Hamiltonian now, we have to find a convention for denoting states with different values of S, m, and n on different lattice sites. Because the unperturbed Hamiltonian (3.12) is local, the ground state of $\hat{H}_0$ has the same quantum numbers on every site, which we will denote by $\{\mathbf{S}, \mathbf{m}, \mathbf{n}\}$. When some sites have different quantum numbers, these will be stated explicitly. For example, the state $|\{\mathbf{S}, \mathbf{m}, \mathbf{n}\}, \{S_i, m_i, n_i\}\rangle$ has the quantum numbers S_i, m_i, n_i on the lattice sites i while the other sites have the quantum S, m, n. Note that our approach is restricted to the case $\eta \neq 0$ because for $\eta = 0$ we have a degenerated ground state for an odd particle number per site. Therefore, the undegenerated perturbation theory does not apply and we would have to consider degenerated perturbation theory instead. However, we will not carry out these calculations here because the finite-temperature approach described later on will provide us with tools to consider this situation in a much easier way. In order to find the correlation functions which read

$$\langle \hat{a}^\dagger_{k\alpha} \hat{a}_{l\alpha} \rangle = \langle \Phi | \hat{a}^\dagger_{k\alpha} \hat{a}_{l\alpha} | \Phi \rangle \quad , \tag{4.11}$$

where Φ is the ground state of the system, we need to find the shifts to the energies first. The first order shifts read

$$E^{(1)}_{\{\mathbf{S},\mathbf{m},\mathbf{n}\}} = \langle\{\mathbf{S},\mathbf{m},\mathbf{n}\}|\hat{H}_1|\{\mathbf{S},\mathbf{m},\mathbf{n}\}\rangle = -Jz\sum_{\alpha}\sum_{<i,j>}\langle\{\mathbf{S},\mathbf{m},\mathbf{n}\}|\hat{a}^{\dagger}_{i\alpha}\hat{a}_{j\alpha}|\{\mathbf{S},\mathbf{m},\mathbf{n}\}\rangle = 0 \quad . \tag{4.12}$$

The corresponding first-order shifts to the eigenstates are given by

$$\begin{aligned}
|\{\mathbf{S},\mathbf{m},\mathbf{n}\}^{(1)}\rangle =& \sum_{\{\mathbf{S},\mathbf{m},\mathbf{n}\}'\neq\{\mathbf{S},\mathbf{m},\mathbf{n}\}} \frac{\langle\{\mathbf{S},\mathbf{m},\mathbf{n}\}'|\hat{H}_1\rangle\{\mathbf{S},\mathbf{m},\mathbf{n}\}\rangle}{E_{\{\mathbf{S},\mathbf{m},\mathbf{n}\}} - E_{\{\mathbf{S},\mathbf{m},\mathbf{n}\}'}}|\{\mathbf{S},\mathbf{m},\mathbf{n}\}'\rangle \\
=& J\sum_{<i,j>}\Bigg[\frac{M_{\alpha,S,m,n}O_{\alpha,S,m,n}}{U_0+(2S+2)U_2}|\{\mathbf{S},\mathbf{m},\mathbf{n}\},\{S_j{+}1,m_j{+}\alpha,n_j{-}1\},\{S_i{+}1,m_i{-}\alpha,n_i{-}1\}\rangle \\
&+\frac{N_{\alpha,S,m,n}O_{\alpha,S,m,n}}{U_0+U_2}|\{\mathbf{S},\mathbf{m},\mathbf{n}\},\{S_j{-}1,m_j{+}\alpha,n_j{-}1\},\{S_i{+}1,m_i{-}\alpha,n_i{-}1\}\rangle \\
&+\frac{M_{\alpha,S,m,n}P_{\alpha,S,m,n}}{U_0+U_2}|\{\mathbf{S},\mathbf{m},\mathbf{n}\},\{S_j{+}1,m_j{+}\alpha,n_j{-}1\},\{S_i{-}1,m_i{-}\alpha,n_i{-}1\}\rangle \\
&+\frac{N_{\alpha,S,m,n}P_{\alpha,S,m,n}}{U_0-2SU_2}|\{\mathbf{S},\mathbf{m},\mathbf{n}\},\{S_j{-}1,m_j{+}\alpha,n_j{-}1\},\{S_i{-}1,m_i{-}\alpha,n_i{-}1\}\rangle\Bigg] \quad .
\end{aligned} \tag{4.13}$$

Inserting (4.13) into (4.11), we can calculate

$$\begin{aligned}
\langle\hat{a}^{\dagger}_{k\alpha}\hat{a}_{l\alpha}\rangle =& \left(\langle\{\mathbf{S},\mathbf{m},\mathbf{n}\}| + \langle\{\mathbf{S},\mathbf{m},\mathbf{n}\}^{(1)}| + \ldots\right)\hat{a}^{\dagger}_{k\alpha}\hat{a}_{l\alpha}\left(|\{\mathbf{S},\mathbf{m},\mathbf{n}\}\rangle + |\{\mathbf{S},\mathbf{m},\mathbf{n}\}^{(1)}\rangle + \ldots\right) \\
=& \langle\{\mathbf{S},\mathbf{m},\mathbf{n}\}|\hat{a}^{\dagger}_{k\alpha}\hat{a}_{l\alpha}|\{\mathbf{S},\mathbf{m},\mathbf{n}\}\rangle + \langle\{\mathbf{S},\mathbf{m},\mathbf{n}\}|\hat{a}^{\dagger}_{k\alpha}\hat{a}_{l\alpha}|\{\mathbf{S},\mathbf{m},\mathbf{n}\}^{(1)}\rangle \\
&+ \langle\{\mathbf{S},\mathbf{m},\mathbf{n}\}^{(1)}|\hat{a}^{\dagger}_{k\alpha}\hat{a}_{l\alpha}|\{\mathbf{S},\mathbf{m},\mathbf{n}\}\rangle + \mathcal{O}(J^2) \quad .
\end{aligned} \tag{4.14}$$

From the denominators in (4.13) we see that the result does depend neither on the chemical nor on the magneto-chemical potential. The reason for this is that we are considering processes where one particle is created and another one annihilated, thus leaving the total particle number constant. Furthermore, these particles both carry $m_F = \alpha$, thus leaving also the magnetization constant. The values of η and μ are nevertheless important because they determine the ground state of the system as described in Section 3.2. Using the orthonormality of the unperturbed eigenstates (2.21), we get the result

$$\langle\hat{a}^{\dagger}_{k\alpha}\hat{a}_{l\alpha}\rangle = \delta_{kl}n_{\alpha} + \delta_{d(k,l),1}2JC_{\alpha} + \mathcal{O}(J^2) \tag{4.15}$$

with the coefficients

$$n_{\alpha} = O^2_{\alpha,S,m,n} + P^2_{\alpha,S,m,n} \tag{4.16}$$

and

$$C_{\alpha} = \frac{M^2_{\alpha,S,m,n}O^2_{\alpha,S,m,n}}{U_0+(2S+2)U_2} + \frac{M^2_{\alpha,S,m,n}P^2_{\alpha,S,m,n}}{U_0+U_2} + \frac{N^2_{\alpha,S,m,n}O^2_{\alpha,S,m,n}}{U_0+U_2} + \frac{N^2_{\alpha,S,m,n}P^2_{\alpha,S,m,n}}{U_0-2SU_2} \quad . \tag{4.17}$$

In a magnetized gas with $\eta > 0$, there is always $m = S$ for a system in the ground state and we can, therefore, use the formulas for the matrix elements in Appendix A to write down the expansion coefficients in a more explicit form:

$$n_1 = \frac{n+(n+2)S+S^2}{3+2S} \quad , \tag{4.18}$$

$$C_1 = \frac{(n-S)(S+1)(n+S+3)}{(2S+1)(2S+3)^2[U_0+(2S+2)U_2]} + \frac{(n+S+3)(n+S+1)(S+1)S}{[4(S+2)S+3](U_0+U_2)} \quad . \tag{4.19}$$

The other two components are calculated in a completely analogous way. The respective results are:

$$n_0 = \frac{n-S}{2S+3} \quad , \tag{4.20}$$

$$C_0 = \frac{2(n-S)(n+S+3}{(2S+3)^2[U_0+2(S+2)U_2]} \tag{4.21}$$

for the component with $\alpha = 0$ and

$$n_{-1} = \frac{(n-S)(S+1)}{2S+3} \quad , \tag{4.22}$$

$$C_{-1} = 2(n-S)(S+1)\left\{\frac{(n-S+2)S}{[3+4S(S+2)](U_0+U_2)} + \frac{n+S+3}{(2S+1)(2S+3)^2[U_0+2(S+1)U_2]}\right\} \tag{4.23}$$

for the one with $\alpha = -1$. When we sum (4.18), (4.20), and (4.22) we obtain the relation

$$n_1 + n_0 + n_{-1} = n \quad , \tag{4.24}$$

which is of course also obvious on physical ground because the sum of the particle number in the different hyperfine spin components must just be the total particle number. Because of its connection to the scalar Bose-Hubbard model, as discussed above, we briefly consider the limit of a fully polarized gas. In order to obtain a result in this limit, we remember that for this special situation, we have $n = S$ and put this together with $U = U_0 + U_2$ into (4.18) to obtain $n_1 = n$, $C_1 = n(n+1)$. From (4.17) we get in this special situation, furthermore, $n_0 = n_{-1} = C_0 = C_{-1} = 0$. This is exactly the result obtained by directly considering the Bose-Hubbard model for scalar Bosons as done in Ref. [23]. To find out more about the correlations, we have a closer look at (4.15). The first term is local, it is just the boson number per site in the state $m_F = \alpha$. The second term is proportional to the hopping element and describes correlations between sites which are nearest neighbors. Because of the simple perturbation theory which we have applied, there are no correlations between sites which are more than one lattice spacing away. In general, we can say that, if we neglect terms of the order J^n, then

$$\langle \hat{a}^\dagger_{k\alpha} \hat{a}_{l\alpha} \rangle = 0 \quad \text{for } d(k,l) \geq n \quad . \tag{4.25}$$

From this fact, one can see that this simple strong-coupling expansion breaks down near the critical point where we expect correlations on all length scales [5, 76]. To get the phase boundary from the strong-coupling expansion, a resummation is necessary, which will be done for the special case of spinless Bosons in Subsection 6.1.2.

The ratio between C_α and n_α in (4.15) is a good measure for the strength of the correlations between different lattice sites. In Fig. 4.1 we have plotted this ratio against U_2. Note that here we did not, like in the previous presentations, normalize to U_0 but to $U_{\text{total}} = U_0 + U_2$. The reason for this is that we want to see the effects resulting from the spin asymmetric interaction and not the trivial lowering of the correlations with higher *total* interaction.

4.1.3 Time-of-Flight Pictures

Now we turn to the calculation of the momentum space density generalizing the approach used in Ref. [23] for the scalar Bose-Hubbard model. It reads

$$n_\alpha(\mathbf{k}) = \langle \hat{\Psi}^\dagger_\alpha(\mathbf{k}) \hat{\Psi}_\alpha(\mathbf{k}) \rangle \quad , \tag{4.26}$$

where the field-operators in momentum-space $\hat{\Psi}^\dagger_\alpha(\mathbf{k})$ and $\hat{\Psi}(\mathbf{k})_\alpha$ are the Fourier transforms of the field-operators in real-space, i.e. $\hat{\Psi}^\dagger(\mathbf{x})_\alpha$ and $\hat{\Psi}(\mathbf{x})_\alpha$, which occur in (2.7). With the definition of the Fourier transform and the Wannier decomposition (2.9) we obtain from (4.26)

$$n_\alpha(\mathbf{k}) = \frac{1}{(2\pi)^3} \sum_{i,j} \int d^3\mathbf{x} \int d^3\mathbf{x}' e^{i\mathbf{k}\mathbf{x}} w^*(\mathbf{x}) e^{-i\mathbf{k}\mathbf{x}'} w(\mathbf{x}') e^{i\mathbf{k}(\mathbf{x}_i - \mathbf{x}_j)} \langle \hat{a}^\dagger_{i\alpha} \hat{a}_{j\alpha} \rangle \quad . \tag{4.27}$$

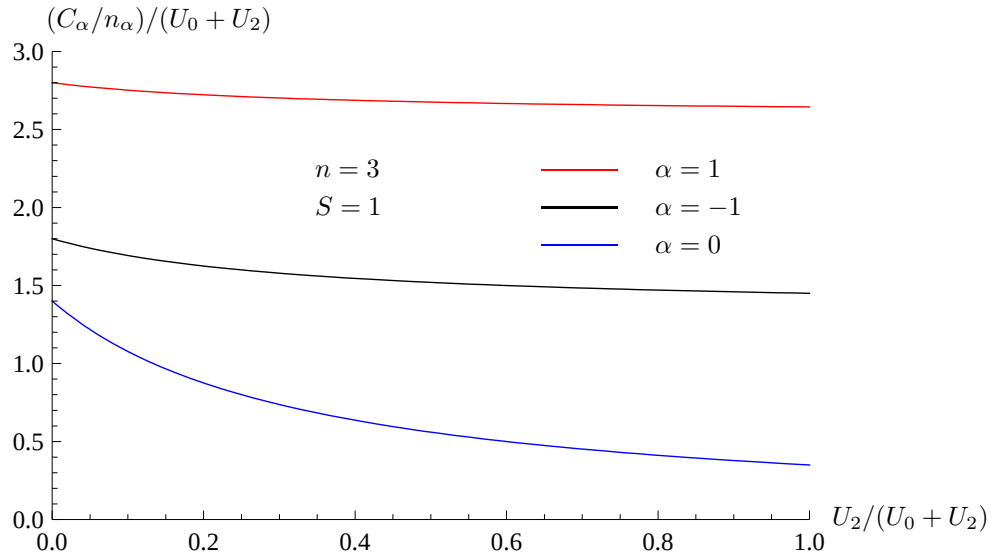

Figure 4.1: Relative amount of correlations between nearest-neighbor sites depending on the spin asymmetric interaction.

Now we introduce the explicit form of the Fourier transform of the Wannier function in the harmonic approximation

$$w(\mathbf{k}) = \frac{a^3}{\pi^{9/2}\sqrt{\tilde{V}_0{}^3}} \exp\left(-\frac{a^3}{\pi^2\sqrt{\tilde{V}_0}}\mathbf{k}^2\right) \tag{4.28}$$

with the dimensionless lattice depth $\tilde{V}_0 = V_0/E_R$. Inserting this together with the quasi-momentum distribution

$$S_\alpha(\mathbf{k}) = \sum_{i,j}\langle \hat{a}^\dagger_{i\alpha}\hat{a}_{j\alpha}\rangle e^{i\mathbf{k}(\mathbf{x}_i-\mathbf{x}_j)} \tag{4.29}$$

into (4.27) allows us to write

$$n_\alpha(\mathbf{k}) = |w(\mathbf{k})|^2 S_\alpha(\mathbf{k}) \quad . \tag{4.30}$$

Inserting (4.15) into (4.29) yields the result

$$S_\alpha(\mathbf{k}) = N_S\left[n_\alpha + 4JC_\alpha\sum_{\nu=1}^{3}\cos(k_\nu a) + \ \ldots\right] \quad . \tag{4.31}$$

Because the experimental absorption pictures are only two-dimensional, we must integrate our result for the momentum-space density (4.30) over one axis, which is here chosen to be the z-axis. Having a closer look at Eqs. (4.29)–(4.30) we see that the only contribution which does not only yield an overall prefactor is

$$\int_{-\infty}^{\infty} dk_z \ \exp\left(-\frac{1}{\pi^2\sqrt{\tilde{V}_0}}\mathbf{k}^2\right)\cos k_z a = \frac{\pi^{3/2}\tilde{V}_0^{1/4}}{a}\exp\left(-\frac{\pi^2\sqrt{\tilde{V}_0}}{4}\right) \quad . \tag{4.32}$$

We note that for large lattice depths, i.e. $\tilde{V}_0 \gg 1$, the contribution from (4.32) in negligible. This means that, deep in the Mott regime, we can drop the term with $\cos(k_z a)$ in (4.29) and skip the integration over the z-axis. Thus, we can consider an effective two-dimensional system. However, for shallow lattices the contribution (4.32) becomes important. Therefore, we have taken it into account when calculating the pictures, which we have plotted in Fig. 4.2.

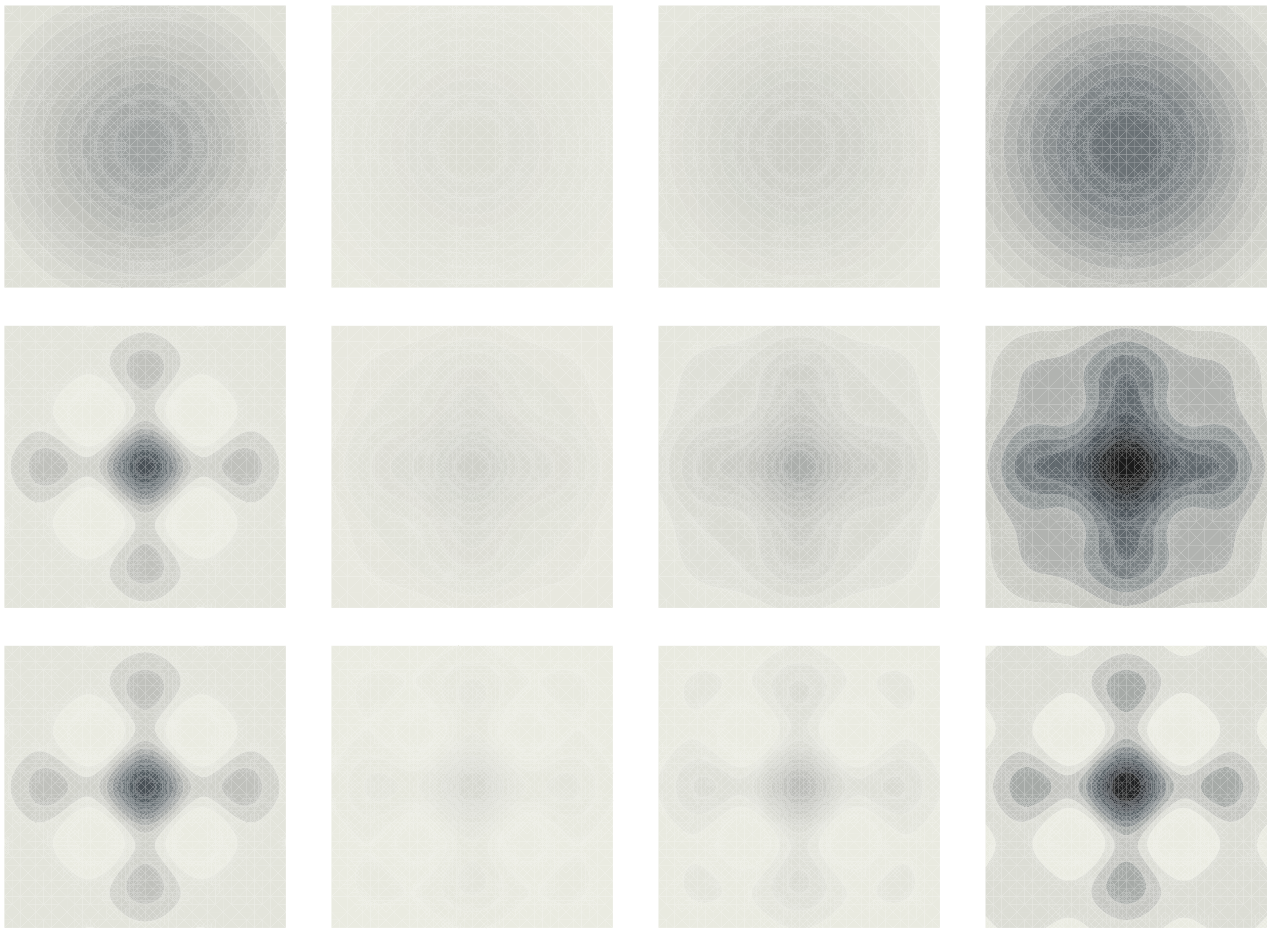

Figure 4.2: Theoretically calculated time-of-flight pictures for $S = 1$, $n = 3$, and $U_2 = 0.04\,U_0$. From left to right: $n_1(\mathbf{k})$, $n_0(\mathbf{k})$, $n_{-1}(\mathbf{k})$, $n(\mathbf{k})$. Lattice depth: $V_0 = 30\,E_R$ (First line), $V_0 = 14\,E_R$ (Second line), $V_0 = 8\,E_R$ (Third line).

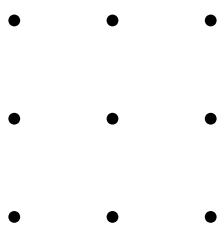

Figure 4.3: Momentum-space density for the limit of vanishing interaction. Note that the black spots are infinitely small.

One can clearly see from these pictures that, for deep lattices, there are no structures. This is understandable because in the deep Mott regime the particles on different sites are completely isolated from each other. Their relative phases are random and there exists no coherence between them. Therefore, one should not expect any interferences. When the lattice is made shallower, more tunneling takes places and interferences occur which lead to the dark spots visible in Fig. 4.2. We want to stress here again that the used strong-coupling expansion is only valid in the Mott phase and it is quite a crude approximation to use it, for example, in Fig. 4.2 where the value $V_0 = 8\,E_R$ clearly corresponds to a system in the superfluid phase. Therefore, the very sharp peaks seen in experiments [17, 77] and which are calculated in Section 4.1.1 are not reproduced by the theory presented here.
The effects arising from the spin-dependent interaction are not clearly visible in Fig. 4.2, because they change the situation not in a *qualitative*, but only in a *quantitative* way, as it is already expected from Eqs. (4.30) and (4.31). The main intensity is concentrated in the spin-component parallel to the external field, while the other components are populated less and also show less correlations, as also seen in Fig. 4.1.

4.1.4 Visibility

The time-of-flight pictures, which were discussed above, are difficult to compare with experimental data in a quantitative way because of various unknown factors. For example, the pictures crucially depend on the sensitivity of the used detector. To overcome this problem, it is useful to define a quantity, which is independent of normalization, but incorporates the essential feature, i.e. the difference between dark and bright spots. The quantity, which is chosen conveniently, is called the visibility. It was used in the experimental work for spinless Bosons in Refs. [77, 78]. We extend this definition to the spin-1 case and write

$$\mathcal{V}_\alpha = \frac{n_{\alpha\max} - n_{\alpha\min}}{n_{\alpha\max} + n_{\alpha\min}} \quad , \tag{4.33}$$

where $n_{\alpha\max}$ and $n_{\alpha\min}$ are the maximal and minimal densities in the $k_x - k_y$ –plane. Restricting ourselves to deep lattices allows us to use the two-dimensional approximation described in Subsection 4.1.2. Thus, we can cancel the Fourier transform of the Wannier function arising from (4.30) and rewrite (4.33) as

$$\mathcal{V}_\alpha = \frac{S_\alpha(\mathbf{k}_{\max}) - S_\alpha(\mathbf{k}_{\min})}{S_\alpha(\mathbf{k}_{\max}) + S_\alpha(\mathbf{k}_{\min})} \quad , \tag{4.34}$$

where $\mathbf{k}_{\max} = (2\pi/a, 0)$ and $\mathbf{k}_{\min} = (\sqrt{2}\pi/a, \sqrt{2}\pi/a)$ are the positions of the first maximum and minimum in the *two*-dimensional $k_x - k_y$-plane.
Because the different hyperfine states enter (4.31) only via the coefficients n_α and C_α, the extremal values of the wave vectors $S_\alpha(\mathbf{k}_{\max})$ and $S_\alpha(\mathbf{k}_{\min})$ do not depend on the spin index α. The maximal value of the relevant cosine factor in the $k_x - k_y$ –plane, i.e.

$$\cos(k_x a) + \cos(k y_a) \quad , \tag{4.35}$$

is $\cos(2\pi) + \cos(2\pi) = 2$ while the minimal value is $\cos(\sqrt{2}\pi) + \cos(\sqrt{2}\pi) \approx -0.53$. Inserting these values into (4.34) yields

$$\mathcal{V}_\alpha = \frac{n_\alpha + 8JzC_\alpha - [n_\alpha + 8JzC_\alpha]\cos(\sqrt{2}\pi) + \ldots}{n_\alpha + 8JzC_\alpha + [n_\alpha + 8JzC_\alpha]\cos(\sqrt{2}\pi) + \ldots} \quad . \tag{4.36}$$

In order get the final first-order result, we must expand (4.36) for small J. Doing this yields

$$\mathcal{V}_\alpha = 4zJ\left[1 - \cos(\sqrt{2}\pi)\right]\frac{C_\alpha}{n_\alpha} + \mathcal{O}(J^2) \quad . \tag{4.37}$$

We see, that the result in (4.37) is directly proportional to the quantity C_α/n_α which we have already plotted in Fig. 4.1 as a function of the spin-dependent interaction.

4.2 Finite Temperature

In the previous section, we have calculated the correlation functions for $T = 0$, from which we were able to derive the corresponding time-of-flight pictures. In this section, we investigate how they are affected by finite temperature.

4.2.1 Correlation Functions

In this subsection, we calculate the correlation function for finite temperature up to first order in the hopping parameter J. In order to do this, we will employ exactly the same formalism which was also used for the calculation of the grand-canonical free energy in mean-field approximation in Section 3.5. The correlation function for finite temperature is defined as the thermal average

$$\langle \hat{a}^\dagger_{k\alpha} \hat{a}_{l\alpha} \rangle = \frac{1}{\tilde{\mathcal{Z}}} \mathrm{Tr} \left\{ \hat{a}^\dagger_{k\alpha} \hat{a}_{l\alpha}\, e^{-\beta \hat{H}} \right\} \quad , \tag{4.38}$$

where $\tilde{\mathcal{Z}}$ is the partition function of the full non-local Hamiltonian (2.18). Now we write Eq. (4.38) in complete analogy to (3.76) as

$$\langle \hat{a}^\dagger_{k\alpha} \hat{a}_{l\alpha} \rangle = \frac{1}{\tilde{\mathcal{Z}}} \mathrm{Tr} \left\{ \hat{a}^\dagger_{k\alpha} \hat{a}_{l\alpha}\, e^{-\beta \hat{H}_0} U_\mathrm{D}(\beta, 0) \right\} \quad , \tag{4.39}$$

where the Dirac time-evolution operator is given by the Dyson series (3.72) with the perturbation operator (3.28) which reads in the Dirac picture:

$$\hat{H}_{1\mathrm{D}}(\tau) = -J \sum_{<i,j,>} e^{\hat{H}_0 \tau} \sum_\alpha \hat{a}^\dagger_{i\alpha} \hat{a}_{j\alpha}\, e^{-\hat{H}_0 \tau} \quad . \tag{4.40}$$

Note that in the denominator in (4.39), we have the full partition function $\tilde{\mathcal{Z}}$ which must be also calculated as a power series in the hopping matrix element J. Because the diagonal matrix elements of the perturbation Hamiltonian (3.28) vanish, which stems from the fact that

$$\langle \{\mathbf{S}, \mathbf{m}, \mathbf{n}\} | \hat{a}^\dagger_{i\alpha} \hat{a}_{j\alpha} | \{\mathbf{S}, \mathbf{m}, \mathbf{n}\} \rangle = 0 \quad , \qquad i \neq j \quad , \tag{4.41}$$

there is no first-order contribution to the partition function. Thus, we can replace the full partition function $\tilde{\mathcal{Z}}$ in (4.39) by the unperturbed partition function $\tilde{\mathcal{Z}}^{(0)}$ which is connected to the known partition function of the local system in Eq. (3.27) by

$$\tilde{\mathcal{Z}}^{(0)} = \left[\mathcal{Z}^{(0)} \right]^{N_S} \quad . \tag{4.42}$$

Now we take (3.72) up to first order and insert it into (4.39). When we now write the trace in a more explicit form, we obtain for the zeroth order

$$\langle \hat{a}^\dagger_{k\alpha} \hat{a}_{l\alpha} \rangle^{(0)} = \delta_{k,l} \langle \hat{n}_\alpha \rangle^{(0)} = \frac{\delta_{k,l}}{\mathcal{Z}^{(0)}} \sum_{S,m,n} \langle S, m, n | \hat{a}^\dagger_\alpha \hat{a}_\alpha | S, m, n \rangle e^{-\beta E_{S,m,n}} \quad , \tag{4.43}$$

where it is worth noting that this result, unlike its zero-temperature analog, does depend on the chemical and the magneto-chemical potential. The reason for this is obvious: Because for finite temperature no integer average particle number or magnetization exists, the parameters μ and η are needed to control those quantities. With the help of (A.89), Eq. (4.43) can be simplified to

$$\langle \hat{a}^\dagger_{k\alpha} \hat{a}_{l\alpha} \rangle^{(0)} = \frac{\delta_{k,l}}{\mathcal{Z}^{(0)}} \sum_{S,m,n} \left[O^2_{\alpha,S,m,n} + P^2_{\alpha,S,m,n} \right] e^{-\beta E_{S,m,n}} \quad . \tag{4.44}$$

The first order in J yields for the correlation function

$$\langle \hat{a}^\dagger_{k\alpha}\hat{a}_{l\alpha}\rangle^{(1)} = \sum_{\{\mathbf{S},\mathbf{m},\mathbf{n}\}} \frac{J}{\tilde{\mathcal{Z}}^{(0)}} \langle\{\mathbf{S},\mathbf{m},\mathbf{n}\}|\hat{a}^\dagger_{k\alpha}\hat{a}_{l\alpha}\, e^{-\beta\hat{H}_0} \sum_\gamma \sum_{<i,j>} \int_0^\beta d\tau\, \hat{a}^\dagger_{i\gamma}\hat{a}_{j\gamma}|\{\mathbf{S},\mathbf{m},\mathbf{n}\}\rangle \quad . \tag{4.45}$$

Because we only sum over diagonal elements, we must have equal numbers of creation and annihilation operators on every sites. Together with the same argument for the magnetic quantum number m, Eq. (4.45) becomes

$$\langle \hat{a}^\dagger_{k\alpha}\hat{a}_{l\alpha}\rangle^{(1)} = \frac{\delta_{d(l,k),1}J}{\mathcal{Z}^{(0)}} \sum_{\{\mathbf{S},\mathbf{m},\mathbf{n}\}} \langle\{\mathbf{S},\mathbf{m},\mathbf{n}\}|\hat{a}^\dagger_{k\alpha}\hat{a}_{l\alpha}\, e^{-\beta\hat{H}_0} \int_0^\beta d\tau\, \hat{a}^\dagger_{k\alpha}\hat{a}_{l\alpha}|\{\mathbf{S},\mathbf{m},\mathbf{n}\}\rangle \quad . \tag{4.46}$$

With the matrix elements from Appendix A and the energy eigenvalues of the unperturbed Hamiltonian (3.14) we obtain from (4.46)

$$\begin{aligned}
\langle \hat{a}^\dagger_{k\alpha}\hat{a}_{l\alpha}\rangle^{(1)} = {} & \frac{\delta_{d(l,k),1}J}{\mathcal{Z}^{(0)2}} \sum_{S_l,m_l,n_l} \sum_{S_k,m_k,n_k} \\
\times \Bigg[& M^2_{\alpha,S_k,m_k,n_k} O^2_{\alpha,S_l,m_l,n_L} \int_0^\beta e^{-\tau(E_{S_l,m_l,n_l}+E_{S_k,m_k,n_k})} e^{(\tau-\beta)(E_{S_l+1,m_l-\alpha,n_l-1}+E_{S_k+1,m_k+\alpha,n_k+1})} \\
& M^2_{\alpha,S_k,m_k,n_k} P^2_{\alpha,S_l,m_l,n_l} \int_0^\beta e^{-\tau(E_{S_l,m_l,n_l}+E_{S_k,m_k,n_k})} e^{(\tau-\beta)(E_{S_l-1,m_l-\alpha,n_l-1}+E_{S_k+1,m_k+\alpha,n_k+1})} \\
& N^2_{\alpha,S_k,m_k,n_k} O^2_{\alpha,S_l,m_l,n_l} \int_0^\beta e^{-\tau(E_{S_l,m_l,n_l}+E_{S_k,m_k,n_k})} e^{(\tau-\beta)(E_{S_l+1,m_l-\alpha,n_l-1}+E_{S_k-1,m_k+\alpha,n_k+1})} \\
& N^2_{\alpha,S_k,m_k,n_k} P^2_{\alpha,S_l,m_l,n_l} \int_0^\beta e^{-\tau(E_{S_l,m_l,n_l}+E_{S_k,m_k,n_k})} e^{(\tau-\beta)(E_{S_l-1,m_l-\alpha,n_l-1}+E_{S_k-1,m_k+\alpha,n_k+1})} \Bigg] \quad .
\end{aligned} \tag{4.47}$$

The following calculation is rather tedious but neither mathematically or physically enlightening and, therefore, deferred to Appendix B. Its final result (B.12) reads

$$\begin{aligned}
\langle \hat{a}^\dagger_{k\alpha}\hat{a}_{l\alpha}\rangle^{(1)} = {} & \frac{\delta_{d(l,k),1}2J}{\mathcal{Z}^{(0)2}} \sum_{S_l,m_l,n_l} \sum_{S_k,m_k,n_k} e^{-\beta(E_{S_k,m_k,n_k}-E_{S_l,m_l,n_l})} \\
\times \Bigg[& \frac{M^2_{\alpha,S_k,m_k,n_k} O^2_{\alpha,S_l,m_l,n_l}}{U_0(n_k-n_l+1)+U_2(S_k+S_l+2)} + \frac{M^2_{\alpha,S_k,m_k,n_k} P^2_{\alpha,S_l,m_l,n_l}}{U_0(n_k-n_l+1)+U_2(S_l-S_k+1)} \\
& + \frac{N^2_{\alpha,S_k,m_k,n_k} O^2_{\alpha,S_l,m_l,n_l}}{U_0(n_k-n_l+1)+U_2(S_k-S_l+1)} + \frac{N^2_{\alpha,S_k,m_k,n_k} P^2_{\alpha,S_l,m_l,n_l}}{U_0(n_k-n_l+1)-U_2(S_k+S_l)} \Bigg] \quad .
\end{aligned} \tag{4.48}$$

When we take the zero-temperature limit of (4.48), we can easily see that we get back (4.17) which is the result we calculated directly with ordinary $T = 0$ perturbation theory. Therefore, our finite temperature calculation is consistent with our previous result.

4.2.2 Particle Number

Before we come to the discussion of the temperature dependence of the correlation function, it is instructive to consider the thermal averages of the on-site particle numbers in the three hyperfine

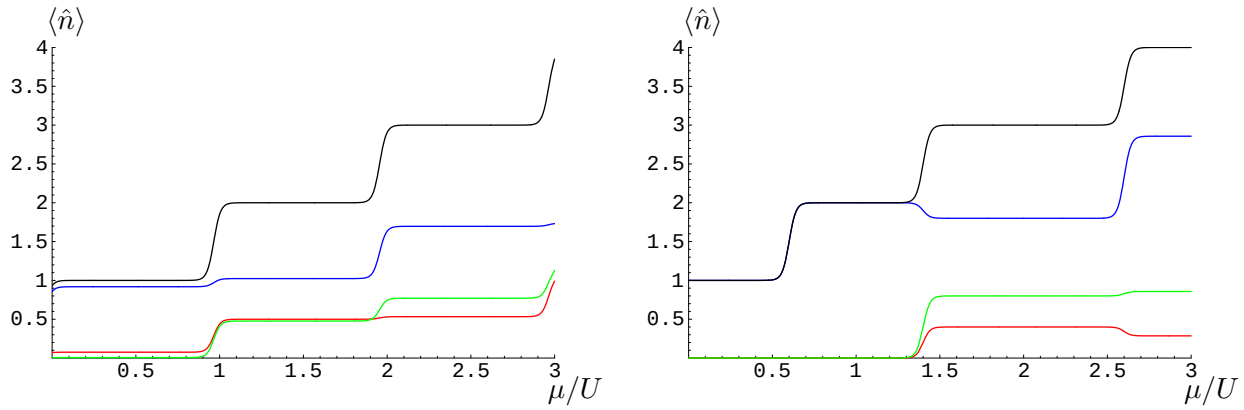

Figure 4.4: Thermal average of particle number per site for the different hyperfine states for the parameters $U_2/U_0 = 0.05$, $\eta/U_0 = 0.05$ (left), and $U_2/U_0 = 0.5$, $\eta/U_0 = 0.9$ (right). Blue: $\langle \hat{n}_1 \rangle$. Red: $\langle \hat{n}_0 \rangle$. Green: $\langle \hat{n}_{-1} \rangle$. Black: total, $\langle \hat{n} \rangle$.

components with respect to the unperturbed Hamiltonian (3.12). These quantities are given by (4.44). Note that in Fig. 3.1 we have only shown the total particle number per site, while we now want to resolve the different spin components. When we consider a non-magnetized system, i.e. $\eta = 0$, all hyperfine components have the same particle numbers, i.e

$$\langle \hat{n}_1 \rangle = \langle \hat{n}_0 \rangle = \langle \hat{n}_{-1} \rangle = \frac{1}{3} \langle \hat{n} \rangle \quad , \tag{4.49}$$

where we have omitted the index $^{(0)}$. This is also clear for symmetry reasons. When the system is magnetized, i.e. $\eta > 0$, the situation becomes more interesting because the occupation numbers of the different hyperfine components differ from each other and change also in a non-trivial way with the chemical potential μ. This effect stems again from the competition between the Zeeman energy η, the spin-dependent interaction energy U_2, and the thermal energy $k_B T$. In Fig. 4.4, we have plotted this dependence for the parameter values which were also used when discussing the phase boundary in Chapter 3.

4.2.3 Visibility

Because of the structure of (4.15), temperature can not change the time-of-flight pictures in a qualitative way. The only quantities which are affected are the coefficients n_α and C_α in (4.17). The first-order expression for the correlation function (4.15) now reads

$$\langle \hat{a}^\dagger_{k\alpha} \hat{a}_{l\alpha} \rangle = \delta_{kl} n_\alpha(T) + \delta_{d(k,l),1} 2J C_\alpha(T) + \mathcal{O}(J^2) \quad . \tag{4.50}$$

Comparing (4.43) and (4.48) with (4.31) we can write the temperature-dependent coefficients in (4.50) as

$$\begin{aligned} n_\alpha(T) =& \langle \hat{a}^\dagger_{k\alpha} \hat{a}_{l\alpha} \rangle^{(0)} = \frac{1}{\mathcal{Z}^{(0)}} \sum_{S,m,n} \langle S,m,n | \hat{a}^\dagger_{k\alpha} \hat{a}_{k\alpha} | S,m,n \rangle e^{-\beta E_{s,m,n}} \\ =& \frac{1}{\mathcal{Z}^{(0)}} \sum_{S,m,n} \left[O^2_{\alpha,S,m,n} + P^2_{\alpha,S,m,n} \right] e^{-\beta E_{S,m,n}} \end{aligned} \tag{4.51}$$

and

$$C_\alpha(T) = \frac{1}{\mathcal{Z}^{(0)2}} \sum_{S_l,m_l,n_l} \sum_{S_k,m_k,n_k} e^{-\beta(E_{S_k,m_k,n_k}+E_{S_l,m_l,n_l})} \times \left[\frac{M^2_{\alpha,S_k,m_k,n_k} O^2_{\alpha,S_l,m_l,n_l}}{U_0(n_k-n_l+1)+U_2(S_k+S_l+2)} + \frac{M^2_{\alpha,S_k,m_k,n_k} P^2_{\alpha,S_l,m_l,n_l}}{U_0(n_k-n_l+1)+U_2(S_l-S_k+1)} + \frac{N^2_{\alpha,S_k,m_k,n_k} O^2_{\alpha,S_l,m_l,n_l}}{U_0(n_k-n_l+1)+U_2(S_k-S_l+1)} + \frac{N^2_{\alpha,S_k,m_k,n_k} P^2_{\alpha,S_l,m_l,n_l}}{U_0(n_k-n_l+1)-U_2(S_k+S_l)} \right] \quad . \tag{4.52}$$

Thus, the temperature-dependent visibility becomes

$$\mathcal{V}_\alpha(T) = 4zJ \left[1-\cos(\sqrt{2}\pi)\right] \frac{C_\alpha(T)}{n_\alpha(T)} + \mathcal{O}(J^2) \quad . \tag{4.53}$$

Furthermore, we define the total visibility as

$$\mathcal{V}(T) = 4zJ \left[1-\cos(\sqrt{2}\pi)\right] \frac{\sum_\alpha C_\alpha(T)}{\sum_\alpha n_\alpha(T)} + \mathcal{O}(J^2) \quad . \tag{4.54}$$

From (4.53) we see, that both the dependence of the visibility on the spin and its temperature dependence is contained in the ratio $C_\alpha(T)/n_\alpha(T)$ whose zero-temperature analog we have already shown in Fig. 4.1. Before turning to the general spinor case, we consider at first place the limiting case of a fully polarized system which is, as already discussed in Chapter 3, equivalent to the scalar Bose-Hubbard model. In Fig. 4.5, we have plotted (4.53) only for $\alpha = 1$ as the other components vanish. Comparing the left and the right side in Fig. 4.5, one notes that the visibility is larger for integer than for fractional fillings. The reason for this is the following: For fractional filling, the thermal fluctuations are larger. This is explained in more detail in Subsection 6.1.4. Thus, the quantum correlations between the sites, which produce the characteristic intensity distribution measured by the visibility, get more suppressed.

After having understood this special case, we now come back to our main problem. For a spinor system without magnetization, the visibility prefactors are the same for all hyperfine components. They get reduced for higher spin-dependent interaction as already encountered for the zero-temperature case in Fig. 4.1. Again, the situation is more interesting for a magnetized system. In Fig. 4.6 we have plotted the visibility prefactors for the three hyperfine components, while we have used the same parameters as in the discussion of the phase transition in Chapter 3. The most striking feature is the fact that the visibility for the components with $\alpha = 0$ and $\alpha = -1$ is not a monotonically decreasing function of the temperature. This seems a bit strange at first sight but becomes understandable after recalling that the zero temperature ground state for the used parameters is $|1,1,3\rangle$. Thus the components with $m = 0$ and $m = -1$ are not occupied at all for $T = 0$. Thermal fluctuations lead to an occupation of these states which results in an increasing visibility. But of course the competing process also takes place, i.e. the thermal fluctuations destroy the quantum correlations. For higher temperatures this process becomes dominant which results in a decreasing visibility.

To conclude the discussion of this chapter, we make the following remark: We have only considered the correlation function $\langle \hat{a}^\dagger_{i\alpha} \hat{a}_{j\alpha} \rangle$ but, of course, there also exist correlation functions $\langle \hat{a}^\dagger_{i\alpha} \hat{a}_{j\beta} \rangle$ with $\beta \neq \alpha$. They are also of interest but because there exists at the present time no experimental way to measure them, we will not consider them further.

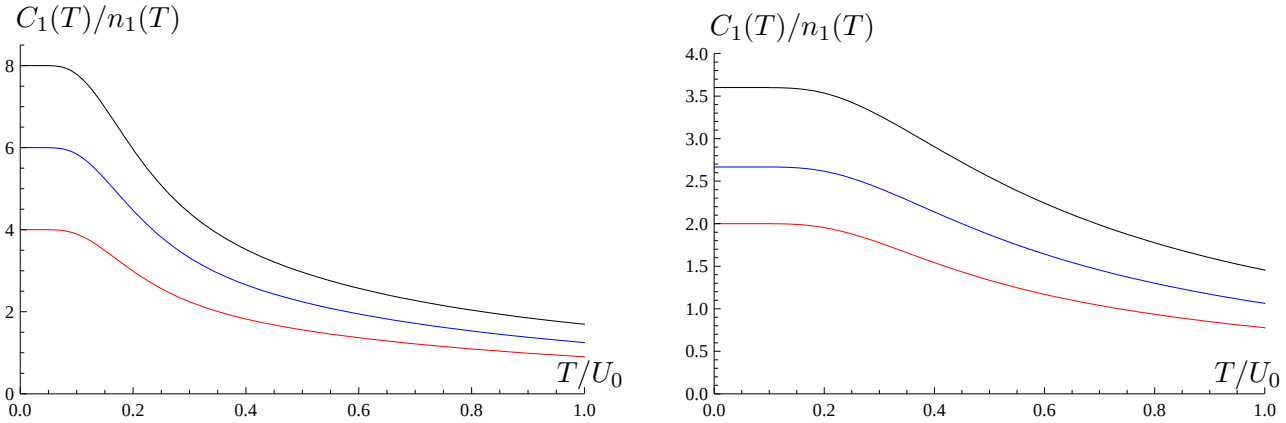

Figure 4.5: Visibility prefactor $C_1(T)/n_1(T)$ for fully polarized system. Left: Integer filling with $\langle n\rangle = 1$ (red), $\langle n\rangle = 2$ (blue), $\langle n\rangle = 3$ (black). Right: fractional filling: $\langle n\rangle = 0.5$ (red), $\langle n\rangle = 1.5$ (blue), $\langle n\rangle = 2.5$ (black).

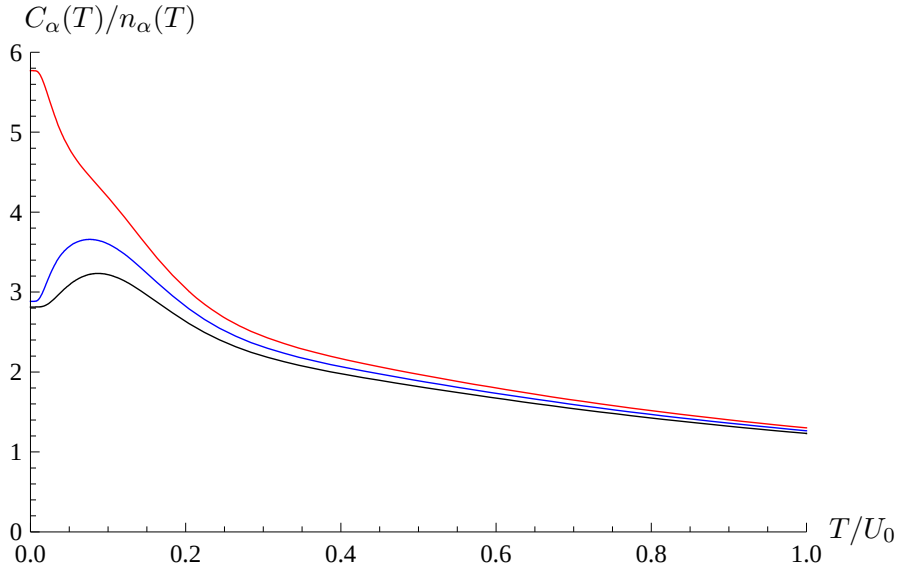

Figure 4.6: Visibility prefactor $C_\alpha(T)/n_\alpha(T)$ for the parameters $\eta = 0.05\,U_0$, $U_2 = 0.04\,U_0$, $\langle n\rangle = 1$ and the hyperfine components $\alpha = 1$ (red), $\alpha = 0$ (blue), $\alpha = -1$ (black).

Chapter 5

Diagrammatic Green's Functions Approach

In this chapter we introduce a different and more general method to calculate various properties of Bosons in optical lattices. We will restrict ourselves to the scalar Bose-Hubbard model which describes Bosons having no spin degrees of freedom. As we have already seen above, this corresponds to a fully polarized system where all atoms are in the same hyperfine state. As this is the experimentally realized situation when condensates are produced in magnetic traps, and these devices are used in most experiments, this case is very relevant.

5.1 Preliminaries

Before we turn to the development of our formalism, we have to state some preliminaries which we do in this section.

5.1.1 Scalar Bose-Hubbard Model

The scalar Bose-Hubbard model can be easily derived from scratch but here we just obtain it from the spin-1 model (2.18) by setting the spin-dependent interaction U_2 to zero. We do not need a magneto-chemical potential in this situation, so we can also set $\eta = 0$. Doing this and renaming $U_0 \to U$, we obtain the Hamiltonian

$$\hat{H} = \sum_i \frac{U}{2} \left[\hat{n}_i(\hat{n}_i - 1) - \mu \hat{n}_i\right] - J \sum_{<i,j>} \hat{a}_i^\dagger \hat{a}_j \quad , \tag{5.1}$$

where $\hat{n} = \hat{a}_i^\dagger \hat{a}_i$ denotes the particle-number operator on site i. As done in the previous chapters, we work in the strong-coupling limit and therefore split (5.1) into two parts:

$$\hat{H} = \hat{H}_0 + \hat{H}_1 \tag{5.2}$$

with

$$\hat{H}_0 = \sum_i \left[\frac{U}{2}\hat{n}_i(\hat{n}_i - 1) - \mu \hat{n}_i\right] \tag{5.3}$$

and

$$\hat{H}_1 = -J \sum_{<i,j>} \hat{a}_i^\dagger \hat{a}_j \quad . \tag{5.4}$$

As we see, the Hamiltonian $\hat{H}_0$ in Eq. (5.3) is diagonal with respect to the lattice sites. Thus, because all lattice sites are equivalent, its eigenstates and eigenvalues are given by

$$\hat{H}_0|n\rangle = N_S E_n|n\rangle \quad , \qquad E_n = \frac{U}{2}n(n-1) - \mu n \quad . \tag{5.5}$$

Because it is needed whenever considering the zero-temperature limit, we state here the connection between the chemical potential and the particle number per site for zero temperature: Minimizing (5.5) yields

$$(n-1) < \mu/U < n \quad , \tag{5.6}$$

which can be also obtained by setting $U_2 = 0$ in the spinor analog in Eqs. (3.15), (3.16).

5.1.2 Importance of Green's Functions

The quantity we are interested in is the one-particle Green function. In imaginary time it is defined as

$$G_1(\tau', j'|\tau, j) = \frac{1}{\mathcal{Z}}\mathrm{Tr}\left\{e^{-\beta\hat{H}}\hat{T}\left[\hat{a}_{j,\mathrm{H}}(\tau)\hat{a}^\dagger_{j',\mathrm{H}}(\tau')\right]\right\} \quad , \tag{5.7}$$

where

$$\hat{O}_\mathrm{H}(\tau) = e^{\hat{H}\tau}\hat{O}e^{-\hat{H}\tau} \tag{5.8}$$

denotes an imaginary-time Heisenberg operator and $\hat{T}$ the time ordering operator. We will see later on that the knowledge of the function (5.7) allows us to calculate both thermodynamic and dynamic quantities of interest. But in addition to regarding it merely as a mathematical tool, we can also associate a physical meaning to it. This is best seen not in imaginary but in real time where the Green function is also called the propagator [62]. It represents the probability amplitude of creating a particle at site j' and time t', transporting it to site j, and annihilating it there at time t. We shall keep that picture in mind even when performing calculations in imaginary time.

5.1.3 Interaction Picture

Because we do not know the eigenstates and energies of the full Hamiltonian (5.1), we cannot calculate the Green function (5.7) exactly. Instead, we aim at a perturbative treatment where the Green function (5.7) is calculated as a power series with respect to the hopping matrix element. To this end, we use once more the Dirac interaction picture which was already employed in Chapter 3. As calculated in Section 3.5, the Dyson series for the Dirac imaginary-time evolution operator reads

$$\hat{U}_\mathrm{D}(\tau, \tau_0) = \sum_{n=0}^{\infty}(-1)^n \int_{\tau_0}^{\tau} d\tau_1 \ldots \int_{\tau_0}^{\tau_{n-1}} d\tau_n \hat{H}_{1\mathrm{D}}(\tau_1)\ldots\hat{H}_{1\mathrm{D}}(\tau_n) \quad . \tag{5.9}$$

Using the imaginary-time ordering operator, Eq. (5.9) can be simplified to

$$\hat{U}_\mathrm{D}(\tau, \tau_0) = \sum_{n=0}^{\infty}\frac{(-1)^n}{n!}\int_{\tau_0}^{\tau} d\tau_1 \ldots \int_{\tau_0}^{\tau} d\tau_n \hat{T}\left[\hat{H}_{1\mathrm{D}}(\tau_1)\ldots\hat{H}_{1\mathrm{D}}(\tau_n)\right] = \hat{T}\exp\left(-\int_{\tau_0}^{\tau} d\tau_1 \hat{H}_{1\mathrm{D}}(\tau_1)\right) \quad . \tag{5.10}$$

Note that the factor $1/n!$ accounts for the number of possible permutations of the operators under the time ordering operator. Now we insert the explicit form of the hopping Hamiltonian (5.4). To shorten our notation, we drop the index D of the creation and annihilation operators in the following.

All time-dependent operators are in the Dirac picture unless explicitly stated otherwise. Thus, the perturbation operator (5.4) becomes

$$\hat{H}_{1\mathrm{D}}(\tau) = -J \sum_{<i,j>} \hat{a}_i^\dagger(\tau)\hat{a}_j(\tau) = -\sum_{i,j} J_{i,j}\hat{a}_i^\dagger(\tau)\hat{a}_j(\tau) \quad , \tag{5.11}$$

where we have introduced the generalized hopping matrix element

$$J_{ij} = \begin{cases} J & \text{if } i,j \text{ nearest neighbors} \\ 0 & \text{otherwise} \end{cases} \quad . \tag{5.12}$$

Inserting (5.11) into (5.10) yields

$$\hat{U}_{\mathrm{D}}(\tau,\tau_0) = \hat{T}\exp\left(\sum_{i,j} J_{ij}\int_{\tau_0}^{\tau} d\tau_1\, \hat{a}_i^\dagger(\tau_1)\hat{a}_j(\tau_1)\right) \quad . \tag{5.13}$$

5.1.4 Partition Function

Before turning to the calculation of (5.7), we determine the partition function which occurs in the denominator of (5.7) but is also an interesting quantity of itself because it determines thermodynamic quantities like the specific heat and the compressibility. As seen in Section 3.5, the partition function (3.8) can also be written as

$$\mathcal{Z} = \mathrm{Tr}\left\{e^{-\beta\hat{H}_0}\hat{U}_{\mathrm{D}}(\beta,0)\right\} \quad . \tag{5.14}$$

When we now insert (5.10) in (5.14), we can write the partition function in a power series in the hopping matrix element J. Doing this yields for the nth-order contribution

$$\mathcal{Z}^{(n)} = \frac{1}{n!}\tilde{\mathcal{Z}}^{(0)}\sum_{i_1,j_1,\ldots,i_n,j_n} J_{i_1j_1}\ldots J_{i_nj_n}\int_0^\beta d\tau_1\int_0^\beta d\tau_2\ldots\int_0^\beta d\tau_n \left\langle \hat{T}\left[\hat{a}_{i_1}^\dagger(\tau_1)\hat{a}_{j_1}(\tau_1)\ldots\hat{a}_{i_n}^\dagger(\tau_n)\hat{a}_{j_n}(\tau_n)\right]\right\rangle^{(0)} \quad . \tag{5.15}$$

Here we have used the partition function of the unperturbed system $\tilde{\mathcal{Z}}^{(0)}$ whose connection to the single-site unperturbed partition function

$$\mathcal{Z}^{(0)} = \sum_{n=0}^{\infty} e^{-\beta E_n} \tag{5.16}$$

is given in Eq. (4.42). Now we make an important observation: The thermal average occurring in (5.15) is just the n-particle Green function of the *unperturbed* system where some pairs of creation and annihilation operators have the same time arguments. The unperturbed n-particle Green function is defined as

$$G_n^{(0)}(\tau_1',i_1';\ldots;\tau_n',i_n'|\tau_1,i_1;\ldots;\tau_n,i_n) = \left\langle \hat{T}\left[\hat{a}_{i_1'}^\dagger(\tau_1')\hat{a}_{i_1}(\tau_1)\ldots\hat{a}_{i_n'}^\dagger(\tau_n')\hat{a}_{i_n}(\tau_n)\right]\right\rangle^{(0)} \quad . \tag{5.17}$$

Thus, we have reduced the problem of calculating the *full* partition function to the calculation of integrals over n-particle Green functions of the *unperturbed* system:

$$\mathcal{Z}^{(n)} = \frac{1}{n!}\tilde{\mathcal{Z}}^{(0)}\sum_{i_1,j_1,\ldots,i_n,j_n} J_{i_1j_1}\ldots J_{i_nj_n}\int_0^\beta d\tau_1\int_0^\beta d\tau_2\ldots\int_0^\beta d\tau_n G_n^{(0)}(\tau_1,i_1;\ldots;\tau_n,i_n|\tau_1,j_1;\ldots;\tau_n,j_n) \quad . \tag{5.18}$$

We will see later on that a similar relation also holds for the full one-particle Green function (5.7).

5.2 Cumulant Decomposition

The next step in our derivation is to decompose $G_n^{(0)}$, which is occurring in the perturbation series for the partition function in (5.18), into simpler parts. As already discussed in Chapter 3, we cannot use Wick's theorem to decompose this n-particle function into one-particle functions but we can decompose it into cumulants. To this end, we follow an approach reviewed by Metzner [79, 80] in the context of electrons in a conductor. A similar technique has been also used to describe systems of electrons and phonons [81, 82].

In order to find a decomposition of $G_n^{(0)}$, we first define a generating functional for them. This is achieved by coupling the creation and annihilation operators to external currents according to a standard technique from field theory [5, 56, 62, 76]. Because we are interested in the correlations of the unperturbed system, we use the Hamiltonian (5.3) and define

$$\hat{H}_0[j, j^*] = \hat{H}_0 - \sum_i \left[j_i(\tau)\hat{a}_i^\dagger + j_i^*(\tau)\hat{a}_i \right] \quad . \tag{5.19}$$

Note that the Hamiltonian is now explicitly time dependent because of the functional dependence on the current fields $j_i(\tau)$ and $j_i^*(\tau)$ on each lattice site. Now we go to the Dirac picture where we consider the currents in (5.19) as the perturbative contribution. Thus, we have

$$\hat{H}_{1\mathrm{S}}(\tau) = -\sum_i \left[j_i(\tau)\hat{a}_i^\dagger + j_i^*(\tau)\hat{a}_i \right] \quad , \tag{5.20}$$

where we have explicitly put the index S for Schrödinger picture. Equation (5.20) becomes in the Dirac picture

$$\hat{H}_{1\mathrm{D}}(\tau) = -\sum_i \left[j_i(\tau)\hat{a}_i^\dagger(\tau) + j_i^*(\tau)\hat{a}_i(\tau) \right] \quad . \tag{5.21}$$

Now we use (5.10) with (5.21) and obtain

$$\hat{U}_{\mathrm{D}}[j, j^*](\tau, \tau_0) = \hat{T} \exp\left\{ \sum_i \int_{\tau_0}^{\tau} d\tau_1 \left[j_i(\tau)\hat{a}_i^\dagger(\tau) + j_i^*(\tau)\hat{a}_i(\tau) \right] \right\} \quad , \tag{5.22}$$

which yields which (5.14)

$$\mathcal{Z}^{(0)}[j, j^*] = \left\langle \hat{T} \exp\left(\sum_i \int_0^{\beta} d\tau \left[j_i^*(\tau)\hat{a}_i(\tau) + j_i(\tau)\hat{a}_i^\dagger(\tau) \right] \right) \right\rangle^{(0)} \quad . \tag{5.23}$$

As it can be easily seen, the Green functions are obtained from this generating functional (5.23) by functional differentiation with respect to the currents:

$$G_n^{(0)}(\tau_1', i_1'; \ldots; \tau_n', i_n' | \tau_1, i_1; \ldots; \tau_n, i_n) = \frac{1}{\mathcal{Z}^{(0)}[j, j^*]} \frac{\delta^{2n} \mathcal{Z}^{(0)}[j, j^*]}{\delta j_{i_1'}(\tau_1') \ldots \delta j_{i_n'}(\tau_n') \delta j_{i_1}^*(\tau_1) \ldots \delta j_{i_n}^*(\tau_n)} \bigg|_{j=j^*=0} \quad . \tag{5.24}$$

This relation is for itself not of great practical value because we already know how to calculate $G_n^{(0)}$ directly according to (5.17). However, the generating functional allows us to find a representation of the Green functions in terms of cumulants. In order to find this connection, we define the generating functional of the cumulants as

$$C_0^{(0)}[j, j^*] = \log \mathcal{Z}^{(0)}[j, j^*] \quad . \tag{5.25}$$

The cumulants follow from (5.25) as the functional derivatives

$$C_n^{(0)}(\tau_1', i_1'; \ldots; \tau_n', i_n' | \tau_1, i_1; \ldots; \tau_n, i_n) = \frac{\delta^{2n}}{\delta j_{i_1'}(\tau_1') \ldots \delta j_{i_n'}(\tau_n') \delta j_{i_1}^*(\tau_1) \ldots \delta j_{i_n}^*(\tau_n)} C_0^{(0)}[j, j^*] \Big|_{j=j^*=0} \quad . \tag{5.26}$$

Because of the property of the logarithm, $\log(x \cdot y) = \log(x) + \log(y)$, and the fact that the unperturbed Hamiltonian (5.3) is a sum of local Hamiltonians on every site, i.e.

$$\hat{H}_0 = \sum_i \hat{H}_{0i} \quad , \quad \hat{H}_{0i} = \frac{1}{2} U \hat{n}_i (\hat{n}_i - 1) - \mu \hat{n}_i \quad , \tag{5.27}$$

we can write the generating functional of the cumulants as

$$C_0^{(0)}[j, j^*] = \sum_i \log \left\langle \hat{T} \exp \left(\int_0^\beta d\tau \left[j_i^*(\tau) \hat{a}_i(\tau) + j_i(\tau) \hat{a}_i^\dagger(\tau) \right] \right) \right\rangle^{(0)} \quad , \tag{5.28}$$

where $\langle \cdot \rangle^{(0)}$ denotes now an expectation value with respect to the *local* Hamiltonian $\hat{H}_{0i}$. Because (5.28) is a sum of local terms, the cumulants (5.26) must be local too. When differentiating (5.28) with respect to the current $j_h(\tau)$, all terms but the one with site index h become zero. When we now differentiate with respect to a current $j_k(\tau)$ with a site index $k \neq l$, we surely get zero.
Because all lattice sites are equivalent in a homogeneous system, which we are considering, and we do not care about normalization constants at the moment, we can drop the sum in (5.28) and work with an one-site creating functional. This allows us to redefine the generating functional of the cumulants as

$$C_0^{(0)}[j, j^*] = \log \left\langle \hat{T} \exp \left(\int_0^\beta d\tau \left[j^*(\tau) \hat{a}(\tau) + j(\tau) \hat{a}^\dagger(\tau) \right] \right) \right\rangle^{(0)} \quad , \tag{5.29}$$

where the square brackets now only denote a functional dependence on $j(\tau)$ and $j^*(\tau)$. With (5.29), the corresponding cumulants read

$$C_n^{(0)}(\tau_1', \ldots, \tau_n' | \tau_1, \ldots, \tau_n) = \frac{\delta^{2n}}{\delta j(\tau_1') \ldots \delta j(\tau_n') \delta j^*(\tau_1) \ldots \delta j^*(\tau_n)} C_0^{(0)}[j, j^*] \Big|_{j=j^*=0} \quad . \tag{5.30}$$

Until now the definition of these cumulants seems a bit artificial but their importance stems from the fact that they form the building blocks for constructing the Green function $G_m^{(0)}$. To see how this works, we discuss as an example the one- and the two-particle unperturbed Green functions. At first, we obtain by performing two functional derivatives on (5.29) according to (5.30)

$$\begin{aligned} G_1^{(0)}(\tau', i' | \tau, i) &= \frac{1}{\mathcal{Z}^{(0)}[j, j^*]} \frac{\delta^2}{\delta j_{i'}(\tau') \delta j_i^*(\tau)} \mathcal{Z}^{(0)}[j, j^*] \Big|_{j=j^*=0} = \frac{\delta^2}{\delta j_{i'}(\tau') \delta j_i^*(\tau)} C_0^{(0)}[j, j^*] \Big|_{j=j^*=0} \\ &= \delta_{i,i'} C_1^{(0)}(\tau' | \tau) \quad . \end{aligned} \tag{5.31}$$

When we calculate the higher n-particle functions, the product rule of functional differentiation produces all possible combinations of the cumulants. For example:

$$\begin{aligned} G_2^{(0)}(\tau_1', i_1'; \tau_2', i_2' | \tau_1, i_1; \tau_2, i_2) =& \delta_{i_1,i_2} \delta_{i_1',i_2'} \delta_{i_1,i_1'} C_2^{(0)}(\tau_1', \tau_2' | \tau_1, \tau_2) \\ &+ \delta_{i_1,i_1'} \delta_{i_2,i_2'} C_1^{(0)}(\tau_1' | \tau_1) C_1^{(0)}(\tau_2' | \tau_2) + \delta_{i_1,i_2'} \delta_{i_2,i_1'} C_1^{(0)}(\tau_2' | \tau_1) C_1^{(0)}(\tau_1' | \tau_2) \quad . \end{aligned} \tag{5.32}$$

This also holds for any higher functional derivatives. All possible ways to distribute the n primed and n unprimed variables equally of the 2, 4, 6, ...-particle functions must be summed. To find all these possible combinations and to connect them in the right way in order to sum and integrate over them according to (5.18) seems quite complicated. Fortunately, there exists a graphical way to manage this task which we introduce in the next section.

5.3 Basic Diagrammatic Calculations

In this section, we introduce diagrammatic rules to calculate the perturbative contributions to the partition function. They build a one-to-one representation of the perturbation series (5.18) with the cumulant decomposition of $G_n^{(0)}$, e.g. (5.32).

5.3.1 Diagrammatic Rules

We denote a m-particle cumulant at a lattice site by a vertex with m entering and m leaving lines with imaginary-time variables. The hopping matrix element is symbolized by a line connecting two vertices. For example:

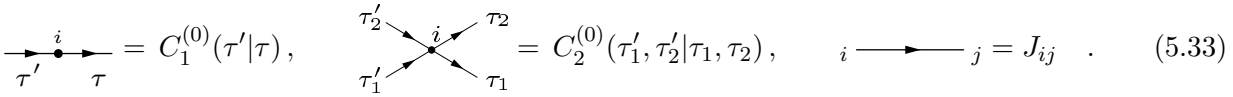

(5.33)

In Eq. (5.18), we must sum over all site indices and integrate all time variables. There are no free variables and because of this there are no external lines. With all this, we can set up the rules for calculating the vacuum diagrams contributing to the partition function in nth order in J:

1. Draw all possible combinations of vertices with total n entering and n leaving lines.
2. Connect them in all possibles ways and assign time variables and hopping matrix elements to the lines.
3. Sum all site indices over all lattice sites and integrate all time variables from 0 to β.

We also note here that we have to sum all site indices over the *whole* lattice, no matter whether two sites in a diagram coincide or not.

5.3.2 Weights and Multiplicities

The diagrammatic rules derived above are not sufficient to calculate the perturbative series for the partition function. In this subsection we introduce the symmetry factor which allows us to calculate the weight of the respective diagram. As discussed in Section 5.2, $G_n^{(0)}$ is decomposed into a sum of products of cumulants. We must know how many of them belong to the same diagram. We do this in a two-step process: For a given diagram there are $n!$ possible permutations of the internal time variables. But not all of them really belong to different terms in the cumulant decomposition. This fact is taken into account by the symmetry factor. Thus, the weight of a diagram can be written, including the prefactor $1/n!$ from the Taylor expansion in (5.18), as

$$\text{weight} = \frac{1}{n!}\,\frac{n!}{\text{symmetry factor}} \quad . \tag{5.34}$$

The symmetry factor can be calculated by counting the permutations of the time variables and vertex indices which do not change the topological structure of the diagram because they correspond to the same term in the cumulant decomposition. As an example, we consider the second-order vacuum diagram

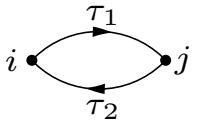

. (5.35)

From (5.32), we see that there is only one term in the decomposition which corresponds to this diagram. One can also see that the symmetry factor is 2, cancelling the two possible permutations of τ and τ'. Thus, the total weight of the considered diagram is 1/2. Weights for the fourth-order vacuum diagrams are given in Ref. [79].

5.3.3 Diagrammatic Series for Partition Function

With the help of the weights discussed in in the previous subsection, the diagrammatic series for the partition function reads

$\mathcal{Z} = \tilde{\mathcal{Z}}^{(0)} +$ 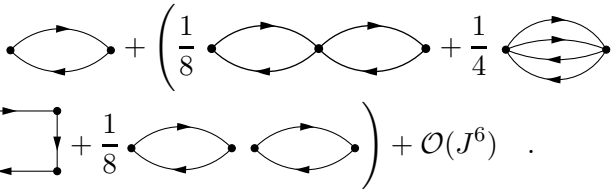 $+ \mathcal{O}(J^6)$.

(5.36)

The first four diagrams are connected while the last one is disconnected. We will see later on that disconnected diagrams do not contribute to any quantities which are of physical relevance.
Here is a good point to make some remarks about the differences between the diagrammatic expansion performed here and the "standard diagrammatic", which is for example employed in Φ^4 - theory and which is extensively discussed in literature [5, 56, 62, 63]. The main difference is that in the latter case the *interaction* between the particles is taken as a perturbation. A Green function without interaction is symbolized by a line and an interaction matrix element by a vertex. Because of the form of the propagators, Wick's theorem can be used to decompose the respective n-particle function into sums of products of one-particle function which makes calculations much easier than in our case.

5.3.4 Calculation of Cumulants

In order to perform explicit calculations in the present formalism, we must first calculate the cumulants explicitly. To this end, we make use of the generating functional (5.29). Differentiating twice according to (5.30) yields

$$C_1^{(0)}(\tau'|\tau) = \langle \hat{T}\left[\hat{a}^\dagger(\tau')\hat{a}(\tau)\right]\rangle^{(0)} = \frac{1}{\mathcal{Z}^{(0)}}\sum_{n=0}^{\infty}\langle n|\hat{T}\left[\hat{a}^\dagger(\tau')\hat{a}(\tau)\right]|n\rangle\, e^{-\beta E_n} \tag{5.37}$$

$$= \frac{1}{\mathcal{Z}^{(0)}}\sum_{n=0}^{\infty}\left[\Theta(\tau-\tau')(n+1)\, e^{(E_n-E_{n+1})(\tau-\tau')} + \Theta(\tau'-\tau)\, n\, e^{(E_n-E_{n-1})(\tau'-\tau)}\right] e^{-\beta E_n} \quad .$$

We see that (5.37) only depends on the difference of the imaginary times τ' and τ. This is a general feature which is also valid for the full Green functions (5.7), because the Hamiltonian (5.1) does not explicitly depend on time. Thus, we will often use the abbreviation

$$C_1^{(0)}(\tau-\tau') = C_1^{(0)}(\tau'|\tau) \quad . \tag{5.38}$$

In order to obtain $C_2^{(0)}$, we have to differentiate (5.29) four times which yields

$$C_2^{(0)}(\tau_1',\tau_2'|\tau_1,\tau_2) = \langle \hat{T}\left[\hat{a}^\dagger(\tau_1')\hat{a}^\dagger(\tau_2')\hat{a}(\tau_1)\hat{a}(\tau_2)\right]\rangle^{(0)} - C_1^{(0)}(\tau_1'|\tau_1)C_1^{(0)}(\tau_2'|\tau_2) - C_1^{(0)}(\tau_1'|\tau_2)C_1^{(0)}(\tau_2'|\tau_1) \quad . \tag{5.39}$$

With the same technique, we can also calculate the n-particle cumulant for any given n. This function will always turn out be a sum of a thermal average of n creation and n annihilation operators and products of lower-order cumulants.

5.3.5 Free Energy

As a first application of the diagrammatic approach and to demonstrate the formalism, we calculate the first correction to the grand-canonical free energy. To do this is interesting because we can see how the effects arising from hopping change the thermodynamic quantities. In the previous subsection, we have stated diagrammatic rules for the calculation of the partition function (5.18). The grand-canonical potential follows from it according to

$$\mathcal{F} = -\frac{1}{\beta}\log \mathcal{Z} \quad . \tag{5.40}$$

The series for $\mathcal{Z}$ in (5.36) contains both connected and disconnected diagrams. Now it turns out that the logarithm in (5.40) just cancels all disconnected diagrams. This can be proved for example with help of the replica method, as further explained in Ref. [56], or in an explicit way, as presented in Ref. [83]. We will not state these proofs here but point out a physical argument why the disconnected diagrams cannot contribute to the grand-canonical free energy. As it is known from thermodynamics, the grand-canonical free energy belongs to the extensive quantities which means that it scales with the size of the system N_S [51]. But when we sum the site indices in a diagram over the lattice, we get a factor N_S for every connected sub-diagram. Thus, all disconnected diagrams scale at least with N_S^2 and such terms cannot contribute to extensive quantities.
There are no vacuum-diagrams with one internal line. Therefore, the first correction is of second order in J and reads

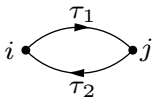

$$= \sum_{i,j} J_{i,j}J_{j,i} \int_0^\beta d\tau \int_0^\beta d\tau'\, C_1^{(0)}(\tau'|\tau)C_1^{(0)}(\tau|\tau') \quad . \tag{5.41}$$

Performing one integration with the help of (5.38) and carrying out the summation of the site indices over all lattice sites, Eq. (5.41) becomes

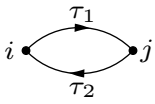

$$= \beta J^2 2DN_S \int_0^\beta d\tau\, C_1^{(0)}(\tau)C_1^{(0)}(-\tau) \quad . \tag{5.42}$$

Inserting (5.37) into (5.42) and performing the remaining integral yields

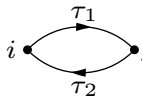

$$= \frac{\beta J^2 2DN_S}{\mathcal{Z}^{(0)2}} \sum_{n,k} \int_0^\beta d\tau (n+1)k\, e^{(E_n - E_{n+1} + E_k - E_{k-1})\tau} e^{-\beta(E_n+E_k)} \tag{5.43}$$

$$= \frac{\beta J^2 2DN_S}{\mathcal{Z}^{(0)2}} \sum_{n,k} \frac{(n+1)k}{E_n - E_{n+1} + E_k - E_{k-1}} \left[e^{(E_n - E_{n+1} + E_k - E_{k-1})\beta} - 1\right] e^{-\beta(E_n+E_k)} \quad ,$$

from which we can obtain by shifting summation indices and using (5.5)

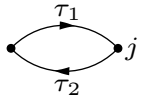

$$= \frac{N_S J^2 2D\beta}{U\mathcal{Z}^{(0)2}} \sum_{n,k} \left[\frac{(k+1)n}{k-n+1} + \frac{k(n+1)}{n-k+1}\right] e^{-\beta(E_n+E_k)} \quad . \tag{5.44}$$

Rearranging the term in the square brackets in Eq. (5.44) yields the final result

$$i \;\underset{\tau_2}{\overset{\tau_1}{\bigcirc}}\; j = \frac{N_S 4DJ^2\beta}{U\mathcal{Z}^{(0)2}} \sum_{n,k} \frac{(n+1)n}{(n-k+1)(k-n+1)} e^{-\beta(E_n+E_k)} \quad . \tag{5.45}$$

Note that these terms are defined not for all values of k and n. For example, the first term in the denominator in (5.45) surely becomes zero for $k = n-1$. This arises from the fact that

$$\int_0^\beta dx\, e^{\epsilon x} = (1-\delta_{\epsilon,0})\frac{e^{\beta\epsilon}-1}{\epsilon} + \delta_{\epsilon,0}\beta \quad , \tag{5.46}$$

where the second possibility was not taken into account when performing the integral in (5.43). It is possible to consider all these cases separately but this becomes quite cumbersome when going to higher orders where we have more integrals to calculate. But fortunately, there exists another solution: The occurring singularities are not real poles but can be removed by means of a well-defined limiting process. To this end, we need two principle limits which we state here in a general form. The first one is

$$\lim_{\epsilon\to 0} \frac{e^{\beta\epsilon}-1}{\epsilon} = \lim_{\epsilon\to 0} \frac{1+\beta\epsilon-1+\ldots}{\epsilon} = \beta \quad , \tag{5.47}$$

where we have used the Taylor expansion of the exponential function. Later on, we will also find terms with ϵ^2 in their denominators where we have to expand, correspondingly, up to second order to obtain

$$\lim_{\epsilon\to 0}\left(\frac{\beta}{\epsilon} + \frac{e^{-\beta\epsilon}-1}{\epsilon^2}\right) = \lim_{\epsilon\to 0}\left(\frac{\beta}{\epsilon} + \frac{1-\beta\epsilon+\frac{1}{2}\beta^2\epsilon^2-1+\ldots}{\epsilon^2}\right) = \frac{\beta^2}{2} \quad . \tag{5.48}$$

Thus, we will think of all integer numbers n, k, ... as being shifted by a suitable smallness parameter ϵ, do our calculation, and perform the limit $\epsilon \to 0$ at the end. After this clarification we return to the calculation of the first correction to the free energy. Inserting (5.45) in (3.1) and using the symmetry factor of the diagram, which we have shown in Subsection 5.3.2 to be 1/2, finally yields

$$\mathcal{F}^{(2)} = -\frac{1}{2\beta}\; i \;\underset{\tau_2}{\overset{\tau_1}{\bigcirc}}\; j \;= -\frac{N_S 2DJ^2}{U\mathcal{Z}^{(0)2}} \sum_{n,k} \frac{(n+1)n}{(n-k+1)(k-n+1)} e^{-\beta(E_n+E_k)} \quad . \tag{5.49}$$

When we perform the zero-temperature limit $\beta \to \infty$ of (5.49), we get the first correction to the ground-state energy per site:

$$E_n^{(2)} = -\frac{2DJ^2}{U} n(n+1) \quad , \tag{5.50}$$

where n in the integer particle number per site or filling factor. Thus, we conclude that the hopping reduces the energy of the system. This result can, of course, also be obtained by using the standard Rayleigh-Schrödinger perturbation theory at $T = 0$. There it even is a theorem that, when the *first* correction to the ground-state energy vanishes, the *second* correction must be negative [61]. Equation (5.50) obviously obeys this rule.

As it is well known and also discussed above, the grand-canonical free energy contains the information about the thermodynamics of a system. When we now investigate these quantities in the lowest non-trivial order in J, we must keep in mind that our results will be only valid for $J \ll U$, i.e. in the deep Mott phase.

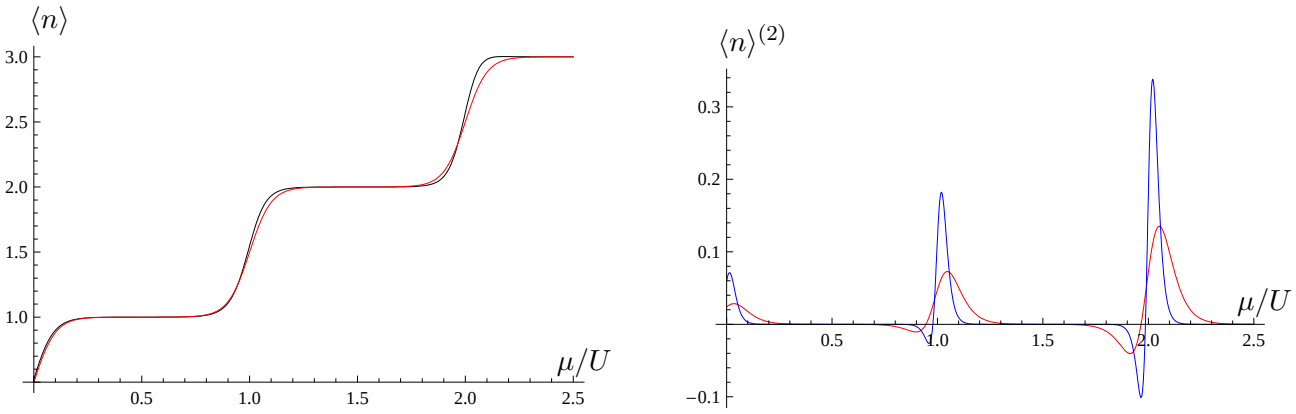

Figure 5.1: Corrections to particle number per site for $J = 0.02\,U$. Left: Unperturbed system (black), Second order in J (red). Right: First hopping correction for $T = 0.02\,U$ (blue) and $T = 0.05\,U$ (red).

5.3.6 Particle Number

Before we turn to the more sophisticated calculation of the specific heat, we investigate how the corrections from the hopping process affect the particle. With the help of the general arguments made in Subsection 3.1, we can write the particle number per site as

$$\langle n\rangle = \langle n\rangle^{(0)} + \langle n\rangle^{(2)} + \mathcal{O}(J)^4 \quad , \tag{5.51}$$

where the zeroth hopping-order reads

$$\langle n\rangle^{(0)} = \frac{1}{\mathcal{Z}^{(0)}} \sum_{l=0}^{\infty} l\, e^{-\beta E_l} \tag{5.52}$$

and the first non-vanishing hopping correction is, according to (3.2), given by

$$\langle n\rangle^{(2)} = -\frac{1}{N_S}\frac{\partial \mathcal{F}^{(2)}}{\partial \mu} \quad . \tag{5.53}$$

Inserting now (5.49) into (5.53) and using (5.5) yields

$$\langle n\rangle^{(2)} = \frac{2DJ^2}{U}\frac{\partial}{\partial \mu}\frac{\sum_{n,k} \frac{(n+1)n}{(n-k+1)(k-n+1)} e^{-\beta(E_n+E_k)}}{\mathcal{Z}^{(0)2}} \quad . \tag{5.54}$$

Performing the derivative in (5.54) and simplifying yields the final result

$$\langle n\rangle^{(2)} = \frac{2DJ^2\beta}{U\mathcal{Z}^{(0)2}}\left[\sum_{n,k}\frac{n(n+1)(n+k)}{(n-k+1)(k-n+1)} e^{-\beta(E_n+E_k)} - 2\langle n\rangle^{(0)}\sum_{n,k}\frac{n(n+1)}{(n-k+1)(k-n+1)} e^{-\beta(E_n+E_k)}\right] \quad . \tag{5.55}$$

Before we consider this result further, we calculate its zero-temperature limit. In order to do this, we remember from Subsection 3.2.2 that all thermal sums get reduced to one term in this situation. Thus, we have $k = n = \langle n\rangle^{(0)}$ where n is the integer filling determined by (5.6). Therefore, the two terms in the bracket in (5.55) cancel each other. Because this process is governed by exponential functions, it is faster than the linear grow in β resulting from the prefactor, and we can state

$$\lim_{\beta\to\infty} \langle n\rangle^{(2)} = 0 \quad . \tag{5.56}$$

Note that this convergence is only pointwise with respect to μ but not uniform [84]. In Fig. 5.1 (left), we can see that the corrections are very small and become slightly larger for larger particle numbers. In Fig. 5.1 (right), it is visible that for lower temperature the region, where the corrections are non-neglectable, becomes smaller, but also more peaked. This is a result of the non-uniform convergence which was mentioned above. In conclusion, we can say that hopping induces only minor changes to the dependence of the particle-number per site on the chemical potential and that these effects are more important for larger temperatures.

5.3.7 Specific Heat

As a second thermodynamic quantity, we calculate now the specific heat at constant volume. It is defined as

$$C_V = \left.\frac{\partial U_{\text{in}}}{\partial T}\right|_{V,\,N\,\text{fixed}} \quad , \tag{5.57}$$

where U_{in} is the inner energy. Note that the role of the volume is played in our system by the number of lattice sites N_S. The connection between them is for a system, which has the form of a D-dimensional cube with lattice-spacing a, given by

$$V = N_S\, a^D \quad . \tag{5.58}$$

We consider here only the unperturbed system, i.e. $J = 0$. To get the specific heat, we need to know the inner energy which is connected to the grand-canonical free energy by the Legendre transformation [51]

$$U_{\text{in}} = \mathcal{F} + TS + \mu N \quad , \tag{5.59}$$

where the entropy is given by

$$S = -\frac{\partial \mathcal{F}}{\partial T} \quad . \tag{5.60}$$

The grand-canonical free energy of the unperturbed system reads

$$\mathcal{F}^{(0)} = -TN_S \log \mathcal{Z}^{(0)} \quad , \tag{5.61}$$

with the single-site unperturbed partition function given by (5.16). Inserting (5.61) into (5.60) yields the entropy

$$S = N_S \log \mathcal{Z}^{(0)} + \frac{N_S}{\mathcal{Z}^{(0)}} \sum_{n=0}^{\infty} E_n e^{-E_n/T}. \tag{5.62}$$

Plugging (5.62) and also the connection between grand-canonical free energy and particle number, which reads for the unperturbed system

$$N = -\frac{\partial \mathcal{F}^{(0)}}{\partial \mu} = \frac{N_S}{\mathcal{Z}^{(0)}} \sum_{n=0}^{\infty} n\, e^{-E_n/T} \quad , \tag{5.63}$$

into (5.59) yields for the inner energy

$$U_{\text{in}} = N_S \frac{1}{\mathcal{Z}^{(0)}} \left[\sum_{n=0}^{\infty} E_n\, e^{-E_n/T} + \mu \sum_{n=0}^{\infty} n\, e^{-E_n/T} \right] \quad . \tag{5.64}$$

This can be simplified by introducing the new energies

$$\tilde{E}_n = E_n + \mu n = \frac{U}{2} n(n-1) \quad , \tag{5.65}$$

which are just the energy eigenvalues (5.5) of the Hamiltonian (5.3) without the additional term $-\mu n$ which was just a consequence of working within the grand-canonical ensemble. Inserting (5.65) into (5.64) yields

$$U_{\rm in} = \frac{N_S}{\mathcal{Z}^{(0)}} \sum_{n=0}^{\infty} \tilde{E}_n \, e^{-E_n/T} = \langle \tilde{E}_n \rangle^{(0)} \quad . \tag{5.66}$$

The expression (5.66) for the inner energy $U_{\rm in}$ is not yet suitable for the calculation of the specific heat because it does not explicitly depend on the total particle number, but only implicitly via the chemical potential. In order to overcome this problem, we use (5.63) and insert it into (5.66) to obtain

$$U_{\rm in} = \frac{\sum_{n=0}^{\infty} \tilde{E}_n \, e^{-E_n/T}}{\sum_{n=0}^{\infty} n \, e^{-E_n/T}} \, N \quad . \tag{5.67}$$

The next step is to perform the derivative of (5.67) with respect to the temperature. Note that this derivative must be performed for fixed particle number which means that we must consider the chemical potential μ as an implicit function of the particle number N. Because of that, we introduce the fugacity $z = e^{\mu/T}$ and rewrite (5.67), according to (5.65) as

$$U_{\rm in} = \frac{\sum_{n=0}^{\infty} \tilde{E}_n \, e^{-\tilde{E}_n/T} z^n}{\sum_{n=0}^{\infty} n \, e^{-\tilde{E}_n/T} z^n} N \quad . \tag{5.68}$$

Now all the complicated dependence on $\mu(N)$ is hidden in the fugacity and we must calculate its derivative with respect to T for fixed total particle number N. This seems to be a problematic task because, in order to calculate the derivative of z, we need $\partial\mu(N,T)/\partial T$ which is impossible to calculate explicitly, because we do not know the explicit form of $\mu(N,T)$. When considering the Bose gas in a harmonic trap, as it is done in Ref. [85], there exists a possibility to overcome this problem. We apply the same method to our present problem of a Bose gas in an optical lattice. To this end we start with the obvious identity

$$\left. \frac{\partial N(\mu,T)}{\partial T} \right|_{N \text{ fixed}} = 0 \quad . \tag{5.69}$$

Inserting now (5.63) into (5.69) and using the definition of the fugacity, we obtain the relation

$$\begin{aligned} &\left[\sum_{n=0}^{\infty} n \left(\frac{\tilde{E}_n}{T^2} z^n + n z^{n-1} \frac{\partial z}{\partial T} \right) e^{-\tilde{E}_n/T} \right] \times \left[\sum_{n=0}^{\infty} e^{-\tilde{E}_n/T} z^n \right] \\ &\qquad - \left[\sum_{n=0}^{\infty} \left(\frac{\tilde{E}_n}{T^2} z^n + n z^{n-1} \frac{\partial z}{\partial T} \right) e^{-\tilde{E}_n/T} \right] \times \left[\sum_{n=0}^{\infty} n \, e^{-\tilde{E}_n/T} z^n \right] = 0 \quad , \end{aligned} \tag{5.70}$$

where all derivatives have to be performed for fixed particle number N. Expanding the sums in (5.70) yields

$$\sum_{n,k=0}^{\infty} z^n \left(\frac{\tilde{E}_k}{T^2} z^k + k z^{k-1} \frac{\partial z}{\partial T} \right) (k-n) e^{-(\tilde{E}_k + \tilde{E}_n)/T} = 0 \quad . \tag{5.71}$$

Equation (5.71) contains the desired derivative of the fugacity with respect to the temperature at fixed particle number. Solving (5.71) for it yields

$$\left. \frac{\partial z}{\partial T} \right|_{N \text{ fixed}} = -\frac{1}{T^2} \frac{\sum_{n,k} z^n \tilde{E}_k z^k (k-n) \, e^{-(\tilde{E}_k + \tilde{E}_n)/T}}{\sum_{n,k} z^n k z^{k-1} (k-n) \, e^{-(\tilde{E}_k + \tilde{E}_n)/T}} \quad . \tag{5.72}$$

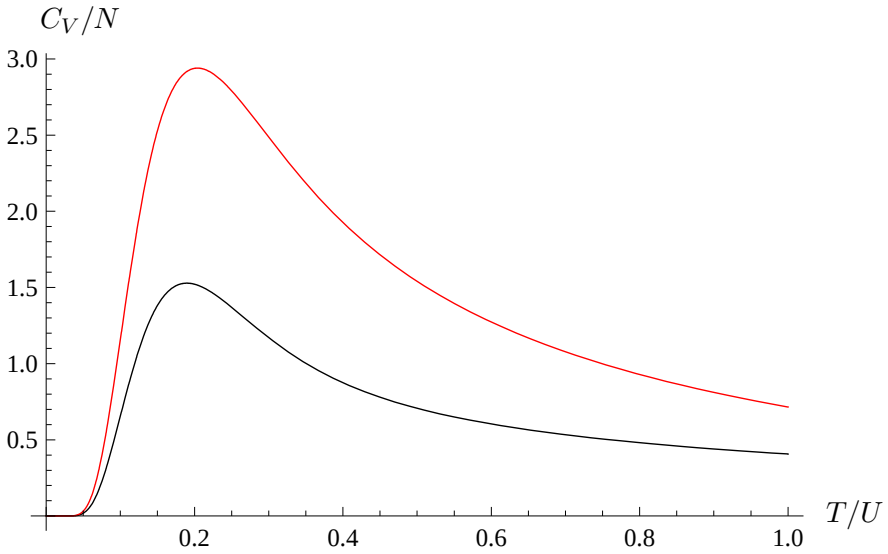

Figure 5.2: Specific heat per particle for a system without hopping and with filling factors $n = 1$ (black) and $n = 2$ (red).

Now we insert (5.68) into (5.57) and obtain

$$C_V = \frac{N}{\left(\sum_n n z^n e^{-\tilde{E}_n/T}\right)^2}\left\{\left[\sum_n \tilde{E}_n\left(\frac{\tilde{E}_n}{T^2}z^n + nz^{n-1}\frac{\partial z}{\partial T}\right)e^{-\tilde{E}_n/T}\right]\times\left[\sum_n nz^n e^{-\tilde{E}_n/T}\right]\right.$$
$$\left. - \left[\sum_n \tilde{E}_n z^n e^{-\tilde{E}_n/T}\right]\times\left[\sum_n n\left(\frac{\tilde{E}_n}{T^2}z^n + nz^{n-1}\frac{\partial z}{\partial T}\right)e^{-\tilde{E}_n/T}\right]\right\} \quad . \tag{5.73}$$

Together with (5.72), Eq. (5.73) is the solution for the specific heat of a system without hopping. Our result, which we have plotted in Fig. 5.2, obeys the third law of thermodynamics, i.e. $\lim_{T\to 0} C_V = 0$, but does not yield the Dulong-Petit law in the limit $T \to \infty$. But this is no drawback because the one-band Bose-Hubbard model is only valid for low temperatures and is not expected to yield meaningful high-temperature results anyway. We note that the functional form of $C_V(T)$ near $T = 0$ is $C_V \propto e^{-\Delta/T}$, where the activation energy Δ is determined by the on-site interaction energy U, i.e. $\Delta \approx U$. We do not consider corrections for finite J here because for *small* J there will be only minor changes, as already observed when discussing the particle. For larger values of J, a superfluid exists which changes the thermodynamic behavior in such a fundamental way that simple low-order perturbation theory is unable to provide significant results.

5.3.8 Green's Functions

Now we turn to our main quantity of interest and calculate the one-particle Green function (5.7) perturbatively in the hopping parameter J. The Green function can be written in complete analogy to (5.14) as

$$G_1(\tau', i'|\tau, i) = \frac{1}{\mathcal{Z}}\mathrm{Tr}\left\{e^{-\beta\hat{H}_0}\hat{T}\left[\hat{a}^\dagger_{i'}(\tau')\hat{a}_i(\tau)\hat{U}_\mathrm{D}(\beta, 0)\right]\right\} \quad , \tag{5.74}$$

where the time-ordering operator acts also on the time variables which are resulting from the expansion of the Dirac time-evolution operator in (5.10). Equation (5.74) has a similar structure as (5.14) and

can, therefore, be treated with the same methods. In complete analogy to (5.18) we get

$$G_1^{(n)}(\tau', i'|\tau, i) = \frac{\tilde{\mathcal{Z}}^{(0)}}{\mathcal{Z}} \frac{1}{n!} \sum_{i_1, j_1, \ldots, i_n, j_n} J_{i_1 j_1} \ldots J_{i_n j_n} \int_0^\beta d\tau_1 \ldots \int_0^\beta d\tau_n \times G_{n+1}^{(0)}(\tau_1, i_1; \ldots; \tau_n, i_n, \tau', i'|\tau_1, j_1; \ldots; \tau_n, j_n; \tau, i) \quad . \tag{5.75}$$

We can use the same cumulant decomposition and a diagrammatic representation with nearly the same rules, but we have to consider the fact that now there are two additional time variables and site indices which are fixed and which are not summed or integrated. We denote them by external lines. With those remarks the zeroth hopping order just reads

$$G_1^{(0)}(\tau', i|\tau, j) = \underset{\tau'}{\overset{i}{\bullet}} \!\!\rightarrow\!\!\!\!\rightarrow \underset{\tau}{\bullet} = \delta_{i,j} C_1^{(0)}(\tau'|\tau) \quad . \tag{5.76}$$

In first order in J there is only one diagram which we now explicitly calculate as an example. However, we only consider the case $\tau' > \tau$, because the other case is calculated in exactly the same manner. The first correction to the Green function reads under consideration of (5.12) and the diagrammatic rules in Subsection 5.3.1.

$$G_1^{(1)}(\tau', i|\tau, j) = \underset{\tau'}{\overset{i}{\bullet}} \!\!\rightarrow\!\!\!\!\rightarrow \underset{\tau_1}{\overset{j}{\bullet}} \!\!\rightarrow\!\!\!\!\rightarrow \underset{\tau}{\bullet} = J\delta_{d(i,j),1} \int_0^\beta d\tau_1 \, C_1^{(0)}(\tau'|\tau_1) C_1^{(0)}(\tau_1|\tau) \quad . \tag{5.77}$$

Inserting (5.38) into (5.77) yields

$$G_1^{(1)}(\tau', i|0, j) = J\delta_{d(i,j),1} \int_0^\beta d\tau_1 \, C_1^{(0)}(\tau' - \tau_1) C_1^{(0)}(\tau_1) \quad , \tag{5.78}$$

so we obtain with (5.37):

$$G_1^{(1)}(\tau', i|0, j) = \frac{J\delta_{d(i,j),1}}{\mathcal{Z}^{(0)2}} \sum_{n,k} \int_0^\beta d\tau_1 \Big[\Theta(\tau_1 - \tau')(n+1) \, e^{(E_n - E_{n+1})(\tau_1 - \tau')} + \Theta(\tau' - \tau_1) \, n \, e^{(E_n - E_{n-1})(\tau' - \tau_1)} \Big] k \, e^{(E_k - E_{k-1})\tau_1} \, e^{-\beta(E_n + E_k)} \quad . \tag{5.79}$$

After carrying out the integral over the internal time variable τ, Eq. (5.79) yields

$$G_1^{(1)}(\tau', i|0, j) = \frac{J\delta_{d(i,j),1}}{\mathcal{Z}^{(0)2}} \sum_{n,k} k(n+1) \Bigg[\frac{e^{\tau'(E_{n+1} - E_n)}}{E_n - E_{n+1} + E_k - E_{k+1}} e^{\beta(E_n - E_{n+1} + E_k - E_{k-1})} - \frac{e^{\tau'(E_k - E_{k-1})}}{E_n - E_{n+1} + E_k - E_{k+1}} + \frac{e^{\tau'(E_k - E_{k-1})} - e^{\tau'(E_n - E_{n-1})}}{E_{n-1} - E_n + E_k - E_{k-1}} \Bigg] e^{-\beta(E_n + E_k)} \quad . \tag{5.80}$$

By shifting summation indices and using (5.5), we can simplify (5.80) and obtain the final result

$$G_1^{(1)}(\tau', i|0, j) = \frac{J\delta_{d(i,j),1}}{U\mathcal{Z}^{(0)2}} \sum_{n,k} \Bigg[\frac{(k+1)n \, e^{\tau'(E_n - E_{n-1})}}{k - n + 1} + \frac{k(n+1) e^{\tau'(E_k - E_{k-1})}}{n - k + 1} + \frac{e^{\tau'(E_k - E_{k-1})} - e^{\tau'(E_n - E_{n-1})}}{k - n} \Bigg] e^{-\beta(E_n + E_k)} \quad , \tag{5.81}$$

where the vanishing denominators have to be treated according to (5.47).

5.4 Diagrammatic Rules in Matsubara Space

After having calculated this example, we return to the general concept. Calculations can often, but not always, be simplified by going to Matsubara space. The Matsubara transform of the one-particle cumulant reads, for instance,

$$C_1^{(0)}(\omega_m'|\omega_m) = \frac{1}{\beta}\int_0^\beta d\tau \int_0^\beta d\tau'\, C_1^{(0)}(\tau'|\tau) e^{i(\omega_m\tau - \omega_m'\tau')} \quad . \tag{5.82}$$

Here the bosonic Matsubara frequencies are

$$\omega_m = \frac{2\pi}{\beta} m \quad , \tag{5.83}$$

with m taking integer values. Because (5.82) depends only on time differences, according to (5.38), we can write it as

$$C_1^{(0)}(\omega_m'|\omega_m) = \delta_{m,m'} C_1^{(0)}(\omega_m) \tag{5.84}$$

with

$$C_1^{(0)}(\omega_m) = \int_0^\beta d\tau\, C_1^{(0)}(\tau) e^{i\omega_m\tau} \quad . \tag{5.85}$$

Explicitly, we obtain from inserting (5.37) and (5.38) into (5.85)

$$C_1^{(0)}(\omega_m) = \frac{1}{\mathcal{Z}^{(0)}}\int_0^\beta d\tau \sum_n e^{-\beta E_n}\, n\, e^{(E_n - E_{n-1} + i\omega_m)\tau} = \frac{1}{\mathcal{Z}^{(0)}} \sum_n e^{-\beta E_n}\, n \frac{e^{\beta(E_n - E_{n-1})} - 1}{E_n - E_{n-1} + i\omega_m} \quad , \tag{5.86}$$

which yields after shifting summation indices

$$C_1^{(0)}(\omega_m) = \frac{1}{\mathcal{Z}^{(0)}} \sum_n \left[\frac{(n+1)}{E_{n+1} - E_n + i\omega_m} - \frac{n}{E_n - E_{n-1} + i\omega_m} \right] e^{-\beta E_n} \quad . \tag{5.87}$$

The inverse Matsubara transform into the time domain reads

$$C_1^{(0)}(\tau'|\tau) = \frac{1}{\beta} \sum_{m=-\infty}^{\infty} C_1^{(0)}(\omega_m) e^{-i\omega_m(\tau - \tau')} \quad . \tag{5.88}$$

The situation is similar for higher n-point functions. Because they all only depend on time differences, always a "frequency conservation" occurs which can be written as

$$C_n^{(0)}(\omega_{m_1}', \ldots, \omega_{m_n}'|\omega_{m_1}, \ldots, \omega_{m_n}) \propto \delta_{\sum_{k=1}^n \omega_{m_k}, \sum_{k=1}^n \omega_{m_k}'} \quad . \tag{5.89}$$

This is the imaginary-time analog of the fact that homogeneity in time implies conservation of energy according to the Noether theorem [19].
Now we can write down how our diagrammatic rules have to be modified in Matsubara space: The lines now carry Matsubara frequencies which obey (5.89) and we have to sum over all free Matsubara frequencies ω_m instead of integrating over the time-variables. This "frequency conservation" will allow us to calculate some kind of diagrams without having to perform Matsubara-sums at all. For example:

$G_1^{(1)}(\omega_m; i, j) =$ 

$= J\delta_{d(i,j),1} C_1^{(0)}(\omega_m)^2 \quad .$ (5.90)

This observation will help us later on to sum infinite series of diagrams to obtain results which go beyond perturbation theory.
It is quite instructive to calculate $G_1^{(1)}(\tau'|\tau)$ by transforming (5.90) back into the time domain. We will again restrict ourselves to the case $\tau' > \tau$. Inserting (5.87) into (5.90) yields

$$G_1^{(1)}(\omega_m; i', i) = \delta_{d(i',i),1} J \left[\frac{1}{\mathcal{Z}^{(0)}} \sum_n \left(\frac{n+1}{E_{n+1} - E_n + i\omega_m} - \frac{n}{E_n - E_{n-1} + i\omega_m} \right) e^{-\beta E_n} \right]^2 \quad . \tag{5.91}$$

Applying (5.88) to (5.91) and rearranging the result allows us to write the Matsubara back-transform as

$$\begin{aligned} G_1^{(1)}(\tau', i'|\tau, i) = &- \frac{J\delta_{d(i',i),1}}{\beta \mathcal{Z}^{(0)2}} \sum_{m=-\infty}^{\infty} \sum_{n,k} \frac{nk}{(E_n - E_{n-1} + i\omega_m)(E_k - E_{k-1} + i\omega_m)} \left[1 - e^{\beta(E_n - E_{n-1})} \right] \\ &\times \left[1 - e^{\beta(E_k - E_{k-1})} \right] e^{-\beta(E_n + E_k)} e^{-i\omega_m(\tau - \tau')} \quad . \end{aligned} \tag{5.92}$$

The next step is to perform a decomposition into partial fractions which yields

$$\begin{aligned} -\frac{1}{(E_n - E_{n-1} + i\omega_m)(E_k - E_{k-1} + i\omega_m)} = &\frac{1}{E_n - E_{n-1} - E_k + E_{k-1}} \\ &\times \left(\frac{1}{E_n - E_{n-1} + i\omega_m} - \frac{1}{E_k - E_{k-1} + i\omega_m} \right) \quad . \end{aligned} \tag{5.93}$$

In order to perform the Matsubara-sums, we use Poisson's sum formula [62, (2.429)]

$$\sum_{m=-\infty}^{\infty} f(\omega_m) = \frac{\beta}{2\pi} \sum_{l=-\infty}^{\infty} \int_{-\infty}^{\infty} d\omega_m \, f(\omega_m) \, e^{i\omega_m l\beta} \quad , \tag{5.94}$$

where ω_m on the right-hand side is a continuous variable. Applying (5.94) to the first term in (5.93) gives

$$\sum_{m=-\infty}^{\infty} \frac{1}{E_n - E_{n-1} + i\omega_m} e^{-i\omega_m(\tau - \tau')} = \frac{\beta}{2\pi} \sum_{l=-\infty}^{\infty} \int_{-\infty}^{\infty} d\omega_m \frac{1}{E_n - E_{n-1} + i\omega_m} e^{i\omega_m[l\beta - (\tau - \tau')]} \quad , \tag{5.95}$$

where the occurring integral can be evaluated with the help of the residue theorem. Because the integrand should vanish at the contour of integration, we must close this contour in the upper half plane for $l > 0$ and in the lower one for $l < 0$. For $l = 0$ we remember that $\tau' > \tau$, so we also close the contour of integration in the upper half-plane. The integrand in (5.95) has one simple pole at $\omega_m = i(E_n - E_{n-1})$. For $E_n > E_{n-1}$ the pole is in the upper half plane. Thus, the integral vanishes for $l < 0$. Inserting this into (5.95) yields

$$\frac{\beta}{2\pi} 2\pi i \frac{1}{i} \sum_{k=0}^{\infty} e^{-[k\beta - (\tau - \tau')](E_{n-1} - E_n)} = \beta \frac{e^{(\tau - \tau')(E_{n-1} - E_n)}}{1 - e^{\beta(E_n - E_{n-1})}} \quad . \tag{5.96}$$

For $E_n < E_{n-1}$ the situation is vice versa: Only $l < 0$ give non-vanishing contributions. Shifting summation variables, it turns out that the result is the same as (5.96). Performing the same calculation with the second term in (5.93) and putting everything together, we obtain

$$\begin{aligned} G_1^{(1)}(\tau', i'|\tau, i) = &\frac{J\delta_{d(i',i),1}}{\mathcal{Z}^{(0)2}} \sum_{n,k} \frac{nk}{E_n - E_{n-1} - E_k + E_{k-1}} \left\{ e^{(\tau - \tau')(E_{k-1} - E_k)} \left[1 - e^{\beta(E_n + E_{n-1})} \right] \right. \\ &\left. - e^{(\tau - \tau')(E_{n-1} - E_n)} \left[1 - e^{\beta(E_k - E_{k-1})} \right] \right\} e^{-\beta(E_n + E_k)} \quad , \end{aligned} \tag{5.97}$$

which yields after shifting indices, inserting (5.5), and setting $\tau = 0$ the same result as (5.81). This result is important for the explanation of the time-of-flight pictures which will be done in Subsection 6.1.1.

Chapter 6

Further Development of Green's Functions Technique

In the last Chapter, we have developed the basic principles of a very powerful approach to the Bose-Hubbard model. In this chapter, we apply this formalism in order to calculate various system properties. Aside from these practical applications, we also develop a resummation method which allows us to improve our perturbative results.

6.1 Applications

In this section, we apply the Green function formalism to calculate quantities which are of relevance for explaining experimental observations.

6.1.1 Time-of-Flight

As discussed in Chapter 4, most experiments performed with Bosons in optical lattices involve time-of-flight measurements [67]. In order to explain them theoretically, we need the density in momentum space which can be calculated from the Green function. At first, we need the equal-time correlation function which we get from (5.7) according to

$$\langle \hat{a}_i^\dagger \hat{a}_j \rangle = \lim_{\tau' \searrow 0} G_1(\tau', i|0, j) \quad . \tag{6.1}$$

Note that the equal-time limit must be performed in this way because in the formula for the quasi-momentum distribution (4.29), the creator stands at the left-hand side of the annihilator. With (5.31), (5.37), and (6.1), we get in zeroth hopping order

$$\langle \hat{a}_i^\dagger \hat{a}_j \rangle^{(0)} = \langle \hat{n} \rangle^{(0)} \delta_{i,j} \quad , \tag{6.2}$$

which is just the thermal average of the particle number per site. Using (5.81), the first-order correction in (6.1) is given by

$$\langle \hat{a}_i^\dagger \hat{a}_j \rangle^{(1)} = \frac{J \delta_{d(i,j),1}}{U \mathcal{Z}^{(0)2}} \sum_{n,k} \left[\frac{(k+1)n}{k-n+1} + \frac{k(n+1)}{n-k+1} \right] e^{-\beta(E_n + E_k)} \quad , \tag{6.3}$$

which becomes in the zero-temperature limit

$$\langle \hat{a}_i^\dagger \hat{a}_j \rangle^{(1)} = 2 \frac{J \delta_{d(i,j),1}}{U} n(n+1) \quad . \tag{6.4}$$

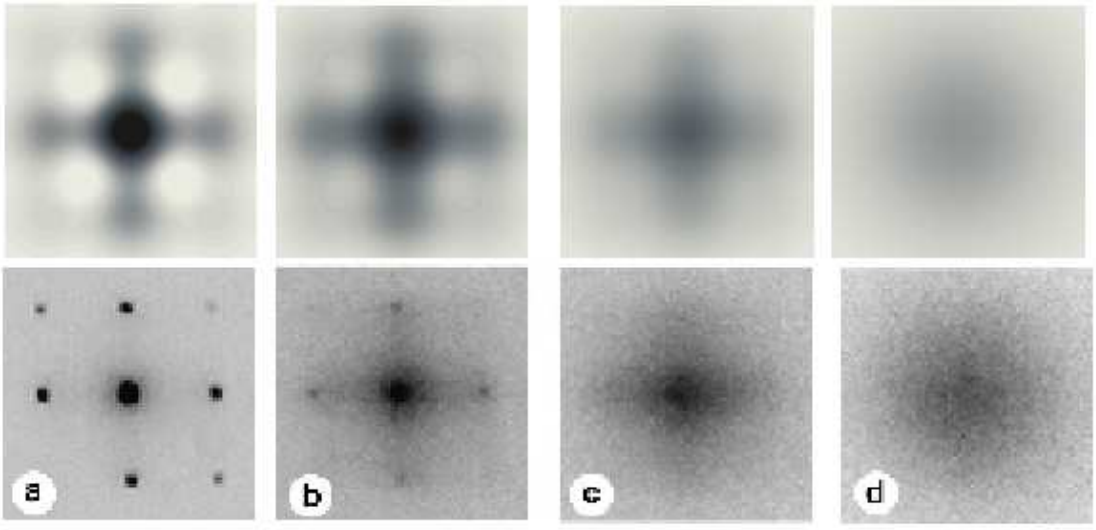

Figure 6.1: First-order time-of-flight pictures at zero-temperature (first row) and comparison with experimental data [17] (second row). $V_0 = 8\ E_R$ (a), $V_0 = 14\ E_R$ (b), $V_0 = 18\ E_R$ (c), $V_0 = 30\ E_R$ (d).

The quasi-momentum distribution reads in an analogous way to (4.29)

$$S(\mathbf{k}) = \langle \hat{n} \rangle^{(0)} + J(\mathbf{k}) S_1(\beta) \quad , \tag{6.5}$$

where we have used the D-dimensional analog of the lattice dispersion (4.6),

$$J(\mathbf{k}) = 2J \sum_{\nu=1}^{D} \cos(k_\nu a) \tag{6.6}$$

and the temperature-dependent coefficient

$$S_1(\beta) = \frac{1}{U \mathcal{Z}^{(0)2}} \sum_{n,k} \left[\frac{(k+1)n}{k-n+1} + \frac{k(n+1)}{n-k+1} \right] e^{-\beta(E_n + E_k)} \quad . \tag{6.7}$$

The zero-temperature limit of (6.7) is

$$S_1 = \frac{2n(n+1)}{U} \quad . \tag{6.8}$$

When we want to compare this result with experimental data, we encounter a problem: Unfortunately, so far, there exists no way to measure the temperature of Bosons which are trapped in an optical lattice. The gas is cooled to the lowest possible temperature, i.e. until no thermal fraction is visible anymore, before the optical lattice is turned on adiabatically [17]. This increase of the lattice depth can lead to a change of the temperature [86] which cannot be measured experimentally. Because of this problem, we have assumed the system to be at $T = 0$ for the calculation of the time-of-flight pictures in Fig. 6.1 as an approximation. Nevertheless, the question how to determine the actual temperature is interesting and shall be discussed later on. In Fig. 6.1, the agreement between our first-order calculation and the experiment is quite good for deep lattices in (c) and (d) and becomes worse when the lattice becomes shallower as in (a) and (b) as already discussed for the spinor case in Chapter 4. However, in Subsection 6.1.6 we show that it is also possible to go beyond simple perturbation theory and to incorporate features arising from long-range correlations, so that we are then able to explain the sharp interference peaks theoretically.

6.1.2 Phase Boundary

In this section, we calculate the phase boundary between the Mott insulator and the superfluid phase [6, 58, 64] which we have addressed for the more general spinor system already in Chapter 3. However, we will see that the approach used in this chapter provides us with more insight and also allows us to improve the respective results.

Within the theory of critical phenomena, it is known that the correlations become infinitely strong at the critical point which means that the Green function diverges [5, 76]. It is not possible to get a diverging Green function from simple finite-order perturbation theory because this yields only analytic functions, i.e. power series in J. Thus, we have to sum an infinite subset of diagrams which we choose to consist of all diagrams which do not have any loops but are single chains. A conceptually similar method was used in Ref. [87] where a system at zero temperature was considered and, therefore, real-time Green functions were calculated. Thus, the resummed Green function reads

$$\tilde{G}_1(\omega_m; i, j) =$$

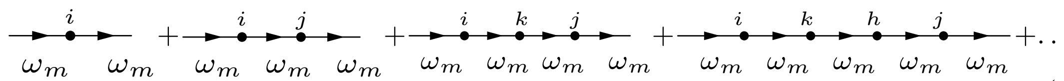

(6.9)

The choice of this particular subset of diagrams seems a bit arbitrary but becomes more reasonable below. A more systematic way to understand the resummation of the perturbation series for the Green functions by means of the self-energy is presented in Subsection 6.2.1.

Because site indices are allowed to coincide on the actual lattice according to rule 3 in Subsection 5.3.1, every line produces just a factor of $J(\mathbf{k})$ and, therefore, the summation (6.9) is easily performed in Fourier space, yielding

$$\tilde{G}_1(\omega_m, \mathbf{k}) = \sum_{l=0}^{\infty} \left[C_1^{(0)}(\omega_m) \right]^{l+1} J(\mathbf{k})^l \quad . \tag{6.10}$$

This is a geometric series which can be immediately evaluated to

$$\tilde{G}_1(\omega_m, \mathbf{k}) = \frac{C_1^{(0)}(\omega_m)}{1 - J(\mathbf{k})\, C_1^{(0)}(\omega_m)} \quad . \tag{6.11}$$

Equation (6.11) diverges at

$$1 - J(\mathbf{k})\, C_1^{(0)}(\omega_m) = 0 \tag{6.12}$$

for some wave vector $\mathbf{k}$ and some Matsubara frequency ω_m. The imaginary part of $C_1^{(0)}$ in (5.87) vanishes only for $\omega_m = 0$. Furthermore, phase transitions are governed by long-wavelength fluctuations [5, 76] and, therefore, the wave vector $\mathbf{k}$ has also to be set to zero. Thus, the condition for the phase transition becomes after inserting (5.87) into (6.12)

$$2DJ_c = \frac{\sum_n e^{-\beta E_n}}{\sum_n e^{-\beta E_n} \left(\frac{n+1}{E_{n+1}-E_n} - \frac{n}{E_n - E_{n-1}} \right)} \quad , \tag{6.13}$$

which coincides with the mean-field result [64, 65]. The zero-temperature limit of (6.13) is [58]

$$2DJ_c = 1 / \left[\frac{n+1}{E_{n+1} - E_n} - \frac{n}{E_n - E_{n-1}} \right] \tag{6.14}$$

for filling n. The phase boundary both for finite and zero temperature is shown in Fig. 6.2. The temperature shifts the phase boundary towards higher critical values of J. This effect is important in the region between the lobes but quite weak near the tips. We shall see later on that this behavior is closely connected to thermal fluctuations.

In order to see that (6.13) becomes exact in the limit of infinite spatial dimension D, one must suitably

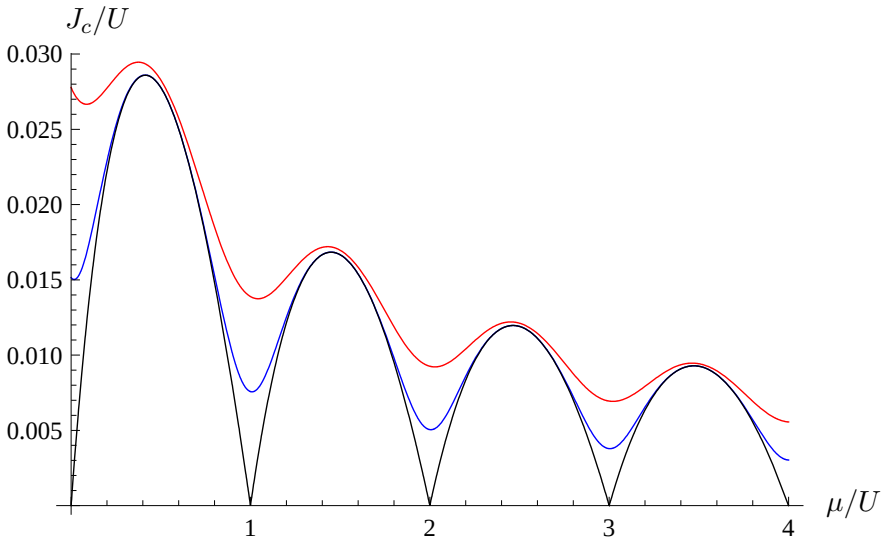

Figure 6.2: First-order (mean-field) phase diagram for different temperatures. $T = 0$ (black), $T = 0.05\,U$ (blue), and $T = 0.1\,U$ (red).

scale the hopping parameter. This is a non-trivial question leading to different answers for Fermions and Bosons, respectively [88, 89]. For our case, we define at first place the rescaled hopping strength $\tilde{J} = 2DJ$ so that the contribution of the kth order chain diagram in (6.9) is proportional to $\tilde{J}^k$. The lowest-order term neglected by our summation is represented by the diagram

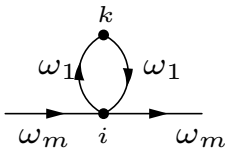

. (6.15)

It has two internal lines and is, for this reason, proportional to J^2. Furthermore, (6.15) hast one free site index, which we must sum. This yields a factor $2D$. Thus, the one-loop diagram (6.15) is proportional to $2DJ^2 = \tilde{J}^2/(2D)$ for which reason it vanishes in the limit of $D \to \infty$. All other neglected diagrams are also at least of the order $1/D$. Therefore, it can be said that the first-order or mean-field result (6.13) is exact at infinite spatial dimension.

6.1.3 Real-Time Green's Functions

The quantum phase diagram (6.13) and also the correlation functions (6.1) are properties of a system in thermal equilibrium which become properties of the ground state for $T = 0$. But we are also interested in dynamic properties which can be also measured experimentally [68]. The dynamic property which is best accessible within the framework employed in this thesis, is the excitation spectrum or dispersion relation. It is especially interesting because it has a characteristic gap in the Mott phase which vanishes when approaching the critical hopping. Furthermore, we are interested to investigate how finite temperature affects the situation.
Until now, we have only dealt with imaginary-time Green functions. To find information on the excitation spectrum, it is necessary to consider the real-time Green function for $T \neq 0$. Of course, the concept of temperature makes no sense when considering systems far from thermal equilibrium but, because we are only considering excitations of a thermal system, it is reasonable to define the retarded

Green function for finite temperature due to causality according to [62, 63, 90]

$$G_1(t', j'|t, j) = \Theta(t - t')\frac{1}{\mathcal{Z}}\mathrm{Tr}\left\{e^{-\beta\hat{H}}\left[\hat{a}_{j\mathrm{H}}(t), \hat{a}^\dagger_{j'\mathrm{H}}(t')\right]\right\} \quad , \tag{6.16}$$

where $\hat{a}^\dagger_{j'\mathrm{H}}(t)$ and $\hat{a}_{j\mathrm{H}}(t)$ are creation and annihilation operators in real-time Heisenberg representation. It is possible to perform a diagrammatic expansion of this expression using the real-time interaction representation but we will not work this out here. We get the retarded Green function in a much simpler way by means of an analytic continuation of the corresponding imaginary-time one (5.7), which we have calculated in the previous chapter. This continuation is not well defined in general because we know $G_1(\omega_m)$ only at a set of *discrete* points ω_m and this is not enough for determining the function in the whole upper half-plane [91]. This problem is also encountered when continuing functions which are determined numerically, as discussed in Ref. [92]. Fortunately, it is known that $G_1(\omega_m)$ must vanish like $1/\omega_m$ for large frequencies [62]. We can also see explicitly that our perturbative result (5.87) obeys this condition. This information is sufficient to make the analytic continuation unique. In order to find a connection between the real- and imaginary-time Green function, we use the general approach in Ref. [62] and adapt it to the particular system discussed here. At first place, we write the imaginary-time Green function in the spectral representation. Because of the already discussed translational invariance in imaginary time, we set $\tau' = 0$ in (5.7) and consider only the case $\tau > 0$. Doing this, Eq. (5.7) becomes

$$G_1(0, j'|\tau, j) = \frac{1}{\mathcal{Z}}\mathrm{Tr}\left\{e^{-\beta\hat{H}}\hat{a}_{j,\mathrm{H}}(\tau)\hat{a}^\dagger_{j',\mathrm{H}}(0)\right\} \quad . \tag{6.17}$$

Now, we denote the eigenstates of the *full* Hamiltonian (5.1) by $|\mathbf{n}\rangle$ and its respective energy eigenvalues by $E_\mathbf{n}$. Note that, of course, we do not know them explicitly, but an explicit formula is not needed for the following derivation. Performing the trace in (6.17) in the base $|\mathbf{n}\rangle$ yields

$$G_1(0, j'|\tau, j) = \frac{1}{\mathcal{Z}}\sum_\mathbf{n} e^{-\beta E_\mathbf{n}}\langle\mathbf{n}|\hat{a}_{j,\mathrm{H}}(\tau)\hat{a}^\dagger_{j',\mathrm{H}}(0)|\mathbf{n}\rangle \quad , \tag{6.18}$$

which can be rewritten with the help of the completeness relation $\sum_{\mathbf{n}'}|\mathbf{n}'\rangle\langle\mathbf{n}'| = 1$ and the connection between operators in Heisenberg and Schödinger picture (5.8) as

$$G_1(0, j'|\tau, j) = \frac{1}{\mathcal{Z}}\sum_{\mathbf{n},\mathbf{n}'} e^{-\beta E_\mathbf{n}}e^{(E_\mathbf{n} - E_{\mathbf{n}'})\tau}\langle\mathbf{n}|\hat{a}_j|\mathbf{n}'\rangle\langle\mathbf{n}'|\hat{a}^\dagger_{j'}|\mathbf{n}\rangle \quad . \tag{6.19}$$

In Eq. (6.19), the dependence on time and on the operators is separated which allows us directly to calculate the Matsubara transform very easily. Inserting (6.19) into (5.85) yields

$$G_1(\omega_m; j', j) = \frac{1}{\mathcal{Z}}\sum_{\mathbf{n},\mathbf{n}'}\langle\mathbf{n}|\hat{a}_j|\mathbf{n}'\rangle\langle\mathbf{n}'|\hat{a}^\dagger_{j'}|\mathbf{n}\rangle\int_0^\beta d\tau'\, e^{(E_\mathbf{n} - E_{\mathbf{n}'} + i\omega_m)\tau'} \quad , \tag{6.20}$$

from which we obtain after carrying out the occurring integral

$$G_1(\omega_m; j', j) = -\frac{1}{\mathcal{Z}}\sum_{\mathbf{n},\mathbf{n}'} e^{-\beta E_\mathbf{n}}\langle\mathbf{n}|\hat{a}_j|\mathbf{n}'\rangle\langle\mathbf{n}'|\hat{a}^\dagger_{j'}|\mathbf{n}\rangle\frac{1 - e^{\beta(E_{\mathbf{n}'} - E_\mathbf{n})}}{E_\mathbf{n} - E_{\mathbf{n}'} + i\omega_m} \quad . \tag{6.21}$$

This spectral representation (6.21) will be the suitable form of the imaginary-time Green function to be compared with its real-time analog which we address now. Its definition (6.16) becomes for $t' = 0$

$$G_1(0, j'|t, j) = \Theta(t)\frac{1}{\mathcal{Z}}\mathrm{Tr}\left\{e^{-\beta\hat{H}}\left[\hat{a}_{j,\mathrm{H}}(t), \hat{a}^\dagger_{j',\mathrm{H}}(0)\right]\right\} \quad . \tag{6.22}$$

Now, we can proceed in a similar way as in (6.17), (6.18) and obtain under consideration of the commutator occurring in (6.22)

$$G_1(j'|t,j) = \Theta(t)\frac{1}{\mathcal{Z}}\sum_{\mathbf{n},\mathbf{n}'} e^{-\beta E_{\mathbf{n}}}\left[e^{i(E_{\mathbf{n}}-E_{\mathbf{n}'})t}\langle\mathbf{n}|\hat{a}_j|\mathbf{n}'\rangle\langle\mathbf{n}'|\hat{a}^\dagger_{j'}|\mathbf{n}\rangle - e^{i(E_{\mathbf{n}'}-E_{\mathbf{n}})t}\langle\mathbf{n}|\hat{a}^\dagger_{j'}|\mathbf{n}'\rangle\langle\mathbf{n}'|\hat{a}_j|\mathbf{n}\rangle\right] \quad . \tag{6.23}$$

The next step is to perform a Fourier transform of (6.23):

$$G_1(\omega; j', j) = \int_{-\infty}^{\infty} dt\, G_1(j'|t,j)\, e^{i\omega t} \quad . \tag{6.24}$$

Inserting (6.23) into (6.24) yields

$$G_1(\omega; j', j) = \frac{1}{\mathcal{Z}}\sum_{\mathbf{n},\mathbf{n}'} e^{-\beta E_{\mathbf{n}}}\left[\langle\mathbf{n}|\hat{a}_j|\mathbf{n}'\rangle\langle\mathbf{n}'|\hat{a}^\dagger_{j'}|\mathbf{n}\rangle\int_0^\infty dt\, e^{i(E_{\mathbf{n}}-E_{\mathbf{n}'})t} - \langle\mathbf{n}|\hat{a}^\dagger_{j'}|\mathbf{n}'\rangle\langle\mathbf{n}'|\hat{a}_j|\mathbf{n}\rangle\int_0^\infty dt\, e^{i(E_{\mathbf{n}'}-E_{\mathbf{n}})t}\right] \quad . \tag{6.25}$$

The two integrals in (6.25) are not well defined because integrals of this form only converge when the exponent has a negative real part. But the energies are of course real and, therefore, the exponent does not have a real part at all. To ensure convergence nevertheless, we add an infinitesimal positive imaginary part to the frequency ω, i.e. set $\omega \to \omega + i\eta$. Note, that if we did not consider the *retarded* Green function but the *advanced* one, which has a prefactor $\Theta(-t)$, the infinitesimal imaginary part $i\eta$ would just change sign. Performing the integrals in (6.25) with this convergence procedure yields

$$G_1(\omega; j', j) = \frac{1}{\mathcal{Z}}\sum_{\mathbf{n},\mathbf{n}'} e^{-\beta E_{\mathbf{n}}}\Big[\langle\mathbf{n}|\hat{a}_j|\mathbf{n}'\rangle\langle\mathbf{n}'|\hat{a}^\dagger_{j'}|\mathbf{n}\rangle\frac{-1}{i(E_{\mathbf{n}} - E_{\mathbf{n}'} + \omega + i\eta)} - \langle\mathbf{n}|\hat{a}^\dagger_{j'}|\mathbf{n}'\rangle\langle\mathbf{n}'|\hat{a}_j|\mathbf{n}\rangle\frac{-1}{i(E_{\mathbf{n}'} - E_{\mathbf{n}} + \omega + i\eta)}\Big] \quad . \tag{6.26}$$

After exchanging $\mathbf{n}$ and $\mathbf{n}'$ in the second term, we can write this as

$$G_1(\omega; j', j) = \frac{i}{\mathcal{Z}}\sum_{\mathbf{n},\mathbf{n}'} e^{-\beta E_{\mathbf{n}}}\langle\mathbf{n}|\hat{a}_j|\mathbf{n}'\rangle\langle\mathbf{n}'|\hat{a}^\dagger_{j'}|\mathbf{n}\rangle\frac{1 - e^{\beta(E_{\mathbf{n}}-E_{\mathbf{n}'})}}{E_{\mathbf{n}} - E_{\mathbf{n}'} + \omega + i\eta} \quad , \tag{6.27}$$

which can now be compared with the spectral representation of the imaginary-time Green function in (6.21). Thus, we see that we get the real-time Green function from the imaginary one by making the replacement $i\omega_m \to \omega + i\eta$ and multiplying the result by $-i$:

$$G_1(\omega; j', j) = -iG_1(i\omega_m = \omega + i\eta; j', j) \quad . \tag{6.28}$$

As a simple example, we state here the real-time Green function for the unperturbed system. Applying the rule (6.28) to (5.87) yields the desired result:

$$G_1^{(0)}(\omega; j', j) = \delta_{j',j}C_1^{(0)}(\omega) = \frac{-i\delta_{i,j}}{\mathcal{Z}^{(0)}}\sum_{n=0}^{\infty}\left[\frac{n+1}{E_{n+1} - E_n + \omega + i\eta} - \frac{n}{E_n - E_{n-1} + \omega + i\eta}\right]e^{-\beta E_n} \quad . \tag{6.29}$$

6.1.4 Dispersion Relations of Excitations

As it is well known within the Kubo formalism [56], the retarded Green function describes the linear response of a system to an external disturbance [56, 62, 90]. We are now interested for which value of

the wave vector $\mathbf{k}$, describing the spatial dependence, and the frequency ω, describing the temporal dependence, this response becomes arbitrarily strong. The analogs in a classical one-particle system, like a pendulum, are the eigenfrequencies where resonances occur. When neglecting damping, the response is infinitely strong and, therefore, the Green function diverges when the frequency hits a resonance frequency. For a quantum many-particle system, like the one discussed here, these resonances can be described in terms of quasiparticles which provides a more intuitive way of understanding them. The dispersion relation of these quasiparticles describes how the resonance frequencies depend on the wave vector $\mathbf{k}$. Thus, we need to find the poles of the real-time Green function. In order to do this, we take the resummed first-order imaginary-time Green function (6.11), continue it to real time according to (6.28) and obtain

$$\tilde{G}_1(\omega, \mathbf{k}) = \frac{-iC_1^{(0)}(\omega)}{1 - J(\mathbf{k})\, C_1^{(0)}(\omega)} \quad , \tag{6.30}$$

where $C_1^{(0)}(\omega)$ is given by (6.29). Equation (6.30) has poles for

$$1 - J(\mathbf{k}) \frac{1}{\mathcal{Z}^{(0)}} \sum_{n=0}^{\infty} \left[\frac{n+1}{E_{n+1} - E_n + \omega} - \frac{n}{E_n - E_{n-1} + \omega} \right] e^{-\beta E_n} \stackrel{!}{=} 0 \quad , \tag{6.31}$$

where we have already set $\eta \to 0$. Now we only need to solve (6.31) for ω. Because of the infinite sum in (6.31), this can be done only numerically. We will come back to this soon but discuss at first place the zero-temperature limit where analytic solutions are possible. For this case, the solution of (6.31) reads with (5.5)

$$\omega_{1,2}(\mathbf{k}) = \frac{U}{2}(2n-1) - \mu - J(\mathbf{k}) \pm \frac{1}{2}\sqrt{U^2 - UJ(\mathbf{k})(4n+2) + [J(\mathbf{k})]^2} \quad . \tag{6.32}$$

To gain some physical insight into (6.32), we set $J = 0$ and obtain

$$\omega_{\mathrm{p}}^{(0)}(\mathbf{k}) = E_{n+1} - E_n = Un - \mu \quad , \qquad \omega_{\mathrm{h}}^{(0)}(\mathbf{k}) = E_n - E_{n-1} = U(n-1) - \mu \quad . \tag{6.33}$$

From this, we can conclude that ω_{p} is the energy needed to add another particle to a site already occupied by n Bosons. Therefore, we shall call this a "particle" excitation. The second solution ω_{h} is the energy gained when removing a particle from an n-fold occupied site, for which reason we shall call it a "hole" excitation. In the Mott-insulator phase, the excitation spectrum is gapped, which means that $\omega_{\mathrm{p,h}}(\mathbf{0}) \neq 0$. This is most obviously seen for $J = 0$ due to (6.33). For a particle excitation one has to add a particle to a site which costs a finite energy given by (6.33). When we allow hopping, this energy is reduced because of delocalization. If a superfluid is present, we expect the spectrum to be gapless because the added particle can delocalize over the whole system leading to a vanishing energy in the long-wavelength limit.

Examining Eq. (6.32) and also its finite-temperature analog, which we have determined numerically, we see that the excitations have a gap for parameters μ and J which correspond to a system in the Mott phase as given by (6.13) and (6.14), respectively. Furthermore, we can see that the phase transition is characterized by a vanishing gap, i.e. $\omega(\mathbf{0}) = 0$. Because of these considerations, it is reasonable to define a Mott insulator through its excitation gap and the phase boundary as the point where this gap vanishes first time. We will see below that this definition of the phase boundary is equivalent to the one used above. In literature, sometimes, as for example in Ref. [58], a different definition of a Mott insulator is used. There it is defined as an *incompressible* phase but this definition is strictly valid only for $T = 0$ [22]. At first place, we have to understand the reason for the incompressibility of the Mott phase at zero-temperature. In order to change the size of the system by one site, a finite energy is required because at least one particle needs to be transferred to another site. Therefore an infinitesimal change in volume is not possible with an infinitesimal energy and the compressibility is zero. However, when a superfluid is present, the energy change is smooth because the superfluid

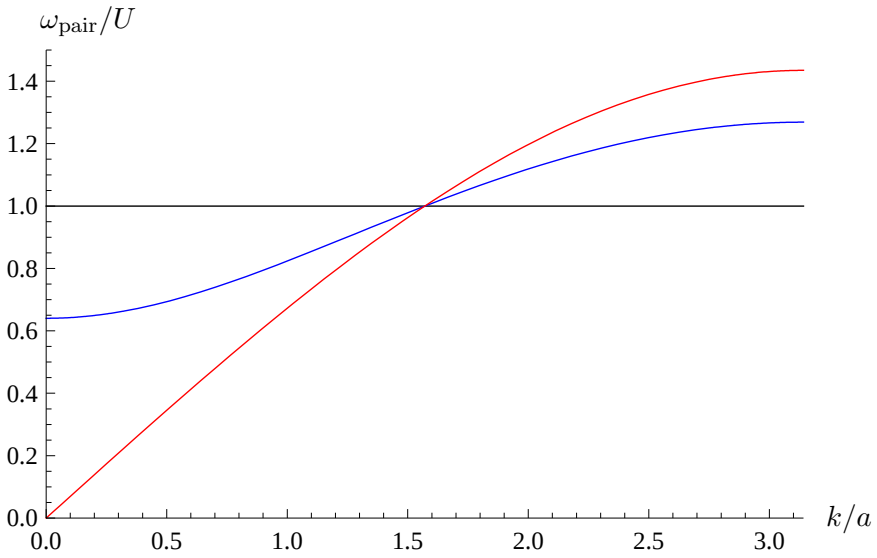

Figure 6.3: Spectrum of the pair excitation for $T = 0$, $n = 1$, and $2DJ = 0$ (black), $2DJ = 0.1\,U$ (blue), $2DJ = 2DJ_{\text{ct}} = 0.1716\,U$ (red) within the first Brillouin zone.

is delocalized and therefore the compressibility is finite. So far the situation for $T = 0$. For finite temperature, thermal fluctuations of the particle number exist also in the Mott phase. Therefore, an infinitesimal change in volume does just change the average particle number per site in an infinitesimal way, leading to a small but finite compressibility [22]. Thus, we calculated in Subsection 6.1.2 the phase-boundary for a transition from a phase with gap to a phase without gap. This definition is equivalent to the one based on the compressibility for $T = 0$ but is also valid and useful for finite temperatures.
The excitations discussed above lack some physical meaning because they involve adding or removing a particle from outside which makes them not very feasible to study experimentally. This is also the reason why they explicitly depend on the chemical potential. Thus, we turn our attention to the dispersion relation of a pair excitation which is explicitly described by removing a particle from one site and putting it to another. Using (6.32), the energy of this process is given for $T = 0$ by

$$\omega_{\text{pair}}(\mathbf{k}) = \omega_{\text{p}}(\mathbf{k}) - \omega_{\text{h}}(\mathbf{k}) = \sqrt{U^2 - UJ(\mathbf{k})(4n+2) + [J(\mathbf{k})]^2} \quad . \tag{6.34}$$

Because such pair excitations do not change the total particle number, they do not depend on the chemical potential μ. Their spectrum is shown in Fig. 6.3. We can now compute the value of J where the gap of the pair excitations vanishes. At this point it does not cost any finite energy to create particle-hole pairs in the long-wavelength limit which leads to the formation of the superfluid. We set (6.34) equal to zero and obtain

$$\omega_{\text{pair}}(\mathbf{0}) = \sqrt{U^2 - 2DUJ_c(4n+2) + (2DJ_c)^2} \stackrel{!}{=} 0 \quad . \tag{6.35}$$

Solving (6.35) yields

$$\frac{2DJ_{\text{ct}}}{U} = 2n + 1 - 2\sqrt{n(n+1)} \quad . \tag{6.36}$$

For $n = 1$, the numerical value of (6.36) is

$$\left.\frac{2DJ_{\text{ct}}}{U}\right|_{n=1} = 3 - 2\sqrt{2} \approx 0.1716 \quad , \tag{6.37}$$

which is just the value at the tip of the first Mott lobe. To prove this connection in general, we have to find the tip in (6.14) which means that we have to maximize it with respect to μ. Performing the differentiation in (6.14) with respect to the chemical potential μ and setting the derivative equal to zero yields

$$\frac{\partial}{\partial\mu}\frac{1}{\frac{n+1}{E_{n+1}-E_n}-\frac{n}{E_n-E_{n-1}}}=\left[\frac{n(n+1)}{(\mu/U+1)^2}-1\right]\stackrel{!}{=}0 \quad . \tag{6.38}$$

When we solve this for μ, we obtain the positive solution

$$\mu_\mathrm{t}/U=\sqrt{n(n+1)}-1 \quad . \tag{6.39}$$

Inserting (6.39) back into (6.14) gives us the same value of the critical hopping at the tip as obtained in (6.36).

Now we examine, how temperature affects the dispersion relation. The presence of thermal fluctuations makes the situation more difficult. Now also the energy of the pair excitation depends on the chemical potential. This is understandable because for finite temperature we do not have an fixed integer filling anymore but only an average one which is related to the chemical potential in a bijective way (see also Chapter 3). This dependence is shown in Fig. 6.5. When solving (6.31) numerically, one can see that the effect of temperature on the dispersion relation is strongest for those values of μ which correspond to fractional filling. Because we know already from examining the phase boundary in Subsection 6.1.2 that thermal fluctuations shift the superfluid transition to higher values of J, it is not unexpected that this suppression of the superfluid can also be seen in the excitation spectrum. To examine the thermal fluctuation in a more quantitative way, we consider the thermal fluctuations of the particle number per site in the unperturbed system. They are defined as

$$\langle\delta n\rangle=\sqrt{\left\langle\left(\hat{n}-\langle\hat{n}\rangle\right)^2\right\rangle} \quad , \tag{6.40}$$

which can be simplified to

$$\langle\delta n\rangle=\sqrt{\langle\hat{n}^2\rangle-\langle\hat{n}\rangle^2} \quad . \tag{6.41}$$

With the definition of the thermal average (3.7), Eq. (6.41) becomes

$$\langle\delta n\rangle=\sqrt{\frac{\sum_n n^2\,e^{-\beta E_n}}{\mathcal{Z}^{(0)}}-\left[\frac{\sum_n n\,e^{-\beta E_n}}{\mathcal{Z}^{(0)}}\right]^2} \quad , \tag{6.42}$$

which is shown in Fig. 6.6. The thermal fluctuations are strongest where the particle number changes most rapidly and the regions of strong fluctuations become larger for increasing temperature.

Thus, it is reasonable that temperature affects the spectrum most for chemical potentials which correspond to fractional fillings as it is clearly visible in Fig. 6.4. In order to clarify this fact further, one can plot the temperature-dependence of the gap $E_\mathrm{gap}=\omega_\mathrm{pair}(\mathbf{0})$ for different hopping parameters and particle numbers, which are controlled by the chemical potential, as we have done in Fig. 6.7. The broadening of the gap for higher temperatures, which was already obtained in Ref. [93], seems a bit counter-intuitive at first sight but we have to keep in mind that we are still in a very low temperature regime. What we observe is the thermal suppression of quantum tunneling. For this reason, it is also obvious that temperature does not affect the gap for vanishing hopping (see black curve in Fig. 6.7). Because the gap is a quantity which is experimentally accessible [68], this effect could be a candidate to serve as a thermometer for Bosons in optical lattices.

6.1.5 Effective Masses

As widely known from condensed matter physics, excitations, which have not too short lifetimes, can by described by quasi-particles propagating through the many-body medium [63]. A prominent

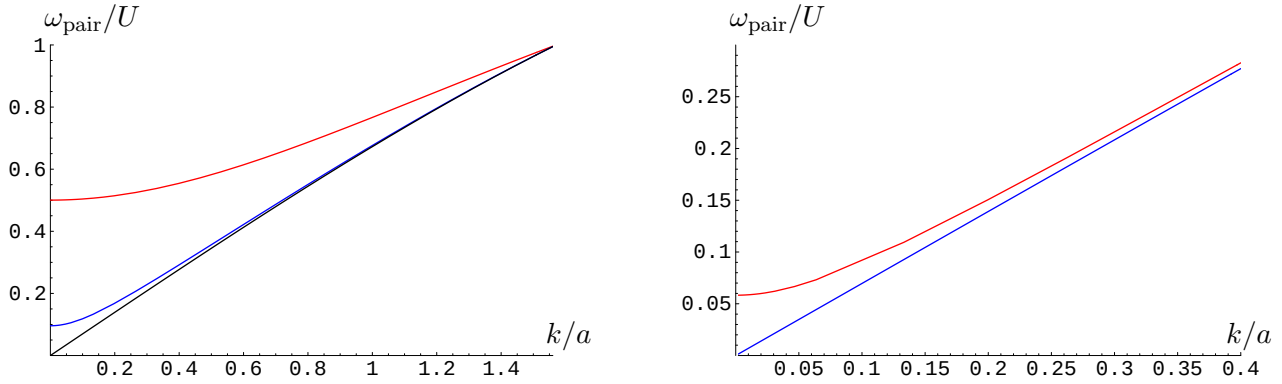

Figure 6.4: Spectrum of a pair excitation for $2DJ = 2DJ_{c(T=0)} = 0.1716$. $T = 0.3\,U$ (red), $T = 0.01\,U$ (blue), $T = 0$ (black). Left: Large thermal fluctuations, fractional filling ($\mu = 0.05\,U$). Right: Small thermal fluctuations, near integer filling ($\mu = 0.2\,U$). Compare Fig. 6.6.

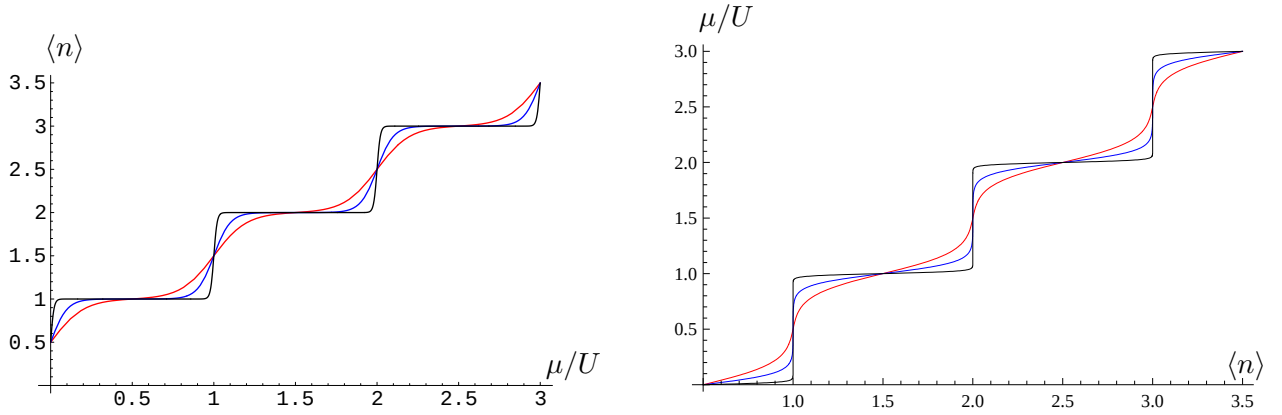

Figure 6.5: Left: Dependence of the average particle number per site on the chemical potential. Right: Dependence of the chemical potential on the average particle number per site. $T = 0.1\,U$ (red), $T = 0.05\,U$ (blue), $T = 0.01\,U$ (black).

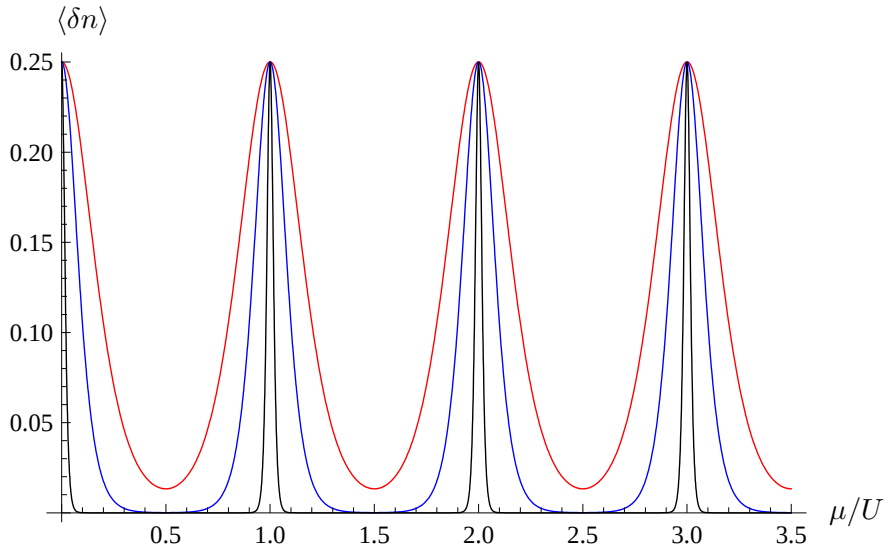

Figure 6.6: Fluctuations of particle number per site for $J = 0$.

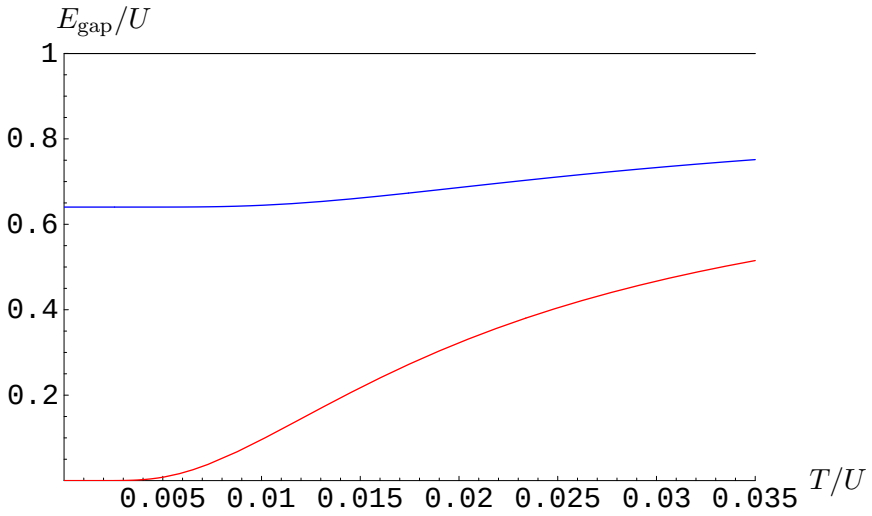

Figure 6.7: Temperature dependence of the gap of pair excitations. Fractional filling, $\mu = 0.05\,U$. $2DJ = 2DJ_{\mathrm{ct}(T=0)} = 0.1716\,U$ (red), $2DJ = 0.1\,U$ (blue), and $J = 0$ (black).

example are particles and holes in a semiconductor [94]. Such quasi-particles bear an effective mass which governs their motion. This effective mass can strongly deviate from the physical mass of the electrons. In this subsection, we calculate such effective masses for the excitations of the Bose-Hubbard model in the Mott phase at zero temperature for a three-dimensional system. The dispersion relation of massive particles is of the form

$$\omega_{\mathrm{p,h}}(\mathbf{k}) = E_{\mathrm{gap}} + \frac{\mathbf{k}^2}{2M_{\mathrm{p,h}}} + \ldots \quad , \tag{6.43}$$

where $M_{\mathrm{p,h}}$ are the effective masses of the particles and holes, respectively. In order to obtain these effective masses, we have to expand (6.32) around $\mathbf{k} = \mathbf{0}$ and solve the coefficient of the $\mathbf{k}^2$ term for $M_{\mathrm{p,h}}$. Doing this yields

$$M_{\mathrm{p,h}}/U = \frac{1}{\tilde{J}} \frac{\sqrt{1 + 36\tilde{J}(\tilde{J}-1)}}{3 - 6\tilde{J} \pm \sqrt{1 + 36\tilde{J}(\tilde{J}-1)}} \quad , \tag{6.44}$$

where we have used the abbreviation $\tilde{J} = J/U$. Thus, we see that the particles and holes become infinitely heavy for vanishing hopping as (6.44) diverges in the limit $\tilde{J} \to 0$. On the other hand, the excitations become massless at the critical point. This is a consequence of the Nambu-Goldstone theorem which states that when a continuous symmetry is broken, massless excitations exist [56]. The symmetry involved here is the $U(1)$ gauge-invariance. In the Mott phase, we can arbitrarily choose the phase of the wave function while in the superfluid the phase is fixed because of the existence of a collective wave function which describes the superfluid. Comparing our result with numerical simulations from Ref. [95] in Fig. 6.8, one sees that they have the same qualitative form and only disagree in the position of the critical point. This is just an obvious consequence of the underestimation of the critical hopping by mean-field theory which was already encountered in Subsection 6.1.2.

6.1.6 Time-of-Flight from Resummed Green's Function

After having successfully calculated the phase boundary and also the excitation spectrum from the resummed Green function (6.11), we use it now to improve also our time-of-flight pictures. As seen

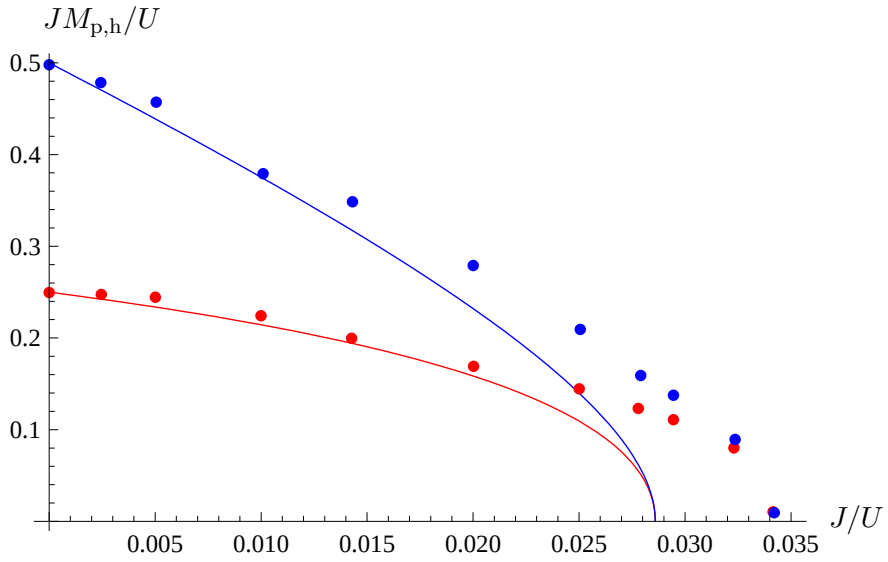

Figure 6.8: Effective masses of particles (red) and holes (blue) in the Mott phase. Dots: Quantum Monte-Carlo data from Ref. [95].

in Subsection 6.1.1, the pictures in Fig. 6.1, which were calculated from the first-order Green function (5.81) are good for deep lattices but do not reproduce the sharp peaks observed in the experiments for low lattice depths, e.g. in Ref. [17]. We show now that we can get better results from the resummed Green function. To this end, we must first transform (6.10) into the time domain. Because of the remarks in Subsection 6.1.1, we focus to the zero-temperature case where the Matsubara frequencies $\omega_m = 2\pi m/\beta$ become infinitely dense, and the sum over all ω_m is replaced by an integral over the continuous variable which we will also call ω_m in order not to mix it up with the real-time frequency ω. We will not introduce a special notation to denote zero-temperature quantities because we will not consider finite-temperature ones in this subsection. The resummed Green function in the time domain is obtained by Fourier transforming (6.11) back into the time domain and reads

$$\tilde{G}_1^{(1)}(\tau'|0;\mathbf{k}) = \frac{1}{2\pi}\int_{-\infty}^{\infty} d\omega_m \, \frac{C_1^{(0)}(\omega_m)}{1 - J(\mathbf{k})\, C_1^{(0)}(\omega_m)} e^{-i\omega_m \tau'} \quad , \tag{6.45}$$

where we restrict ourselves to the case $\tau' > 0$. The one-particle cumulant (5.87) reads in the zero-temperature limit

$$C_1^{(0)}(\omega_m) = \frac{n+1}{E_{n+1} - E_n + i\omega_m} - \frac{n}{E_n - E_{n-1} + i\omega_m} \quad . \tag{6.46}$$

Inserting (6.46) into (6.45) yields with (5.5)

$$\tilde{G}_1^{(1)}(\tau'|0;\mathbf{k}) = \frac{1}{2\pi}\int_{-\infty}^{\infty} d\tilde{\omega}_m \, \frac{1 + \tilde{\mu} - i\tilde{\omega}_m}{\tilde{J}(\mathbf{k})(-\tilde{\mu} - 1 + i\tilde{\omega}_m) - (n - \tilde{\mu} - 1 + i\tilde{\omega}_m)(n - \tilde{\mu} + i\tilde{\omega}_m)} e^{-i\omega_m \tau'} \quad , \tag{6.47}$$

where we have introduced a dimensionless chemical potential $\tilde{\mu} = \mu/U$ and Matsubara frequency $\tilde{\omega}_m = \omega_m/U$. The poles of the integrand in Eq. (6.47) lie at

$$\tilde{\omega}_{1/2} = \frac{i}{2}\left[2n - 2\tilde{\mu} - 1 - \tilde{J}(\mathbf{k}) \pm \sqrt{\tilde{J}(\mathbf{k})^2 - \tilde{J}(\mathbf{k})(4n+2) + 1}\,\right] \quad . \tag{6.48}$$

For the further derivations, the sign of the radicand in (6.48) is crucial. First we note that the radicand is positive for $J = 0$. Therefore, we consider this case first. Now we make use of the residue theorem

again. The pole $\tilde{\omega}_1$ lies in the upper half of the complex plane and, therefore, does not contribute to this integral, while $\tilde{\omega}_2$ lies in the lower one. Thus, we obtain in the limit $\tau' \searrow 0$:

$$\tilde{G}_1^{(1)}(\mathbf{k}) = -\frac{\tilde{J}(\mathbf{k}) - 1 - 2n + \sqrt{\tilde{J}(\mathbf{k})^2 - \tilde{J}(\mathbf{k})(4n+2)+1}}{2\sqrt{\tilde{J}(\mathbf{k})^2 - \tilde{J}(\mathbf{k})(4n+2)+1}} \quad . \tag{6.49}$$

We note that (6.49) does no longer depend on the chemical potential. The physical reason for this is the same as already discussed in Subsection 4.1.2. As the next step, we look for the value of $\tilde{J}(\mathbf{k})$ for which the radicand in (6.48) becomes zero. Setting

$$\tilde{J}(\mathbf{k})^2 - \tilde{J}(\mathbf{k})(4n+2) + 1 \stackrel{!}{=} 0 \tag{6.50}$$

yields

$$\frac{J_c(\mathbf{k})}{U} = 2n + 1 \pm \sqrt{n(n+1)} \quad , \tag{6.51}$$

which is just the generalization of (6.36) to arbitrary wave vectors $\mathbf{k}$. Thus, we can state that the radicand is positive for $\tilde{J}(\mathbf{k}) < 2n+1-\sqrt{n(n+1)}$ and for $\tilde{J}(\mathbf{k}) > 2n+1+\sqrt{n(n+1)}$. Recalling (6.6) we see that $J(\mathbf{0}) = 2DJ$. Thus, Eq. (6.49) is valid only in the Mott phase. Furthermore, we observe that because $J(\mathbf{0}) \geq J(\mathbf{k})$ for all $\mathbf{k}$, the Green function really diverges first in the long-wavelength limit which is exactly the behavior expected at a phase transition [4]. Unfortunately, it is not possible to get results in the superfluid phase. When the radicand in (6.48) is negative, the poles obtain a real-part which leads a to complex unphysical Green function. The second region where the radicand in (6.49) is positive, i.e. $\tilde{J}(\mathbf{k}) > 2n+1+\sqrt{n(n+1)}$, is not physically reasonable either because its positivity is not true for *all* values of $\tilde{J}(\mathbf{k})$ which leads to complex Green functions for some wave-vectors $\mathbf{k}$. Because of these problems, we proceed now in a different way. In order to be able to extract meaningful information in the superfluid region nevertheless, we expand (6.45) back into a geometrical series and integrate term by term:

$$\tilde{G}_1^{(1)}(\tau'|0;\mathbf{k}) = \frac{1}{2\pi}\sum_{l=0}^{\infty} J(\mathbf{k})^l \int_{-\infty}^{\infty} d\omega_m \, C_1^{(0)}(\omega_m)^{l+1} e^{-i\omega_m\tau'} \quad . \tag{6.52}$$

Now we can insert (6.46) into (6.52) and get

$$\tilde{G}_1^{(1)}(\tau'|0;\mathbf{k}) = \frac{1}{2\pi}\sum_{l=0}^{\infty} J(\mathbf{k})^l \int_{-\infty}^{\infty} d\omega_m \left[\frac{n+1}{E_{n+1}-E_n+i\omega_m} - \frac{n}{E_n - E_{n-1}+i\omega_m}\right]^{l+1} e^{-i\omega_m\tau'} \quad . \tag{6.53}$$

As a next step we have to calculate the remaining integral. This is most easily done with the help of the residue theorem again. We insert (5.5) and obtain

$$\tilde{G}_1^{(1)}(\tau'|0;\mathbf{k}) = \frac{1}{2\pi}\sum_{l=0}^{\infty} \frac{J(\mathbf{k})^l}{U^l} \int_{-\infty}^{\infty} d\tilde{\omega}_m \frac{(\tilde{\mu}+1-i\tilde{\omega}_m)^{l+1}}{[(\tilde{\mu}-n+1-i\tilde{\omega}_m)(n-\tilde{\mu}+i\tilde{\omega}_m)]^{l+1}} e^{-i\tilde{\omega}_m\tilde{\tau}'} \quad , \tag{6.54}$$

where we have introduced a dimensionless imaginary time $\tilde{\tau}' = U\tau'$. The integrand in (6.54) has two $(l+1)$-fold poles at $\tilde{\omega}_1 = i(n-\tilde{\mu}-1)$ and $\tilde{\omega}_2 = i(n-\tilde{\mu})$. Because of the relation between the chemical potential and the particle number per site for $T = 0$ (5.6), $\tilde{\omega}_1$ is always in the lower half plane of the the complex ω_m-plane, while $\tilde{\omega}_2$ is always in the upper half plane. To calculate the residue of the contributing pole at $\tilde{\omega}_1$, we need the general formula for a n-fold pole [91]:

$$\mathrm{Res}_a f(z) = \frac{1}{(n-1)!}\lim_{z\to a}\frac{\partial^{n-1}}{\partial z^{n-1}}\left[(z-a)^n f(z)\right] \quad . \tag{6.55}$$

Applying this to our case yields

$$(\tilde{\omega}_m - \tilde{\omega}_1)^{l+1} f(\tilde{\omega}) = \frac{1}{i^{l+1}} \left(\frac{\tilde{\mu} + 1 + i\tilde{\omega}_m}{n - \tilde{\mu} - i\tilde{\omega}_m} \right)^{l+1} e^{-i\tilde{\omega}_m \tilde{\tau}'} \quad . \tag{6.56}$$

With the help of (6.56) we obtain from Eq. (6.54)

$$\tilde{G}_1^{(1)}(\tau'|0;\mathbf{k}) = -\sum_{l=0}^{\infty} \frac{1}{i^l l!} \frac{J(\mathbf{k})^l}{U^l} \frac{\partial^l}{\partial \tilde{\omega}_m^l} \left[\left(\frac{\tilde{\mu} + 1 - i\tilde{\omega}_m}{n - \tilde{\mu} + i\tilde{\omega}_m} \right)^{l+1} e^{-i\tilde{\omega}_m \tilde{\tau}'} \right]_{\tilde{\omega}_m = \tilde{\omega}_1} \quad . \tag{6.57}$$

Now we have to differentiate (6.56) l-times with respect to $\tilde{\omega}_m$, which is a quite cumbersome task in general. But because we are, in the end, only interested in the limit $\tau' \searrow 0$, it is possible to simplify (6.57) to

$$\tilde{G}_1^{(1)}(\mathbf{k}) = -\sum_{l=0}^{\infty} \frac{1}{i^l l!} \frac{J(\mathbf{k})^l}{U^l} \frac{\partial^l}{\partial \tilde{\omega}_m^l} \left[\left(\frac{\tilde{\mu} + 1 - i\tilde{\omega}_m}{n - \tilde{\mu} + i\tilde{\omega}_m} \right)^{l+1} \right]_{\tilde{\omega}_m = \tilde{\omega}_1} \quad . \tag{6.58}$$

Note that the derivatives of $e^{-i\tilde{\omega}_m \tilde{\tau}'}$ cannot contribute, because they all contain at least one factor of $\tilde{\tau}$ and therefore vanish in the considered limit. In order to check the intermediate result (6.58), it is useful to consider the term with $l = 0$, because this is just the equal-time Green function of the unperturbed system. Doing this, we obtain from (6.58):

$$G_1^{(0)}(\mathbf{k}) = n \quad . \tag{6.59}$$

This is just the Fourier transform of the zero-temperature limit of (5.76) with (5.37). Setting $l = 1$ in (6.58) also reproduces the first-order result calculated in (6.8).
For the further development, it is useful to write (6.58) in the form

$$\tilde{G}_1^{(1)}(\mathbf{k}) = \sum_{l=0}^{\infty} \left(\frac{J(\mathbf{k})}{U} \right)^l S_l \quad , \tag{6.60}$$

where the respective dimensionless coefficients are determined according to

$$S_l = -\frac{1}{i^l l!} \frac{\partial^l}{\partial \tilde{\omega}_m^l} \left[\left(\frac{\tilde{\mu} + 1 - i\tilde{\omega}_m}{n - \tilde{\mu} + i\tilde{\omega}_m} \right)^{l+1} \right]_{\tilde{\omega}_m = \tilde{\omega}_1} \quad . \tag{6.61}$$

When explicitly performing the derivatives with respect to $\tilde{\omega}_m$ in (6.61), the chain and product rule of differentiation produce terms with all powers of n up to $l + 1$. In order to find a simpler expression for the coefficients (6.61), we perform a transformation of variables which yields

$$S_l = \frac{1}{l!} \left[\frac{\partial^l}{\partial y^l} \left(\frac{y + n}{1 - y} \right)^{l+1} \right]_{y=0} \quad , \tag{6.62}$$

which can be rewritten as

$$S_l = \frac{1}{l!} \left\{ \frac{\partial^l}{\partial y^l} \left[\sum_{k=0}^{l+1} \binom{l+1}{k} \frac{(n+1)^k}{(1-y)^k} (-1)^{l+1-k} \right] \right\}_{y=0} \quad . \tag{6.63}$$

Now the derivatives can be performed with the help of the formula

$$\frac{\partial^l}{\partial y^l} (1 - y)^{-k} = \frac{(k + l - 1)!}{(k - 1)!} (1 - y)^{-k-l} \quad . \tag{6.64}$$

S_0	n
S_1	$2n + 2n^2$
S_2	$3n + 9n^2 + 6n^3$
S_3	$4n + 24n^2 + 40n^3 + 20n^4$
S_4	$5n + 50n^2 + 150n^3 + 175n^4 + 70n^5$

Figure 6.9: Coefficients for the calculation of the equal-time correlation from the resummed Green function.

Inserting (6.64) into (6.63) yields the final result

$$S_l = (l+1) \sum_{k=0}^{l+1} \frac{(l+k-1)!(-1)^{l-k+1}(n+1)^k}{(l-k+1)!k!(k-1)!} \quad . \tag{6.65}$$

We note that with the help of the hypergeometric function ${}_2F_1(\alpha, \beta; \gamma; z)$ [96, (9.100)], Eq. (6.65) can be written as

$$S_l = (-1)^l (n+1)(l+1)\, {}_1F_2(-l, l+1; 2; n+1) \quad . \tag{6.66}$$

Now one can use a symbolic computer-algebra program like Mathematica to calculate the coefficients S_l explicitly from (6.66). The first few of them are tabulated in Fig. 6.9. The coefficients (6.66) are closely related to the closed form of the resummed Green function in the Mott phase in Eq. (6.49). When Eq. (6.49) is expanded into powers of $J(\mathbf{k})$, the expansion coefficients are just given by S_l in Eq. (6.65), which is a good crosscheck for the correctness of our results.

We note that the series (6.60) only converges within the Mott phase, i.e. for $J < J_{\mathrm{ct}}$ with J_{ct} given by (6.36) Nevertheless, we can also get meaningful results in the superfluid phase. We only need to deal with the problem of the divergence of the series (6.60). Because we have summed in (6.60) only a subset of diagrams of a given order, the Green functions and, therefore, the pictures are not normalized anymore. This is meant in that sense, that the overall intensity becomes arbitrarily strong. But this is no real problem at all because only differences between regions with high and low intensity in the $k_x - k_y$-plane, corresponding to dark and light spots, are of interest and everything else is just a matter of suitably choosing the scale. When we plot the time-of-flight pictures resulting from Eq. (6.60), we need to truncate the infinite series after a finite order which we call N. One can see that it is enough to take $N \approx 20$ because a larger N does not lead to visible differences. Therefore, we call the corresponding pictures the *resummed* time-of-flight pictures which we have plotted in Fig. 6.10. These pictures show a notable difference between the Mott insulator and the superfluid phase. In the former, the pictures from the resummed Green function and the one from the first-order perturbation theory show only minor differences as it can bee seen in Fig. 6.10 (a) and (b). This is reasonable because we already noted in Subsection 6.1.1 that our perturbation theory is good in the Mott phase. In the superfluid phase, the situation is different, as shown in (c) and (d). The resummed pictures show the characteristic sharp peaks which were also observed in the experiment while the first-order ones lack them as discussed in Subsection 6.1.1. Thus, we can say that the resummation procedure allowed us to explain experimental results which were not explainable by the low-order perturbative calculation performed in Subsection 6.1.1. However, the results are not completely satisfactory because of the unphysical non-convergent nature of the series (6.60). Furthermore, we note that Fig. 6.10 (d) does not only show the expected and experimentally measured peaks corresponding to the sites of the reciprocal lattice but also additional ones between them. As they do not occur when considering the quasi-momentum distribution in the limit of vanishing interaction, as done in Section 4.1.1, we can surely say that they are only an artefact of using the series (6.60) in the region of non-convergence.

To conclude this discussion, we briefly sketch the reason for the sharp interference peaks in the superfluid phase on physical ground: When the system is in the superfluid phase, a fraction of the Bosons

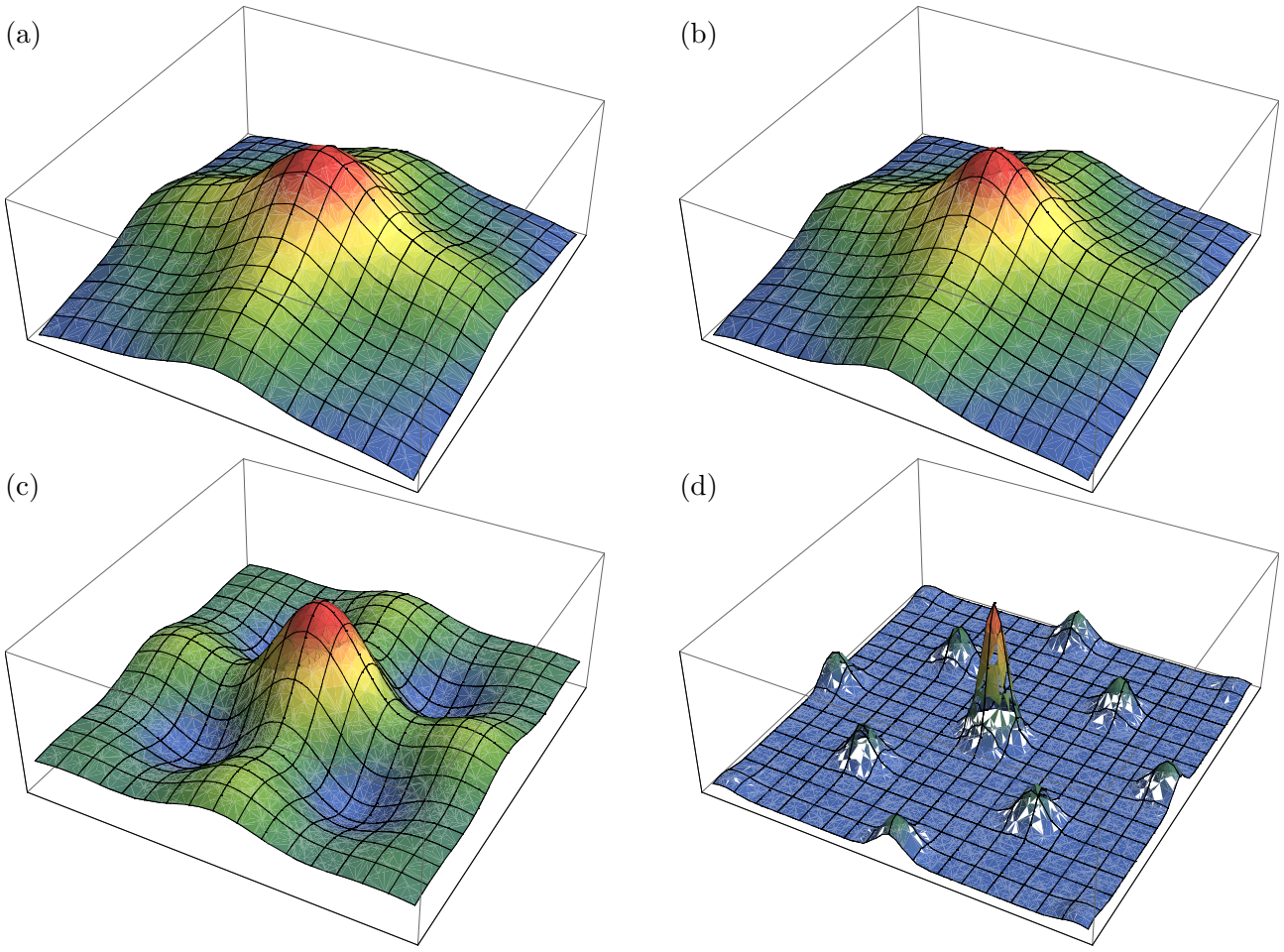

Figure 6.10: Representation of time-of-flight pictures with arbitrary scale and two different lattice depths V_0. (a) and (b): $V_0 = 18\,E_R$. (c) and (d): $V_0 = 8\,E_R$. (a) and (c): First-order perturbation theory. (b) and (d): Resummed (see text).

is completely delocalized over the whole lattice and forms a uniform superfluid which is described in mean-field theory by the order-parameter Ψ, as extensively discussed for the spinor case in Chapter 3. Because the superfluid is spatially uniform, it leads to a constant correlation function in *real* space which corresponds to local correlations in *momentum* space. This is the case because the Fourier transform of a constant is a Kronecker-delta. In order to study these features in more detail, one has to introduce an order parameter into the theory, for example by means of an effective-action formalism [85,97] and calculate the respective Green functions in the presence of this additional background field. This goes beyond the scope of this thesis and will, therefore, not be done.

6.1.7 Visibility from Resummed Green's Function

After having successfully calculated the crucial features in the time-of-flight pictures from the resummed Green function, we now turn to the visibility which was already addressed in Subsection 4.2.3 for the case of a spin-1 system. In this subsection, we use the straightforward specification of (4.34) to a scalar system which reads

$$\mathcal{V} = \frac{n_{\max} - n_{\min}}{n_{\max} + n_{\min}} \quad . \tag{6.67}$$

Because we are now especially interested in the visibility for low lattice depths, we do not use the two-dimensional approximation from Subsection 4.1.2 but carry out the integration over the z axis which leads to

$$n_{\max} = \int_{-\infty}^{\infty} dk_z \, \frac{|w(\mathbf{k})|^2}{a^2} \tilde{G}_1^{(1)}((2\pi/a, 0, k_z/a)) \;, \quad n_{\min} = \int_{-\infty}^{\infty} dk_z \, \frac{|w(\mathbf{k})|^2}{a^2} \tilde{G}_1^{(1)}((\sqrt{2}\pi/a, \sqrt{2}\pi/a, k_z a)) \quad , \tag{6.68}$$

where we have used the resummed Green function in Fourier space (6.60) and the Fourier transform of the Wannier function (4.28). Now we are in the position to calculate the visibility for arbitrary lattice depths. Before we do this, we take a moment to discuss the connection between the parameters of the Bose-Hubbard model U and J and the experimentally adjustable parameter, which is the lattice depth V_0. In order to obtain the parameter J, one must use (2.13). To evaluate the occurring integrals, one has to know the Wannier function. When we approximate it by a Gaussian (4.28) and use the dimensionless lattice depth $\tilde{V}_0 = V_0/E_R$ again, we get for not too low lattice depths [23]

$$J \approx E_R \left(\frac{\pi^2}{4} - 1 \right) \tilde{V}_0 \, e^{-\pi^2 \sqrt{\tilde{V}_0}/4} \quad , \tag{6.69}$$

from which we see that J decays with V_0 exponentially. This is reasonable because it is well known that tunneling probabilities have an exponential dependence on the barrier height. In order to get a formula for the interaction energy, we specify (2.14) to the scalar Bose-Hubbard Model and get

$$U = a_S \int d^3\mathbf{x} |w(\mathbf{x} - \mathbf{x}_i)|^4 \quad , \tag{6.70}$$

where a_S is the s-wave scattering length. In the harmonic approximation Eq. (6.70) becomes [23]

$$U = \sqrt{8\pi} E_R \frac{a_S}{a} \tilde{V}_0^{3/4} \quad , \tag{6.71}$$

where the ratio between the s-wave scattering length a_S and the lattice constant a occurs. From (6.71) we see that U depends only algebraically on $\tilde{V}_0$.

Because the harmonic approximation (6.69), (6.71) has quite large errors, as extensively discussed in Ref. [23], we will not employ it here but use the numerically determined parameters $J(\tilde{V}_0)$ and $U(\tilde{V}_0)$ instead, which we have obtained with the help of a Mathematica program [59]. In Fig. 6.11, we have shown the visibility for varying values of $U/(2DJ)$ in a double-logarithmic plot. Comparing the red and the black curve, one can see that they fairly agree in the deep Mott phase. The visibility depends nearly linearly on J/U in this region. In the superfluid phase, the result from the first-order perturbation theory (black) clearly shows unphysical behavior because it gets larger than unity which is impossible according to the definition (6.67). This it not suprising because the simple perturbation theory breaks down in this region. However, the result from the curve from the resummed Green function (red) does not show these problems but approaches unity as it is expected and also measured experimentally in Ref. [77]. Thus, our resummation procedure allows us to extend the calculation of the visibility, which was calculated for systems in the Mott phase in Ref. [23], to the whole parameter space, i.e. even deep into the superfluid phase. Note that unlike the corresponding result for the time-of-flight in the previous subsection, the visibility does not need any artificial scaling because the respective series for the visibility converges for all values of J/U. To be more precise, it converges to unity for parameter values in the superfluid phase. This seems to be not absolutely correct because it is expected from Bogoliubov theory [71] that the visibility is smaller than unity also in the superfluid phase and approaches unity only for vanishing interaction $U \to 0$. When we compare our theoretical result with experimental data in Fig. 6.11, we see that their exists quite a large disagreement. One main reason is the fact that the experimentally determined particle numbers have quite large errors. Thus, we do not know exactly how many particles occupy one lattice site. Furthermore, in the experiment,

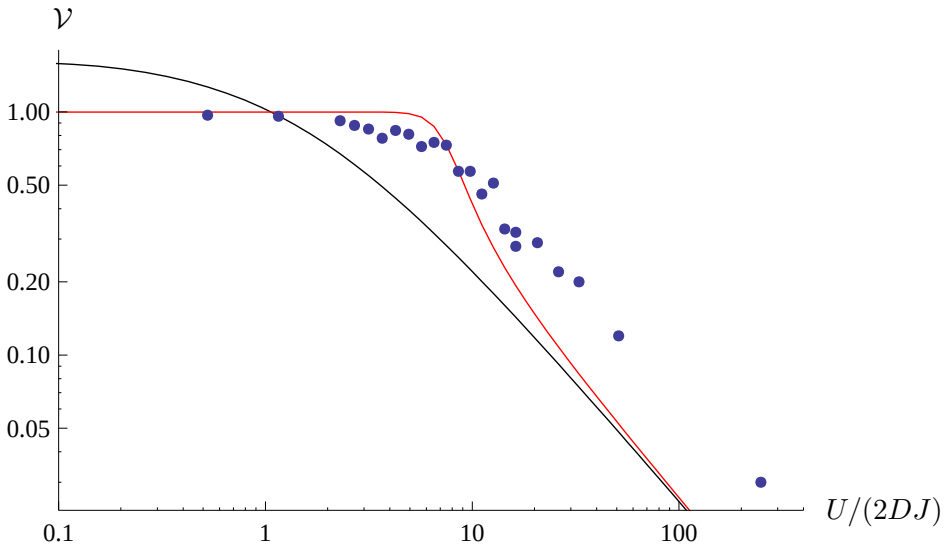

Figure 6.11: Visibility for $n = 2$ and $T = 0$. Black: Result from first-order perturbation theory. Red: Result from resummed Green's function. Dots: Experimental data from Ref. [77]

the system is not homogeneous as in our theoretical consideration. An additional confining trap is used, as mentioned in Chapter 1, which leads to the formation of a so-called wedding-cake structure where Mott shells with different particle numbers per site exist [23,68]. Here we have only considered the innermost one, thus, we have overestimated the visibility. In addition to these complications, superfluid regions exist between these shells which lead to an increased visibility.

6.1.8 Correlation Functions

While we were discussing the phase boundary in Subsection 6.1.2 we noted that the phase transition is characterized by diverging long wave-length correlations. In this subsection we investigate in more details how the correlations between different lattice sites behave. We restrict ourselves to the zero-temperature case again. We explain the main concepts for a one-dimensional system for reasons of simplicity but generalization to arbitrary spatial dimension is straightforward. In order to study the correlation function as a function of the distance between the sites, we define

$$K(r) = \langle \hat{a}_i^\dagger \hat{a}_j \rangle = \lim_{\tau' \searrow 0} G_1(\tau', i|0, j) \qquad \text{with} \qquad d(i,j) = r/a \quad . \tag{6.72}$$

Because we are interested in the behavior of $K(r)$ for large distances r, we cannot use finite-order perturbation theory but we have to use the resummed Green's function instead. Thus, we consider the resummed equal-time Green function (6.60) and Fourier transform it into real-space:

$$\tilde{K}^{(1)}(j) = \frac{a}{2\pi} \int_{-\pi/a}^{\pi/a} dk\, \tilde{G}^{(1)}(k)\, e^{-ikr} \quad . \tag{6.73}$$

From the explicit form of (6.60) we can see that the calculation of the Fourier transform boils down to the evaluation of the integrals

$$I_l = \frac{a}{2\pi} \int_{-\pi/a}^{\pi/a} dk\ [2\cos(ka)]^l\ e^{-ikr} \quad . \tag{6.74}$$

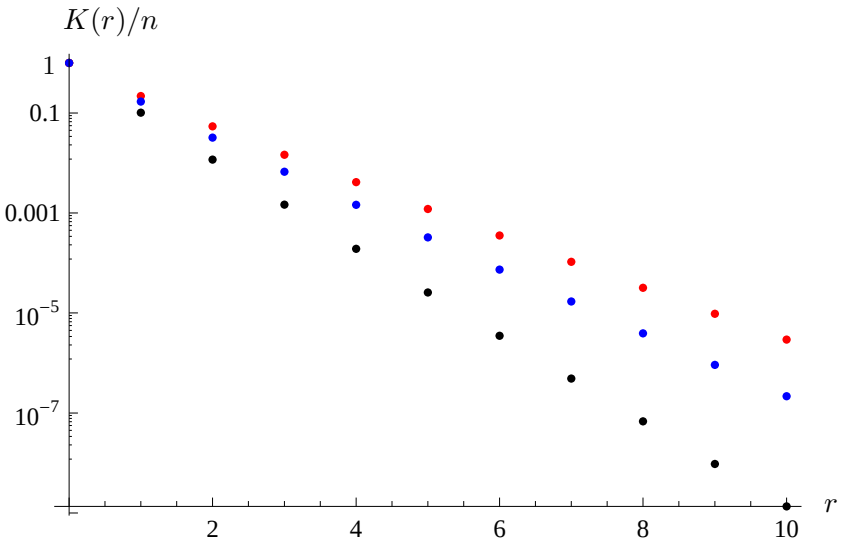

Figure 6.12: Logarithmic plot of decay of correlations in Mott phase for hopping parameters $2DJ = 0.04\,U$ (black), $2DJ = 0.06\,U$ (blue), and $2DJ = 0.09\,U$ (red). The corresponding correlation-lengths are $\xi_1 = 0.31\,a$, $\xi_2 = 0.48\,a$, and $\xi_3 = 0.66\,a$.

As an example we just state the result of (6.74) for $l = 2$ which reads

$$I_2 = \frac{4(\tilde{r}^2 - 2)\sin(\pi\tilde{r})}{\pi(\tilde{r}^3 - 4\tilde{r})} \quad , \tag{6.75}$$

where $\tilde{r} = r/a$. Evaluating (6.75) at the discrete values $\tilde{r} = 0, 1, \ldots$ yields

$$I_2 = 2\delta_{\tilde{r},0} + \delta_{\tilde{r},2} \quad , \tag{6.76}$$

which is the same result as obtained when just counting the possibilities to make two jumps on a one-dimensional lattice starting from the origin. The formula for general values of J is difficult to state in a closed form but easily calculated with the help of an symbolic computer algebra program. We note that an equivalent result could, in principle, be obtained by Fourier transforming Eq. (6.49) back into real-space. However, this is not possible analytically but only by means of numerical integration. Thus, it is more convenient to use the series respresentation (6.60) instead. In Fig. 6.12, we have shown the exponential decay of the correlations which is described by the functional form

$$K(r) \propto e^{-r/\xi} \quad , \tag{6.77}$$

where ξ is the correlation length [5], which can be obtained by fitting (6.77) to Fig. 6.12. For a system in the Mott phase, the correlation-length ξ is of the order of the lattice constant a (see Fig. 6.12), as it is expected. The divergence of ξ when approaching the critical point is discussed below.

6.1.9 Extension to Spin-1 Systems

In this subsection, we sketch how to extend the Green function approach to the spin-1 Bose-Hubbard model which was discussed in the Chapters 2–4. In the definition of the Green function in (5.7) we have to give the operators additional indices α' and α which correspond to the three hyperfine states α. Thus, the full one-particle Green function becomes

$$G_1(\tau', j', \alpha'|\tau, j, \alpha) = \frac{1}{\mathcal{Z}}\mathrm{Tr}\left\{e^{-\beta\hat{H}}\hat{T}\left[\hat{a}_{\alpha j,\mathrm{H}}(\tau)\hat{a}^{\dagger}_{\alpha' j',\mathrm{H}}(\tau')\right]\right\} \quad . \tag{6.78}$$

The same applies to the n-particle Green function and also to the cumulants. Now we proceed like in the scalar case but with one slight change: The perturbative Hamiltonian in Dirac representation now reads

$$\hat{H}_{1\mathrm{D}}(\tau) = -\sum_{\alpha}\sum_{i,j} J_{i,j}\hat{a}^{\dagger}_{i\alpha}(\tau)\hat{a}_{j\alpha}(\tau) \quad , \tag{6.79}$$

where we have to sum over all hyperfine states wherever a perturbation operator occurs. For the diagrammatic rules, this means the following: Every internal line gets an additional spin index which must be summed from -1 to $+1$. External lines get *fixed* spin indices corresponding to α and α' in (6.78). The second important difference occurs, when calculating the cumulants. There we have to use the states $|S,m,n\rangle$ instead of the states $|n\rangle$ and perform the trace over the full Fock space. As the easiest example we calculate the zeroth-order result:

$$G_1^{(0)}(\tau',\alpha'|\tau,\alpha) = \frac{1}{\mathcal{Z}^{(0)}}\sum_{S,m,n}\langle S,m,n|\hat{T}\left[\hat{a}^{\dagger}_{\alpha'}(\tau')\hat{a}_{\alpha}(\tau)\right]|S,m,n\rangle e^{-\beta E_{S,m,n}} \quad . \tag{6.80}$$

Using the matrix elements M, N, O, and P from Appendix A, we can write this as

$$\begin{aligned} G_1^{(0)}(\tau',\alpha'|\tau,\alpha) = \frac{\delta_{\alpha\alpha'}}{\mathcal{Z}^{(0)}}\sum_{S,m,n}\Bigg\{ &\Theta(\tau-\tau')\Big[M^2_{\alpha,S,m,n}\, e^{(E_{S,m,n}-E_{S+1,m+\alpha,n+1})(\tau-\tau')} \\ &+ N^2_{\alpha,S,m,n}\, e^{(E_{S,m,n}-E_{S-1,m+\alpha,n+1})(\tau-\tau')}\Big] + \Theta(\tau'-\tau)\Big[O^2_{\alpha,S,m,n}\, e^{(E_{S,m,n}-E_{S+1,m-\alpha,n-1})(\tau'-\tau)} \\ &+ P^2_{\alpha,S,m,n}\, e^{(E_{S,m,n}-E_{S-1,m-\alpha,n-1})(\tau'-\tau)}\Big]\Bigg\} e^{-\beta E_{S,m,n}} \quad . \end{aligned} \tag{6.81}$$

Note that the higher n-particle functions do not have the Kronecker symbol $\delta_{\alpha\alpha'}$ and we must not drop the spin indices. With these tools we can find the corresponding quasi-momentum distribution yielding the same result as in Chapter 4. To find the phase boundary to the different superfluid phases, we perform a resummation as described in Subsection 6.1.2 and look for the divergence of $G_1(\alpha,\alpha;\omega_m = 0, \mathbf{k} = \mathbf{0})$ which yields the same result as with the mean-field approach described in Chapter 3.

6.2 Second Order

After having seen how to get the thermodynamic and dynamic quantities of interest from our Green function approach, we push this method further and see how the respective results improve. To be able to treat the corrections to the mean-field result systematically, it is useful to introduce basic diagrams from which we can get non-perturbative results by summing a geometric series as done in (6.11). A diagram shall be called "one-particle irreducible" when it cannot be divided into two parts by cutting a single line. We denote the sum of all these one-particle irreducible diagrams with their respective weights like a one-particle cumulant but with a big dot. Thus, we define

$\mathcal{C}_1(\omega_m,\mathbf{k}) =$ 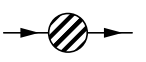 $=$ $+$ 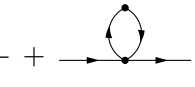 $+\left(\frac{1}{2}\right.$ 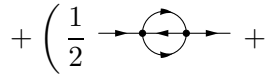 $\left.+\ldots\right)$. (6.82)

From (6.82) we can build up the full Green function by the Dyson-like series

$$G_1(\omega_m,\mathbf{k}) = \sum_{l=0}^{\infty}\Big(\text{ 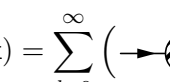 }\Big)^{l+1} J(\mathbf{k})^l = \frac{\mathcal{C}_1(\omega_m,\mathbf{k})}{1-J(\mathbf{k})\mathcal{C}_1(\omega_m)} \quad . \tag{6.83}$$

The procedure used above to get the first-order resummed Green function (6.11) corresponds to the lowest-order approximation in (6.82) which reads

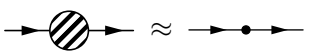 . (6.84)

In this section, we go beyond this.

6.2.1 Self-Energy

A suitable way to describe the dynamics and thermodynamics of a single particle in a many-particle background is to introduce the self-energy [56, 63, 85, 90]. It is defined as

$$\Sigma = \frac{1}{G_1^{(0)}} - \frac{1}{G_1} \quad , \tag{6.85}$$

from which the full Green function can be obtained according to

$$G_1 = \frac{1}{1/G_1^{(0)} - \Sigma} \quad . \tag{6.86}$$

Comparing (6.85) with (6.83) and using (5.76) allows us to write (6.85) as

$$\Sigma(\omega_m, \mathbf{k}) = \frac{1}{C_1^{(0)}(\omega_m)} - \frac{1}{\mathcal{C}_1(\omega_m, \mathbf{k})} + J(\mathbf{k}) \quad , \tag{6.87}$$

which can now be calculated in powers of J. Because no first-order contribution to $\mathcal{C}_1$ exist in (6.82), the first-order self-energy reads

$$\Sigma^{(1)}(\omega_m, \mathbf{k}) = J(\mathbf{k}) \quad . \tag{6.88}$$

Inserting (6.88) into (6.86) just yields again our first-order resummed Green function (6.10). For the calculation of the second-order self-energy we need the second diagram in (6.82) which we will compute in the next subsection.

6.2.2 Calculation of One-Loop Diagram

Of course, we could calculate the one-loop diagram in Matsubara space, but because this involves the quite complicated calculation of a sum over all Matsubara frequencies, we perform the calculation in the time domain. Using the diagrammatic rules in Subsection 5.3.1, the second diagram in (6.82) is evaluated according to

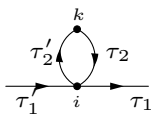

$$= G_1^{(2B)}(\tau_1', i'|\tau_1, i) = 2DJ^2\delta_{i,i'} \int_0^\beta d\tau_2 \int_0^\beta d\tau_2' \, C_2^{(0)}(\tau_1', \tau_2'|\tau_1, \tau_2) G_1^{(0)}(\tau_2|\tau_2') \quad , \tag{6.89}$$

where $G_1^{(2B)}$ is just an abbreviation for the respective diagram and the symmetry factor is one. With the explicit form of the two-particle cumulant (5.39) we get three terms from (6.89) which we calculate

separately for $\tau_1 = 0$. The first one reads

$$G_1^{(2B')}(\tau_1', i'|0, i) = \frac{\delta_{i',i} 2DJ^2}{\mathcal{Z}^{(0)2}} \sum_{k,l} e^{-\beta(E_l+E_k)}$$

$$\times \Bigg\{ k(k-1)(l+1)\, e^{\tau_1'(E_{k-1}-E_{k-2})} \int_{\tau_1'}^{\beta} d\tau_2'\, e^{\tau_2'(E_k-E_{k-1}+E_l-E_{l+1})} \int_0^{\tau_1'} d\tau_2\, e^{\tau_2(E_{k-2}-E_{k-1}-E_l+E_{l+1})} \tag{6.90a}$$

$$+ k^2(l+1)\, e^{\tau_1'(E_k-E_{k-1})} \int_{\tau_1'}^{\beta} d\tau_2'\, e^{\tau_2'(E_k-E_{k-1}+E_l-E_{l+1})} \int_{\tau_1'}^{\tau_2'} d\tau_2\, e^{\tau_2(E_{k-1}-E_k-E_l+E_{l+1})} \tag{6.90b}$$

$$+ k(k+1)l\, e^{\tau_1'(E_k-E_{k-1})} \int_{\tau_1'}^{\beta} d\tau_2\, e^{\tau_2(E_k-E_{k+1}+E_l-E_{l-1})} \int_{\tau_1'}^{\tau_2} d\tau_2'\, e^{\tau_2'(E_{k+1}-E_k-E_l+E_{l-1})} \tag{6.90c}$$

$$+ k(k-1)(l+1)\, e^{\tau_1'(E_k-E_{k-1})} \int_0^{\tau_1'} d\tau_2'\, e^{\tau_2'(E_{k-1}-E_{k-2}+E_l-E_{l+1})} \int_0^{\tau_2'} d\tau_2\, e^{\tau_2(E_{k-2}-E_{k-1}-E_l+E_{l+1})} \tag{6.90d}$$

$$+ k^2 l\, e^{\tau_1'(E_k-E_{k-1})} \int_0^{\tau_1'} d\tau_2\, e^{\tau_2(E_{k-1}-E_k+E_l-E_{l-1})} \int_0^{\tau_2} d\tau_2'\, e^{\tau_2'(E_k-E_{k-1}-E_l+E_{l-1})} \tag{6.90e}$$

$$+ (k+1)kl\, e^{\tau_1'(E_{k+1}-E_k)} \int_{\tau_1'}^{\beta} d\tau_2\, e^{\tau_2(E_k-E_{k+1}+E_l-E_{l-1})} \int_0^{\tau_1'} d\tau_2'\, e^{\tau_2'(E_k-E_{k-1}-E_l+E_{l-1})} \Bigg\} \quad . \tag{6.90f}$$

We note that the two integrals in (6.90a) and (6.90f) are independent from each other and factorize while the remaining terms contain "real" double integrals. The integrations can now be easily carried out and we obtain

$$\begin{aligned}
\text{(6.90a)} =& k(k-1)(l+1)\, e^{\tau_1'(E_{k-1}-E_{k-2})} \frac{e^{\beta(E_k-E_{k-1}+E_l-E_{l+1})} - e^{\tau_1'(E_k-E_{k-1}+E_l-E_{l+1})}}{E_k - E_{k-1} + E_l - E_{l+1}} \\
& \times \frac{e^{\tau_1'(E_{k-2}-E_{k-1}-E_l+E_{l+1})} - 1}{E_{k-2} - E_{k-1} - E_l + E_{l+1}} \quad , && \text{(6.91a)} \\
\text{(6.90b)} =& \frac{k^2(l+1)\, e^{\tau_1'(E_k-E_{k-1})}}{E_{k-1} - E_k - E_l + E_{l+1}} \left[(\beta - \tau_1') - \frac{e^{(\beta-\tau_1')(E_k-E_{k-1}+E_l-E_{l+1})} - 1}{E_k - E_{k-1} + E_l - E_{l+1}} \right] \quad , && \text{(6.91b)} \\
\text{(6.90c)} =& \frac{k(k+1)l\, e^{\tau_1'(E_k-E_{k-1})}}{E_{k+1} - E_k - E_l + E_{l-1}} \left[(\beta - \tau_1') - \frac{e^{(\beta-\tau_1')(E_k-E_{k+1}+E_l-E_{l-1})} - 1}{E_k - E_{k+1} + E_l - E_{l-1}} \right] \quad , && \text{(6.91c)} \\
\text{(6.90d)} =& \frac{k(k-1)(l+1)\, e^{\tau_1'(E_k-E_{k-1})}}{E_{k-2} - E_{k-1} - E_l + E_{l+1}} \left[\tau_1' - \frac{e^{\tau_1'(E_{k-1}-E_{k-2}+E_l-E_{l+1})} - 1}{E_{k-1} - E_{k-2} + E_l - E_{l+1}} \right] \quad , && \text{(6.91d)} \\
\text{(6.90e)} =& \frac{k^2 l\, e^{\tau_1'(E_k-E_{k-1})}}{E_k - E_{k-1} - E_l + E_{l-1}} \left[\tau_1' - \frac{e^{\tau_1'(E_{k-1}-E_k+E_l-E_{l-1})} - 1}{E_{k-1} - E_k + E_l - E_{l-1}} \right] \quad , && \text{(6.91e)} \\
\text{(6.90f)} =& (k+1)kl\, e^{\tau_1'(E_{k+1}-E_k)} \frac{e^{\beta(E_k-E_{k+1}+E_l-E_{l-1})} - e^{\tau_1'(E_k-E_{k+1}+E_l-E_{l-1})}}{E_k - E_{k+1} + E_l - E_{l-1}} \\
& \times \frac{e^{\tau_1'(E_k-E_{k-1}-E_l+E_{l-1})} - 1}{E_k - E_{k-1} - E_l + E_{l-1}} \quad . && \text{(6.91f)}
\end{aligned}$$

By suitably shifting summation indices in (a), (b), (c), and (f), we can get rid of all exponentials containing β which yields

$$\begin{aligned}
(6.90a) =& k(k-1)(l+1)\frac{e^{\tau_1'(E_k-E_{k-2}+E_l-E_{l+1})}-e^{\tau_1'(E_k-E_{k-1})}}{(E_k-E_{k-1}+E_l-E_{l+1})(E_{k-2}-E_{k-1}-E_l+E_{l+1})} \\
&+(k+1)kl\frac{e^{\tau_1'(E_l-E_{l-1})}-e^{\tau_1'(E_k-E_{k-1})}}{(E_{k+1}-E_k+E_{l-1}-E_l)(E_{k-1}-E_k-E_{l-1}+E_l)} \quad , \qquad (6.92a)\\
(6.90b) =& k^2(l+1)\frac{e^{\tau_1'(E_k-E_{k-1})}}{E_{k-1}-E_k-E_l+E_{l+1}}\left[(\beta-\tau_1')+\frac{1}{E_k-E_{k-1}+E_l-E_{l+1}}\right] \\
&+(k+1)^2l\frac{e^{\tau_1'(E_l-E_{l-1})}}{(E_k-E_{k+1}-E_{l-1}+E_l)^2} \quad , \qquad (6.92b)\\
(6.90c) =& k(k+1)l\frac{e^{\tau_1'(E_k-E_{k-1})}}{E_{k+1}-E_k-E_l+E_{l-1}}\left[(\beta-\tau_1')+\frac{1}{E_k-E_{k+1}+E_l-E_{l-1}}\right] \\
&+(k-1)k(l+1)\frac{e^{\tau_1'(E_k-E_{k-2}-E_{l+1}+E_l)}}{(E_k-E_{k-1}-E_{l+1}+E_l)^2} \quad , \qquad (6.92c)\\
(6.90f) =& (k+1)kl\frac{e^{\tau_1'(E_l-E_{l-1})}-e^{\tau_1'(E_k-E_{k-1})}}{(E_k-E_{k+1}+E_l-E_{l-1})(E_k-E_{k-1}-E_l+E_{l-1})} \\
&+(k-1)k(l+1)\frac{e^{\tau_1'(E_k-E_{k-2}-E_{l+1}+E_l)}-e^{\tau_1'(E_k-k-1)}}{(E_{k-1}-E_k+E_{l+1}-E_l)(E_{k-1}-E_{k-2}-E_{l+1}+E_l)} \quad . \qquad (6.92d)
\end{aligned}$$

The next step is to transform this result into Matsubara space. This is straightforward to do, yielding after some rearrangements the result

$$\begin{aligned}
G_1^{(2B')}(\omega_m;i',i) =& \frac{\delta_{i,j}2DJ^2}{\mathcal{Z}^{(0)2}}\sum_{k,l}e^{-\beta(E_l+E_k)} \\
&\times\Bigg\{\frac{k(k-1)(l+1)}{E_k-E_{k-2}+E_l-E_{l+1}+i\omega_m}\Bigg[\frac{2}{(E_{k-1}-E_k-E_l+E_{l+1})(E_k-E_{k-1}+i\omega_m)} \\
&\quad+\frac{1}{(E_k-E_{k-1}-E_{l+1}+E_l)^2}-\frac{1}{(E_k-E_{k-1}+i\omega_m)^2}\Bigg] \\
&+\frac{(k+1)kl}{(E_k-E_{k+1}-E_{l-1}+E_l)(E_k-E_{k-1}+i\omega_m)}\Bigg[\frac{-2}{E_l-E_{l-1}+i\omega_m} \\
&\quad+\frac{1}{E_k-E_{k-1}+i\omega_m}+\frac{1}{E_k-E_{k+1}-E_{l-1}+E_l}\Bigg] \\
&+\frac{(k+1)k(l+1)}{(E_{k-1}+E_k-E_l-E_{l+1})(E_{k+1}-E_k+i\omega_m)}\Bigg[\frac{2}{E_{l+1}-E_l+i\omega_m} \\
&\quad+\frac{-1}{E_{k+1}-E_k+i\omega_m}+\frac{-1}{E_{k-1}-E_k-E_l+E_{l+1}}\Bigg] \\
&+\frac{(k+1)(k+2)l}{E_{k+2}-E_k+E_{l-1}-E_l+i\omega_m}\left[\frac{1}{E_k-E_{k+1}-E_{l-1}+E_l}+\frac{-1}{E_{k+1}-E_k+i\omega_m}\right]^2 \\
&+k^2(l+1)\Bigg[\frac{-1}{(E_{k-1}-E_k-E_l+E_{l+1})(E_k-E_{k-1}+i\omega_m)^2} \\
&\quad+\frac{1}{(E_{k-1}-E_k-E_l-E_{l+1})^2(E_k-E_{k-1}+i\omega_m)}
\end{aligned}$$

$$
\begin{aligned}
&+\frac{1}{(E_k-E_{k-1}-E_{l+1}+E_l)^2(E_{l+1}-E_l+i\omega_m)}\Bigg]\\
&+(k+1)^2 l\Bigg[\frac{-1}{(E_k-E_{k+1}-E_{l-1}+E_l)^2(E_l-E_l-E_{l-1}+i\omega_m)}\\
&+\frac{-1}{(E_k-E_{k+1}-E_{l-1}+E_l)(E_l-E_l-E_{l-1}+i\omega_m)^2}\Bigg]\\
&+\frac{(k+1)^2(l+1)}{(E_{k+1}-E_k+i\omega_m)^2(E_{l+1}-E_l+i\omega_m)}+\frac{-k^2 l}{(E_k-E_{k-1}+i\omega_m)^2(E_l-E_{l-1}+i\omega_m)}\\
&+\beta\Bigg[\frac{k+1}{E_{k+1}-E_k+i\omega_m}-\frac{k}{E_k-E_{k-1}+i\omega_m}\Bigg]\\
&\quad\times\Bigg[\frac{k(l+1)}{E_{k-1}-E_k-E_l+E_{l+1}}+\frac{(k+1)l}{E_{k+1}-E_k-E_l+E_{l-1}}\Bigg]\Bigg\} \quad . \qquad (6.93)
\end{aligned}
$$

We note that every term in (6.93) but the one proportional to β in the last line has a well defined zero-temperature limit. We will see soon how this term is compensated in the limit $\beta\to\infty$. From the second term in (5.39), we get the contribution to (6.89)

$$
G_1^{(2B'')}(\tau_1',i'|\tau_1,i)=-2DJ^2\delta_{i,i'}C_1^{(0)}(\tau_1'|\tau_1)\int_0^\beta d\tau_2\int_0^\beta d\tau_2' C_1^{(0)}(\tau_2'|\tau_2)C_1^{(0)}(\tau_2|\tau_2') \quad . \qquad (6.94)
$$

The integrals in (6.94) have been already calculated in (5.43)–(5.44). Thus, we get in Matsubara space

$$
\begin{aligned}
G_1^{(2B'')}(i',i;\omega_m)=&-\frac{\beta\delta_{i,i'}2DJ^2}{\mathcal{Z}^{(0)3}}\Bigg\{\sum_k e^{-\beta E_k}\Bigg[\frac{k+1}{E_{k+1}-E_k+i\omega_m}-\frac{k}{E_k-E_{k-1}+i\omega_m}\Bigg]\Bigg\}\\
&\times\Bigg\{\sum_{k,l}e^{\beta(E_k+E_l)}\Bigg[\frac{k(l+1)}{E_{k-1}-E_k-E_l+E_{l+1}}+\frac{(k+1)l}{E_{k+1}-E_k-E_l+E_{l-1}}\Bigg]\Bigg\} \quad . \qquad (6.95)
\end{aligned}
$$

Comparing (6.95) with the last term in (6.93), it becomes obvious that they cancel each other in the low-temperature limit $\beta\to\infty$. We must only remember that in this limit all thermal sums get reduced to a single term which is determined by the particle number per site n. Thus, the respective terms cancel for the same reason as already discussed when considering the specific heat in Subsection 5.3.7. Finally, we obtain from the third term in (5.39) for (6.89)

$$
G_1^{(2B''')}(\tau_1',i'|\tau_1,i)=-2DJ^2\delta_{i,i'}\int_0^\beta d\tau_2\int_0^\beta d\tau_2' C_1^{(0)}(\tau_1'|\tau_2)C_1^{(0)}(\tau_2'|\tau_1)C_1^{(0)}(\tau_2,\tau_2') \quad . \qquad (6.96)
$$

When we examine the integral in (6.96), we see that it is, apart from prefactors, the same as the one occurring when calculating the diagram

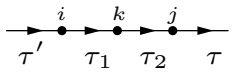

But because of frequency conservation this term is best calculated in Matsubara space and we obtain

$$
G_1^{(2B''')}(i',i;\omega_m)=-2DJ^2\delta_{i,i'}C_1^{(0)}(\omega_m)^3 \quad . \qquad (6.97)
$$

In order to obtain the final result for (6.89), we must only combine (6.93), (6.95), and (6.97) which yields

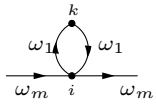

$$= G_1^{(2B)}(i', i|\omega_m) = G_1^{(2B')}(i', i|\omega_m) + G_1^{(2B'')}(i', i|\omega_m) + G_1^{(2B''')}(i', i|\omega_m) \quad . \tag{6.98}$$

Note that because (6.98) is proportional to $\delta_{i,i'}$, it does not depend on $\mathbf{k}$ in momentum space. For this reason, we will drop the variable $\mathbf{k}$ in the following.
Now, we use the definition of the self-energy (6.87) and obtain for the second order in the hopping matrix element

$$\Sigma^{(2)}(\omega_m, \mathbf{k}) = -\frac{G_1^{(2B)}(\omega_m)}{\left[C_1^{(0)}(\omega_m)\right]^2} \quad . \tag{6.99}$$

Note that the proportionality to J^2 is contained in the definition of $G_1^{(2B)}$ in Eq. (6.89). Plugging (6.99) in (6.86) yields

$$\tilde{G}_1^{(2)}(\omega_m, \mathbf{k}) = \frac{1}{1/C_1^{(0)}(\omega_m) - J(\mathbf{k}) + G_1^{(2B)}(\omega_m)/\left[C_1^{(0)}(\omega_m)\right]^2} \quad . \tag{6.100}$$

Because of the topology of the occurring diagram, we call (6.100) the one-loop corrected Green function. To get the phase boundary from it, we must set again $\mathbf{k} = 0$ and $\omega_m = 0$ as described in Subsection 6.1.2

$$\tilde{G}_1^{(2)}(0, \mathbf{0}) = \frac{1}{1/C_1^{(0)}(0) - 2DJ + G_1^{(2B)}(0)/\left[C_1^{(0)}(0)\right]^2} \quad . \tag{6.101}$$

Now we must find the parameter values where (6.101) diverges. Setting the denominator equal to zero provides us with a quadratic equation which has the two solutions

$$J_c = 1/\left\{ C_1^{(0)}(0)D \pm \sqrt{\frac{G_1^{(2B)}(0)}{J^2 C_1^{(0)}(0)} + D^2\left[C_1^{(0)}(0)\right]^2} \right\} \quad . \tag{6.102}$$

Note that this Eq. (6.102) is perfectly defined because the factor J^2 on the right-hand side just cancels the factor J^2 which is contained in the one-loop contribution (6.98). Because we are looking for the phase boundary, which corresponds to the *first* value of J at which G_1 diverges when starting from $J = 0$, we must always take that sign in (6.102) which yields the lower value of J_c. Another fact worth noting is that (6.102) depends on the spatial dimension of the system in a non-trivial way and we can, therefore, see how the quantum-corrections, which we have calculated, affect the mean-field phase diagram for the different dimensions of interest, i.e. $D = 3$, $D = 2$, and $D = 1$. This is done in the next subsections.

6.2.3 One-Loop Corrected Phase Boundary at Zero Temperature

The Mott insulator-superfluid transition at zero temperature is of great theoretical interest as the quantum nature of this phenomenon becomes most transparent in this situation and is not obfuscated by thermal fluctuations. Furthermore, we can compare our findings with the corresponding results in the literature [58, 75, 95, 98]. To find the zero-temperature limit of (6.102) is straightforward. In order to obtain this limit, we have to take the zero-temperature limit of the one-loop diagram (6.98) first.

Together with the Matsubara zero-mode $\omega_m = 0$ and the zero-momentum Fourier component $\mathbf{k} = \mathbf{0}$, we obtain from (6.98), (6.93), (6.95), and (6.97)

$$G_1^{(2B)}(0,\mathbf{0})\Big|_{T=0} = \frac{2DJ^2}{4U^2}\left[\frac{7n(n^2-1)}{n-\tilde{\mu}-3} + \frac{n(n^2+3)}{n-\tilde{\mu}-1} + \frac{4(n+1)^3}{(n-\tilde{\mu})^3} + \frac{2n(n+2)(n+1)}{(n-\tilde{\mu})^2} + \frac{(n+2)(n+1)n}{n-\tilde{\mu}+2} + \frac{(n^2+2n+4)(n+1)}{\tilde{\mu}-n} + \frac{4n^3}{(\tilde{\mu}-n+1)^3} + \frac{2n(n^2-1)}{(\tilde{\mu}-n+1)^2}\right] \quad , \tag{6.103}$$

where n is the filling factor and we have used again the dimensionless chemical potential $\tilde{\mu} = \mu/U$. Inserting now (6.103) into (6.102) and using (5.37), we obtain the phase boundary

$$\begin{aligned}\frac{J_c}{U}\Big|_{T=0} =& \frac{\tilde{\mu}+1}{(\tilde{\mu}-n+1)(n-\tilde{\mu})} \Bigg/ \Bigg[\left[\frac{\tilde{\mu}+1}{(\tilde{\mu}-n+1)(n-\tilde{\mu})}\right]^2 + \Bigg(\frac{(\tilde{\mu}+1)D}{(\tilde{\mu}-n+1)(n-\tilde{\mu})} \\ &\times \Bigg\{(D-2)\left[\frac{\tilde{\mu}+1}{(\tilde{\mu}-n+1)(n-\tilde{\mu})}\right]^3 + \frac{7n(n^2-1)}{2(n-\tilde{\mu}-3)} + \frac{2(n+1)^3}{(n-\tilde{\mu})^3} + \frac{(n+2)(n+1)n}{(n-\tilde{\mu})^2} \\ &+ \frac{(n+2)(n+1)n}{2(n-\tilde{\mu}+2)} + \frac{(n+2)(n+1)n}{2(\tilde{\mu}-n)} + \frac{2n^3}{(\tilde{\mu}-n+1)^2} + \frac{n^2(n-1)}{2(\tilde{\mu}-n+1)}\Bigg\}\Bigg)^{1/2}\Bigg] \quad . \end{aligned} \tag{6.104}$$

Setting $n = 1$ and $D = 3$ in (6.104) yields the important special case

$$\frac{J_c}{U}\Big|_{T=0} = \frac{\tilde{\mu} - \tilde{\mu}^3}{3\tilde{\mu}^2 + 6\tilde{\mu} + 3 + 3\sqrt{\frac{9\tilde{\mu}^5 - 7\tilde{\mu}^4 - 26\tilde{\mu}^3 - 6\tilde{\mu}^2 + \tilde{\mu} - 3}{\tilde{\mu}-3}}} \quad . \tag{6.105}$$

The same result was also found in Ref. [99] where a different field-theoretic approach was used, which is based on the effective potential method. The result in (6.105) and also the corresponding one for $D = 2$ from (Eq. 6.104) is shown in Fig. 6.13 and compared to results from quantum Monte-Carlo simulations. Comparing the results for $D = 2$ and $D = 3$, one can see two things: First, the difference between the first and second order is larger in two dimensions. Second, the deviation of our analytic result from the quantum Monte-Carlo simulation is also larger for lower dimension. This is both reasonable as we have seen in Subsection 6.1.2 that all neglected contributions in (6.82) are smaller for higher dimensions.

When considering $D = 1$ in Fig. 6.14, one encounters a region where (6.102) has no real solutions but two complex ones. Therefore, in this region no phase transition exists in our approximation. But other methods like extrapolated strong-coupling expansion [100], quantum Monte-Carlo simulations [101], and the density-matrix-renormalization-group (DMRG) [102] show that a phase transition exists for all values of μ. Because of this special problem, we will restrict our discussion in the following always to the case $D \geq 2$.

6.2.4 Critical Properties of Mott Insulator-Superfluid Transition

In this subsection, we have a closer look at the zero-temperature phase transition and connect our result (6.104) to the theory of critical phenomena in general [5,76] and to the theory of quantum phase transitions [6] in particular.

The most important point at the phase boundary is the tip because this gives us the value of the hopping parameter for which the Mott phase vanishes for a given filling. Therefore, we call this point of the phase diagram the critical point and the corresponding hopping parameter the critical hopping. In the following, we focus for simplicity on the case $n = 1$. In order to obtain the critical hopping, one has to extremize the function $J_c(\mu)$ as done for the first-order result in Subsection 6.1.4 where

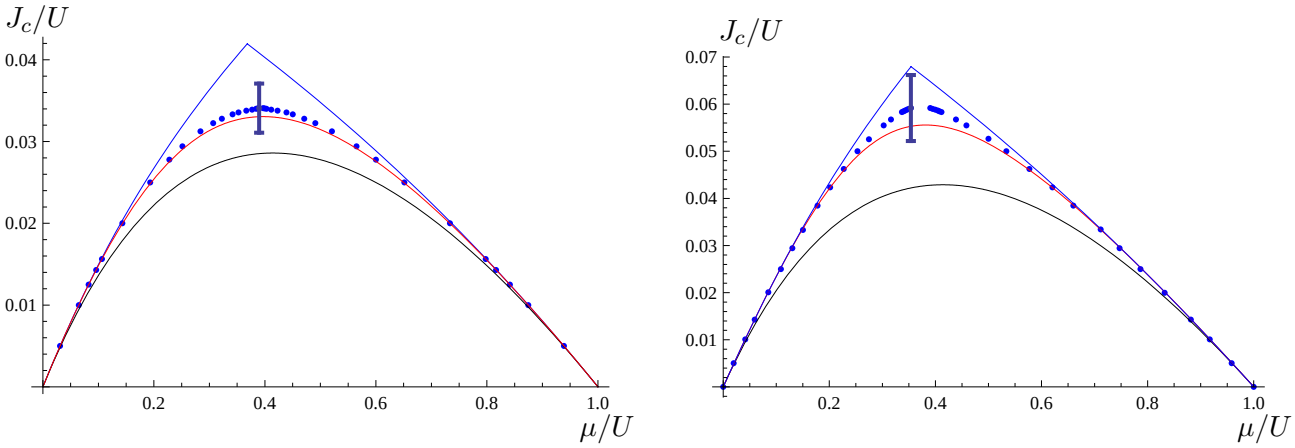

Figure 6.13: Phase diagram for $n = 1$, $T = 0$. Black: First order (mean-field). Red: Second order (one-loop corrected). Blue: Third-order strong-coupling expansion [75]. Error bar: Extrapolated strong-coupling expansion [75]. Dots: Quantum Monte-Carlo data [95,98]. Left: $D = 3$, right: $D = 2$.

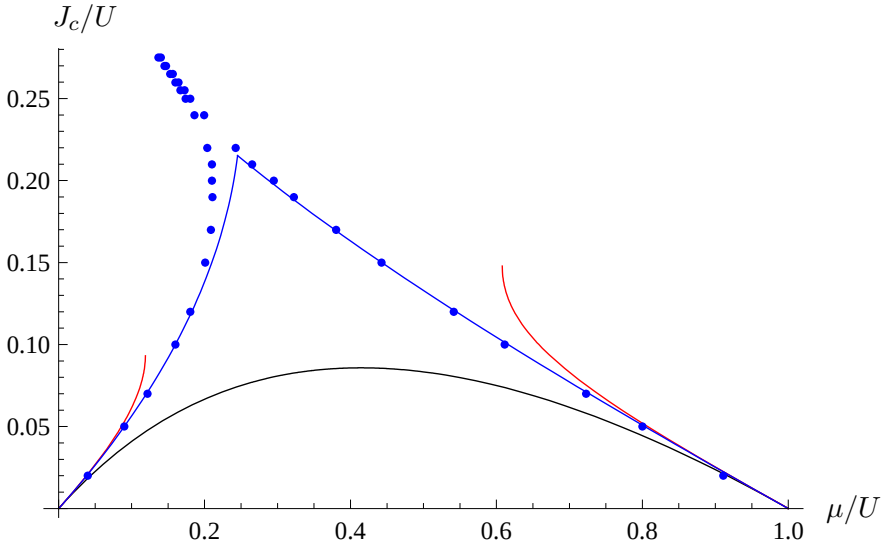

Figure 6.14: Phase diagram for $n = 1$, $T = 0$, $D = 1$. Black: order (mean-field). Red: Second order (one-loop corrected). Blue: Third order strong-coupling expansion [75]. Dots: DMRG data [102].

the analytic expression (6.37) was found. For the second order discussed in Subsection 6.2.3, it is not possible to extremize (6.104) analytically. Therefore, we have computed the critical point numerically. The results are given for different dimensions in Table 6.15 and are compared with results taken from Ref. [75]. The latter values were obtained by extrapolating results from a third-order strong-coupling expansion at zero-temperature by taking into account the general form of the phase boundary around the tip as described in Ref. [58]. We see that our second-order results agree with the values in Ref. [75] for $D = 3$ and $D = 2$ while we cannot find a respective result for $D = 1$ as discussed in the previous subsection.

After this encouraging observation for the position of the critical point, we investigate the region around it in more detail. As discussed in Subsection 6.1.4, the phase boundary can be interpreted as the gap for adding or removing a single particle. Inverting the function of the critical hopping in dependence of the chemical potential $J_c(\mu)$ allows us to show this gap as a function of $|J - J_{\mathrm{ct}}|$ where J_c is the critical hopping parameter (see Fig. 6.16). For the second-order result, this inversion leads to an algebraic equation of fourth order. It is possible to solve this kind of equations in a closed form but because the analytic expressions for the solutions are very complicated and do not provide any additional physical insight, we consider the numerical solution instead. We note that these curves start with an infinite slope, i.e. the derivative diverges at $|J - J_{\mathrm{ct}}| = 0$.

It is well known that the microscopic details of the considered system become irrelevant at a phase transition, at least for most thermodynamic quantities of interest, and the critical behavior is governed by a single length scale, the coherence length. At a classical phase transition, ξ diverges according to [5, 76]

$$\xi \propto |T - T_{\mathrm{ct}}|^{-\nu} \quad . \tag{6.106}$$

Here T_c is the critical temperature and ν the critical exponent of the coherence length. This exponent only depends on the symmetry of the system, its spatial dimension, and the number of components of the respective order parameter. Such critical exponents can be calculated very accurately using field-theoretical methods and combining them with extrapolation techniques like variational perturbation theory [5, 76]. For the zero-temperature quantum phase transition discussed here, the quantum fluctuations drive the transition and the role of the critical temperature is played by the critical hopping parameter. Therefore, we must consider the dynamic system and introduce a characteristic time scale which diverges as $t \propto \xi^z$, where the coherence length now has the behavior $\xi \propto |J - J_{\mathrm{ct}}|^{-\nu}$. The additional parameter z is called the dynamic critical exponent [58, 103]. Because a time scale is inversely proportional to a frequency or energy scale, we can write down the formation of the gap as

$$E_{\mathrm{gap}} \propto |J - J_{\mathrm{ct}}|^{z\nu} \quad . \tag{6.107}$$

Because we see from Fig. 6.16 that E_{gap} is zero at the origin while its first derivative diverges, we can immediately state that $0 < z\nu < 1$. To obtain this exponent quantitatively, we make a double-logarithmic plot of $E_{\mathrm{gap}}(|J - J_{\mathrm{ct}}|)$ for small $|J - J_{\mathrm{ct}}|$. The value of $z\nu$ can then be easily read off from the slope because power functions become straight lines in double-logarithmic plots. This is done both for $D = 2$ and $D = 3$ in Fig. 6.17. Thus, we obtain $z\nu = 0.5$ both for the first- and the second-order result as well as for both considered dimensions. For the first-order calculation this is also obvious from examining the analytic expression for $\mu(J_c)$ which has a square-root behavior. In order to compare these exponents with literature values, we first note that a quantum phase transition in D dimensions has the same critical properties as a classical phase transition in $d = D + 1$ dimensions because the additional dynamic degree of freedom enters the theory exactly like an additional spatial dimension [6, 58]. Because our order parameter has two components, i.e. one *complex* number, it resembles the classical xy-model. The upper critical dimension is $d_c = 4$ for which reason we expect mean-field like behavior for the quantum phase transition for $D = 3$ with the critical exponent $z\nu = 1/2$. For $D = 2$, which corresponds to a classical model with $d = 3$, the result from Ref. [5] is $z\nu = 0.67$. Thus, we can say that our theory correctly describes the qualitative form of the tip but fails to account for the correction to the square-root form in two dimensions. However, we mention that other analytical

	First order	Second order	Ref. [75]
$D = 1$	0.0858	N/A	0.245 ± 0.012
$D = 2$	0.0429	0.0556	0.057 ± 0.007
$D = 3$	0.0286	0.0330	0.034 ± 0.003

Figure 6.15: Critical hopping parameters J_{ct}/U for different spatial dimensions and comparison with values from Ref. [75].

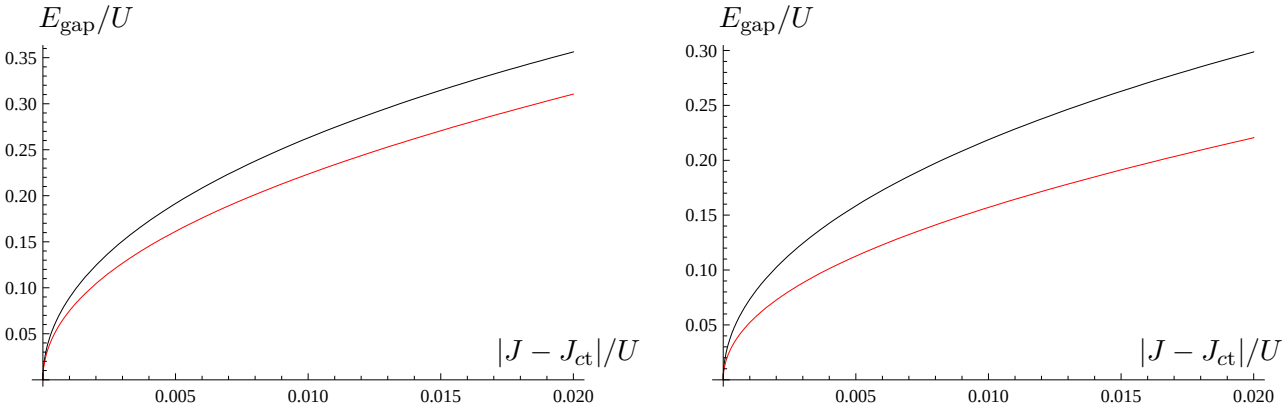

Figure 6.16: Gap for removing of a particle. Black: First-order. Red: Second-order. Left: $D = 3$. Right: $D = 2$

methods like the strong-coupling approach [75, 100] and also some numerical work [98] have obtained Mott lobes which have cusps at the tip even in three dimensions. This means that the slope becomes not infinite at the critical point and, therefore, corresponds to a critical exponent $z\nu > 1$ which strongly disagrees with well established facts [5, 6, 58, 103]. To close this subsection, we make some additional remarks about the one-dimensional case. As this situation corresponds to a classical two-dimensional system, there exists no second-order phase transition, as for $D \geq 2$, but a transition of the Kosterlitz-Thouless type where the gap has an exponential dependence on $|J - J_{\mathrm{ct}}|$ [104]. Presumably, this special behavior is the reason that our approach fails to produce a phase boundary for the one-dimensional system.

6.2.5 One-Loop Corrected Phase Boundary at Finite Temperature

In this subsection, we discuss the phase boundary for finite temperatures. Because there is no other analytical or numerical data available in the literature at the moment, we can only compare our findings with the first-order result in Eq. (6.13) which we have done in Fig. 6.18. Because it is, both from the theoretical and experimental point of view, the most relevant case, we restrict ourselves to the case $D = 3$. The situation for $D = 2$ is very similar, only the differences between first- and second-order results are larger. Effects from temperature are, again, as already seen in Subsection 6.1.2, most important between the lobes, while the effects arising from the one-loop correction play an important role only near the tip. Thus, we can say that we have a thermally dominated region where thermal fluctuations are large (see also Fig. 6.6), and a quantum dominated region where the corrections from the one-loop diagram are large.

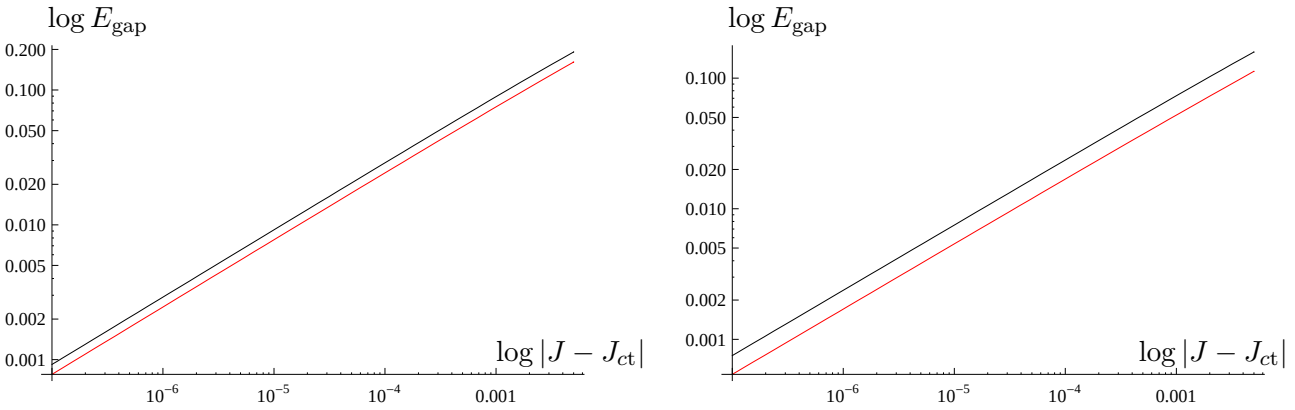

Figure 6.17: Double-logarithmic plot of gap from Fig. 6.16. Black: First-order. Red: Second-order. Left: $D = 3$. Right: $D = 2$. The slope of all curves is $z\nu = 0.5$.

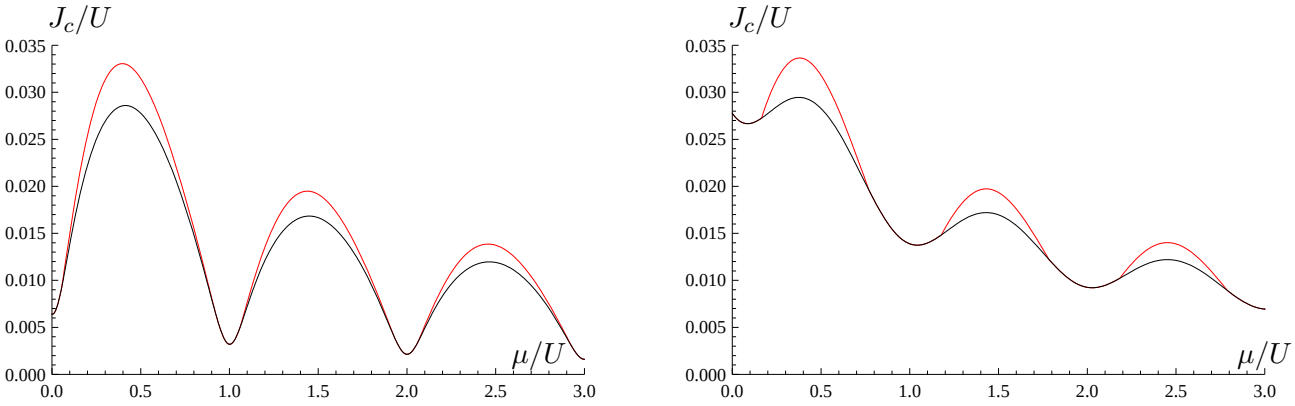

Figure 6.18: Phase diagram for finite temperature and $D = 3$. Black: First order (mean-field). Red: Second order (one-loop-corrected). Left: $T = 0.02\,U$. Right: $T = 0.1\,U$.

6.2.6 One-Loop Corrected Excitation Spectrum

In Subsection 6.1.4 we have calculated the excitation spectrum from the first-order resummed Green function (6.11). Now we investigate, how the one-loop corrections affect this excitation spectrum. In order to this, we proceed exactly like above, which means that we continue $\tilde{G}_1^{(2)}(\omega_m, \mathbf{k})$ in (6.100) to real time and solve it for the poles. Unfortunately, because of the complicated structure of (6.98), this procedure leads to equations for ω which are not solvable analytically. Therefore, we have solved the respective equation, i.e.

$$1 - J(\mathbf{k})C_1^{(0)}(\omega) + G_1^{(2B)}(\omega)/C_1^{(0)}(\omega) \stackrel{!}{=} 0 \tag{6.108}$$

for ω numerically. The respective results are plotted in Fig. 6.19 for $D = 3$ and in Fig. 6.20 for $D = 2$. The quantum-corrections are larger for hopping parameters near the critical value and especially important for long wave-lengths. Of course the vanishing of the gap now takes place at the one-loop corrected value which is given in Fig. 6.15. As expected, the deviations between the two orders are larger for two than for three spatial dimensions.

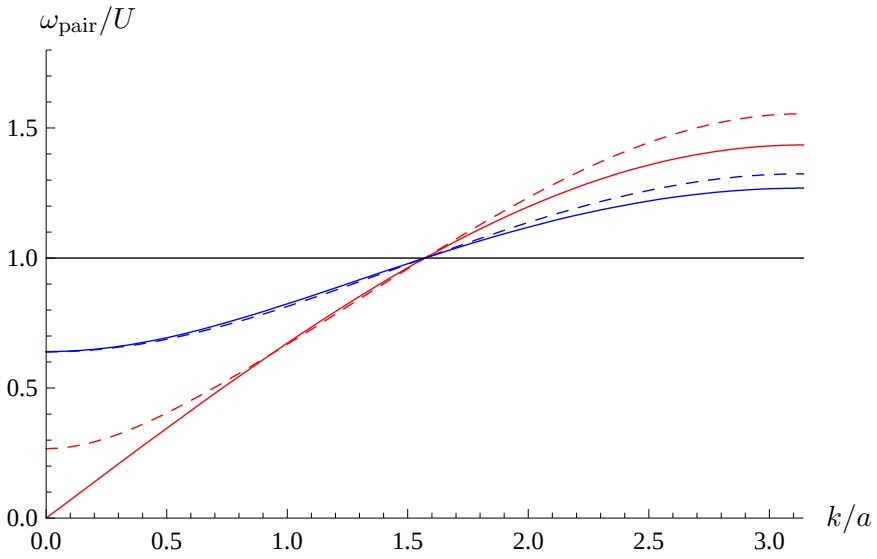

Figure 6.19: Spectrum of the pair excitation for $D = 3$, $T = 0$, $n = 1$, and $2DJ = 0$ (black), $2DJ = 0.1\,U$ (blue), $2DJ = 0.1716\,U$ (red) within the first Brillouin zone. The solid curves are results from the first-order calculation (compare Fig. 6.3), while the dashed curves are the one-loop corrected results.

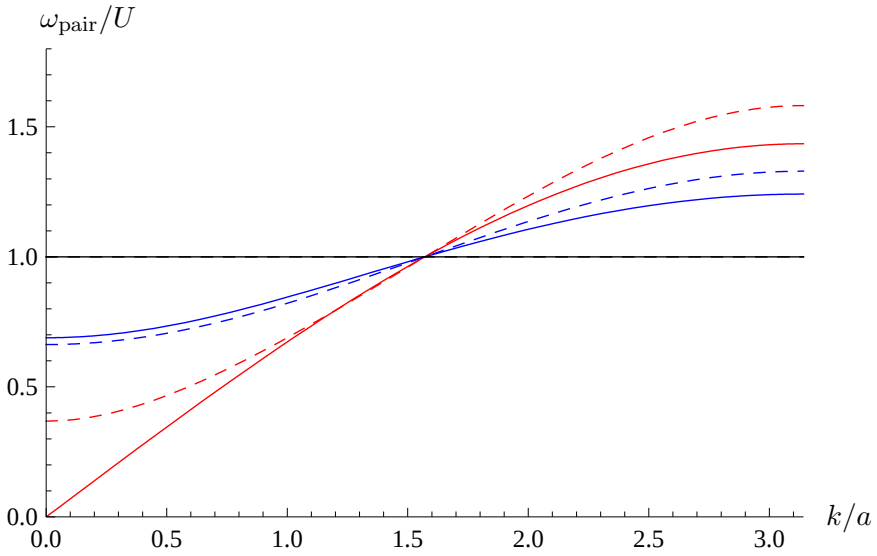

Figure 6.20: Spectrum of the pair excitation for $D = 2$, $T = 0$, $n = 1$, and $2DJ = 0$ (black), $2DJ = 0.1\,U$ (blue), $2DJ = 0.1716\,U$ (red) within the first Brillouin zone. The solid curves are results from the first-order calculation, while the dashed curves are the one-loop corrected results.

Chapter 7

Summary and Outlook

In the present thesis, we have discussed various aspects of the physics of Bosonic gases in optical lattices. In the first part, we have considered Bosons which carry an effective spin $F = 1$. In Chapter 2, we have derived a generalization of the widely used Bose-Hubbard model for their description where the Hamiltonian was given in Eq. (2.18).
Chapter 3 was devoted to the discussion of the Mott insulator-superfluid transition in such a spin-1 system, both for zero and finite temperature, within the framework of perturbative mean-field theory. In contrast to the literature [53, 60], where the discussion was restricted to $T = 0$ and special ground states, we have considered systems in arbitrary zero-temperature ground states in Section 3.4 with the main result (3.45). In order to obtain this result, we have derived recursion relations for the matrix elements of particle creation and annihilation operators with respect to the eigenstates of the spin-1 Bose-Hubbard Hamiltonian in absence of hopping in Appendix A. Our findings (3.45), (3.57), (3.63) agreed with Refs. [53,60] for the special cases discussed there. The result for finite temperature (3.94) showed the new effect of a crossing of phase boundaries belonging to different temperatures which is shown in Fig. 3.12 and explained in Subsection 3.5.2.
In Chapter 4, we have shown the spin-resolved time-of-flight pictures in Fig. 4.2 and generalized the concept of the visibility, which measures the interference patterns in a quantitative way, from scalar Bosons [23, 77] to spinor ones in Eq. (4.33). We have calculated its dependence on the spin-dependent interaction (see Fig. 4.1). Effects arising from finite temperature have been discussed in Section 4.2. The dependence of the visibility of the different hyperfine components on the temperature, as plotted in Fig. 4.6, shows an interesting non-monotonic behavior which could, in principle, be measured experimentally in the very near future.
An interesting open problem, which could not be considered within the framework of this thesis, is the question of phase transitions between different superfluid phases which are characterized by the direction of the order-parameter vector $\mathbf{\Psi}$ as discussed in Chapter 3. But also the Mott phase bears interesting additional features because tunneling leads to an effective interaction between the lattice sites which can result in a transition between different phases that are known from the study of classical spin models [48]. The reason for these features is that tunneling induces an effective interaction between neighboring lattice sites. Thus, for example, an anti-ferromagnetic phase with alternating spin order can occur.
In the second part, we have considered the extensively discussed scalar Bose-Hubbard model where we employed a new analytical approach. We have used the diagrammatic technique reviewed by W. Metzner for Fermions in Ref. [79] and adapted it for the treatment of the present Bosonic problem. The general formalism was developed in Chapter 5 and some diagrams were calculated explicitly. Chapter 6 was devoted to the application of this formalism where we developed, in particular, a resummation procedure (6.83) which allowed us to go beyond simple perturbation theory. With this procedure, we were able to obtain time-of-flight pictures which qualitatively agreed with the experiment in the full

parameter range (see Fig. 6.10) and a formula for the visibility which is both correct in the limit of strong and weak interactions (see Fig. 6.11). Furthermore, we have calculated the excitation spectrum both for zero and finite temperature and proposed a method to measure the temperature of these systems by the width of the gap in the Mott phase (see Fig. 6.7).
Equipped with a general resummation procedure by means of the self-energy, we calculated in Section 6.2 the one-loop corrected Green function (6.100). This allowed us to write down an analytic formula for the phase boundary at zero-temperature (6.104) which improved the zero-temperature mean-field result in Ref. [58] and is close to recent high precision Monte Carlo data in both two and three dimensions (see Fig. 6.13) [95, 98]. The same result was also obtained in Ref. [99] with a different method. The key idea behind that particular approach is to couple currents to the Bose-Hubbard Hamiltonian (5.1) and perform a Legendre transform to obtain the effective action which is suitable to describe the phase transition. Furthermore, we have also shown the analytic one-loop corrected phase diagram for finite temperature for which no other results to compare with exist so far (see Fig. 6.18). We have identified the regions in the phase digram where thermal effects dominate and the ones where quantum effects govern the behavior.
The most pressing question in the context of the Green function approach is the calculation of the Green function within the superfluid phase. Although our resummation allowed us to calculate some properties within this phase, a well-founded description must explicitly take into account the non-vanishing expectation value of the field-operators. A suitable starting point for this goal is the effective action [62, 85], and first results in this direction have been already reported in Ref. [97].

Appendix A

Properties of Spin-1 Eigenstates

The aim of this appendix is to derive properties of the eigenstates of the Hamiltonian (3.12), i.e. the one characterizing the system without hopping. These properties are needed in order to perform the perturbative calculations in Chapters 3 and 4.

A.1 Matrix Elements of Creation and Annihilation Operators

In this section, we calculate the matrix elements of the creation and annihilation operators in the basis of the eigenstates of the local Hamiltonian in absence of hopping, which reads

$$\hat{H}_0 = \frac{1}{2}U_0\hat{n}(\hat{n}-1) + \frac{1}{2}U_2(\hat{\mathbf{S}}^2 - 2\hat{n}) - \mu\hat{n} - \eta\hat{S}^z \quad . \tag{A.1}$$

Note, that in this whole appendix, we work only with quantities, which are local with respect to the lattice sites, so we have dropped all site indices. The matrix elements form an important foundation for the calculations which are performed in this theses, because they provide us with a tool to consider arbitrary perturbations to the Hamiltonian (A.1), for example arising from hopping, as long as they can be expressed in terms of the creation and annihilation operators $\hat{a}_\alpha^\dagger$ and $\hat{a}_\alpha$. The eigenstates of (A.1) are the common eigenstates of $\hat{\mathbf{S}}^2$, S^z and

$$\hat{n} = \sum_\alpha \hat{n}_\alpha = \sum_\alpha \hat{a}_\alpha^\dagger \hat{a}_\alpha \quad . \tag{A.2}$$

We denote them by the quantum numbers S, m and n, i.e.

$$\Phi = |S, m, n\rangle \quad . \tag{A.3}$$

Note that the states (A.3) are defined to be normalized. The calculations in this whole Appendix are based on previous work on spin-1 Bosons in optical lattices at zero temperature [50, 53, 60], on the discussion of spinor Bose gases in general [34, 35, 43, 46] and also on some older work on cavity QED [105].

A.1.1 Further Properties of Spin Operators

The three components of the spin operator $\hat{\mathbf{S}}$ are

$$\begin{aligned}\hat{S}^x &= \frac{1}{\sqrt{2}}(\hat{a}_0^\dagger\hat{a}_1 + \hat{a}_1^\dagger\hat{a}_0 + \hat{a}_{-1}^\dagger\hat{a}_0 + \hat{a}_0^\dagger\hat{a}_{-1}) \quad , \\ \hat{S}^y &= \frac{1}{\sqrt{2}}(\hat{a}_0^\dagger\hat{a}_1 - \hat{a}_1^\dagger\hat{a}_0 + \hat{a}_{-1}^\dagger\hat{a}_0 - \hat{a}_0^\dagger\hat{a}_{-1}) \quad , \\ \hat{S}^z &= \hat{a}_1^\dagger\hat{a}_1 - \hat{a}_{-1}^\dagger\hat{a}_{-1} \quad . \end{aligned} \tag{A.4}$$

from which one can easily calculate

$$\hat{\mathbf{S}}^2 = 2\hat{n}_1\hat{n}_0 + 2\hat{n}_0\hat{n}_{-1} + \hat{n}_1 + 2\hat{n}_0 + \hat{n}_{-1} + \hat{n}^2 + \hat{n}_{-1}^2 - 2\hat{n}_1\hat{n}_{-1} + 2\hat{a}_1^\dagger\hat{a}_{-1}^\dagger\hat{a}_0^2 + 2\hat{a}^{\dagger 2}\hat{a}_1\hat{a}_{-1} \quad . \tag{A.5}$$

With the help of the Bose commutator relation $[\hat{a}_\alpha, \hat{a}_\beta^\dagger] = \delta_{\alpha,\beta}$ we obtain the commutator relations

$$[\hat{S}_j^\alpha, \hat{S}_k^\beta] = i\delta_{jk}\sum_\gamma \epsilon_{\alpha\beta\gamma}\hat{S}_j^\gamma \quad , \tag{A.6}$$

which are just the standard commutator relations for angular momentum operators. For instance, they are also encountered when describing the states of an electron in the hydrogen atom. Inspired by this, we introduce the ladder operators

$$\hat{S}_\pm = \hat{S}^x \pm i\hat{S}^y \quad , \tag{A.7}$$

which can be expressed in terms of the components of $\hat{\mathbf{S}}$ according to

$$\hat{S}^x = \frac{1}{2}\left(\hat{S}_+ + \hat{S}_-\right) \quad , \qquad \hat{S}^y = -\frac{i}{2}\left(\hat{S}_+ - \hat{S}_-\right) \quad . \tag{A.8}$$

Thus, we obtain

$$\hat{\mathbf{S}}^2 = (\hat{S}^x)^2 + (\hat{S}^y)^2 + (\hat{S}^z)^2 = \frac{1}{2}\left(\hat{S}_+\hat{S}_- + \hat{S}_-\hat{S}_+\right) + (\hat{S}^z)^2 \quad . \tag{A.9}$$

The ladder operators (A.7) have the known property [61]

$$\hat{S}_\pm|S,m,n\rangle = \sqrt{S(S+1) - m(m\pm 1)}|S,m\pm 1,n\rangle \quad . \tag{A.10}$$

From (A.4) and (A.7), we get their explicit form in terms of creation and annihilation operators

$$\begin{aligned}\hat{S}_+ &= \sqrt{2}\,(\hat{a}_1^\dagger\hat{a}_0 + \hat{a}_0^\dagger\hat{a}_{-1}) \quad , \\ \hat{S}_- &= \sqrt{2}\,(\hat{a}_0^\dagger\hat{a}_1 + \hat{a}_{-1}^\dagger\hat{a}_0) \quad . \end{aligned} \tag{A.11}$$

A.1.2 Creation of Basis States from Vacuum State

Our aim in this Appendix is to calculate

$$\hat{a}_\alpha^\dagger|S,m,n\rangle \quad \text{and} \quad \hat{a}_\alpha|S,m,n\rangle \quad . \tag{A.12}$$

Therefore, we want to know how the eigenstates of $\hat{H}_0$ can be obtained by letting combinations of the creation operators $\hat{a}_\alpha^\dagger$ act on the vacuum state $|0\rangle$. In order to answer this question, we introduce the singlet creation operator

$$\hat{\Theta}^\dagger = \hat{a}_0^{\dagger 2} - 2\hat{a}_1^\dagger\hat{a}_{-1}^\dagger \quad . \tag{A.13}$$

Below we will see that it creates, when acting on the vacuum state, a state with two particles and zero spin. In order to understand this operator better, it is necessary to calculate some commutator relations first:

$$[\hat{a}_1, \hat{\Theta}^\dagger] = -2\hat{a}_{-1}^\dagger\,, \qquad [\hat{a}_0, \hat{\Theta}^\dagger] = 2\hat{a}_0^\dagger \quad , \tag{A.14}$$

$$[\hat{a}_{-1}, \hat{\Theta}^\dagger] = -2\hat{a}_1^\dagger\,, \qquad [\hat{S}_\pm, \hat{\Theta}^\dagger] = 0 \quad , \tag{A.15}$$

$$[\hat{a}_\alpha, \hat{\Theta}^\dagger] = 0\,, \qquad [\hat{S}^z, \hat{\Theta}^\dagger] = 0 \quad , \tag{A.16}$$

$$[\hat{n}, \hat{\Theta}^\dagger] = 2\hat{\Theta}^\dagger \quad . \tag{A.17}$$

With the help of these relations, we can prove that (A.13) really creates a singlet pair:

$$\hat{\mathbf{S}}^2\hat{\Theta}^{\dagger Q}|0\rangle = \hat{\Theta}^{\dagger Q}\hat{\mathbf{S}}^2|0\rangle + [\hat{\mathbf{S}}^2, \hat{\Theta}^{\dagger Q}]|0\rangle = 0 \quad , \tag{A.18}$$

$$\hat{n}\hat{\Theta}^{\dagger Q}|0\rangle = [\hat{n}, \hat{\Theta}^{\dagger Q}]|0\rangle = Q\hat{\Theta}^{Q-1}[\hat{n}, \Theta^\dagger]|0\rangle = 2Q\hat{\Theta}^{\dagger Q}|0\rangle \quad . \tag{A.19}$$

Here we have introduced the new quantum number Q which denotes the number of spin singlet pairs. It is connected to the quantum numbers n and S by the obvious relation $Q = (n - S)/2$. Because we do not only want to produce spin singlet states, but also states with arbitrary S and m, we now show how to create n particles with aligned spin. This is achieved by successively applying the creation operator $\hat{a}_1^\dagger$. In order to be able to prove this, we need its commutator relations with the constituents of the operator $\hat{\mathbf{S}}^2$ in (A.9). They read

$$\begin{aligned}
&[\hat{a}_1, \hat{S}_+] = \sqrt{2}\hat{a}_0\,, && [\hat{a}_1, \hat{S}_-] = 0 \quad ,\\
&[\hat{a}_0, \hat{S}_+] = \sqrt{2}\hat{a}_{-1}\,, && [\hat{a}_0, \hat{S}_-] = \sqrt{2}\hat{a}_1 \quad ,\\
&[\hat{a}_{-1}, \hat{S}_+] = 0\,, && [\hat{a}_{-1}\hat{S}_-] = \sqrt{2}\hat{a}_0 \quad ,\\
&[\hat{a}_1^\dagger, \hat{S}_+] = 0\,, && [\hat{a}_1^\dagger, \hat{S}_-] = -\sqrt{2}\hat{a}_0^\dagger \quad ,\\
&[\hat{a}_0^\dagger, \hat{S}_+] = -\sqrt{2}\hat{a}_1^\dagger\,, && [\hat{a}_0^\dagger, \hat{S}_-] = -\sqrt{2}\hat{a}_{-1} \quad ,\\
&[\hat{a}_{-1}^\dagger, \hat{S}_+] = -\sqrt{2}\hat{a}_0\,, && [\hat{a}_{-1}^\dagger, \hat{S}_-] = 0 \quad ,
\end{aligned} \tag{A.20}$$

where we have also stated, for the sake of completeness, the respective formulas for the other creation and annihilation operators. With the help of (A.20), we can now show in a way completely analogous to (A.18) and (A.19) that

$$\hat{n}\,\hat{a}_1^{\dagger S}|0\rangle = n\,\hat{a}_1^{\dagger S}|0\rangle \quad , \tag{A.21}$$

$$\hat{\mathbf{S}}^2\,\hat{a}_1^{\dagger S}|0\rangle = S(S+1)\,\hat{a}_1^{\dagger S}|0\rangle \quad , \tag{A.22}$$

$$\hat{S}^z\,\hat{a}_1^{\dagger S}|0\rangle = S\,\hat{a}_1^{\dagger S}|0\rangle \quad . \tag{A.23}$$

Because the singlet creation operator (A.13) contains no annihilation operators, it commutes with all $\hat{a}_\alpha^\dagger$ and we can state that

$$|S, S, n\rangle \propto \hat{a}_1^{\dagger S}\hat{\Theta}^{\dagger Q}|0\rangle \quad . \tag{A.24}$$

Thus, creating Q singlet pairs and S particles of spin one yields a state which is characterized by $n = 2Q + S$ particles with spin S and $m = S$. Introducing a yet unknown normalization factor, we can write (A.24) as

$$|S, S, n\rangle = \frac{1}{\sqrt{f(Q,S)}}\hat{a}_1^{\dagger S}\hat{\Theta}^{\dagger Q}|0\rangle \quad . \tag{A.25}$$

The value of this normalization factor will be proven in the next section to be

$$f(Q,S) = S!Q!2^Q\frac{(2Q+2S+1)!!}{(2S+1)!!} \quad , \tag{A.26}$$

where

$$n!! = n(n-2)(n-4)\dots 1 \tag{A.27}$$

denotes the double factorial. States with lower m can then be obtained by successively applying $\hat{S}_-$ to (A.25). Thus, we are now in the position to express every eigenstate of (A.1) in terms of the vacuum state $|0\rangle$ and three known, commuting operators, which are the singlet creation operator $\hat{\Theta}^\dagger$ in (A.13), the creation operators $\hat{a}_1^\dagger$ and the lowering ladder operator $\hat{S}_-$ in (A.11).

A.1.3 Recursion Relations

After this preliminary discussion, we come back to our main problem (A.12). When we add one spin-1 particle to a state with total spin quantum number S and magnetic quantum number m, we end in a superposition of only two states. The reason for this is provided by various conservation rules. The first two of them are the conservation of the particle number and the magnetization parallel to the z-axis. Thus, applying $\hat{a}_\alpha^\dagger$ on a state $|S,m,n\rangle$, the resulting states must have the form $|\tilde{S},m+\alpha,n+1\rangle$. The third conservation rule states, that when adding a particle, the total spin quantum number S can only change by $\Delta S = \pm 1$ and, therefore, $\tilde{S} = S \pm 1$. Thus, we can write (A.12) in the following form:

$$\hat{a}_\alpha^\dagger|S,m,n\rangle = M_{\alpha,S,m,n}|S+1,m+\alpha,n+1\rangle + N_{\alpha,S,m,n}|S-1,m+\alpha,n+1\rangle \quad . \tag{A.28}$$

When removing a particle, the situation is completely analogous, yielding

$$\hat{a}_\alpha|S,m,n\rangle = O_{\alpha,S,m,n}|S+1,m-\alpha,n-1\rangle + P_{\alpha,S,m,n}|S-1,m-\alpha,n-1\rangle \quad . \tag{A.29}$$

Our task is now to calculate the respective coefficients in (A.28) and (A.29). The first important observation is that states $|S,m,n\rangle$ with $m > S$ do not exist. Therefore, we can state immediately that $N_{1,S,S,n} = 0$ and

$$\hat{a}_1^\dagger|S,S,n\rangle = M_{1,S,S,m}|S+1,m+1,n+1\rangle \quad . \tag{A.30}$$

Thus, it is now possible to obtain $M_{1,S,S,n}$ by calculating:

$$\hat{a}_1^\dagger|S,S,n\rangle = \hat{a}_1^\dagger \frac{1}{\sqrt{f(Q,S)}} \hat{a}_1^{\dagger S}\hat{\Theta}^{\dagger Q}|0\rangle \quad . \tag{A.31}$$

Applying (A.25) yields

$$\hat{a}_1^\dagger|S,S,n\rangle = \frac{\sqrt{f(Q,S+1)}}{\sqrt{f(Q,S)}}|S+1,S+1,n+1\rangle \quad , \tag{A.32}$$

which becomes after inserting the explicit form of the normalization constant (A.26)

$$\hat{a}_1^\dagger|S,S,n\rangle = \sqrt{\frac{(S+1)(2Q+2S+3)}{2S+3}}|S+1,S+1,n+1\rangle \quad . \tag{A.33}$$

Comparing this with (A.30) yields

$$M_{1,S,S,n} = \sqrt{\frac{(S+1)(2Q+2S+3)}{2S+3}} \quad . \tag{A.34}$$

Thus, we have found the first matrix element which will serve us as a starting point for the recursion relation to be derived. In order to find this recursion for $M_{1,S,m,n}$ with $m < S$, we start with (A.28) and act on it with $\hat{S}_+$, yielding

$$\hat{S}_+\hat{a}_1^\dagger|S,m,n\rangle = M_{1,S,m,n}\hat{S}_+|S+1,m+1,n+1\rangle + N_{1,S,m,n}\hat{S}_+|S-1,m+1,n+1\rangle \quad . \tag{A.35}$$

Using the fact from (A.20) that $\hat{a}_1^\dagger$ and $\hat{S}_+$ commute and applying (A.10), this can be rewritten as

$$\begin{aligned}\hat{a}_1^\dagger &\sqrt{S(S+1)-m(m+1)}\,|S,m+1,n\rangle \\ &= \sqrt{(S+1)(S+2)-(m+1)(m+2)}\,M_{1,S,m,n}|S+1,m+2,n+1\rangle \\ &\quad + \sqrt{(S-1)S-(m+1)(m+2)}\,N_{1,S,m,n}|S-1,m+1,n+1\rangle \quad , \end{aligned} \tag{A.36}$$

which takes, after using (A.28) on the left-hand side again, the form

$$\begin{aligned}&\sqrt{S(S+1)-m(m+1)}\Big(M_{1,S,m+1,n}|S+1,m+2,n+1\rangle + N_{1,S,m+1,n}|S-1,m+2,n+1\rangle\Big) \\ &\quad = \sqrt{(S+1)(S+2)-(m+1)(m+2)}\,M_{1,S,m,n}|S+1,m+2,n+1\rangle \\ &\qquad + \sqrt{(S-1)S-(m+1)(m+2)}\,N_{1,S,m,n}|S-1,m+1,n+1\rangle \quad . \end{aligned} \tag{A.37}$$

Comparing the coefficients of the state $|S+1,m+2,n+1\rangle$ on the left- and right-hand side, one can easily read off from (A.76)

$$M_{1,S,m,n} = \sqrt{\frac{(S+1)S-m(m+1)}{(S+1)(S+2)-(m+1)(m+2)}}M_{1,S,m+1,n} \quad , \tag{A.38}$$

which is a recursion relation that tells us how to calculate $M_{1,S,m-1,n}$ from $M_{1,S,m,n}$. The starting point is $M_{1,S,S,n}$ for which we have found the explicit formula (A.34). Together with this, we do now have a formula for the calculation of $M_{1,S,m,n}$ for all $|m| \leq S$.
Motivated by this, we now turn to the calculation of $M_{0,S,m,n}$. We proceed in a way analogous to the one employed above, use (A.29) for $\alpha = 0$, and obtain

$$\hat{S}_+\hat{a}_0^\dagger|S,m,n\rangle = M_{0,S,m,n}\hat{S}_+|S+1,m,n+1\rangle + N_{0,S,m,n}\hat{S}_+|S-1,m,n+1\rangle \quad . \tag{A.39}$$

Because $\hat{a}_0^\dagger$ and $\hat{S}_+$ do not commute, we must use (A.20) on the left-hand side of (A.39) and write

$$\begin{aligned}&\sqrt{S(S+1)-m(m+1)}\,\hat{a}_0^\dagger|S,m+1,n\rangle + \sqrt{2}\hat{a}_1|S,m,n\rangle \\ &\quad = M_{0,S,m,n}\sqrt{(S+1)(S+2)-m(m+1)}\,|S+1,m+1,n+1\rangle \\ &\qquad + N_{0,S,m,n}\sqrt{(S+1)(S-1)-m(m+1)}\,|S-1,m+1,n+1\rangle \quad . \end{aligned} \tag{A.40}$$

Finally, we use (A.28) twice in order to express the remaining operators on the left-hand side of (A.40) by their respective matrix elements. Thus, we get

$$\begin{aligned}&\sqrt{S(S+1)-m(m+1)}\Big(M_{0,S,m+1,n}|S+1,m+1,n+1\rangle + N_{0,S,m+1,n}|S-1,m+1,n+1\rangle\Big) \\ &\qquad + \sqrt{2}\,M_{1,S,m,n}|S+1,m+1,n+1\rangle + \sqrt{2}\,N_{1,S,m,n}|S-1,m+1,n+1\rangle \\ &\quad = M_{0,S,m,n}\sqrt{(S+1)(S+2)-m(m+1)}|S+1,m+1,n+1\rangle \\ &\qquad + N_{0,S,m,n}\sqrt{(S+1)(S-1)-m(m+1)}|S-1,m+1,n+1\rangle \quad . \end{aligned} \tag{A.41}$$

Comparing the coefficients of the state $|S+1,m+1,n+1\rangle$ in (A.41), we can read off the following relation:

$$M_{0,S,m,n} = \sqrt{\frac{S(S+1)-m(m+1)}{(S+1)(S+2)-m(m+1)}}M_{0,S,m+1,n} + \sqrt{\frac{2}{(S+1)(S+2)-m(m+1)}}M_{1,S,m,n} \quad , \tag{A.42}$$

which is a bit more complicated than (A.38), because it involves not only $M_{0,S,m+1,n}$ on the right-hand side, but also $M_{1,S,m,n}$. But this is no problem at all because we know how to calculate $M_{1,S,m,n}$ for

all allowed values of m due to (A.38). To find the right starting point for the recursion (A.42), we recall that $M_{\alpha,S,S+1,n} = 0$. This is trivially true because the corresponding states do not even exist. Thus, the starting point for (A.42) reads with (A.34)

$$M_{0,S,S,n} = \sqrt{\frac{1}{S+1}} M_{1,S,S,n} = \sqrt{\frac{2Q+2S+3}{2S+3}} \quad . \tag{A.43}$$

In order to calculate $M_{-1,S,m,n}$, we proceed exactly as done above but replace $\hat{a}_0^\dagger$ by $\hat{a}_{-1}^\dagger$. Doing this yields after a short calculation

$$M_{-1,S,m,n} = \sqrt{\frac{S(S+1)-m(m+1)}{(S+1)(S+2)-m(m-1)}} M_{-1,S,m+1,n} + \sqrt{\frac{2}{(S+1)(S+2)-m(m-1)}} M_{0,S,m,n} \quad . \tag{A.44}$$

Evaluating (A.44) for $m = S$ yields under consideration of (A.42), (A.38), and (A.34) the starting point

$$M_{-1,S,S,n} = \sqrt{\frac{3+n+S}{(1+2S)(3+2S)}} \quad . \tag{A.45}$$

Now we turn to the calculation of $N_{\alpha,S,m,n}$. One of these coefficients, i.e. $N_{-1,S,S,m}$, can be calculated directly. In order to do this, we make use of the properties of the particle number operator (A.2) and write the particle number as

$$n = \langle S,S,n|\hat{n}|S,S,n\rangle = \sum_\alpha \langle S,S,n|\hat{a}_\alpha^\dagger \hat{a}_\alpha|S,S,n\rangle = \sum_\alpha \langle S,S,n|\hat{a}_\alpha \hat{a}_\alpha^\dagger|S,S,n\rangle - 3 \quad . \tag{A.46}$$

By applying (A.28) and rearranging the resulting expression, we get

$$N_{-1,S,S,n} = -\sqrt{3+n-\sum_\alpha M_{\alpha,S,S,n}^2} \tag{A.47}$$

in terms of what we already know. Following now the same recipe, which was also used in the calculation of $M_{\alpha,S,m,n}$, we apply $\hat{S}_-$ on (A.28) which yields

$$\hat{S}_- \hat{a}_{-1}^\dagger |S,m,n\rangle = M_{-1,S,m,n} \hat{S}_- |S+1,m-1,n+1\rangle + N_{-1,S,m,n} \hat{S}_- |S-1,m-1,n+1\rangle \quad . \tag{A.48}$$

Performing calculations similar to (A.35)–(A.38) we conclude from (A.48)

$$N_{-1,S,m,n} = \sqrt{\frac{S(S-1)-m(m-1)}{S(S+1)-m(m+1)}} N_{-1,S,m+1,n} \quad . \tag{A.49}$$

By replacing $\hat{a}_{-1}^\dagger$ by $\hat{a}_0^\dagger$, respectively $\hat{a}_1^\dagger$, we obtain

$$N_{0,S,m,n} = \sqrt{\frac{S(S-1)-m(m+1)}{S(S+1)-m(m+1)}} N_{0,S,m+1,n} - \sqrt{\frac{2}{S(S+1)-m(m+1)}} N_{-1,m+1,n} \quad , \tag{A.50}$$

$$N_{0,S,m,n} = \sqrt{\frac{S(S-1)-(m+2)(m+1)}{S(S+1)-m(m+1)}} N_{1,S,m+1,n} - \sqrt{\frac{2}{S(S+1)-m(m+1)}} N_{0,m+1,n} \quad . \tag{A.51}$$

After having successfully calculated the matrix elements of the creation operators $\hat{a}_\alpha^\dagger$, our next goal is to do the same for the annihilation operators $\hat{a}_\alpha$. Because the way how this is done is very similar to the one used above, we restrict ourselves to a brief sketch of the derivation. At first place, we consider the matrix elements $O_{\alpha,S,m,n}$. As encountered above, we need again one starting point, which means

that we need to calculate one of them explicitly, for instance $O_{-1,S,S,n}$. In order to obtain it, we use (A.25) and apply the operator $\hat{a}_{-1}$ on it:

$$\hat{a}_{-1}|S,S,n\rangle = \frac{1}{\sqrt{f(Q,S)}}\hat{a}_{-1}\hat{a}_1^{\dagger S}\hat{\Theta}^{\dagger Q}|0\rangle \quad , \tag{A.52}$$

which can be rewritten with the help of some commutator algebra as

$$\hat{a}_{-1}|S,S,n\rangle = \frac{1}{\sqrt{f(Q,S)}}\hat{a}_1^{\dagger S}(-2\hat{a_1}^{\dagger})\hat{\Theta}^{\dagger(Q-1)}Q|0\rangle \quad . \tag{A.53}$$

Using (A.25) again and inserting the explicit form of the normalization factor (A.26) into (A.53) gives

$$\hat{a}_{-1}|S,S,n\rangle = \frac{\sqrt{f(Q-1,S+1)}}{\sqrt{f(Q,S)}}(-2Q)|S+1,S+1,n-1\rangle = -\sqrt{\frac{2Q(2S+1)}{2S+3}}|S+1,m+1,n-1\rangle \quad , \tag{A.54}$$

which yields after comparison with (A.29)

$$O_{-1,S,S,n} = -\sqrt{\frac{2Q(2S+1)}{2S+3}} \quad . \tag{A.55}$$

Acting with $\hat{S}_+$ on (A.29) one finds the three recursion relations

$$O_{-1,S,m,n} = \sqrt{\frac{S(S+1)-m(m+1)}{(S+2)(S+1)-(m+2)(m+1)}}O_{-1,S,m+1,n} \quad , \tag{A.56}$$

$$O_{0,S,m,n} = \sqrt{\frac{S(S+1)-m(m+1)}{(S+2)(S+1)-m(m+1)}}O_{0,S,m+1,n} - \sqrt{\frac{2}{(S+2)S(S+1)-m(m+1)}}O_{-1,m,n} \quad , \tag{A.57}$$

$$O_{1,S,m,n} = \sqrt{\frac{S(S+1)-m(m+1)}{(S+2)(S+1)-m(m-1)}}O_{0,S,m+1,n} - \sqrt{\frac{2}{(S+2)(S+1)-m(m-1)}}O_{0,m+1,n} \quad , \tag{A.58}$$

where the starting point is given by (A.55). At last, we determine now the remaining class of matrix elements. Here the starting point is provided by $P_{-1,S,S,n}$. In order to calculate it, we use the particle number operator $\hat{n}$ once more and obtain

$$n = \langle S,S,n|\hat{n}|S,S,n\rangle = \sum_\alpha \langle S,S,n|\hat{a}_\alpha^\dagger\hat{a}_\alpha|S,S,n\rangle \quad . \tag{A.59}$$

Rearranging (A.59) with the help of (A.29) gives us

$$P_{1,S,S,n} = \sqrt{n - \sum_\alpha O_{\alpha,S,S,n}^2} \quad . \tag{A.60}$$

Applying now $\hat{S}_{-1}$ on (A.29) one can obtain the last three recursion relations, which read

$$P_{1,S,m,n} = \sqrt{\frac{S(S-1)-m(m-1)}{S(S+1)-m(m+1)}}P_{1,S,m+1,n} \quad , \tag{A.61}$$

$$P_{0,S,m,n} = \sqrt{\frac{S(S-1)-m(m+1)}{S(S+1)-m(m+1)}}P_{0,S,m+1,n} + \sqrt{\frac{2}{S(S+1)-m(m+1)}}P_{1,S,m+1,n} \quad , \tag{A.62}$$

S	m	$M_{1,S,m,n}$	$M_{0,S,m,n}$	$M_{-1,S,m,n}$	$N_{1,S,m,n}$	$N_{0,S,m,n}$	$M_{-1,S,m,n}$
0	0	$\sqrt{\frac{n+3}{3}}$	$\sqrt{\frac{n+3}{3}}$	$\sqrt{\frac{n+3}{3}}$	0	0	0
1	1	$\sqrt{\frac{2(n+4)}{5}}$	$\sqrt{\frac{n+4}{5}}$	$\sqrt{\frac{n+4}{15}}$	0	0	$-\sqrt{\frac{n+1}{3}}$
1	0	$\sqrt{\frac{n+4}{5}}$	$2\sqrt{\frac{n+4}{15}}$	$\sqrt{\frac{n+4}{5}}$	0	$\sqrt{\frac{n+1}{3}}$	0
1	-1	$\sqrt{\frac{n+4}{14}}$	$\sqrt{\frac{n+4}{5}}$	$\sqrt{\frac{2(n+4)}{5}}$	$-\sqrt{\frac{n+1}{3}}$	0	0
2	2	$\sqrt{\frac{3(n+5)}{7}}$	$\sqrt{\frac{n+5}{7}}$	$\sqrt{\frac{3(n+5)}{105}}$	0	0	$-\sqrt{\frac{2n}{5}}$
2	1	$\sqrt{\frac{2(n+5)}{7}}$	$2\sqrt{\frac{6(n+5)}{105}}$	$3\sqrt{\frac{n+5}{105}}$	0	$\sqrt{\frac{n}{5}}$	$-\sqrt{\frac{n}{5}}$
2	0	$2\sqrt{\frac{2(n+5)}{105}}$	$3\sqrt{\frac{3(n+5)}{105}}$	$2\sqrt{\frac{2(n+5)}{105}}$	$-\sqrt{\frac{n}{15}}$	$2\sqrt{\frac{n}{15}}$	$-\sqrt{\frac{n}{15}}$
2	-1	$3\sqrt{\frac{n+5}{105}}$	$\sqrt{2\frac{6(n+5)}{105}}$	$\sqrt{\frac{2(n+5)}{7}}$	$-\sqrt{\frac{n}{5}}$	$\sqrt{\frac{n}{5}}$	0
2	-2	$\sqrt{\frac{3(n+5)}{105}}$	$\sqrt{\frac{n+5}{7}}$	$\sqrt{\frac{3(n+5)}{7}}$	$-\sqrt{\frac{2n}{5}}$	0	0

Figure A.1: Matrix elements of the creation operators $\hat{a}^\dagger_\alpha$.

$$P_{-1,S,m,n} = \sqrt{\frac{S(S+1)-(m+2)(m+1)}{S(S+1)-m(m+1)}} P_{-1,S,m+1,n} + \sqrt{\frac{2}{S(S+1)-m(m+1)}} P_{0,m+1,n} \quad . \quad \text{(A.63)}$$

With the formulas derived in this section, we can calculate arbitrary matrix elements between states with arbitrary quantum numbers S, m, n in a recursive way. In literature, so far, only matrix elements for some particular states were given [50, 53, 60]. Thus, our result is especially important in view of calculations for finite temperature which are performed in Section 3.2.2. There it is necessary to perform a trace over all states and, therefore, those arbitrary matrix elements are needed. However, the *zero*-temperature ground state for an unmagnetized, anti-ferromagnetic system is $|0,0,n\rangle$ for even and $|1,m,n\rangle$, $(m=0,\pm 1)$ for odd particle number n. Thus, when only considering the lowest orders in zero-temperature perturbation theory, we only need the matrix elements of these states and of the states $|S,m,n\rangle$ with $S \leq 2$ and $|m| \leq 2$. In order to be able to work with explicit formulas and to compare our results, stemming from the general recursion relations, with the particular formulas in Ref. [60], we have stated the matrix elements of the creation and annihilation operators for these states in Table A.1 and Table A.2. They agree with the findings from Ref. [60].

A.2 Calculation of Normalization Constant of Eigenstates

In this section, we prove that the normalization constant occurring in (A.25) has the value which was already given in (A.26). We carry out the prove according to the sketch in Ref. [46]. In order to do

S	m	$O_{1,S,m,n}$	$O_{0,S,m,n}$	$O_{-1,S,m,n}$	$P_{1,S,m,n}$	$P_{0,S,m,n}$	$P_{-1,S,m,n}$
0	0	$-\sqrt{\frac{n}{3}}$	$\sqrt{\frac{n}{3}}$	$-\sqrt{\frac{n}{3}}$	0	0	0
1	1	$\sqrt{\frac{n+2}{3}}$	$\sqrt{\frac{n-1}{5}}$	$-\sqrt{\frac{2(n-1)}{5}}$	$-\sqrt{\frac{n-1}{15}}$	0	0
1	0	$-\sqrt{\frac{n-1}{5}}$	$\sqrt{\frac{n+2}{3}}$	$-\sqrt{\frac{n-1}{5}}$	0	$2\sqrt{\frac{n-1}{15}}$	0
1	-1	$-\sqrt{\frac{2(n-1)}{5}}$	$\sqrt{\frac{n-1}{5}}$	$\sqrt{\frac{n+2}{3}}$	0	0	$-\sqrt{\frac{n-1}{15}}$
2	2	$-\sqrt{\frac{3(n-2)}{105}}$	$\sqrt{\frac{n-2}{7}}$	$-\sqrt{\frac{3(n-2)}{7}}$	$\sqrt{\frac{2(n+2)}{5}}$	0	0
2	1	$-3\sqrt{\frac{n-2}{105}}$	$2\sqrt{\frac{6(n-2)}{105}}$	$-\sqrt{\frac{2(n-2)}{7}}$	$\sqrt{\frac{n+3}{5}}$	$\sqrt{\frac{n+3}{5}}$	0
2	0	$-3\sqrt{\frac{2(n-2)}{105}}$	$3\sqrt{\frac{3(n-2)}{105}}$	$-3\sqrt{\frac{2(n-2)}{105}}$	$\sqrt{\frac{n+3}{15}}$	$2\sqrt{\frac{n+3}{15}}$	$\sqrt{\frac{n+3}{15}}$
2	-1	$-\sqrt{\frac{2(n-2)}{7}}$	$2\sqrt{\frac{6(n-2)}{105}}$	$-3\sqrt{\frac{n-2}{105}}$	0	$\sqrt{\frac{n+3}{5}}$	$\sqrt{\frac{n+3}{5}}$
2	-2	$-\sqrt{\frac{3(n-2)}{7}}$	$\sqrt{\frac{n-2}{7}}$	$-\sqrt{\frac{3(n-2)}{105}}$	0	0	$\sqrt{\frac{2(n+2)}{5}}$

Figure A.2: Matrix elements of the annihilation operators $\hat{a}_\alpha$

this, we define at first place the operator

$$\hat{\mathbf{A}} = \begin{pmatrix} (\hat{a}_{-1} - \hat{a}_1)/\sqrt{2} \\ -i(\hat{a}_1 + \hat{a}_{-1})/\sqrt{2} \\ \hat{a}_0 \end{pmatrix} \quad . \tag{A.64}$$

The connection of this operator to our problem is the fact, that its square is just the adjoined of our singlet creation operator (A.13), i.e.

$$\hat{\mathbf{A}}^2 = \hat{A}_x^2 + \hat{A}_y^2 + \hat{A}_z^2 = 2\hat{a}_0^2 - \hat{a}_{-1}\hat{a}_1 = \hat{\Theta} \quad . \tag{A.65}$$

In order to create the state $|0, 0, 2Q\rangle$, we need to apply $\hat{\Theta}^{\dagger Q}$ on the vacuum state $|0\rangle$. Therefore, we define a creating function, from which we can get all powers of $\hat{\Theta}^\dagger$ by means of a simple derivative calculation. The easiest function containing all powers is the exponential, which is defined for an operator by its Taylor series. Thus, we write

$$e^{\hat{\mathbf{A}}^\dagger \cdot \mathbf{x}} = \sum_{l=0}^{\infty} \frac{1}{l!} (\hat{\mathbf{A}}^\dagger \cdot \mathbf{x})^l \quad . \tag{A.66}$$

Acting with the Laplace operator on a term in the exponential series (A.66) yields under consideration of (A.65)

$$\nabla^2 (\hat{\mathbf{A}}^\dagger \cdot \mathbf{x})^l = l(l-1)\hat{\Theta}^\dagger (\hat{\mathbf{A}}^\dagger \cdot \mathbf{x})^{l-2}. \tag{A.67}$$

Repeating this Q times yields

$$\left(\nabla^2\right)^Q (\hat{\mathbf{A}}^\dagger \cdot \mathbf{x})^l = \begin{cases} \frac{l!}{(l-2Q)!} \hat{\Theta}^{\dagger Q} (\hat{\mathbf{A}}^\dagger \cdot \mathbf{x})^{l-2Q} & \text{for} \quad l \geq 2Q \\ 0 \quad \text{otherwise} \end{cases} \quad . \tag{A.68}$$

With the help of (A.68), we can write

$$\hat{\Theta}^{\dagger Q}|0\rangle = \left(\nabla^2\right)^Q e^{\hat{\mathbf{A}}^\dagger\cdot\mathbf{x}}|0\rangle\Big|_{\mathbf{x}=\mathbf{0}} \quad . \tag{A.69}$$

Because we are also interested in producing powers of $\hat{a}_1^\dagger$, we note that

$$\left(\frac{\partial}{\partial x} + i\frac{\partial}{\partial y}\right)(\hat{\mathbf{A}}^\dagger\cdot\mathbf{x})^l = l(\hat{A}_x^\dagger + i\hat{A}_y^\dagger)(\hat{\mathbf{A}}^\dagger\cdot\mathbf{x})^{l-1} \quad , \tag{A.70}$$

which becomes after insertion of (A.64)

$$\left(\frac{\partial}{\partial x} + i\frac{\partial}{\partial y}\right)(\hat{\mathbf{A}}^\dagger\cdot\mathbf{x})^l = l(-\sqrt{2})\hat{a}_1^\dagger(\hat{\mathbf{A}}^\dagger\cdot\mathbf{x})^{l-1} \quad . \tag{A.71}$$

Combining this with (A.69), we can write

$$\hat{a}_1^{\dagger S}\hat{\Theta}^{Q\dagger}|0\rangle = \hat{T}_S^Q e^{\hat{\mathbf{A}}^\dagger\cdot\mathbf{x}}|0\rangle\Big|_{\mathbf{x}=\mathbf{0}} \quad . \tag{A.72}$$

where we have introduced the operator

$$\hat{T}_S^Q(\mathbf{x}) = (-2^{-1/2})^S\left(\frac{\partial}{\partial x} + i\frac{\partial}{\partial y}\right)^S\left(\nabla^2\right)^Q \quad . \tag{A.73}$$

Because the eigenstates (A.3) are, by definition, normalized, the desired normalization constant (A.26) can be written as

$$f(Q,S) = \langle 0|\left(\hat{a}_1^{\dagger S}\hat{\Theta}^{Q\dagger}\right)^\dagger\left(\hat{a}_1^{\dagger S}\hat{\Theta}^{Q\dagger}\right)|0\rangle \quad . \tag{A.74}$$

Now we insert (A.73) into (A.74) and use the fact, that only $\hat{\mathbf{A}}^\dagger$ and $\hat{\mathbf{A}}$ act on the vacuum state $|0\rangle$. Furthermore, we note that $\left(e^{\hat{\mathbf{A}}^\dagger\cdot\mathbf{x}}\right)^\dagger = e^{\hat{\mathbf{A}}\cdot\mathbf{x}}$ and introduce the complex conjugate of (A.73) which reads

$$\hat{T}_S^{*Q}(\mathbf{x}) = (-2^{-1/2})^S\left(\frac{\partial}{\partial x} - i\frac{\partial}{\partial y}\right)^S\left(\nabla^2\right)^Q \quad . \tag{A.75}$$

Finally, we obtain

$$f(Q,S) = \hat{T}_S^Q(\mathbf{x}')\hat{T}_S^{*Q}(\mathbf{x})\langle 0|e^{\hat{\mathbf{A}}\cdot\mathbf{x}'}e^{\hat{\mathbf{A}}^\dagger\cdot\mathbf{x}}|0\rangle\Big|_{\mathbf{x}=\mathbf{x}'=\mathbf{0}} \quad . \tag{A.76}$$

In order to simplify (A.76) further, we need the commutator relation

$$[\hat{\mathbf{A}},\hat{\mathbf{A}}^\dagger] = \mathbf{1} \quad , \tag{A.77}$$

which allows us to use the Baker-Campbell-Hausdorff formula [62]. This relation reads in the suitable form

$$e^{\hat{X}}e^{\hat{Y}} = e^{\hat{Y}}e^{\hat{X}}e^{[\hat{X},\hat{Y}]} \quad , \tag{A.78}$$

where $\hat{X}$ and $\hat{Y}$ are operators with the property

$$\left[\hat{X},[\hat{X},\hat{Y}]\right] = \left[\hat{Y},[\hat{X},\hat{Y}]\right] = 0 \quad . \tag{A.79}$$

Together with the fact, that $\hat{\mathbf{A}}|0\rangle$ vanishes and the normalization of the vacuum state, i.e. $\langle 0|0\rangle = 1$, we can simplify

$$\langle 0|e^{\hat{\mathbf{A}}\cdot\mathbf{x}'}e^{\hat{\mathbf{A}}^\dagger\cdot\mathbf{x}}|0\rangle = e^{\mathbf{x}\cdot\mathbf{x}'} \quad . \tag{A.80}$$

Inserting (A.80) into (A.76) and expanding the occurring exponential yields

$$f(Q,S) = \frac{1}{(2Q+S)!}\hat{T}_S^{*Q}(\mathbf{x}')\hat{T}_S^{Q}(\mathbf{x})(\mathbf{x}\cdot\mathbf{x}')^{2Q+S}\Big|_{\mathbf{x}=\mathbf{x}'=\mathbf{0}} \quad . \tag{A.81}$$

The only thing left to do is to carry out the differentiations in $\hat{T}_S^Q$ on the simple function $(\mathbf{x}\cdot\mathbf{x}')^{2Q+S}$ which is straightforward, yielding

$$f(Q,S) = S!Q!2^Q(2Q+2S+1)(2Q+2S-1)(2Q+2S-3)\ldots(2S+3) \quad . \tag{A.82}$$

This can be simplified with the help of (A.27) to the final result (A.26).

A.3 Relations Between Matrix Elements

The matrix elements, which we have calculated in Section A.1, are not independent but obey relations between each others. Some of these relations, which are used in this thesis to simplify equations, are derived in this section. At first place, we use (A.28) and consider

$$\begin{aligned}\langle S,m,n|\hat{a}_\alpha^\dagger|S-1,m-\alpha,n-1\rangle &= \langle S,m,n|\Big(M_{\alpha,S-1,m-\alpha,n-1}|S,m,n\rangle + N_{\alpha,S-1,m-\alpha,n-1}|S-2,m,n\rangle\Big)\\ &= M_{\alpha,S-1,m-\alpha,n-1} \quad .\end{aligned} \tag{A.83}$$

But we can calculate the same quantity also by letting the adjoined operator of $\hat{a}_\alpha^\dagger$, which is $\hat{a}_\alpha$, act on the left-hand side of the scalar product and apply (A.29) to get

$$\begin{aligned}\langle S,m,n|\hat{a}_\alpha^\dagger|S-1,m-\alpha,n-1\rangle =&\Big(O_{\alpha,S,m,n}\langle S+1,m-\alpha,n-1| + P_{\alpha,S,m,n}\langle S-1,m-\alpha,n-1|\Big)\\ &\times|S-1,m-\alpha,n-1\rangle = P_{\alpha,S,m,n} \quad .\end{aligned} \tag{A.84}$$

Comparing (A.83) and (A.84) one can derive the relation

$$M_{\alpha,S-1,m-\alpha,n-1} = P_{\alpha,S,m,n} \quad . \tag{A.85}$$

Furtheremore, we can also prove with the same technique

$$N_{\alpha,S+1,m-\alpha,n-1} = O_{\alpha,S,m,n} \quad , \tag{A.86}$$

$$O_{\alpha,S-1,m+\alpha,n+1} = N_{\alpha,S,m,n} \quad , \tag{A.87}$$

$$P_{\alpha,S+1,m+\alpha,n+1} = M_{\alpha,S,m,n} \quad . \tag{A.88}$$

These relations can be exemplarily checked in Figs. A.1 and A.2. With the help of these formulas, we can calculate the quantum mechanical expectation value of the particle number operator in a given hyperfine spin state, which is given by $\hat{n}_\alpha = \hat{a}_\alpha^\dagger\hat{a}_\alpha$, and obtain

$$\langle S,m,n|\hat{n}_\alpha|S,m,n\rangle = O_{\alpha,S,m,n}^2 + P_{\alpha,S,m,n}^2 \quad . \tag{A.89}$$

A.4 Calculation of Matrix Elements for Unmagnetized System

In this section, we calculate the matrix elements (3.98) which were appearing in Subsection 3.5.2. They are defined by

$$\tilde{M}_{\alpha,S,n} = \sum_{m=-S}^{S} M_{\alpha,S,m,n}^2 \quad . \tag{A.90}$$

Completely analogous definitions hold for $\tilde{N}_{\alpha,S,n}$, $\tilde{N}_{\alpha,S,n}$, $\tilde{O}_{\alpha,S,n}$, and $\tilde{P}_{\alpha,S,n}$. At first place, we write down $M^2_{1,S,m,n}$ in an explicit form. Using (A.34) and (A.38) yields

$$M^2_{1,S,m,n} = \frac{(S+1)(n+S+3)}{2S+3} \times \frac{(S+1)S - S(S-1)}{(S+2)(S+1) - (S+1)S} \times \frac{(S+1)S - (S-1)(S-2)}{(S+2)(S+1) - S(-1)} \times \cdots \times \frac{(S+1)S - m(m+1)}{(S+2)(S+1) - (m+2)(m+1)} \quad . \tag{A.91}$$

As a next step, we rewrite (A.90) with the help of (A.91) as

$$\tilde{M}_{1,S,n} = \frac{(S+1)(n+S+3)}{2S+3} \left(\frac{(S+1)S - S(S-1)}{(S+2)(S+1) - (S+1)S} \left(\frac{(S+1)S - (S-1)(S-2)}{(S+2)(S+1) - S(S-1)} \times \left(\ldots \left(\frac{(S+1)S - (-S)(-S+1)}{(S+2)(S+1) - (-S+1)(-S+2)} + 1 \right) + 1 \right) \ldots \right) + 1 \right) \quad , \tag{A.92}$$

which becomes after simplifying the respective fractions

$$\tilde{M}_{S,n} = \frac{(n+S+3)(S+1)}{3} \quad , \tag{A.93}$$

For reasons of symmetry, the matrix elements for the unmagnetized system must be the same for all hyperfine components α because there exists no preferred direction. Therefore, we have dropped this index in (A.93). This result is also obtained when calculating $\tilde{M}_{0,S,n}$ and $\tilde{M}_{-1,S,n}$ explicitly. The calculation for the other matrix elements are so similar that we will skip them and only state their results:

$$\tilde{N}_{S,n} = \frac{(n-S+2)S}{3} \quad , \tag{A.94}$$

$$\tilde{O}_{S,n} = \frac{(n-S)(S+1)}{3} \quad , \tag{A.95}$$

$$\tilde{P}_{S,n} = \frac{(n+S+1)S}{3} \quad . \tag{A.96}$$

Appendix B

Correlation Function for Finite Temperature

In this Appendix, we carry out the details of the calculation of the finite temperature correlation function which were deferred in Section 4.2. We start with (4.47), carry out the occurring integrals and obtain

$$\begin{aligned}
\langle \hat{a}^\dagger_{k\alpha}\hat{a}_{l\alpha}\rangle^{(1)} = \frac{\delta_{d(l,k),1}J}{\mathcal{Z}^{(0)2}} \sum_{S_l,m_l,n_l} \sum_{S_k,m_k,n_k} \\
\Bigg[M^2_{\alpha,S_k,m_k,n_k} O^2_{\alpha,S_l,m_l,n_l} \frac{e^{-\beta(E_{S_l,m_l,n_l}+E_{S_k,m_k,n_k})} - e^{-\beta(E_{S_l+1,m_l-\alpha,n_l-1}+E_{S_k+1,m_k+\alpha,n_k+1})}}{E_{S_l+1,m_l-\alpha,n_l-1}+E_{S_k+1,m_k+\alpha,n_k+1}-E_{S_l,m_l,n_l}-E_{S_k,m_k,n_k}} \\
+ M^2_{\alpha,P_k,m_k,n_k} P^2_{\alpha,S_l,m_l,n_l} \frac{e^{-\beta(E_{S_l,m_l,n_l}+E_{S_k,m_k,n_k})} - e^{-\beta(E_{S_l-1,m_l-\alpha,n_l-1}+E_{S_k+1,m_k+\alpha,n_k+1})}}{E_{S_l-1,m_l-\alpha,n_l-1}+E_{S_k+1,m_k+\alpha,n_k+1}-E_{S_l,m_l,n_l}-E_{S_k,m_k,n_k}} \\
+ N^2_{\alpha,S_k,m_k,n_k} O^2_{\alpha,S_l,m_l,n_l} \frac{e^{-\beta(E_{S_l,m_l,n_l}+E_{S_k,m_k,n_k})} - e^{-\beta(E_{S_l+1,m_l-\alpha,n_l-1}+E_{S_k-1,m_k+\alpha,n_k+1})}}{E_{S_l+1,m_l-\alpha,n_l-1}+E_{S_k-1,m_k+\alpha,n_k+1}-E_{S_l,m_l,n_l}-E_{S_k,m_k,n_k}} \\
+ N^2_{\alpha,S_k,m_k,n_k} P^2_{\alpha,S_l,m_l,n_l} \frac{e^{-\beta(E_{S_l,m_l,n_l}+E_{S_k,m_k,n_k})} - e^{-\beta(E_{S_l-1,m_l-\alpha,n_l-1}+E_{S_k-1,m_k+\alpha,n_k+1})}}{E_{S_l-1,m_l-\alpha,n_l-1}+E_{S_k-1,m_k+\alpha,n_k+1}-E_{S_l,m_l,n_l}-E_{S_k,m_k,n_k}} \Bigg] \quad . \qquad \text{(B.1)}
\end{aligned}$$

We plug the explicit formulas for the energy eigenvalues (3.14) in the denominators of (B.1) and split the resulting formula into two parts according to

$$\langle \hat{a}^\dagger_{k\alpha}\hat{a}_{l\alpha}\rangle^{(1)} = A + B \quad , \qquad \text{(B.2)}$$

with

$$\begin{aligned}
A = &\frac{\delta_{d(l,k),1}J}{\mathcal{Z}^{(0)2}} \sum_{S_l,m_l,n_l} \sum_{S_k,m_k,n_k} e^{-\beta(E_{S_k,m_k,n_k}+E_{S_l,m_l,n_l})} \\
&\Bigg[\frac{M^2_{\alpha,S_k,m_k,n_k} O^2_{\alpha,S_l,m_l,n_l}}{U_0(n_k-n_l+1)+U_2(S_k+S_l+2)} + \frac{M^2_{\alpha,S_k,m_k,n_k} P^2_{\alpha,S_l,m_l,n_l}}{U_0(n_k-n_l+1)+U_2(S_l-S_k+1)} \\
&+ \frac{N^2_{\alpha,S_k,m_k,n_k} O^2_{\alpha,S_l,m_l,n_l}}{U_0(n_k-n_l+1)+U_2(S_k-S_l+1)} + \frac{N^2_{\alpha,S_k,m_k,n_k} P^2_{\alpha,S_l,m_l,n_l}}{U_0(n_k-n_l+1)-U_2(S_k+S_l)} \Bigg] \quad , \qquad \text{(B.3)}
\end{aligned}$$

and

$$
\begin{aligned}
B = -\frac{\delta_{d(l,k),1}J}{\mathcal{Z}^{(0)2}} \sum_{S_l,m_l,n_l} \sum_{S_k,m_k,n_k} \Bigg[& \frac{M^2_{\alpha,S_k,m_k,n_k} O^2_{\alpha,S_l,m_l,n_l} e^{-\beta(E_{S_l+1,m_l-\alpha,n_l-1}+E_{S_k+1,m_k+\alpha,n_k+1})}}{U_0(n_k-n_l+1)+U_2(S_k+S_l+2)} \\
& + \frac{M^2_{\alpha,S_k,m_k,n_k} P^2_{\alpha,S_l,m_l,n_l} e^{-\beta(E_{S_l-1,m_l-\alpha,n_l-1}+E_{S_k+1,m_k+\alpha,n_k+1})}}{U_0(n_k-n_l+1)+U_2(S_l-S_k+1)} \\
& + \frac{N^2_{\alpha,S_k,m_k,n_k} O^2_{\alpha,S_l,m_l,n_l} e^{-\beta(E_{S_l+1,m_l-\alpha,n_l-1}+E_{S_k-1,m_k+\alpha,n_k+1})}}{U_0(n_k-n_l+1)+U_2(S_k-S_l+1)} \\
& + \frac{N^2_{\alpha,S_k,m_k,n_k} P^2_{\alpha,S_l,m_l,n_l} e^{-\beta(E_{S_l-1,m_l-\alpha,n_l-1}+E_{S_k-1,m_k+\alpha,n_k+1})}}{U_0(n_k-n_l+1)-U_2(S_k+S_l)} \Bigg] \quad . \qquad \text{(B.4)}
\end{aligned}
$$

Now, we consider the first term in (B.4), which we call B_1, and perform the following shifts of variables:

$$
\begin{aligned}
& S_k+1 \to S_k \quad , && m_k+\alpha \to m_k \quad , && n_k+1 \to n_k \quad , \\
& S_l+1 \to S_l \quad , && m_l-\alpha \to m_l \quad , && n_l-1 \to n_l \quad . \qquad \text{(B.5)}
\end{aligned}
$$

Of course, we also have to shift the summation indices and furtheremore, adjust the boundaries of summation. This is, in principle, a bit complicated because the different indices depend on each other. For example, we have to sum S from $S=0$ to $S=n$ under the constraint that only even (odd) values of S are allowed for even (odd) values of n. This constraint does not cause a problem because we shift both S and n by ± 1 and, therefore, their relative parity remains unchanged. The boundary terms arising from the shifted summation variables vanish because at least one of the respective matrix elements is zero, e.g. $O_{\alpha,S,m,S}=0$. Thus, we can write

$$
\begin{aligned}
B_1 &= -\frac{\delta_{d(l,k),1}J}{\mathcal{Z}^{(0)2}} \sum_{S_l,m_l,n_l} \sum_{S_k,m_k,n_k} \frac{M^2_{\alpha,S_k,m_k,n_k} O^2_{\alpha,S_l,m_l,n_l} e^{-\beta(E_{S_l+1,m_l-\alpha,n_l-1}+E_{S_k+1,m_k+\alpha,n_k+1})}}{U_0(n_k-n_l+1)+U_2(S_k+S_l+2)} \\
&= -\frac{\delta_{d(l,k),1}J}{\mathcal{Z}^{(0)2}} \sum_{S_l,m_l,n_l} \sum_{S_k,m_k,n_k} \frac{M^2_{\alpha,S_k-1,m_k-\alpha,n_k-1} O^2_{\alpha,S_l-1,m_l+\alpha,n_l+1} e^{-\beta(E_{S_k,m_k,n_k}-E_{S_l,m_l,n_l})}}{U_0(n_k-n_l-1)+U_2(S_k+S_l)} \quad . \qquad \text{(B.6)}
\end{aligned}
$$

Using now (A.85) and (A.87), we obtain from (B.6)

$$
B_1 = \frac{\delta_{d(l,k),1}J}{\mathcal{Z}^{(0)2}} \sum_{S_l,m_l,n_l} \sum_{S_k,m_k,n_k} e^{-\beta(E_{S_k,m_k,n_k}-E_{S_l,m_l,n_l})} \frac{N^2_{\alpha,S_k,m_k,n_k} P^2_{\alpha,S_l,m_l,n_l}}{U_0(n_l-n_k+1)-U_2(S_l+S_k)} \qquad \text{(B.7)}
$$

with the same technique of shifting summation indices we get

$$
B_2 = \frac{\delta_{d(l,k),1}J}{\mathcal{Z}^{(0)2}} \sum_{S_l,m_l,n_l} \sum_{S_k,m_k,n_k} e^{-\beta(E_{S_k,m_k,n_k}+E_{S_l,m_l,n_l})} \frac{N^2_{\alpha,S_k,m_k,n_k} O^2_{\alpha,S_l,m_l,n_l}}{U_0(n_l-n_k+1)+U_2(S_l-S_k+1)} \quad , \qquad \text{(B.8)}
$$

$$
B_3 = \frac{\delta_{d(l,k),1}J}{\mathcal{Z}^{(0)2}} \sum_{S_l,m_l,n_l} \sum_{S_k,m_k,n_k} e^{-\beta(E_{S_k,m_k,n_k}+E_{S_l,m_l,n_l})} \frac{M^2_{\alpha,S_k,m_k,n_k} P^2_{\alpha,S_l,m_l,n_l}}{U_0(n_l-n_k+1)+U_2(S_k-S_l+1)} \quad , \qquad \text{(B.9)}
$$

$$
B_4 = \frac{\delta_{d(l,k),1}J}{\mathcal{Z}^{(0)2}} \sum_{S_l,m_l,n_l} \sum_{S_k,m_k,n_k} e^{-\beta(E_{S_k,m_k,n_k}+E_{S_l,m_l,n_l})} \frac{M^2_{\alpha,S_k,m_k,n_k} O^2_{\alpha,S_l,m_l,n_l}}{U_0(n_l-n_k+1)+U_2(S_l+S_k+2)} \quad . \qquad \text{(B.10)}
$$

Before simplifying further, we note that there exist possible divergences. For example, B_2 in (B.8), diverges when $n_l-n_k+1=0$ and at the same time $S_l-S_k+1=0$. However, the same divergence occurs also with different sign in the thermal sum and they cancel for this reason. Thus, we can just skip divergent terms when performing the sum over all states. Because we sum both the indices S_l,

m_l, n_l and S_k, m_k, n_k over all allowed values, we do not change the result if we exchange n_l with n_k, S_l with S_k and m_l with m_k. Applying these replacements to (B.7) and comparing the result with (B.3) yields

$$B_1 = \frac{\delta_{d(l,k),1} J}{\mathcal{Z}^{(0)2}} \sum_{S_l,m_l,n_l} \sum_{S_k,m_k,n_k} e^{-\beta(E_{S_k,m_k,n_k} - E_{S_l,m_l,n_l})} \frac{N^2_{\alpha,S_k,m_k,n_k} P^2_{\alpha,S_l,m_l,n_l}}{U_0(n_k - n_l + 1) - U_2(S_k + S_l)} = A_4 \quad . \tag{B.11}$$

With the same method we can show that $B_2 = A_3$, $B_3 = A_3$, and $B_4 = A_1$. Thus, we can finally write

$$\langle \hat{a}^\dagger_{k\alpha} \hat{a}_{l\alpha} \rangle^{(1)} = 2A \quad , \tag{B.12}$$

with A given by (B.3).

Bibliography

[1] W. Pauli, *The Connection Between Spin and Statistics*, Phys. Rev. **58** (1940) 716.

[2] L. Pitaevskii, S. Stringari, *Bose-Einstein Condensation*, Oxford University Press, 2003.

[3] K. Glaum, *Bose-Einstein-Konenstation in endlichen Systemen*, Ph.D. thesis, Freie Universität Berlin (2008).

[4] H. E. Stanley, *Introduction to Phase Transitions and Critical Phenomena*, Oxford University Press, 1971.

[5] H. Kleinert, V. Schulte-Frohlinde, *Critical Properties of Φ^4-Theories*, World Scientific, 2001.

[6] S. Sachdev, *Quantum Phase Transitions*, Cambridge University Press, 1999.

[7] W. D. Phillips, *Nobel Lecture: Laser cooling and trapping of neutral atoms*, Rev. Mod. Phys. **70** (1998) 721.

[8] O. Penrose, L. Onsager, *Bose-Einstein Condensation and Liquid Helium*, Phys. Rev. **104** (1956) 576.

[9] M. H. Anderson, J. R. Ensher, M. R. Matthews, C. E. Wieman, E. A. Cornell, *Observation of Bose-Einstein Condensation in a Dilute Atomic Vapor*, Science **269** (1995) 198.

[10] K. B. Davis, M. O. Mewes, M. R. Andrews, N. J. van Druten, D. S. Durfee, D. M. Kurn, W. Ketterle, *Bose-Einstein Condensation in a Gas of Sodium Atoms*, Phys. Rev. Lett. **75** (1995) 3969.

[11] T. Hänsch, A. Schawlow, *Cooling of Gases by Laser Radiation*, Opt. Comm. **13** (1975) 68.

[12] D. Wineland, J. Dalibard, C. Cohen-Tannoudji, *Sisyphus Cooling of a Bound Atom*, J. Opt. Soc. Am. **9** (1992) 32.

[13] W. Ketterle, N. Van Druten, *Evaporative cooling of trapped atoms*, Adv. At., Mol., Opt. Phys. **37** (1996) 181.

[14] University of York,
`http://www-users.york.ac.uk/~phys24/Pages/Techniques/MDS/index2.shtml`.

[15] University of Otago,
`http://www.physics.otago.ac.nz/research/jackdodd/resources/exp_aspects.html`.

[16] P. Soltan-Panahi, *Spinor Bose-Einstein Condensation*, Diploma thesis, Freie Universität Berlin, 2006.

[17] M. Greiner, O. Mandel, T. Esslinger, T. W. Hänsch, I. Bloch, *Quantum phase transition from a superfluid to a Mott insulator in a gas of ultracold atoms*, Nature **415** (2002) 39.

[18] K. Xu, Y. Liu, J. R. Abo-Shaeer, T. Mukaiyama, J. K. Chin, D. E. Miller, W. Ketterle, K. M. Jones, E. Tiesinga, *Sodium Bose-Einstein condensates in an optical lattice*, Phys. Rev. A **72** (2005) 043604.

[19] W. Nolting, *Grundkurs Theoretische Physik 1. Klassische Mechanik*, 8th Edition, Springer, 2006.

[20] F. Schwabl, *Quantenmechanik für Fortgeschrittene (QM 2)*, Springer, 1997.

[21] U. Gavish, Y. Castin, Matter-wave localization in disordered cold atom lattices, Phys. Rev. Lett. **95** (2005) 020401.

[22] K. V. Krutitsky, A. Pelster, R. Graham, *Mean-field phase diagram of disordered bosons in a lattice at nonzero temperature*, New Journ. Phys. **8** (2006) 187.

[23] A. Hoffmann, *Bosonen im optischen Gitter*, Diploma thesis, Freie Universität Berlin, 2007.

[24] D. Jaksch, C. Bruder, J. I. Cirac, C. W. Gardiner, P. Zoller, *Cold Bosonic Atoms in Optical Lattices*, Phys. Rev. Lett. **81** (1998) 3108.

[25] D. Jaksch, H.-J. Briegel, J. I. Cirac, C. W. Gardiner, P. Zoller, *Entanglement of Atoms via Cold Controlled Collisions*, Phys. Rev. Lett. **82** (1999) 1975.

[26] G. K. Brennen, C. M. Caves, P. S. Jessen, I. H. Deutsch, *Quantum Logic Gates in Optical Lattices*, Phys. Rev. Lett. **82** (1999) 1060.

[27] A. Klein, D. Jaksch, *Simulating high-temperature superconductivity model Hamiltonians with atoms in optical lattices*, Phys. Rev. A **73** (2006) 053613.

[28] R. Schutzhold, S. Mostame, *Quantum simulator for the O(3) nonlinear sigma model*, JETP Lett. **82** (2005) 248.

[29] W. Hofstetter, J. I. Cirac, P. Zoller, E. Demler, M. D. Lukin, *High-Temperature Superfluidity of Fermionic Atoms in Optical Lattices*, Phys. Rev. Lett. **89** (2002) 220407.

[30] I. Bloch, *Ultracold quantum gases in optical lattices*, Nature Physics **1** (2005) 23.

[31] D. M. Stamper-Kurn, H.-J. Miesner, S. Inouye, M. R. Andrews, W. Ketterle, *Collisionless and Hydrodynamic Excitations of a Bose-Einstein Condensate*, Phys. Rev. Lett. **81** (1998) 500.

[32] C. K. Law, H. Pu, N. P. Bigelow, *Quantum Spins Mixing in Spinor Bose-Einstein Condensates*, Phys. Rev. Lett. **81** (1998) 5257.

[33] M.-S. Chang, C. D. Hamley, M. D. Barrett, J. A. Sauer, K. M. Fortier, W. Zhang, L. You, M. S. Chapman, *Observation of Spinor Dynamics in Optically Trapped Rb Bose-Einstein Condensates*, Phys. Rev. Lett. **92** (2004) 140403.

[34] M. Koashi, M. Ueda, *Exact Eigenstates and Magnetic Response of Spin-1 and Spin-2 Bose-Einstein Condensates*, Phys. Rev. Lett. **84** (2000) 1066.

[35] M. Ueda, M. Koashi, *Theory of spin-2 Bose-Einstein condensates: Spin correlations, magnetic response, and excitation spectra*, Phys. Rev. A **65** (2002) 063602.

[36] D. M. Stamper-Kurn, M. R. Andrews, A. P. Chikkatur, S. Inouye, H.-J. Miesner, J. Stenger, W. Ketterle, *Optical Confinement of a Bose-Einstein Condensate*, Phys. Rev. Lett. **80** (1998) 2027.

[37] R. Grimm, M. Weidemuller, Y. Ovchinnikov, *Optical dipole traps for neutral atoms*, Adv. At., Mol., Opt. Phys **42** (2000) 95.

[38] Universität Hamburg, *Website of the group of K. Sengstock*.

[39] H. Haken, H. Wolf, *Atom- und Quantenphysik*, 9th Edition, Springer, 2004.

[40] K. Huang, *Statistical Mechanics*, 2nd Edition, Wiley and Sons, 1987.

[41] A. Griesmaier, J. Werner, S. Hensler, J. Stuhler, T. Pfau, *Bose-Einstein Condensation of Chromium*, Phys. Rev. Lett. **94** (2005) 160401.

[42] K. Glaum, A. Pelster, H. Kleinert, T. Pfau, *Critical Temperature of Weakly Interacting Dipolar Condensates*, Phys. Rev. Lett. **98** (2007) 080407.

[43] T.-L. Ho, *Spinor Bose Condensates in Optical Traps*, Phys. Rev. Lett. **81** (1998) 742.

[44] E. G. M. van Kempen, S. J. Kokkelmans, D. J. Heinzen, B. J. Verhaar, *Interisotope Determination of Ultracold Rubidium Interactions from Three High-Precision Experiments*, Phys. Rev. Lett. **88** (2002) 093201.

[45] A. Crubellier, O. Dulieu, F. Masnou-Seeuws, M. Elbs, H. Knöckel, E. Tiemann, *Simple Determination of Na2 Scattering Length Using Observed Bound Levels at the Ground State Asymptote*, Eur. Phys J. D **6** (1999) 211.

[46] T.-L. Ho, S. K. Yip, *Fragmented and Single Condensate Ground States of Spin-1 Bose Gas*, Phys. Rev. Lett. **84** (2000) 4031.

[47] M. Snoek, F. Zhou, *Microscopic wave functions of spin-singlet and nematic Mott states of spin-one bosons in high-dimensional bipartite lattices*, Phys. Rev. B **69** (2004) 094410.

[48] E. Demler, F. Zhou, *Spinor Bosonic Atoms in Optical Lattices: Symmetry Breaking and Fractionalization*, Phys. Rev. Lett. **88** (2002) 163001.

[49] P. B. Blakie, C. W. Clark, *Wannier states and Bose-Hubbard parameters for 2D optical lattices*, Journ. Phys. B **37** (2004) 1391.

[50] T. Kimura, S. Tsuchiya, S. Kurihara, *Possibility of a First-Order Superfluid–Mott-Insulator Transition of Spinor Bosons in an Optical Lattice*, Phys. Rev. Lett. **94** (2005) 110403.

[51] F. Schwabl, *Statistische Mechanik*, 3rd Edition, Springer Verlag, 2006.

[52] N. Uesugi, M. Wadati, *Superfluid–Mott Insulator Transition of Spinor Gases with External Magnetic Fields*, J. Phys. Soc. Japan 72 (2003) 1041.

[53] T. Kimura, S. Tsuchiya, M. Yamashita, S. Kurihara, *Superfluid–Mott insulator transition of spin-1 bosons in optical lattice under magnetic field*, J. Phys. Soc. Japan **75** (2006) 074601.

[54] A. A. Svidzinsky, S. T. Chui, *Insulator-superfluid transition of spin-1 bosons in an optical lattice in magnetic field*, Phys. Rev. A **68** (2003) 043612.

[55] L. D. Landau, E. M. Lifshitz, *Statistical Physics*, 3rd Edition, Pergamon Press, 1980.

[56] J. W. Negele, H. Orland, *Quantum Many-Particle Systems*, Addison-Wesley Publishing Company, 1988.

[57] S. Inouye, R. Andrews, J. Stenger, H.-J. Miesner, D. M. Stamper-Kurn, W. Ketterle, *Observation of Feshbach Resonances in a Bose-Einstein Condensate*, Nature **392** (1998) 151.

[58] M. P. A. Fisher, P. B. Weichman, G. Grinstein, D. S. Fisher, *Boson localization and the superfluid-insulator transition*, Phys. Rev. B **40** (1989) 546.

[59] K. Krutitsky, Private communication.

[60] S. Tsuchiya, S. Kurihara, T. Kimura, *Superfluid–Mott insulator transition of spin-1 bosons in an optical lattice*, Phys. Rev. A **70** (2004) 043628.

[61] F. Schwabl, *Quantenmechanik (QM I)*, 6th Edition, Springer, 2002.

[62] H. Kleinert, *Path Integrals in Quantum Mechanics, Statistics, Polymer Physics, and Financial Markets*, 4th Edition, World Scientific, 2006.

[63] A. A. Abrikosov, L. P. Gorkov, I. E. Dzyaloshinski, *Methods of Quantum Field Theory in Statistical Physics*, Dover Publications, 1963.

[64] P. Buonsante, A. Vezzani, *Phase Diagram for Ultracold Bosons in Optical Lattices and Superlattices*, Phys. Rev. A **70** (2004) 033608.

[65] K. V. Krutitsky, A. Pelster, R. Graham, *Mean-field phase diagram of disordered bosons in a lattice at nonzero temperature*, New J. Phys. **8** (2006) 187.

[66] A. Imambekov, M. Lukin, E. Demler, *Spin-exchange interactions of spin-one bosons in optical lattices: Singlet, nematic, and dimerized phases*, Phys. Rev. A **68** (2003) 063602.

[67] V. A. Kashurnikov, N. V. Prokof'ev, B. V. Svistunov, *Revealing the superfluid–Mott-insulator transition in an optical lattice*, Phys. Rev. A **66** (2002) 031601.

[68] S. Fölling, A. Widera, T. Müller, F. Gerbier, I. Bloch, *Formation of Spatial Shell Structure in the Superfluid to Mott Insulator Transition*, Phys. Rev. Lett. **97** (2006) 060403.

[69] A. Imambekov, M. Lukin, E. Demler, *Magnetization Plateaus for Spin-One Bosons in Optical Lattices: Stern-Gerlach Experiments with Strongly Correlated Atoms*, Phys. Rev. Lett. **93** (2004) 120405.

[70] D. E. Platt, *A modern analysis of the Stern–Gerlach experiment*, Am. J. Phys. **60** (1992) 306.

[71] D. van Oosten, P. van der Straten, H. T. Stoof, *Quantum phases in an optical lattice*, Phys. Rev. A **63** (2001) 053601.

[72] J. M. Ziman, *Prinzipien der Festkörpertheorie*, 2nd Edition, Cambridge University Press, 1998.

[73] F. Dalfovo, S. Giorgini, L. P. Pitaevskii, S. Stringari, *Theory of Bose-Einstein condensation in trapped gases*, Rev. Mod. Phys. **71** (1999) 463.

[74] C. J. Pethick, H. Smith, *Bose-Einstein Condensation in Dilute Gases*, Cambridge University Press, 2002.

[75] J. K. Freericks, H. Monien, *Strong-coupling expansions for the pure and disordered Bose-Hubbard model*, Phys. Rev. B **53** (1996) 2691.

[76] J. Zinn-Justin, *Quantum Field Theory and Critical Phenomena*, 3rd Edition, Clarendon Press, 1996.

[77] F. Gerbier, A. Widera, S. Fölling, O. Mandel, T. Gericke, I. Bloch, *Interference pattern and visibility of a Mott insulator*, Phys. Rev. A **72** (2005) 053606.

[78] F. Gerbier, A. Widera, S. Fölling, O. Mandel, T. Gericke, I. Bloch, *Phase coherence of an atomic Mott insulator*, Phys. Rev. Lett. **95** (2005) 050404.

[79] W. Metzner, *Linked-cluster expansion around the atomic limit of the Hubbard model*, Phys. Rev. B **43** (1993) 8549.

[80] A. Sherman, *One-loop approximation for the Hubbard model*, Phys. Rev. B **73** (2006) 155105.

[81] V. A. Moskalenko, P. Entel, D. F. Digor, *Strong interaction of correlated electrons with phonons: A diagrammatic approach*, Phys. Rev. B **59** (1999) 619.

[82] V. A. Moskalenko, P. Entel, D. F. Digor, *Strong interaction of correlated electrons with acoustical phonons using the extended Hubbard-Holstein model*, Phys. Rev. B **74** (2006) 075109.

[83] K. Kubo, *Magnetic Susceptibility of the Strongly Correlated Hubbard Model*, Progr. Theo. Phys. **64** (1980) 758.

[84] O. Forster, *Analysis 2*, 7th Edition, Vieweg, 2006.

[85] A. Pelster, *Bose-Einstein-Kondensation*, Vorlesungsmanuskript Universität Duisburg-Essen, 2004.

[86] T.-L. Ho, Q. Zhou, Intrinsic heating and cooling in adiabatic processes for bosons in optical lattices, Phys. Rev. Lett. **99** (2007) 120404.

[87] F. Nogueira, *A Primer to the Bose-Hubbard Model*.

[88] W. Metzner, D. Vollhardt, *Correlated Lattice Fermions in $d = \infty$ Dimensions*, Phys. Rev. Lett. **62** (1989) 324.

[89] L. Amico, V. Penna, *Dynamical Mean Field Theory of the Bose-Hubbard Model*, Phys. Rev. Lett. **80** (1998) 2189.

[90] G. D. Mahan, *Many-Particle Physics*, 3rd Edition, Kluwer Academic, 2000.

[91] H. Jänich, *Funktionentheorie*, Springer Verlag, 2004.

[92] R. N. Silver, D. S. Sivia, J. E. Gubernatis, *Maximum-entropy method for analytic continuation of quantum Monte Carlo data*, Phys. Rev. B **41** (1990) 2380.

[93] D. B. M. Dickerscheid, D. van Oosten, P. J. H. Denteneer, H. T. C. Stoof, *Ultracold atoms in optical lattices*, Phys. Rev. A **68** (2003) 043623.

[94] C. Kittel, *Einführung in die Festkörperphysik*, Oldenbourg, 2005.

[95] B. Capogrosso-Sansone, N. V. Prokof'ev, B. V. Svistunov, *Phase diagram and thermodynamics of the three-dimensional Bose-Hubbard model*, Phys. Rev. B **75** (2007) 134302.

[96] I. S. Gradshteyn, I. M. Ryzhik, *Table of Integrals, Series and Products*, Academic Press, 1965.

[97] K. Sengupta, N. Dupuis, *Mott-insulator–to–superfluid transition in the Bose-Hubbard model: A strong-coupling approach*, Phys. Rev. A **71** (2005) 033629.

[98] B. Capogrosso-Sansone, S. G. Söyler, N. Prokof'ev, B. Svistunov, *Monte Carlo study of two-dimensional Bose-Hubbard model*, eprint: `arXiv:0710.2703v3`.

[99] E. Santos, A. Pelster, *In preparation*.

[100] N. Elstner, H. Monien, *Dynamics and thermodynamics of the Bose-Hubbard model*, Phys. Rev. B **59** (1999) 12184.

[101] G. Mazzarella, S. M. Giampaolo, F. Illuminati, *Extended Bose Hubbard model of interacting bosonic atoms in optical lattices: From superfluidity to density waves*, Phys. Rev. A **73** (2006) 013625.

[102] T. D. Kühner, H. Monien, *Phases of the one-dimensional Bose-Hubbard model*, Phys. Rev. B **58** (1998) R14741.

[103] P. C. Hohenberg, B. I. Halperin, *Theory of dynamic critical phenomena*, Rev. Mod. Phys. **49** (1977) 435.

[104] J. M. Kosterlitz, D. J. Thouless, *Ordering, metastability and phase transitions in two-dimensional systems*, J. Phys. C **6** (1973) 1181.

[105] W. Ying, *Simple algebraic method to solve a coupled-channel cavity QED model*, Phys. Rev. A **54** (1996) 4534.

List of Figures

1.1 Cooling methods . . . 3
1.2 Two- and three dimensional optical lattices . . . 4

2.1 Intensity distribution in optical trap . . . 8
2.2 Different hyperfine components in a spinor BEC . . . 8
2.3 Scattering lengths . . . 9

3.1 Particle number at zero temperature . . . 16
3.2 Particle number for different temperatures . . . 17
3.3 Total spin expectation value . . . 18
3.4 Magnetization as function of μ . . . 19
3.5 Magnetization as function of η . . . 19
3.6 First- and second-order phase transition . . . 24
3.7 Phase diagram for $T = 0$ . . . 24
3.8 Phase diagram for $T = 0$ and large U_2 . . . 25
3.9 Phase diagram for $T = 0$ and vanishing magnetization . . . 26
3.10 Difference between small an vanishing η . . . 27
3.11 Phase diagram for scalar BHM . . . 32
3.12 Phase boundary for finite temperature . . . 33
3.13 Phase boundary for finite temperature and large U_2 . . . 33

4.1 Nearest-neighbor correlations . . . 40
4.2 Time-of-flight pictures for spin-1 BHM . . . 41
4.3 Momentum-space density for $V_0 = 0$ . . . 41
4.4 On-site occupation number for different hyperfine states. . . . 45
4.5 Visibility prefactor for scalar BHM . . . 47
4.6 Visibility prefactor for spin-1 BHM . . . 47

5.1 Corrections to particle number per site . . . 58
5.2 Specific heat . . . 61

6.1 First-order time-of-flight pictures and experiment 66
6.2 1st order phase diagram 68
6.3 Spectrum of pair excitations 72
6.4 Finite T excitation spectrum 74
6.5 On-site number statistic for scalar BHM 74
6.6 Fluctuations of particle number 74
6.7 Temperature dependence of gap 75
6.8 Effective masses 76
6.9 Coefficients for equal-time correlation 79
6.10 Resummed TOF pictures 80
6.11 Visibility 82
6.12 Spatial correlations in Mott phase 83
6.13 One-loop phase diagram. $T = 0$, $D = 3, D = 2$ 91
6.14 One-loop phase diagram. $T = 0$, $D = 1$ 91
6.15 Critical hopping parameters 93
6.16 Gap for first and second order 93
6.17 Critical exponent 94
6.18 One-loop phase diagram at finite T 94
6.19 One-loop corrected spectrum of a pair excitations for $D = 3$ 95
6.20 One-loop corrected spectrum of a pair excitations for $D = 2$ 95

A.1 Matrix elements of creation operators 106
A.2 Matrix elements of annihilation operators 107

Danksagung

Als erstes möchte ich Herrn Prof. Dr. Dr. h.c. Hagen Kleinert für die Möglichkeit danken, diese Diplomarbeit in seiner Arbeitsgruppe anzufertigen. In Gesprächen mit ihm konnte ich lernen, daß theoretische Physik nicht nur aus Formeln und Rechnungen besteht, sondern auch tiefe Einsichten in die Natur der Dinge liefern kann. Sein enormes physikalisches Wissen, das sich auch in seinen zahlreichen Büchern widerspiegelt, erlaubte auch mir meinen Horizont zu erweitern.
Desweiteren gilt mein großer Dank Herrn Priv.-Doz. Dr. Axel Pelster für seine Betreuung. Er hat mich nicht nur an seinem großen physikalischen Erfahrungsschatz teilhaben lassen, sondern auch immer Zeit gefunden, mir bei der Lösung kleinerer und größerer Probleme zu helfen. Außerdem lieferte er mir große Unterstützung bei der Niederschrift der Arbeit. Ohne ihn wäre diese Diplomarbeit nicht möglich gewesen.
Alexander Hoffmann und Dr. Konstantin Glaum bin ich dafür zu Dank verpflichtet, daß sie mir, gerade zu Beginn meiner Arbeit, bereitwillig viele Fragen zu Bose-Einstein Kondensaten und anderem beantwortet haben und außerdem, wie auch Aristeu Lima, mit schonungsloser Kritik geholfen haben, meine Arbeit zu verbessern.
Ich bedanke mich bei Dr. Konstantin Krutitsky für sein Mathematica-Programm, das in dieser Arbeit für die numerische Berechnung der Modell-Parameter verwendet wurde.
Herrn Prof. Dr. Dr. h.c. Robert Graham und Herrn Prof. Dr. Ralf Schützhold möchte ich für die Gastfreundschaft bei meinen Aufenthalten in Duisburg danken, bei denen ich die Gelegenheit hatte, unsere Arbeit vorzustellen und viele stimulierende Diskussionen zu führen.
Allen Gruppenmitgliedern, insbesondere Walja Korolesvski, Dr. Jürgen Dietel, Dr. Flavio Nogueira, Ednilson Santos, Markus Düttmann und Victor Bezerra, danke ich für eine vorzügliche Arbeitsatmosphäre und viele, auch über die Physik hinausgehende, Gespräche und Diskussion.
Zum Schluß möchte ich noch meinen Eltern und Anja dafür danken, daß sie mich in jeder Form unterstützt haben und immer für mich da waren.